FAA-76-14
REPORT NO. FAA-RD-76-93

# WAKE VORTEX AND GROUNDWIND METEOROLOGICAL MEASUREMENTS

M. R. Brashears
K. R. Shrider
D. A. Love
S. J. Robertson
A. D. Zalay

Lockheed Missiles & Space Company, Inc.
Huntsville Research & Engineering Center
4800 Bradford Drive
Huntsville AL 35807


MAY 1976
FINAL REPORT



Prepared for

U.S. DEPARTMENT OF TRANSPORTATION
FEDERAL AVIATION ADNINISTRATION
Systems Research and Development Service
Washington DC 20590

**Technical Report Documentation Page**

| 1. Report No. | 2. Government Accession No. | 3. Recipient's Catalog No. |
|---|---|---|
| FAA-RD-76-93 | | |

| 4. Title and Subtitle | 5. Report Date |
|---|---|
| WAKE VORTEX AND GROUNDWIND METEOROLOGICAL MEASUREMENTS | May 1976 |
| | 6. Performing Organization Code |

| 7. Author(s) | 8. Performing Organization Report No. |
|---|---|
| M.R. Brashears, K.R. Shrider, D.A. Love, S.J. Robertson, and A.D. Zalay | DOT-TSC-FAA-76-14<br>LMSC-HREC TR D496558 |

| 9. Performing Organization Name and Address | 10. Work Unit No. (TRAIS) |
|---|---|
| Lockheed Missiles & Space Company, Inc.*<br>Huntsville Research & Engineering Center<br>4800 Bradford Drive<br>Huntsville AL 35807 | FA605/R6122 |
| | 11. Contract or Grant No.<br>DOT-TSC-904 |

| 12. Sponsoring Agency Name and Address | 13. Type of Report and Period Covered |
|---|---|
| U.S. Department of Transportation<br>Federal Aviation Administration<br>Systems Research and Development Service<br>Washington DC 20590 | Final Report<br>Aug. 1974 - Sept. 1975 |
| | 14. Sponsoring Agency Code |

15. Supplementary Notes

*Under contract to: U.S. Department of Transportation
Transportation Systems Center
Kendall Square
Cambridge MA 02142

16. Abstract

Wake vortex groundwind and meteorological measurements obtained by DOT-TSC at John F. Kennedy (JFK) International Airport have been reduced, analyzed, and correlated with a theoretical vortex transport model. The predictive Wake Vortex Transport Model has been updated so that detailed on-site meteorological measurements can be interpreted and utilized to predict more accurately the vortex transport and decay characteristics. A discussion of the wake vortex test data analysis and software development is presented, including a description of the JFK wake vortex test program, the computer processing of wake vortex measurements, the analysis of groundwind sensor measurements, and the analysis of meteorological measurements.

| 17. Key Words | 18. Distribution Statement |
|---|---|
| Vortices, Wind Shear, Turbulence, Vortex Transport, Wake Vortex Hazard, Groundwind, Aircraft Wakes | DOCUMENT IS AVAILABLE TO THE U.S. PUBLIC THROUGH THE NATIONAL TECHNICAL INFORMATION SERVICE, SPRINGFIELD, VIRGINIA 22161 |

| 19. Security Classif. (of this report) | 20. Security Classif. (of this page) | 21. No. of Pages | 22. Price |
|---|---|---|---|
| Unclassified | Unclassified | 174 | |

Form DOT F 1700.7 (8-72) Reproduction of completed page authorized

## PREFACE

This document is the final report for Contract DOT-TSC-904. The contract was initiated on 28 August 1974 to develop optimum techniques for processing groundwind sensor data to determine the location of aircraft wake vortices. This effort was to be completed on 16 February 1975. The basic contract was modified on 9 January 1975 to provide for the development of a unified algorithm incorporating previously developed computer algorithms into a single software package for processing digital tapes recorded during the wake vortex test program at John F. Kennedy International Airport. This effort was completed on 5 September 1975.

This research effort was performed by Lockheed Missiles & Space Company, Inc., Huntsville Research & Engineering Center, Huntsville, Alabama, for the Department of Transportation, Transportation Systems Center, Cambridge, Massachusetts. The Lockheed project Engineer for this study was Dr. M. R. Brashears, and the TSC Contracting Officer's Technical Monitor was Dr. J. N. Hallock. The authors are grateful for Dr. Hallock's assistance and interest during the performance of this study.

## METRIC CONVERSION FACTORS

### Approximate Conversions to Metric Measures

| Symbol | When You Know | Multiply by | To Find | Symbol |
|---|---|---|---|---|
| | | **LENGTH** | | |
| in | inches | 2.5 | centimeters | cm |
| ft | feet | 30 | centimeters | cm |
| yd | yards | 0.9 | meters | m |
| mi | miles | 1.6 | kilometers | km |
| | | **AREA** | | |
| $in^2$ | square inches | 6.5 | square centimeters | $cm^2$ |
| $ft^2$ | square feet | 0.09 | square meters | $m^2$ |
| $yd^2$ | square yards | 0.8 | square meters | $m^2$ |
| $mi^2$ | square miles | 2.6 | square kilometers | $km^2$ |
| | acres | 0.4 | hectares | ha |
| | | **MASS (weight)** | | |
| oz | ounces | 28 | grams | g |
| lb | pounds | 0.45 | kilograms | kg |
| | short tons (2000 lb) | 0.9 | tonnes | t |
| | | **VOLUME** | | |
| tsp | teaspoons | 5 | milliliters | ml |
| Tbsp | tablespoons | 15 | milliliters | ml |
| fl oz | fluid ounces | 30 | milliliters | ml |
| c | cups | 0.24 | liters | l |
| pt | pints | 0.47 | liters | l |
| qt | quarts | 0.95 | liters | l |
| gal | gallons | 3.8 | liters | l |
| $ft^3$ | cubic feet | 0.03 | cubic meters | $m^3$ |
| $yd^3$ | cubic yards | 0.76 | cubic meters | $m^3$ |
| | | **TEMPERATURE (exact)** | | |
| °F | Fahrenheit temperature | 5/9 (after subtracting 32) | Celsius temperature | °C |

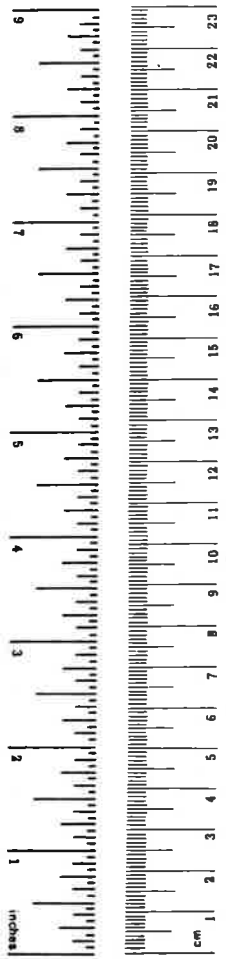


### Approximate Conversions from Metric Measures

| Symbol | When You Know | Multiply by | To Find | Symbol |
|---|---|---|---|---|
| | | **LENGTH** | | |
| mm | millimeters | 0.04 | inches | in |
| cm | centimeters | 0.4 | inches | in |
| m | meters | 3.3 | feet | ft |
| m | meters | 1.1 | yards | yd |
| km | kilometers | 0.6 | miles | mi |
| | | **AREA** | | |
| $cm^2$ | square centimeters | 0.16 | square inches | $in^2$ |
| $m^2$ | square meters | 1.2 | square yards | $yd^2$ |
| $km^2$ | square kilometers | 0.4 | square miles | $mi^2$ |
| ha | hectares (10,000 $m^2$) | 2.5 | acres | |
| | | **MASS (weight)** | | |
| g | grams | 0.035 | ounces | oz |
| kg | kilograms | 2.2 | pounds | lb |
| t | tonnes (1000 kg) | 1.1 | short tons | |
| | | **VOLUME** | | |
| ml | milliliters | 0.03 | fluid ounces | fl oz |
| l | liters | 2.1 | pints | pt |
| l | liters | 1.06 | quarts | qt |
| l | liters | 0.26 | gallons | gal |
| $m^3$ | cubic meters | 35 | cubic feet | $ft^3$ |
| $m^3$ | cubic meters | 1.3 | cubic yards | $yd^3$ |
| | | **TEMPERATURE (exact)** | | |
| °C | Celsius temperature | 9/5 (then add 32) | Fahrenheit temperature | °F |

CONTENTS



LIST OF TABLES

## LIST OF ILLUSTRATIONS

LIST OF ILLUSTRATIONS (Continued)

LIST OF ILLUSTRATIONS (Continued)

LIST OF ILLUSTRATIONS (Continued)

LIST OF ILLUSTRATIONS (Concluded)

# 1. INTRODUCTION

In order to ensure passenger safety and to increase present day airport capacity, the Department of Transportation (DOT) is spearheading the development of a wake vortex avoidance system for airports. Essentially, the system consists of a computerized wake vortex predictive model supplemented by active vortex tracking and meteorological sensors. The Predictive Wake Vortex Transport Models and the meteorological data analysis program were developed by Lockheed-Huntsville for DOT under previous research efforts and are described in Refs. 1 through 4.

As a step toward the development of a wake vortex avoidance system, comprehensive wake vortex monitoring and tracking systems are currently being developed and tested by DOT-TSC at the John F. Kennedy (JFK) International Airport. For this program, Lockheed-Huntsville is developing the computer software to reduce, analyze and correlate meteorological and groundwind wake vortex measurements with predicted vortex tracks. The research effort described in this report consisted of two basic parts. The first was directed toward the development of optimum analytical techniques for processing groundwind sensor data to determine the location of wake vortices. The second was to integrate the selected optimum techniques with previously developed algorithms for analyzing meteorological data and predicting vortex tracks into a single time-efficient software package. This software package was to be suitable for processing large amounts of data obtained during the test program at JFK. The output of the software package was to be an atmospheric characterization and plots of measured vortex tracks obtained with the various vortex tracking systems compared with predicted vortex tracks.

The capability has been developed at TSC to process raw data tapes containing digitized groundwind and meteorological measurements with the results being displayed graphically or numerically. The predictive wake vortex transport model has been updated so that the detailed on-site meteorological measurements can be used as input parameters to compute vortex transport and decay characteristics. Under this research program, the different computer routines have been integrated into one software package enabling comparisons to be made between observed and predicted vortex transport phenomena in the terminal area.

A discussion is given in this report of the analysis of groundwind sensor data to select an optimum analytical technique for identifying and tracking vortices. Some results in the analysis of meteorological data are also described. Finally, a complete description is given of the complete software package developed for processing and analyzing test data obtained in the JFK wake vortex test program.

## 2. WAKE VORTEX TEST PROGRAM

A test program is being conducted at the John F. Kennedy (JFK) International Airport at Jamaica, New York, to test several wake vortex tracking systems and to collect data on the transport of wake vortices under various meteorological conditions. The wake vortex tracks measured by the tracking systems will be compared with predicted tracks computed using a wake vortex transport model computer program. Data collected during the test program will be used to evaluate the tracking systems and to refine the predictive model.

Five different vortex sensor types are currently installed at JFK. Of these five, three utilize acoustics to detect the vortices, one utilizes a laser beam to detect the vortices and one senses the vortex flow with a series of anemometers in a ground array oriented perpendicular to the flight corridor. These sensors are arranged as depicted on the plan view schematic of Fig. 2-1. Auxiliary instrumentation is also depicted in these figures.

The three arrays of anemometers (Ground Wind Vortex Sensing System – GWVSS Nos. 1, 2 and 3) are arranged at locations just beyond the runway 31R middle marker, between the middle marker and runway 22L/4R, and at the threshold of runway 31R.

The Monostatic Acoustic Vortex Sensing System (MAVSS) is arranged in a single array of ten sensors in proximity to GWVSS No. 2. These sensors are used to determine an approximate vortex height and strength when the wind is transporting the vortices over the sensors.

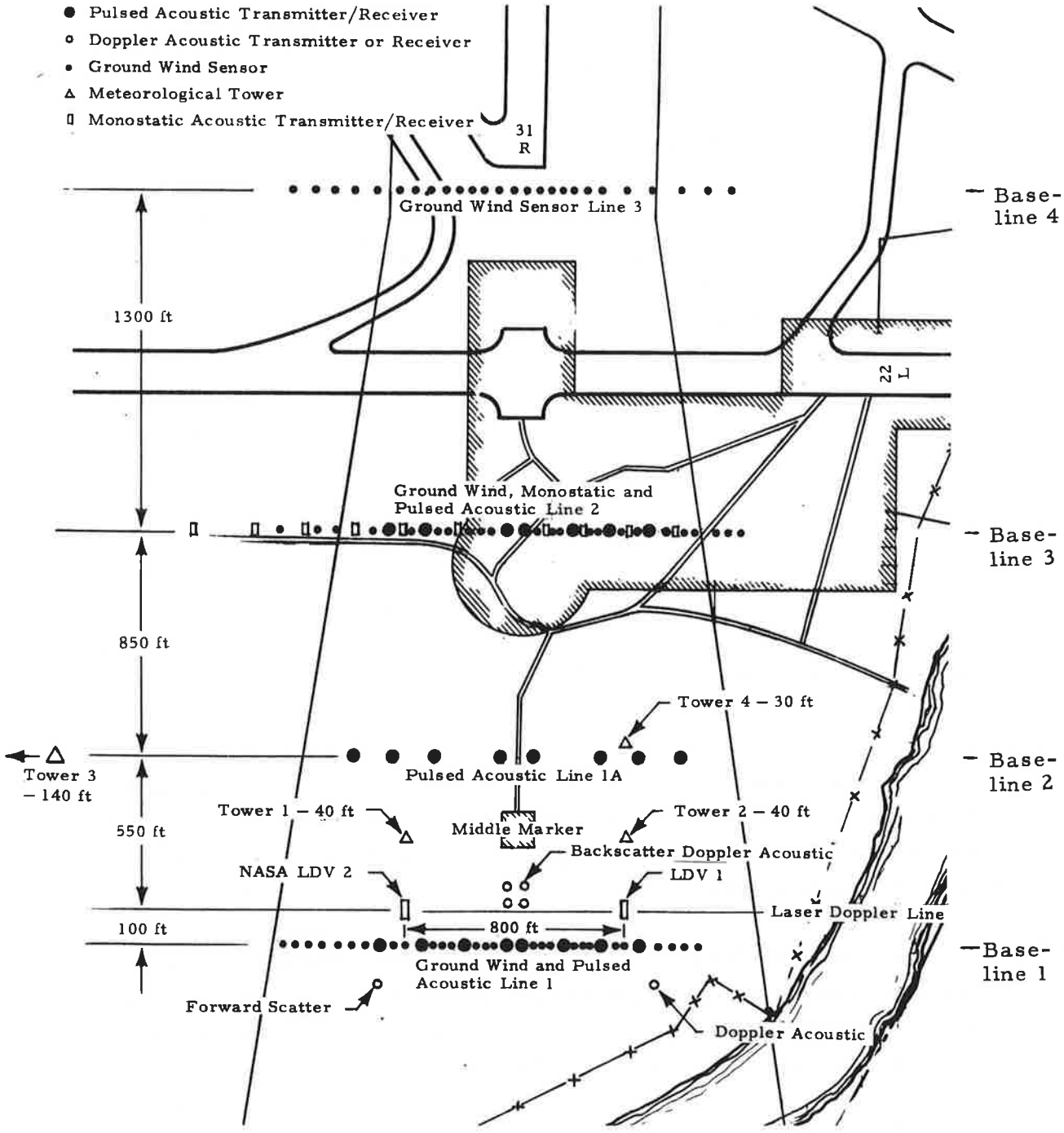


**Fig. 2-1 - Plan View of JFK Vortex Test Site Configuration**

The Doppler Acoustic Vortex Sensor System (DAVSS) is located as depicted in Fig. 2-1. This system is designed to provide vortex position in the plane defined by the sensors. Data from these sensors are processed via computer in the control instrumentation van and are displayed on-line. This sensor is configured to operate in either bistatic or monostatic configurations.

The Laser Doppler Vortex Sensing System (LDVSS) is located in two vans, each positioned 400 feet from the runway extended centerline in the vicinity of the runway 31R middle marker. These systems each operate independently in a backscatter (monostatic) mode. They monitor overlapping regions of space between sensor vans.

In addition to the vortex sensors, the site is equipped with three pressure sensor aircraft detectors designed to sequence the vortex sensor activations. A video camera is also provided to survey aircraft position within the flight corridor.

In order to allow correlation of observed vortex transport to local meteorological conditions, a number of meteorological measurements, including wind speed, temperature, barometric pressure and humidity, are recorded on the network of four meteorological towers depicted in Fig. 2-1. Towers 1 and 2 are 40 feet high, tower 3 is 140 feet high and tower 4 is 30 feet high. A summary of the meteorological tower instrumentation is given in Table 2-1.

## Table 2-1

## SUMMARY OF METEOROLOGICAL TOWER INSTRUMENTATION

METEOROLOGICAL TOWER 1 INSTRUMENTATION

| Level (ft) | Measurements | Instrument(s) |
|---|---|---|
| 20 | u, v, w wind velocity components | R.M. Young Model 27003 3-axis wind velocity sensor |
| 40 | u, v, w wind velocity components | R.M. Young Model 27003 3-axis wind velocity sensor. |
| 40 | Wind magnitude and direction | J-Tech Assoc. VR 300 |
| 40 | Wind magnitude and direction | MRI Model 1074-2 Wind magnitude and direction sensor. |

METEOROLOGICAL TOWER 2 INSTRUMENTATION

| Level (ft) | Measurements | Instrument(s) |
|---|---|---|
| 10 | Temperature<br>Relative Humidity | MRI Model 840-6 temperature and relative humidity sensor |
| 15 | Barometric pressure | MRI Model 751 pressure sensor |
| 20 | u,v,w wind velocity components | R.M. Young Model 27003 3-axis wind velocity sensor |
| 40 | u,v,w wind velocity components | R.M. Young Model 27003 3-axis wind velocity sensor |
| 40 | Wind magnitude and direction. | MRI Model 1074-2 wind speed and direction sensor. |
| | Temperature | MRI Model 840-1 Temperature sensor |
| | ΔT (10 to 40 ft)<br>Horizontal sigma | Performed in transmuter. MRI-1001 located in instrumentation van. |

METEOROLOGICAL TOWER 3 INSTRUMENTATION

| Level (ft) | Measurements | Instrument(s) |
|---|---|---|
| 10 | Temperature | Weather Measure Model T621-TP18X Temperature probe mounted in a Model ISG model aspirated radiation shield. |
| 25 | u,v,w wind velocity components | R.M. Young Model 27003 3-axis wind velocity sensor. |
| 50 | u,v,w wind velocity components. Temperature | R.M. Young Model 27003 sensor. Weather Measure Model T621-TP18X Temperature probe in a Model ISG shield |
| 100 | u,v,w wind velocity components | R.M. Young Model 27003 sensor. |
| 135 | u,v,w wind velocity components. | R.M. Young Model 27003 sensor |
| 140 | Wind magnitude and direction | Weather Measure Model W103/3L/A wind magnitude sensor, Model 101-2 wind dir. sensor |
| | Temperature | Model T621-TP18X Temp. sensor in ISG shield |
| | ΔT (10 to 50 ft)<br>ΔT (10 to 140 ft) | Performed in SC 603 interface unit located at base of tower. |

METEOROLOGICAL TOWER 4 INSTRUMENTATION

| Level (ft) | Measurements | Instrument(s) |
|---|---|---|
| 20 | u,v,w wind velocity components | R.M. Young Model 27003 3-axis wind velocity sensor |
| 40 | u,v,w wind velocity components | R.M. Young Model 27003 3-axis wind velocity sensor. |

# 3. COMPUTER PROCESSING OF WAKE VORTEX MEASUREMENTS

A computer program has been developed to analyze data taken during the wake vortex test program at JFK by TSC. The computer program analyzes groundwind sensor and meteorological data and computes a vortex track based on these data. In addition, a predicted track is computed utilizing the wake vortex transport predictive model described in Ref. 2, and both the groundwind and predictive vortex tracks are compared with tracks determined from other sensing and tracking systems.

A flow chart of the data analysis computer program is given in Fig. 3-1. The driver reads a tape containing the groundwind sensor and meteorological data recorded during a series of aircraft landings. The aircraft type and time of day are recorded for proper identification.

The Statistical Analysis (STAT) program processes the meteorological data to provide averages and variances for use in the Meteorological Analysis (MET) program. The STAT program also has options for performing a number of other operations on the groundwind and meteorological data to yield auto and cross correlations, and power and cross-spectral densities. A flow chart showing the various operations performed by the STAT program is given in Fig. 3-2.

The MET program uses the processed meteorological tower data to provide atmospheric characterization information. The MET program, among other things, computes wind speed and direction profiles, roughness lengths, friction velocities, potential temperature gradients and Richardson numbers. A flow chart showing the various meteorological parameters computed is given in Fig. 3-3.

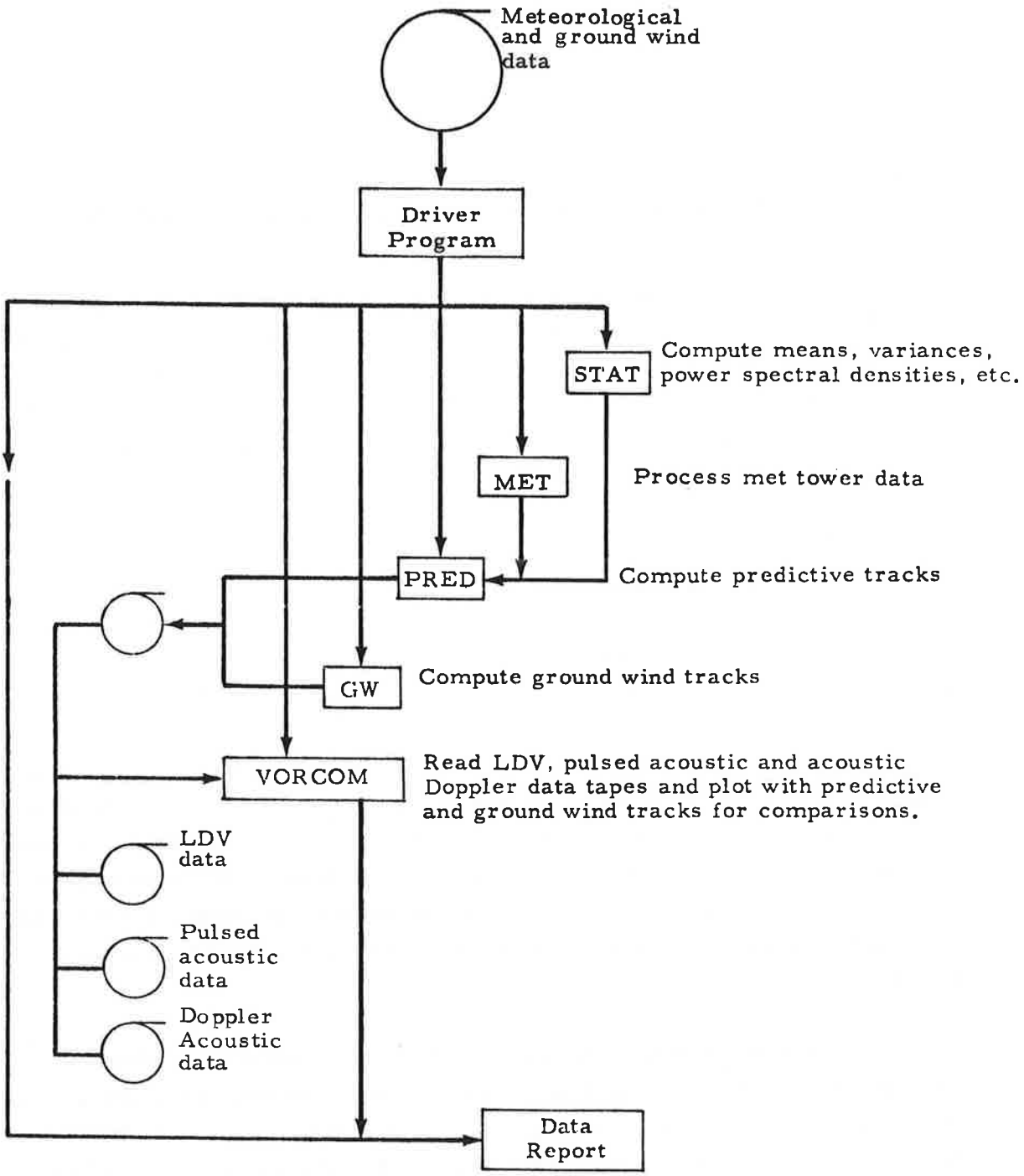


Fig. 3-1 - Flow Chart of Computer Program for Processing Aircraft Wake Vortex Test Data

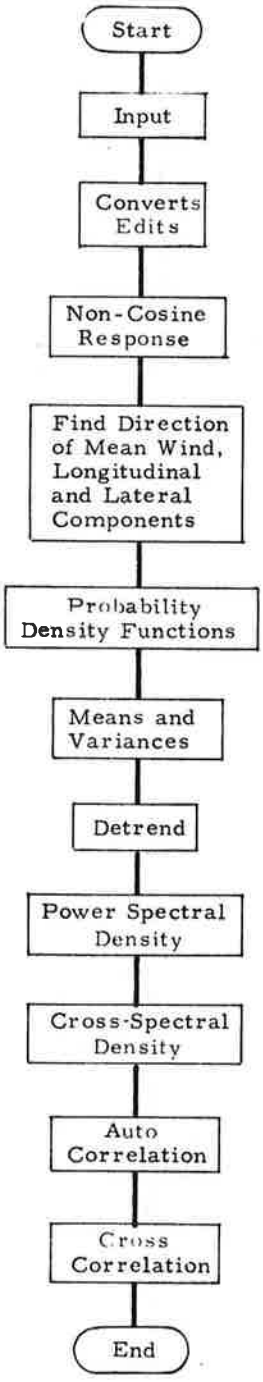


Fig. 3-2 - Statistical Analysis Computer Program Flow Chart

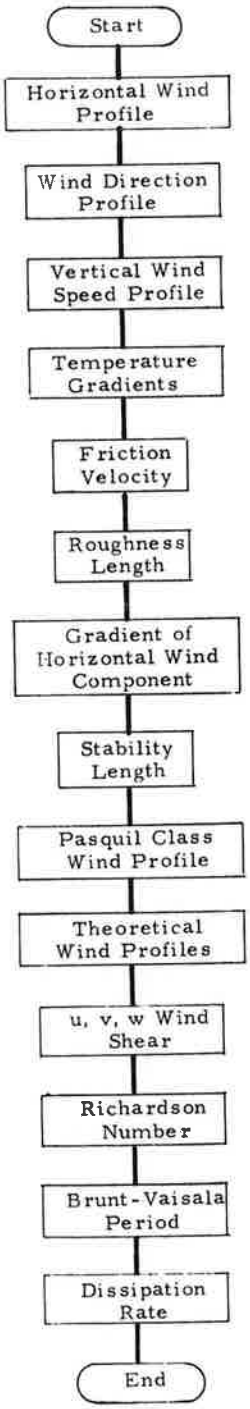


Fig. 3-3 - Meteorological Tower Data Analysis Computer Program Flow Chart

The Predictive Model (PRED) program is used to compute a predicted vortex track based on the analytical vortex transport model. The model utilizes initial vortex strengths and spacing based on aircraft type, and wind profile data computed in the MET program. The initial altitude at vortex formation is determined from an assumed aircraft landing trajectory. The predicted vortex track is stored on a magnetic tape for later use in comparing with tracks measured with the various wake vortex sensing and tracking systems.

The Ground Wind Tracker (GW) program developed at TSC (Ref. 5) analyzes the groundwind sensor data to compute the tracks of the aircraft wake vortices. Two algorithms are used in this determination. The first compares the measured wind speeds of all sensors at given times and selects the sensor locations where the vortex-induced wind speeds are highest. The vortices are then assumed to be located over these selected sensors. A plot is made on the line printer showing the location of the port and starboard vortices at various times. The second algorithm examines the measured wind speeds at each sensor location separately to determine the exact time at which a vortex passed over the sensor. The algorithm uses a cross correlation between a sinusoidal shaped "peak" passed over the data record to locate maximums and minimums in the measured wind speed. This method of location of the maximum and minimum points smooths out irregularities in the curve due to turbulence and other noise in the data. The vortex tracks determined from this algorithm are stored on tape for later comparison with tracks determined from other vortex sensing and tracking systems.

The Vortex Comparison (VORCOM) program reads vortex track data stored on tapes which have been computed by the PRED and GW programs, and which have been measured by the other vortex sensing and tracking systems. After reading in the recorded data, plots are made comparing simultaneously obtained vortex tracks.

VORCOM consists of basically two major routines, DECODE and VORPLT. The main function of DECODE is to read in all of the sensor data and write them on a disk file in a random fashion. This routine calls one routine to read each tape. The routine is written in a manner which will allow other tape reading routines to be added at a future date Presently groundwind, predictive, pulsed acoustic, laser Doppler and bistatic Doppler acoustic data can be read and stored on a disk file. Detailed flow charts of all major routines are shown in Appendix A.

Routine VORPLT calls other routines to retrieve data from the disk as requested and plot these data. There will be three plots for each baseline: altitude versus displacement from runway extended centerline, altitude versus time after aircraft passage, and time after aircraft passage versus displacement from runway extended centerline Sample plots are shown in Figs. 3-4a through 3-6c for one flyby. This sample data consists of actual wake vortex measurements conducted with different types of sensors on different days Since no simultaneous measurements were available, the superimposed data are shown to demonstrate the capability of the program rather than to present consistent vortex trends. Both predictive and groundwind data are shown with data from the laser Doppler, pulsed acoustic and Doppler acoustic bistatic sensor overlaid. Lines of constant time between predictive tracks and the sensor data are shown on the first plot for each baseline (see Fig 3-4). As additional sensor tapes are received, software will be added to read and plot them. Table 3-1 defines the symbols utilized in the plots

Table 3-1

SYMBOL CODE USED IN VORTEX
TRACK COMPARISON

| System | Port | Starboard |
|---|---|---|
| Predictive Tracks | O | * |
| Ground Wind Tracks | P | S |
| LDV Van 1 | 3 | 2 |
| LDV Van 2 | 6 | 5 |
| Bistatic Acoustic-Doppler | Y | X |
| Pulsed Acoustic | L | R |

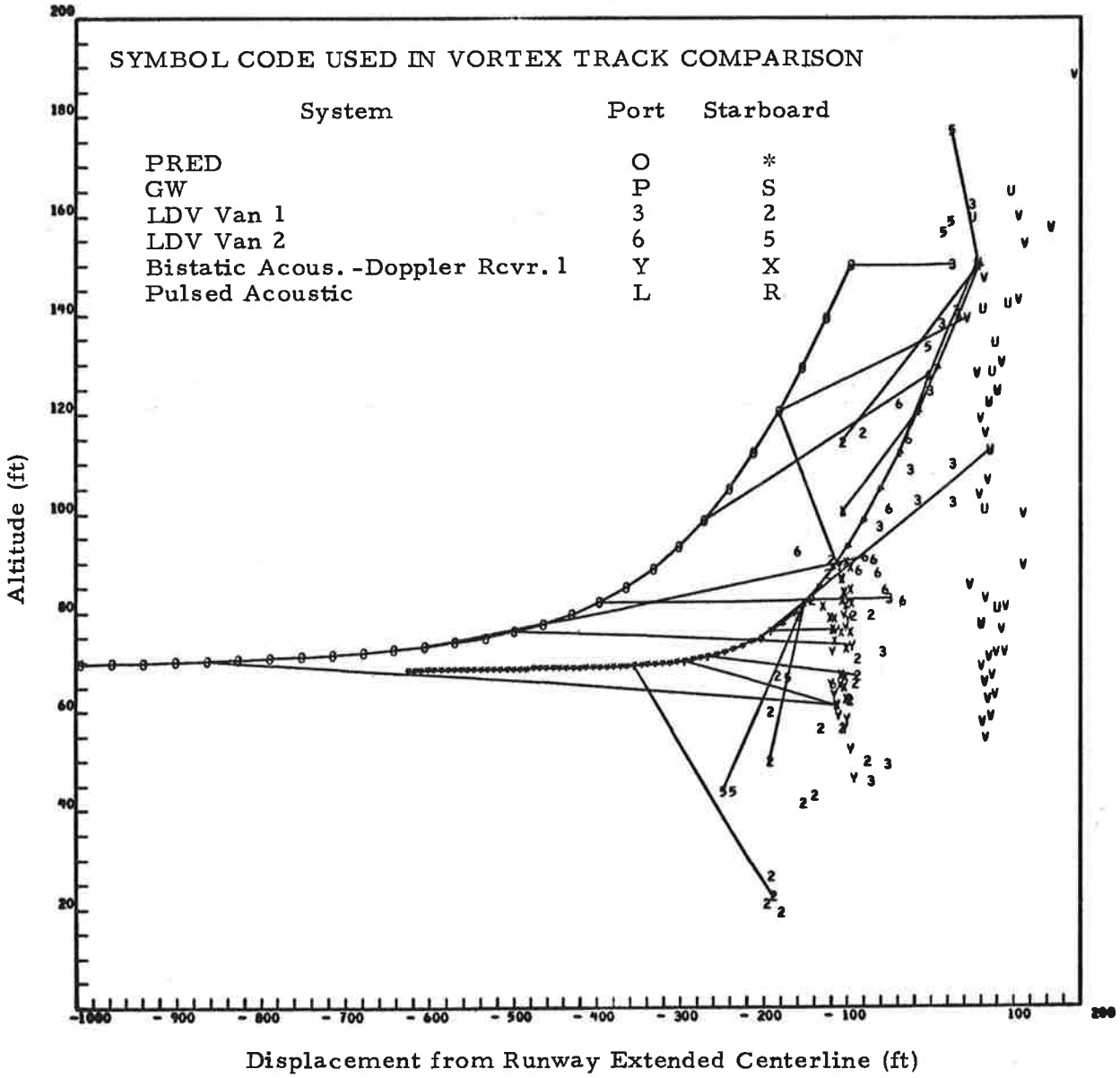


Fig. 3-4a - Comparison of Predicted Vortex Tracks with Sensor Data for Baseline 1

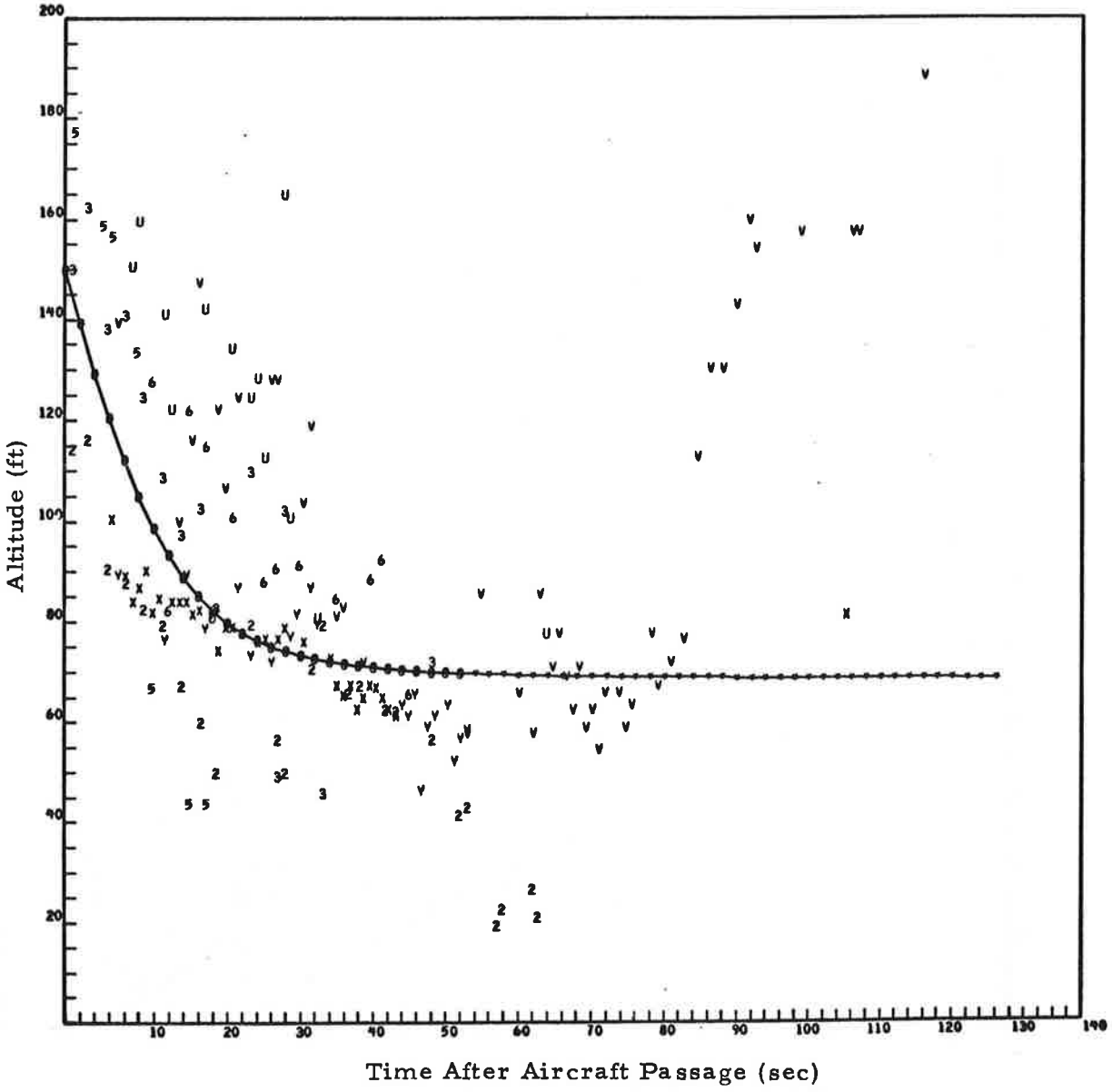


Fig. 3-4b - Comparison of Predicted Vortex Tracks with Sensor Data for Baseline 1

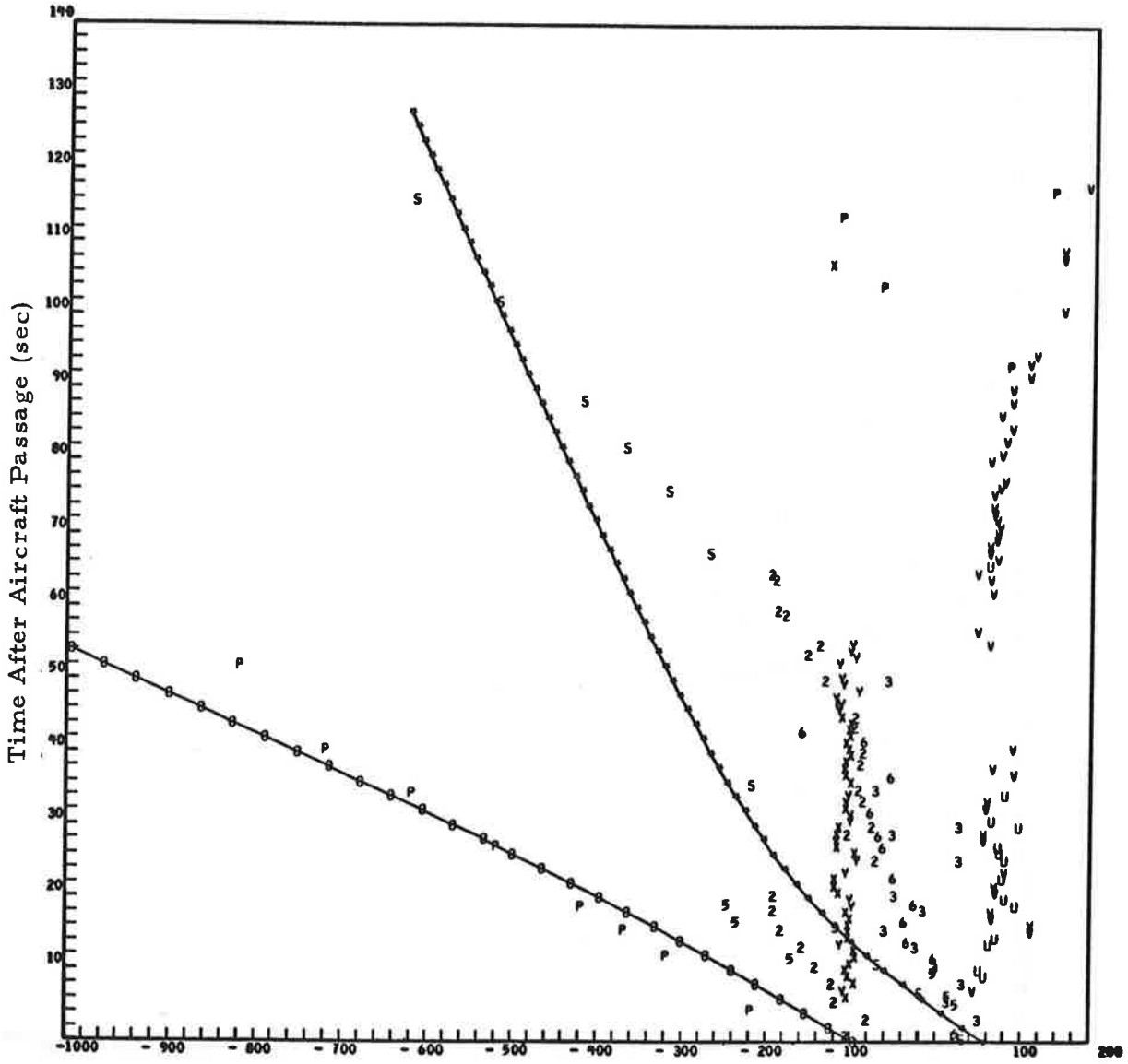


Fig. 3-4c - Comparison of Predicted Vortex Tracks with Sensor Data for Baseline 1

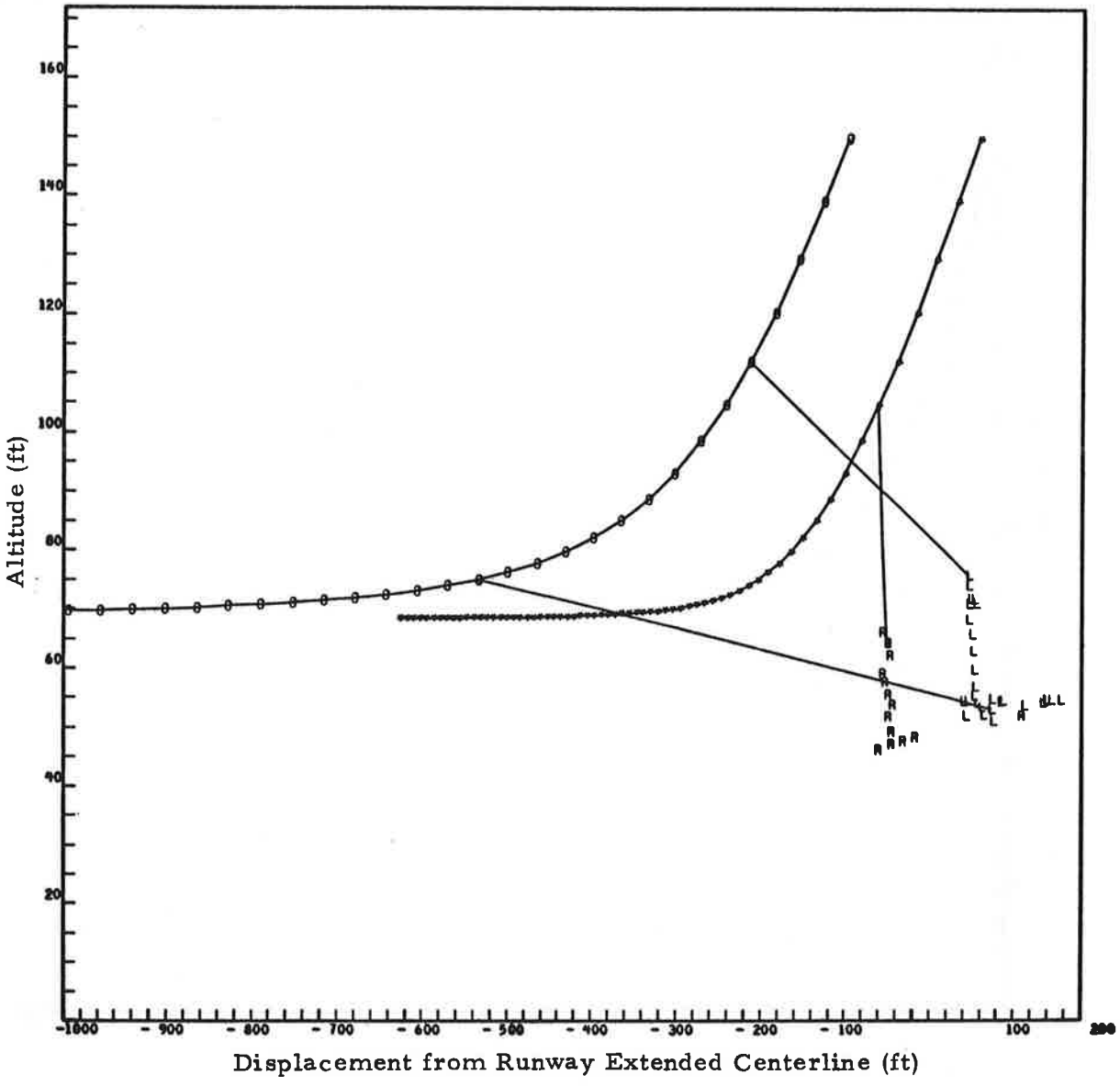


Fig. 3-5a - Comparison of Predicted Vortex Tracks with Sensor Data for Baseline 2

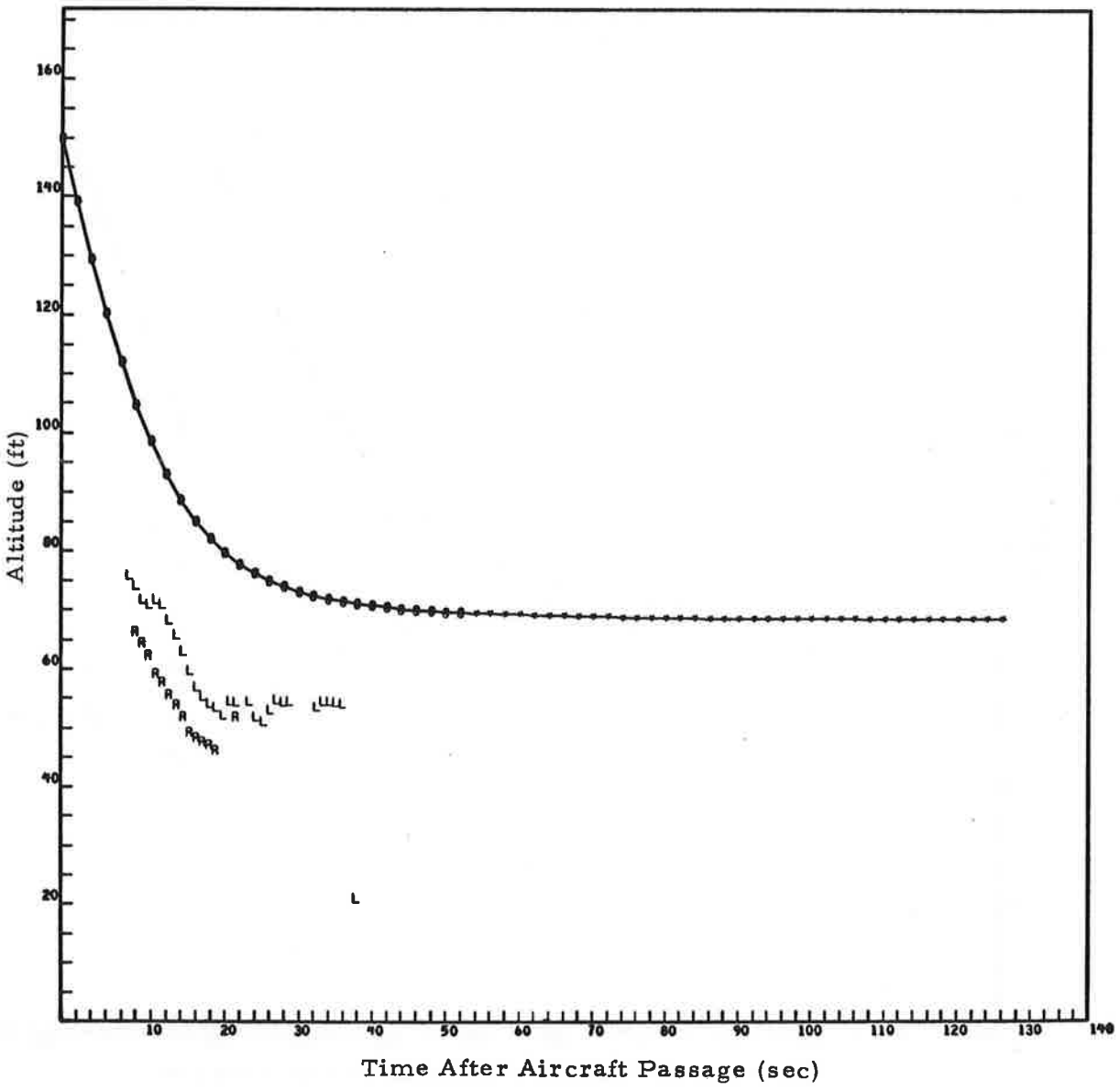


Fig. 3-5b - Comparison of Predicted Vortex Tracks with Sensor Data for Baseline 2

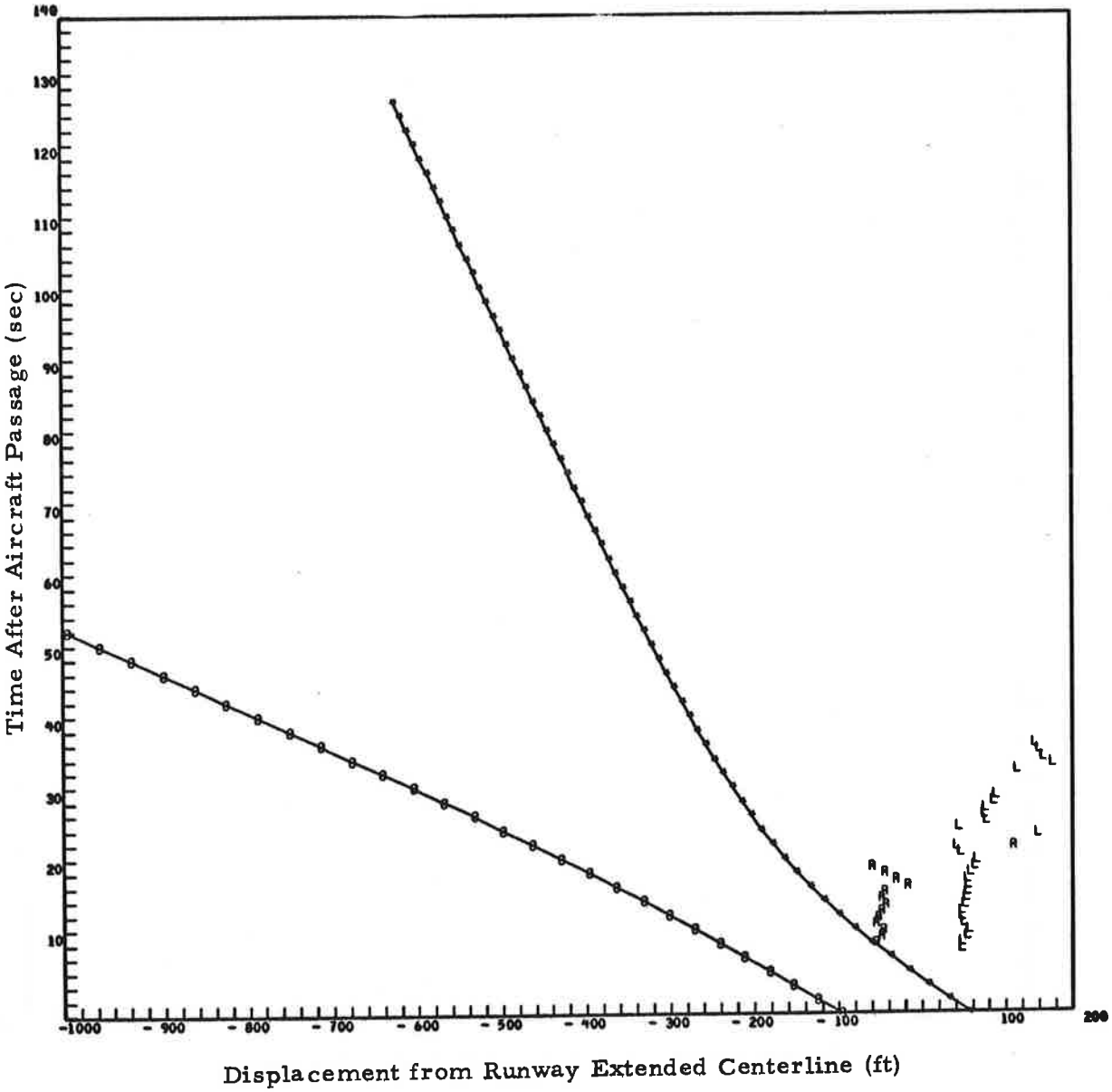


Fig. 3-5c - Comparison of Predicted Vortex Tracks with Sensor Data for Baseline 2

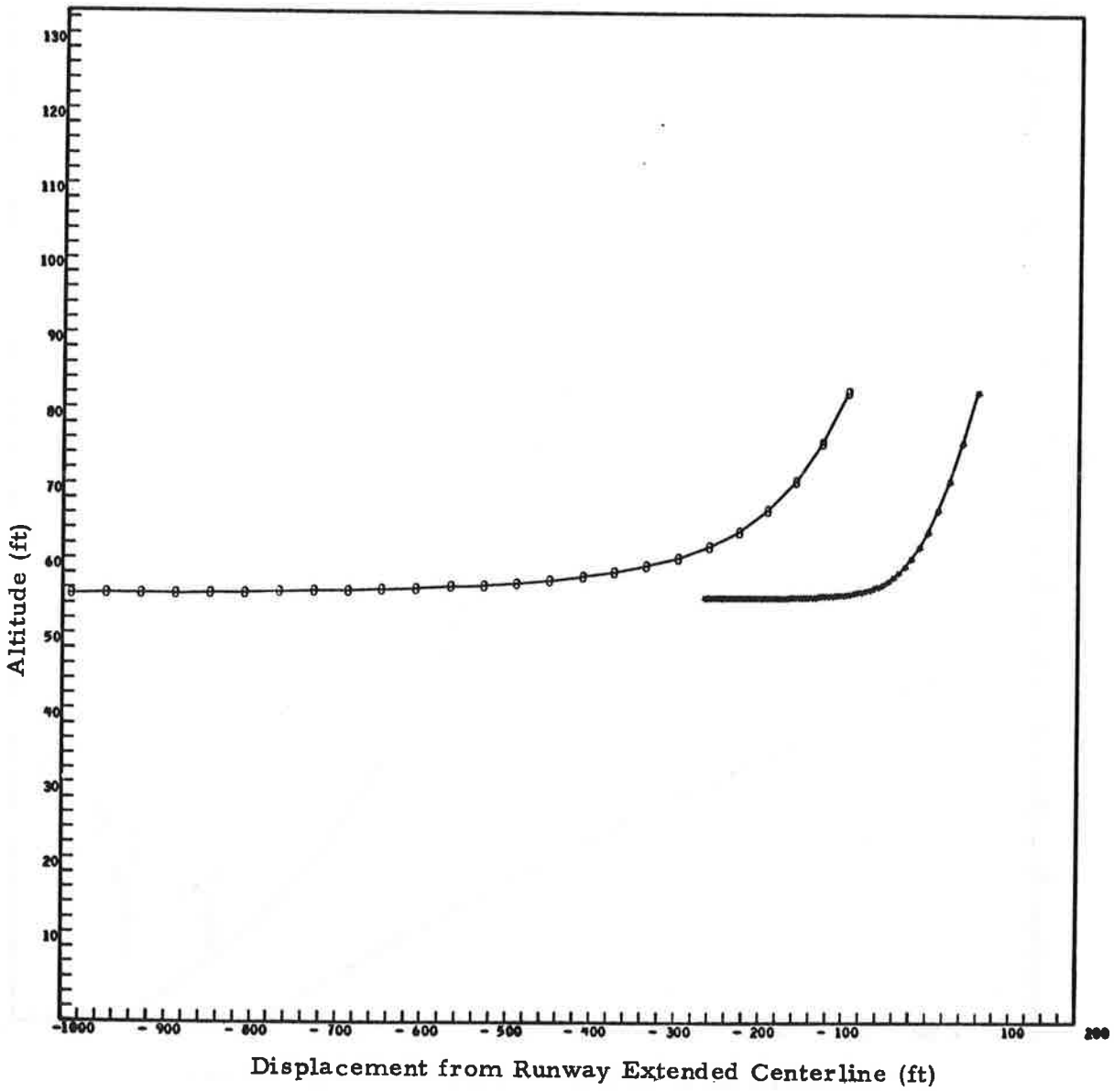


Fig. 3-6a - Comparison of Predicted Vortex Tracks with Sensor Data for Baseline 3 (No data available)

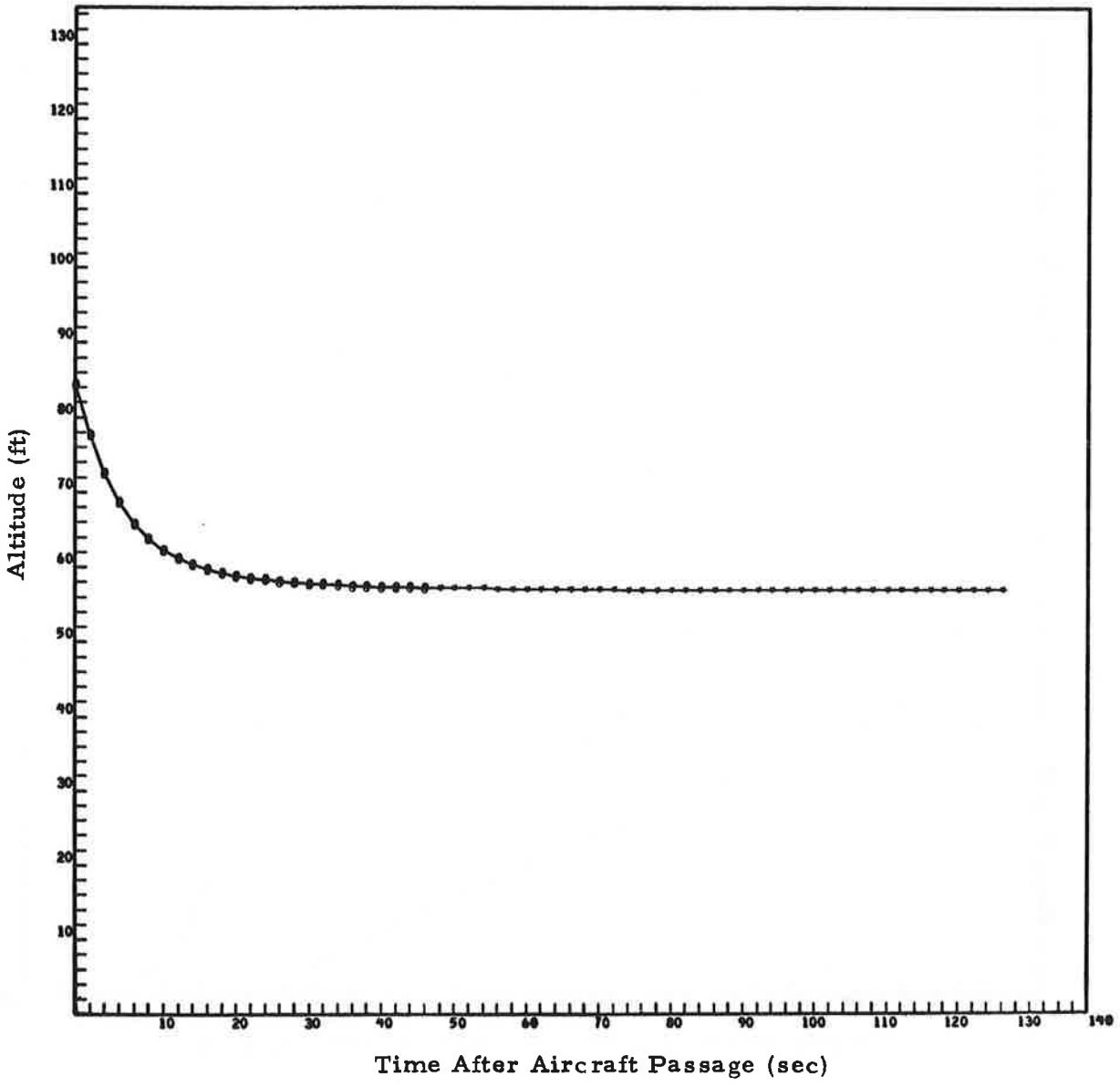


Fig. 3-6b - Comparison of Predicted Vortex Tracks with Sensor Data for Baseline 3 (No data available)

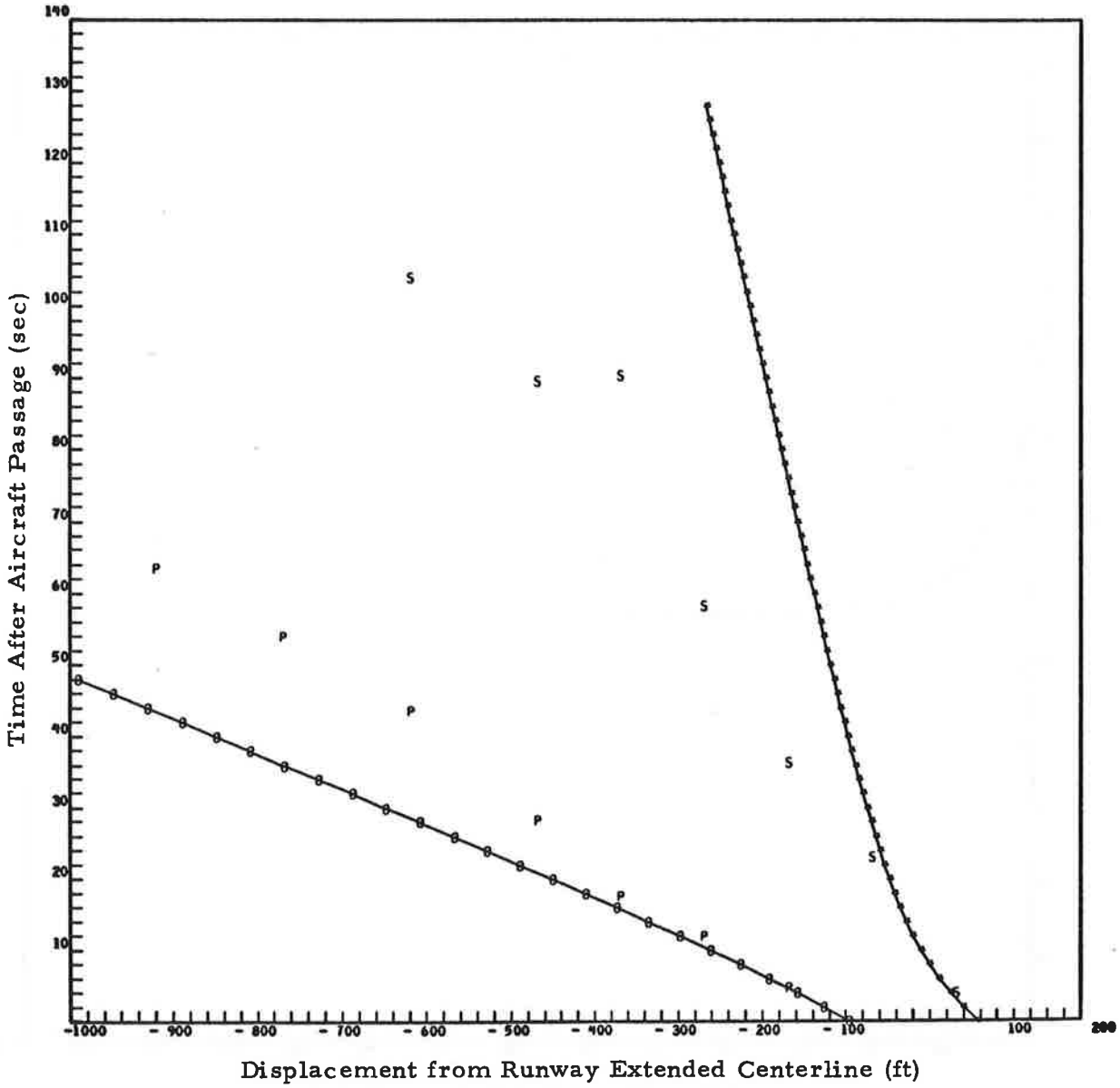


Fig. 3-6c - Comparison of Predicted Vortex Tracks with Sensor Data for Baseline 3

# 4. ANALYSIS OF GROUNDWIND SENSOR MEASUREMENTS

The groundwind sensor data taken at JFK have been analyzed using a number of statistical processing techniques to explore possible means for recognizing wake vortex signatures and determining the vortex locations. The data analyzed in this study were taken at JFK on 10 May 1974 and recorded on DOT-TSC tape No. K122 at a sampling rate of 7.5 data points per second. At that time, only meteorological tower 1 and groundwind sensor lines 1 and 2 were operational. Shown in Figs. 4-1 through 4-20 are plots of the groundwind and meteorological tower data filtered by a moving average over 1, 3, 5, 7 and 9 second intervals for the case of a Boeing 747 aircraft landing at a time designated as 0/02/16 (2 minutes and 16 seconds from the beginning of the tape). Sensors 201 through 226 refer to groundwind sensors on sensor line 1 starting at 800 feet on the port side to 900 feet on the starboard side of the runway. Sensors 101 through 118 refer to groundwind sensors on sensor line 2 starting at 1050 feet on the port side to 1050 feet on the starboard side. Sensor 119 is an unassigned channel actually recording a duplicate of sensor 118. Sensor 120 records temperature data on the meteorological tower. Sensors 121, 222 and 223 and sensors 124, 125 and 126 record three-component wind velocities at the 20-foot and 50-foot elevations, respectively, on the meteorological tower. A list of the MET sensors is given in Appendix E in terms of the notation used in Fig. 4-1 through 4-20.

Considerable smoothing of the data is noted by averaging over the longer time intervals. The 5-second interval is seen to be very effective in removing random fluctuations from the data and allowing the characteristic vortex signature to be easily recognized. Additional data plots are shown in Figs. 4-21 through 4-44 for the cases of a Boeing 707 landing at 0/10/38, a Boeing 747 at 0/12/26 and a Boeing 707 at 0/18/30. The plots show 1- and 5-second averaged data. These cases also show effective smoothing of the data using a 5-second moving average.

The various statistical analysis techniques performed by the STAT program were applied to both predicted and actual groundwind sensor measurements. The predicted results were obtained using the PRED program with a wind profile obtained from the meteorological tower data. The predicted groundwind measurements were examined because they were free of contamination by random wind fluctuations and, therefore, permitted an unobstructed view of the effect of the various statistical analysis techniques on the pure vortex signature. Figures 4-45 through 4-51 show predicted results for sensors 108 and 109 for the case of a Boeing 747 landing at 0/2/16. These sensors are located 250 and 200 feet, respectively, to the port side of the extended runway centerline. Since the vortices were traveling in the direction of the port side, the comparisons between the two sensors were made in that direction (109 to 108). The sensors were labeled in these plots, therefore,as signal one for sensor 109 and signal two for sensor 108. The predicted groundwind signatures for the two sensors are shown in Fig. 4-45 with the probability density functions for wind speed variations given in Fig. 4-46. A normal (Gaussian) distribution is shown for comparison. The cumulative (integrated) distributions are shown in 4-47, again compared with the normal distribution. Both the probability densities and cumulative distributions are seen to be similar to those of the normal distributions, even though there are no random fluctuations in the data.

The power spectral densities of the two theoretical groundwind signatures are given in Fig. 4-48. The intensity is seen to increase as the frequency decreases toward the fundamental frequency corresponding to the 128-second duration of the curves. There does not appear to be any pronounced characteristic frequency representative of the vortex signature. The cross-spectral density phase and magnitude for the correlation between the two curves are shown in Fig. 4-49. Although the phase plot is semi-log, the phase can be seen to be nearly a linear function of frequency for the first five multiples of the fundamental, with the average ratio of phase angle to frequency being 1856 degree-second. The cross spectral density provides some indication of signal transmission time t between the two sensors through the relation:

$$t = \phi/2\pi f \qquad (4.1)$$

where $\phi$ is phase angle and f is frequency. Based on this relation and the average ratio of phase angle to frequency of 1856 degree-second, an average transmission time of 5.2 seconds is computed. For the 50-foot separation distance between the two sensors, this corresponds to a signal transmission velocity of about 10 feet/second. This agrees very well with the 12 foot/second average cross wind velocity at the altitude of the vortices as they passed over the sensors (see Figs. 5-2 and 5-3 at the 40-foot elevations). Since the two vortices are traveling in opposite directions with respect to the wind, the average speed of the two vortices is the same as the cross wind speed. The magnitude of the cross-spectral density increases as the frequency decreases toward the fundamental in the same manner as the power spectral densities of the separate curves. No pronounced characteristic frequency for the cross spectral density is noted.

The autocorrelation for the two theoretical curves is shown in Fig. 4-50. The computation procedure provides only the absolute values, hence, the apparent discontinuities in the first derivative. These curves give some indication of an average period or wave length for the shape of the groundwind signatures. Referring to the upper figure, the approximately 15-second time interval involved in the first decrease of the autocorrelation to zero corresponds roughly to the time between the minimum and maximum in the upper curve in Fig. 4-45. The minimum and maximum points correspond, respectively, to the times at which the downwind and upwind vortices pass over the sensor.

The cross-correlation between the two theoretical groundwind signatures is given in Fig. 4-51. The pronounced peak at a lag time of about 5 seconds corresponds to the signal transmission time discussed earlier in connection with the cross-spectral density.

Shown in Figs. 4-52 through 4-58 are statistically processed data for actual groundwind sensor measurements corresponding to the predicted data in Figs. 4-45 through 4-51. The measured groundwind signatures for sensors 108 and 109 are given in Fig. 4-52 and averaged over 1-second intervals. The

same general shape of the groundwind signature as predicted in Fig. 4-45 is easily recognized in the measured data, although the minimum and maximum points differ by as much as 10 seconds. The probability density functions for the two curves are given in Fig. 4-53, and the cumulative probability densities are given in Fig. 4-54. The power spectral densities are given in Fig. 4-55, and the cross-spectral densities are given in 4-56. The autocorrelations are given in Fig. 4-57, and the cross correlation is given in Fig. 4-58.

In general, the same comments that were made concerning the predicted results are applicable to the measured results. Unfortunately, the linearity in the phase to frequency relationships in the cross-spectral density (Fig. 4-56) appears to be lost in the measured results. Taking the first two points on the phase-frequency plot, an average ratio of phase to frequency of 7296 degree-second is found. From Eq. (4.1), this corresponds to a signal transmission time of about 22 seconds. This is very close to the observed time between the two maximums in Fig. 4-52 and to the lag time at maximum cross correlation in Fig. 4-58. In this case, the upwind vortex is drifting down wind at a slower speed than was predicted, and the peak in the groundwind signature caused by the upwind vortex is broadened and forms a more prominent part of the overall signature than the downwind vortex. Hence, the cross correlation is more strongly influenced by the upwind vortex than the downwind vortex.

Figures 4-59 through 4-68 show some comparisons between predicted and actual groundwind sensor data for the Boeing 747 landing at 0/2/16. Figures 4-59 through 4-64 present comparisons for sensors located on the port side of sensor line one at distances 400, 300 and 200 feet from the runway centerline. Figures 4-65 through 4-68 show comparisons for sensors on the port side of sensor line two at distances of 450 and 250 feet. Each comparison has two figures with the first showing the experimental and theoretical signatures and the second showing a cross correlation between the two signatures. High values in cross correlation at zero lag time indicate good agreement between the two curves. High values at some lag time indicate similarity in shape, but a time difference corresponding to the lag

time. In Fig. 4-59, there appears to be a negative lag time of about 10 seconds between the dips corresponding to passage of the downwind vortex over the sensor. This apparently shows up as a peak in the cross-correlation curve in Fig. 4-60 at the positive lag time of about 120 sec (negative $\tau$ corresponds to positive $128-\tau$). The large peak at 80 seconds is actually negative (only absolute values are computed) and probably corresponds to the anti-correlation between the dip in the experimental curve and the maximum in the theoretical. Figure 4-61 shows overall good agreement between the experimental and theoretical curves, and this is reflected in Fig. 4-62 as a maximum cross correlation at zero lag time. The large negative peak at about 70 seconds corresponds to the anti-correlation between the minimum in the experimental curve and the maximum in the theoretical curve. Similar observations can be made for the results in Figs. 4-63 through 4-68.

These statistical analysis results show some interesting effects which could conceivably be used in identifying and locating aircraft vortices. The moving average results indicate effective smoothing of data by applying a 5-second moving average. Smoothing the data to remove random wind fluctuations will permit more accurate identification of the vortex signature and easier discrimination of the location of the maximum and minimum points corresponding to the passage of the two vortices over the sensor. Of the other statistical processing techniques, some were shown to reveal certain characteristics of the vortex signature, but no positive improvements over the existing TSC algorithms were found.

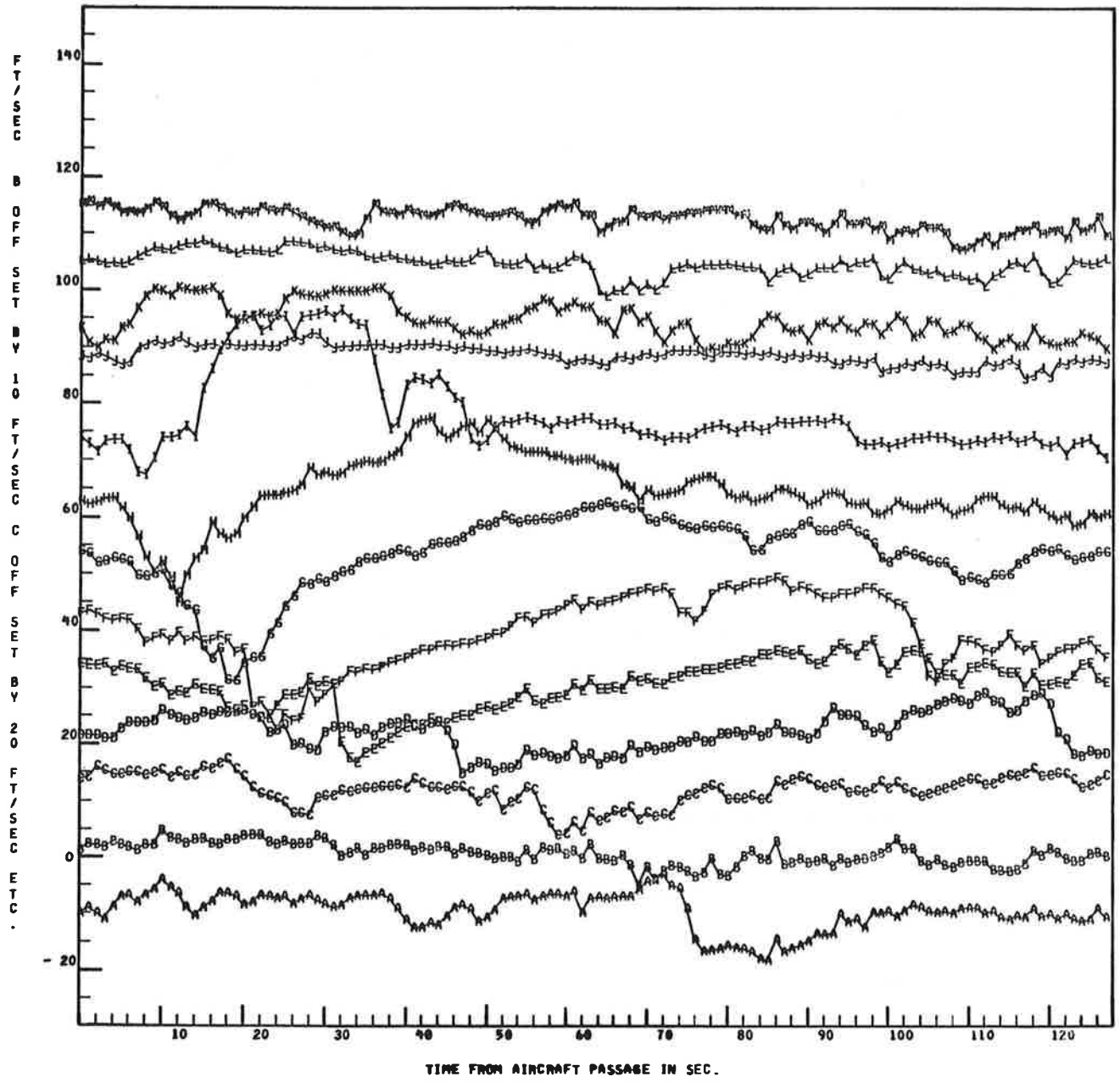


Fig.4-1 - Groundwind Sensor Data Averaged over 1-sec Intervals (Sensors 101-113)

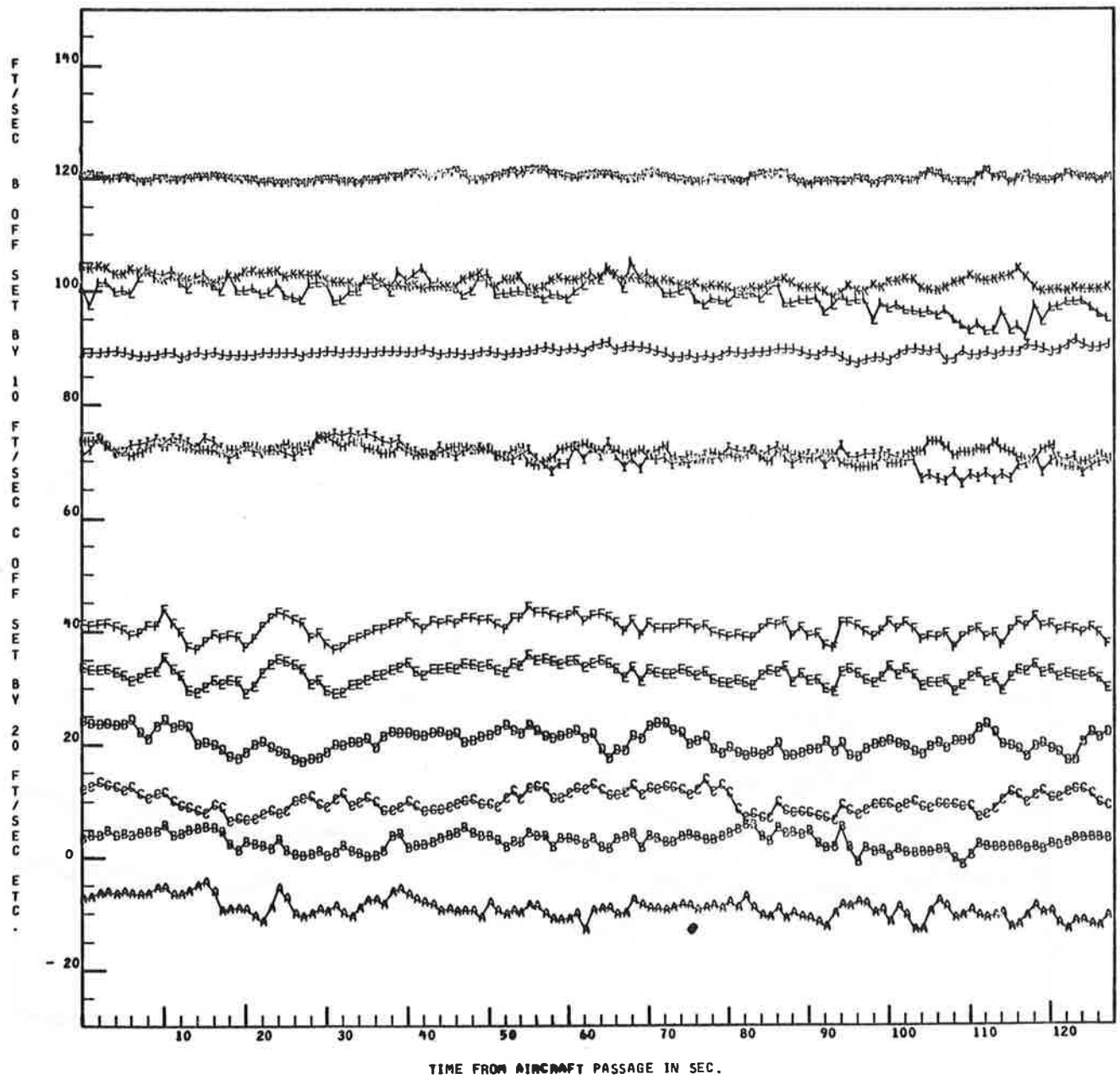


Fig.4-2 - Groundwind Sensor Data Averaged over 1-sec Intervals (Sensors 114-126)

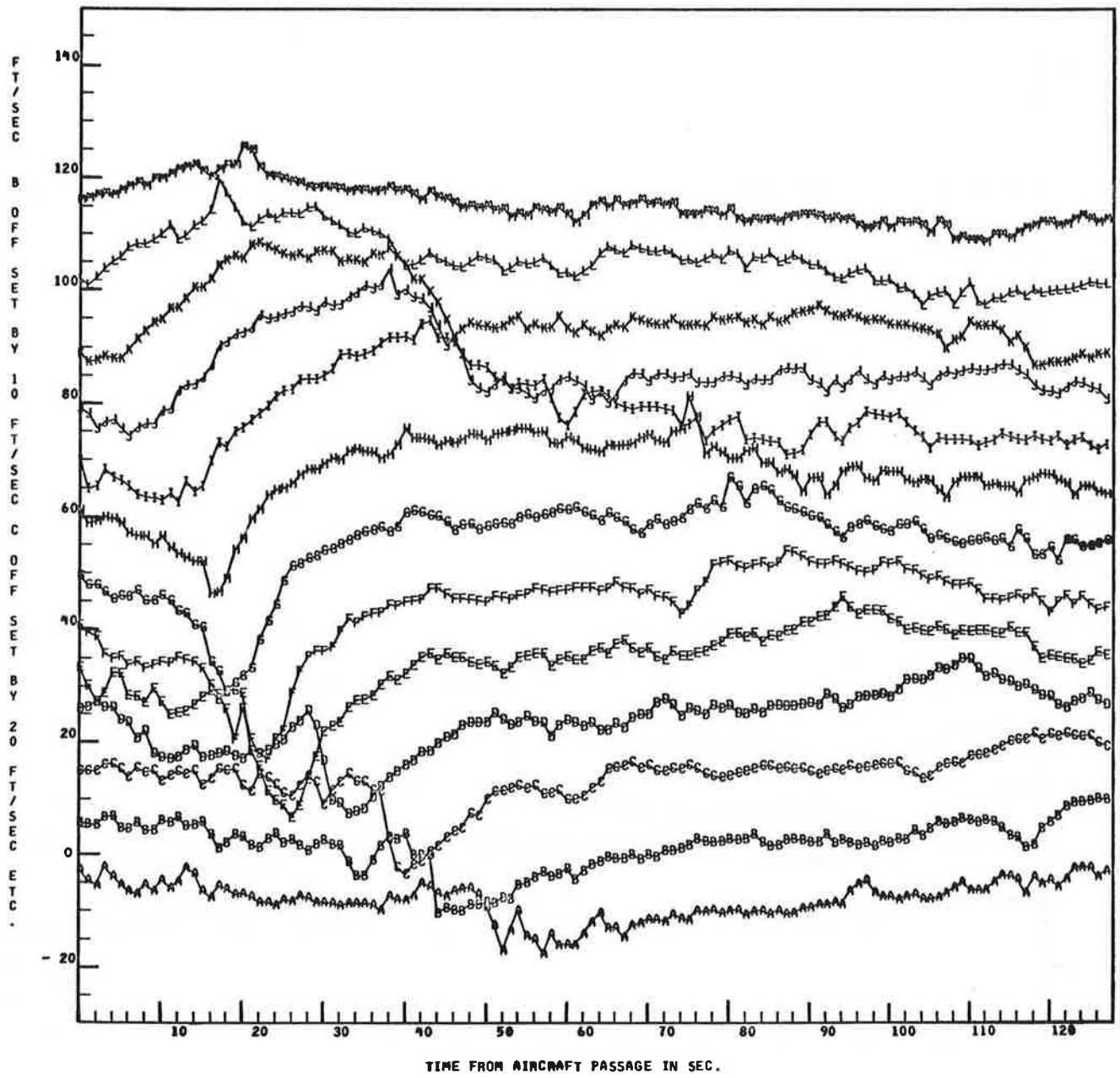


Fig. 4-3 - Groundwind Sensor Data Averaged over 1-sec Intervals (Sensors 201-213)

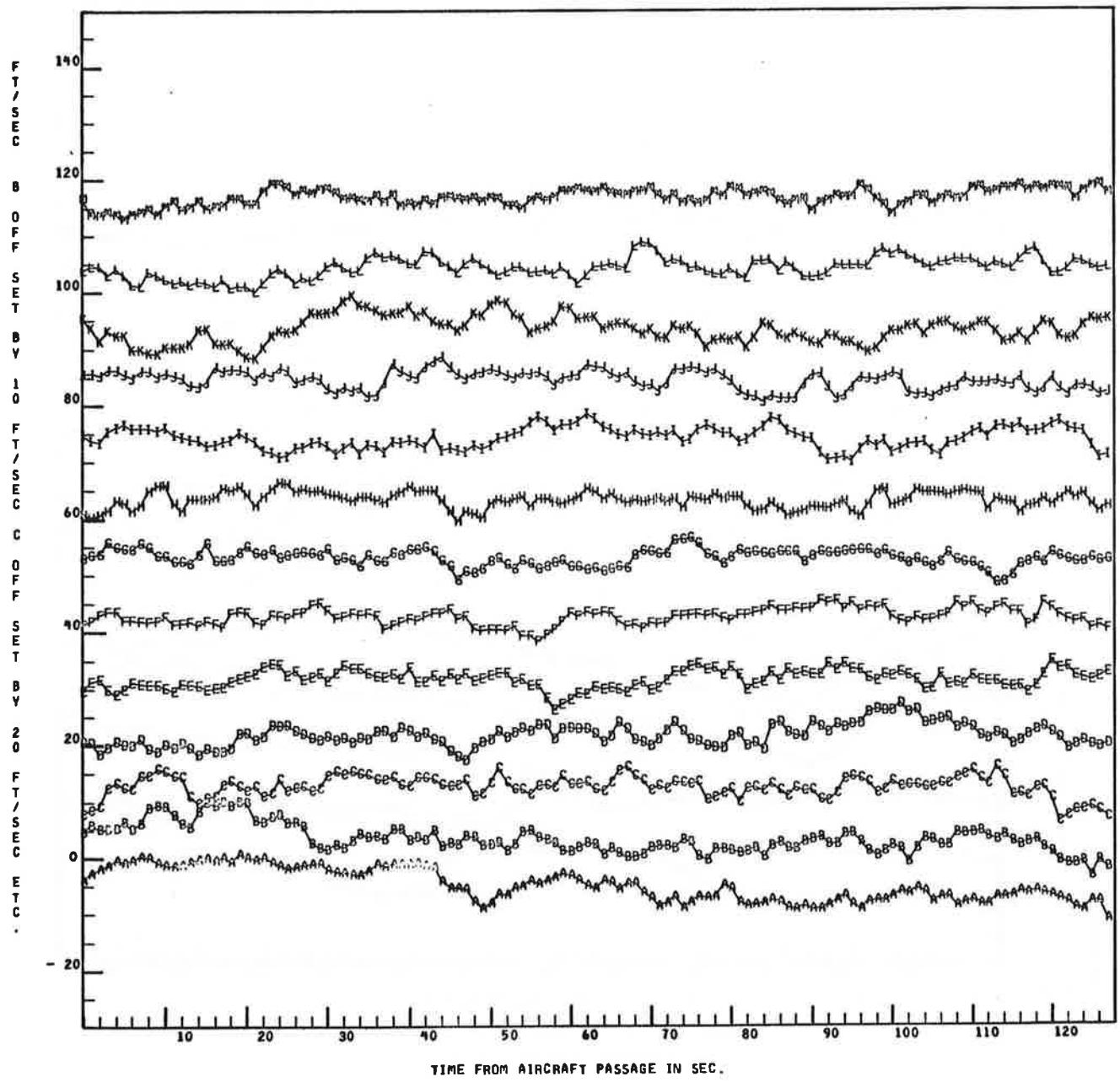


Fig.4-4 - Groundwind Sensor Data Averaged over 1-sec Intervals (Sensors 214-226)

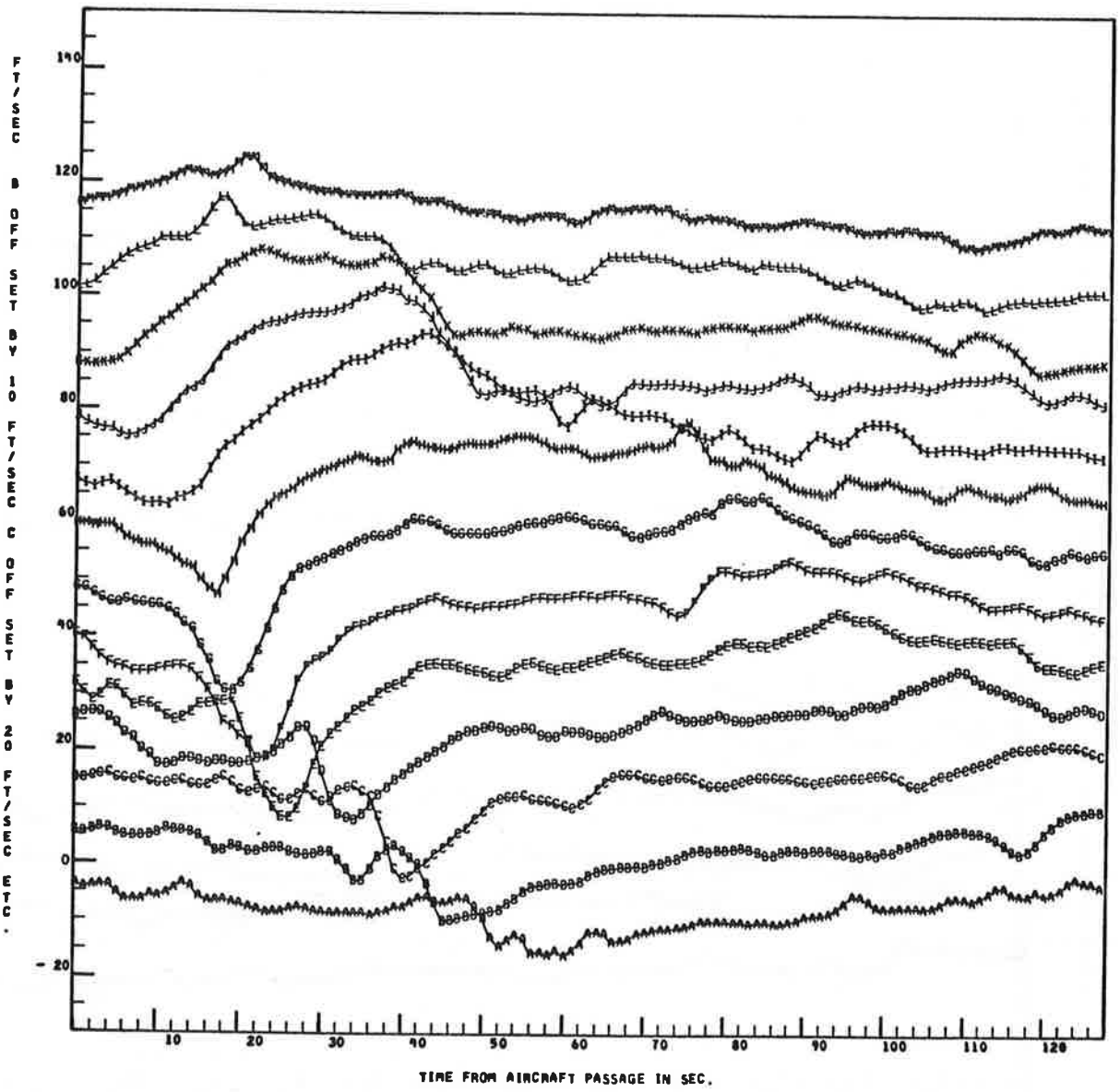


Fig.4-7 - Groundwind Sensor Data Averaged over 3-sec Intervals (Sensors 201-213)

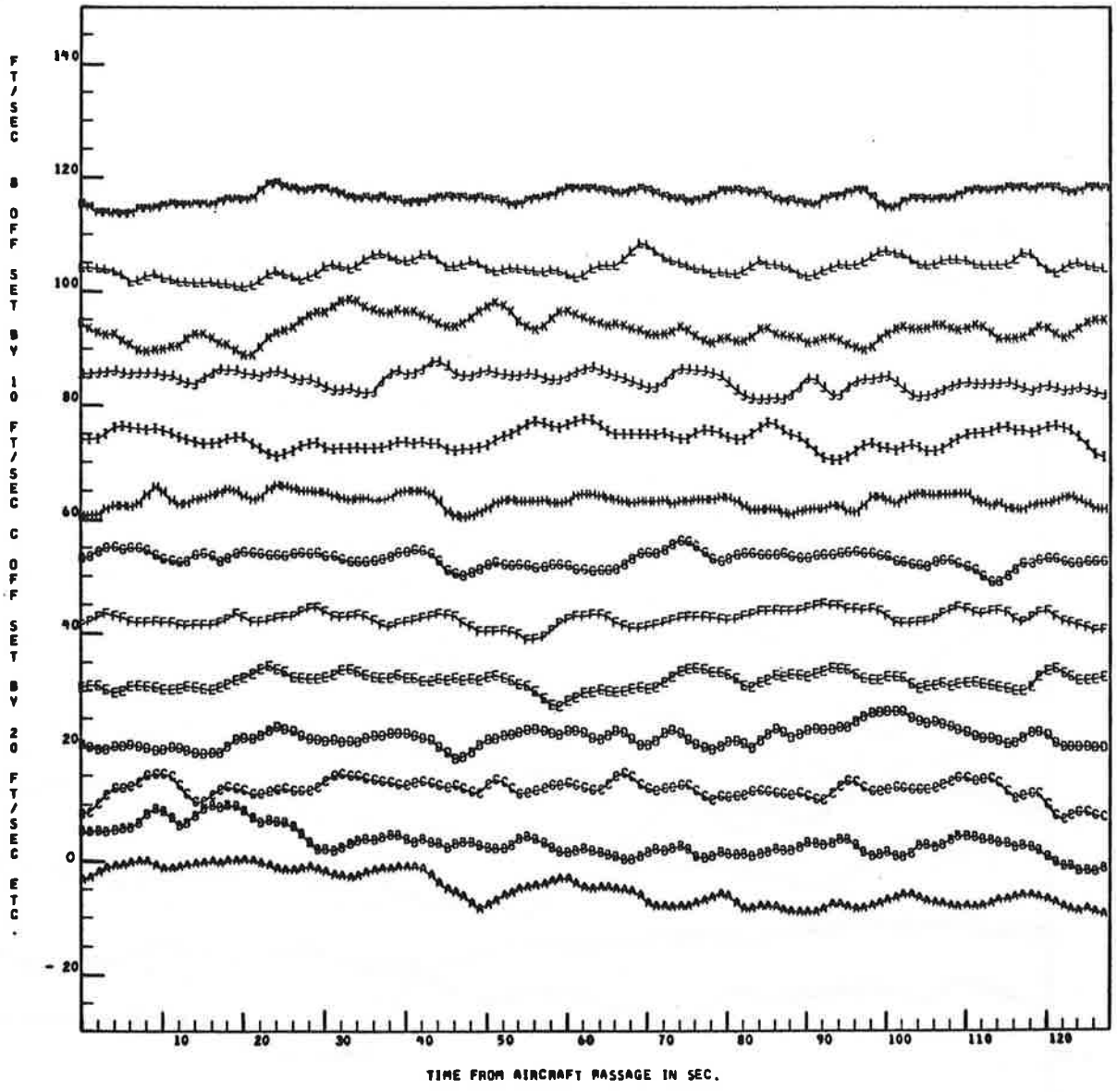


Fig.4-8 - Groundwind Sensor Data Averaged over 3-sec Intervals (Sensors 214-226)

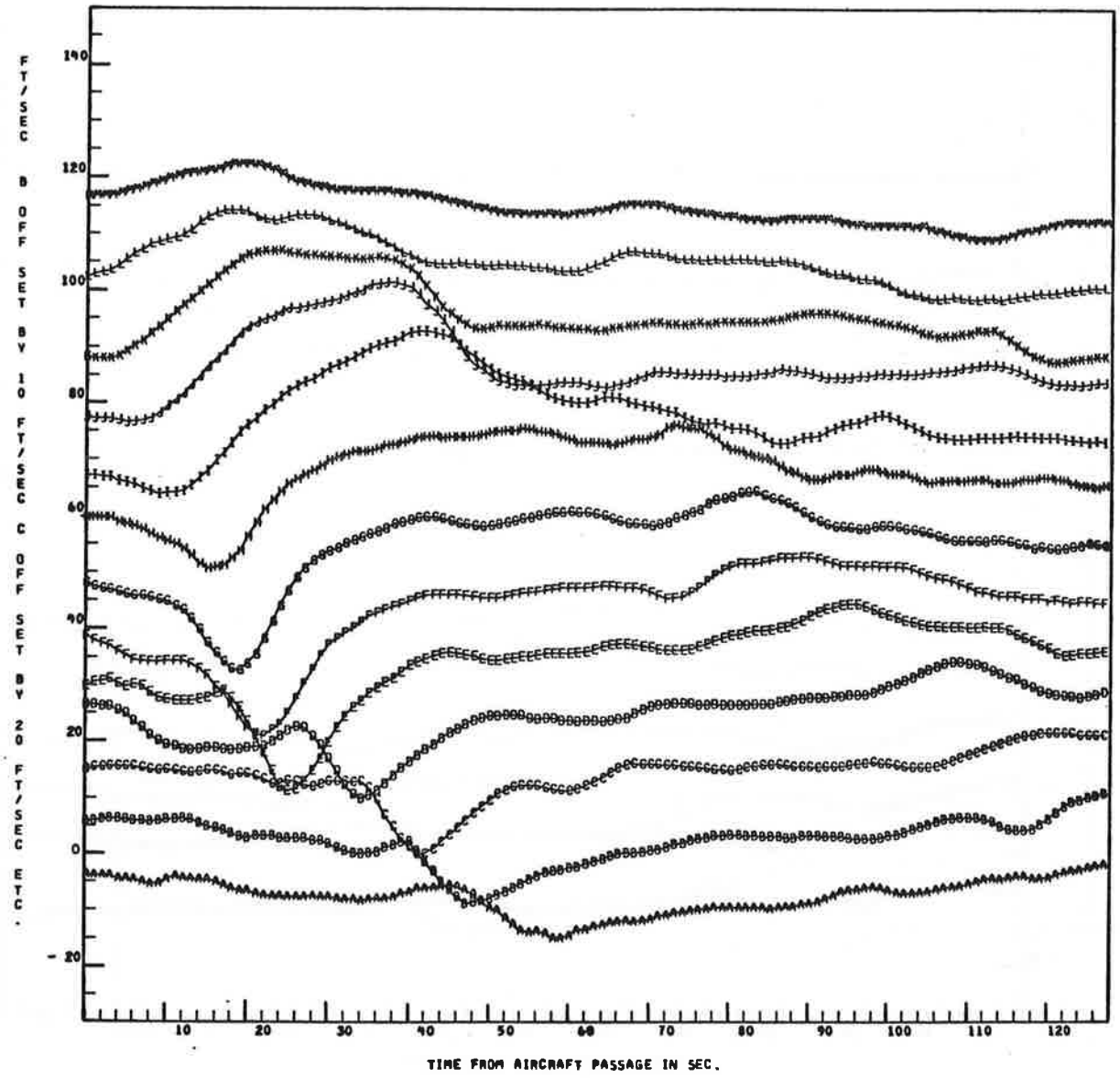


Fig.4-15 - Groundwind Sensor Data Averaged over 7-sec Intervals (Sensors 201-213)

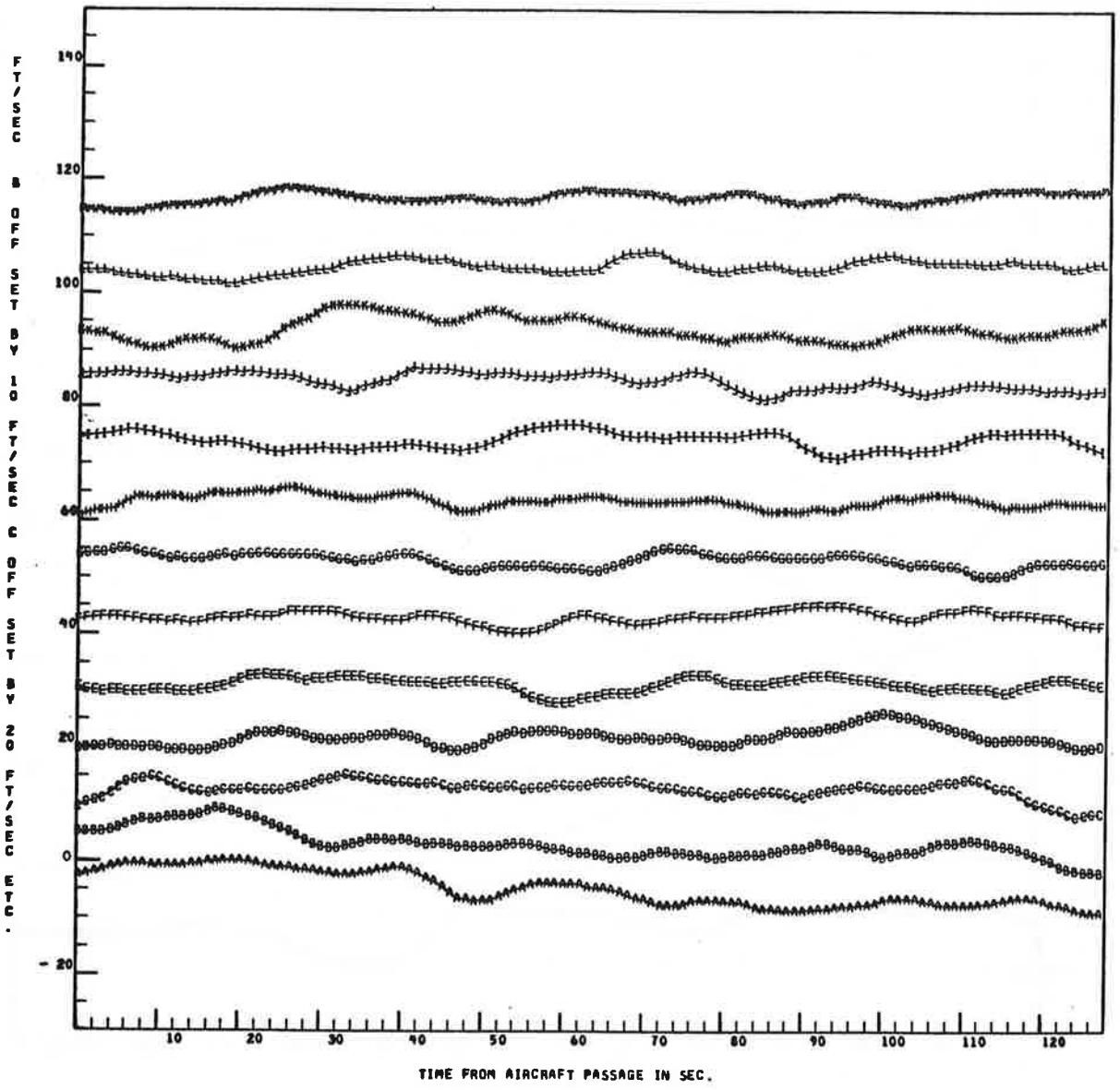


Fig. 4-16 - Groundwind Sensor Data Averaged over 7-sec Intervals (Sensors 214-226)

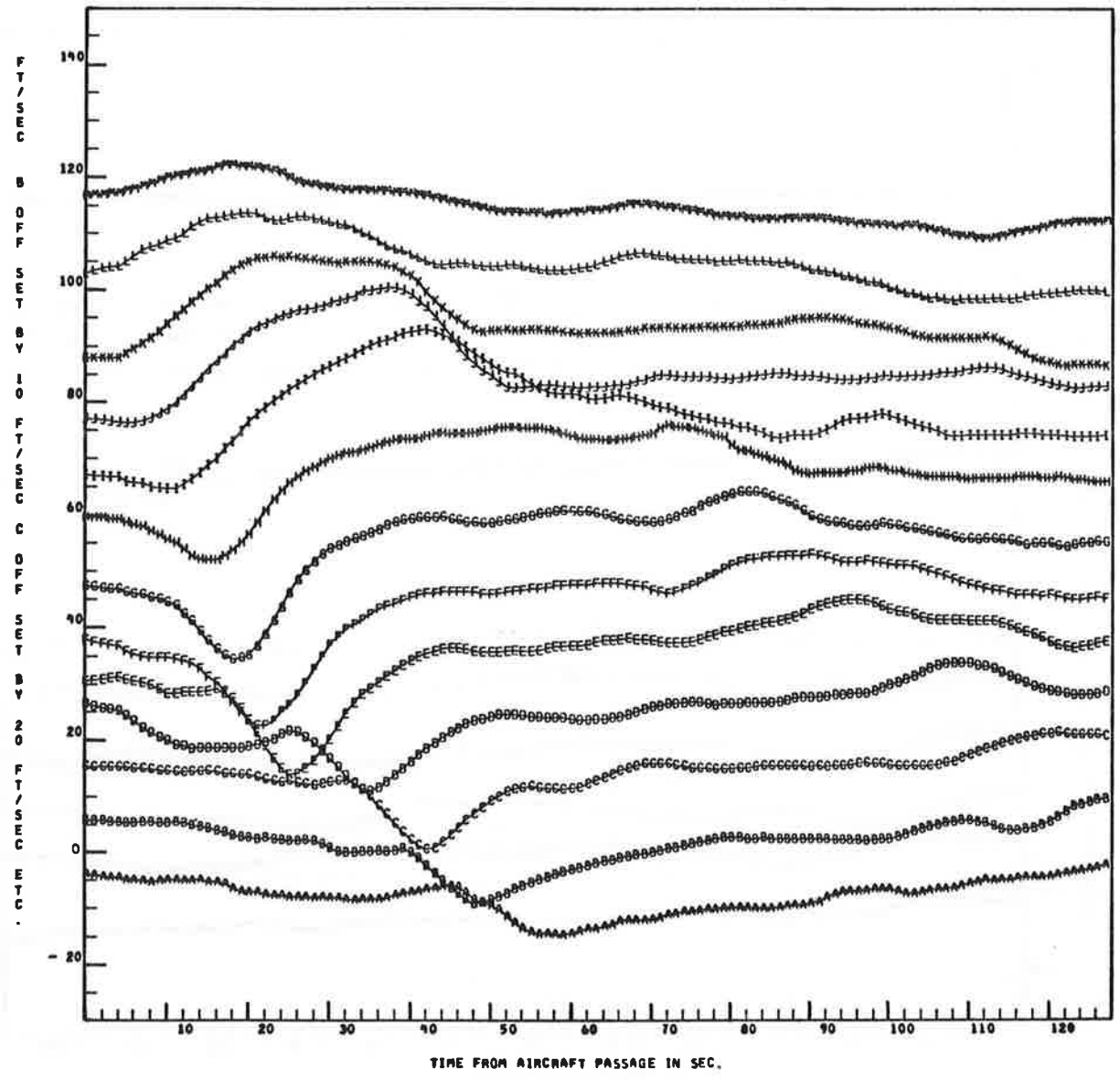


Fig. 4-19 - Groundwind Sensor Data Averaged over 9-sec Intervals (Sensors 201-213)

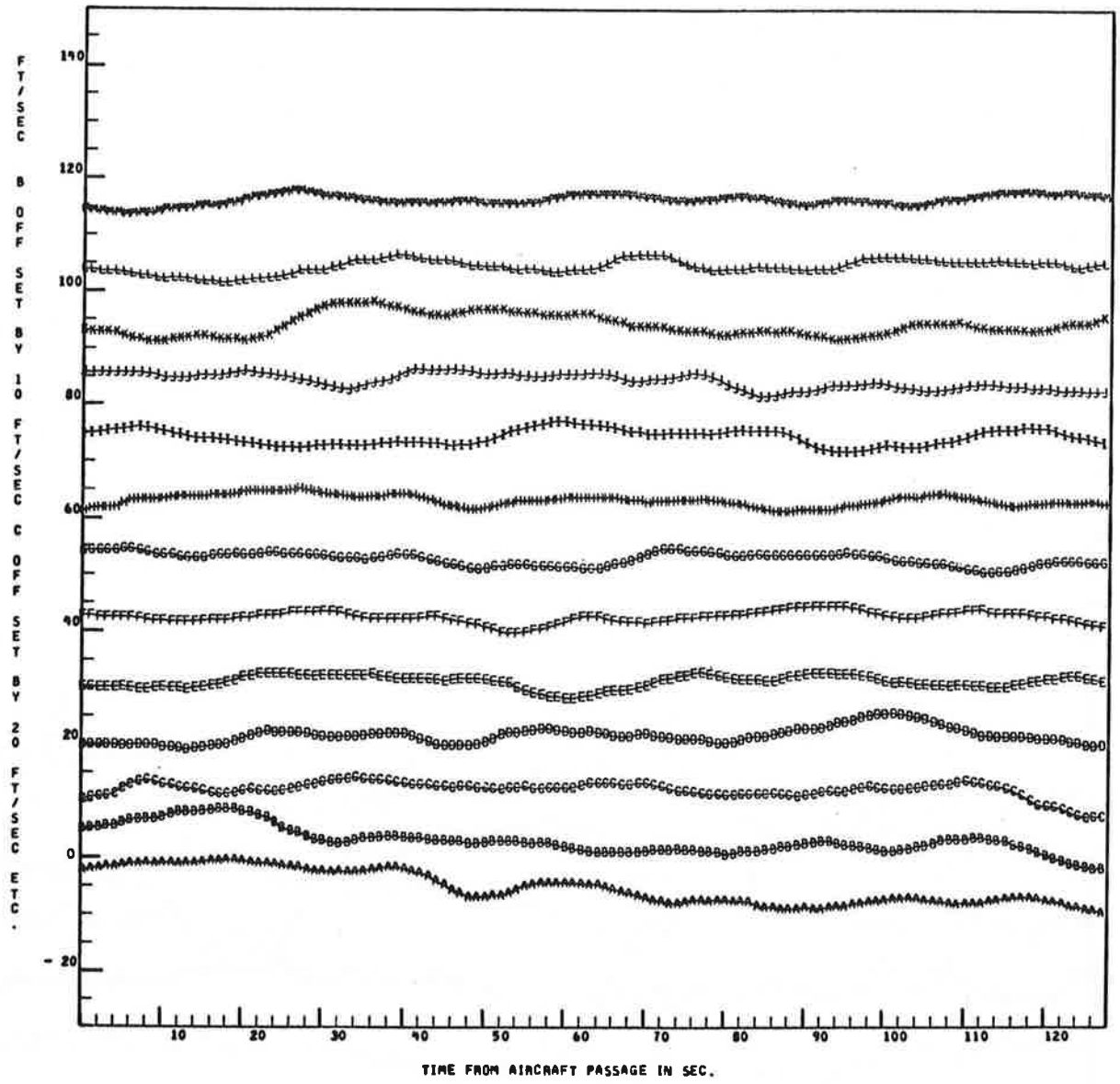


Fig.4-20 - Groundwind Sensor Data Averaged over 9-sec Intervals (Sensors 214-226)

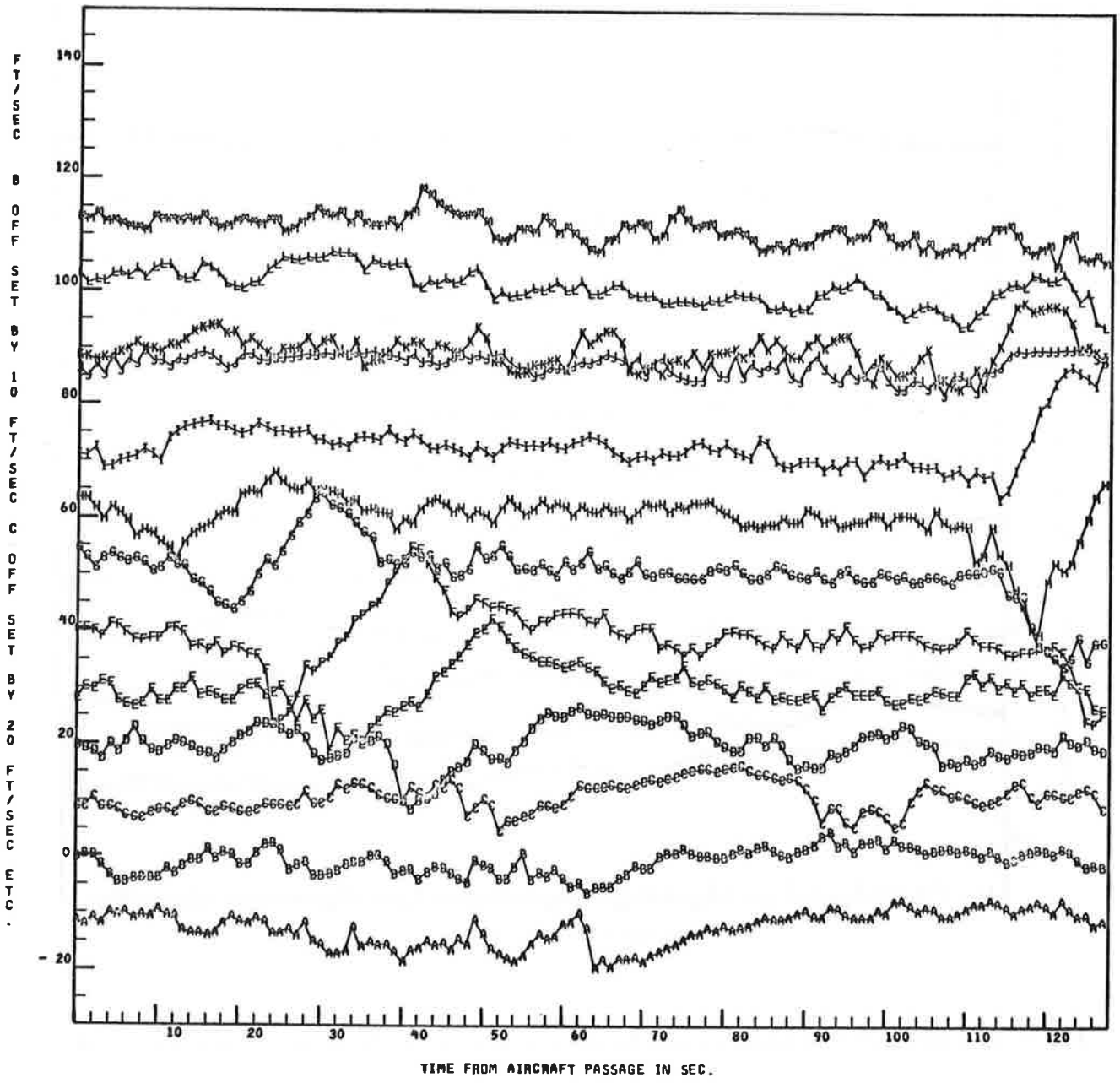


Fig. 4-21 - Groundwind Sensor Data Averaged over 1-sec Intervals (Sensors 101-113)

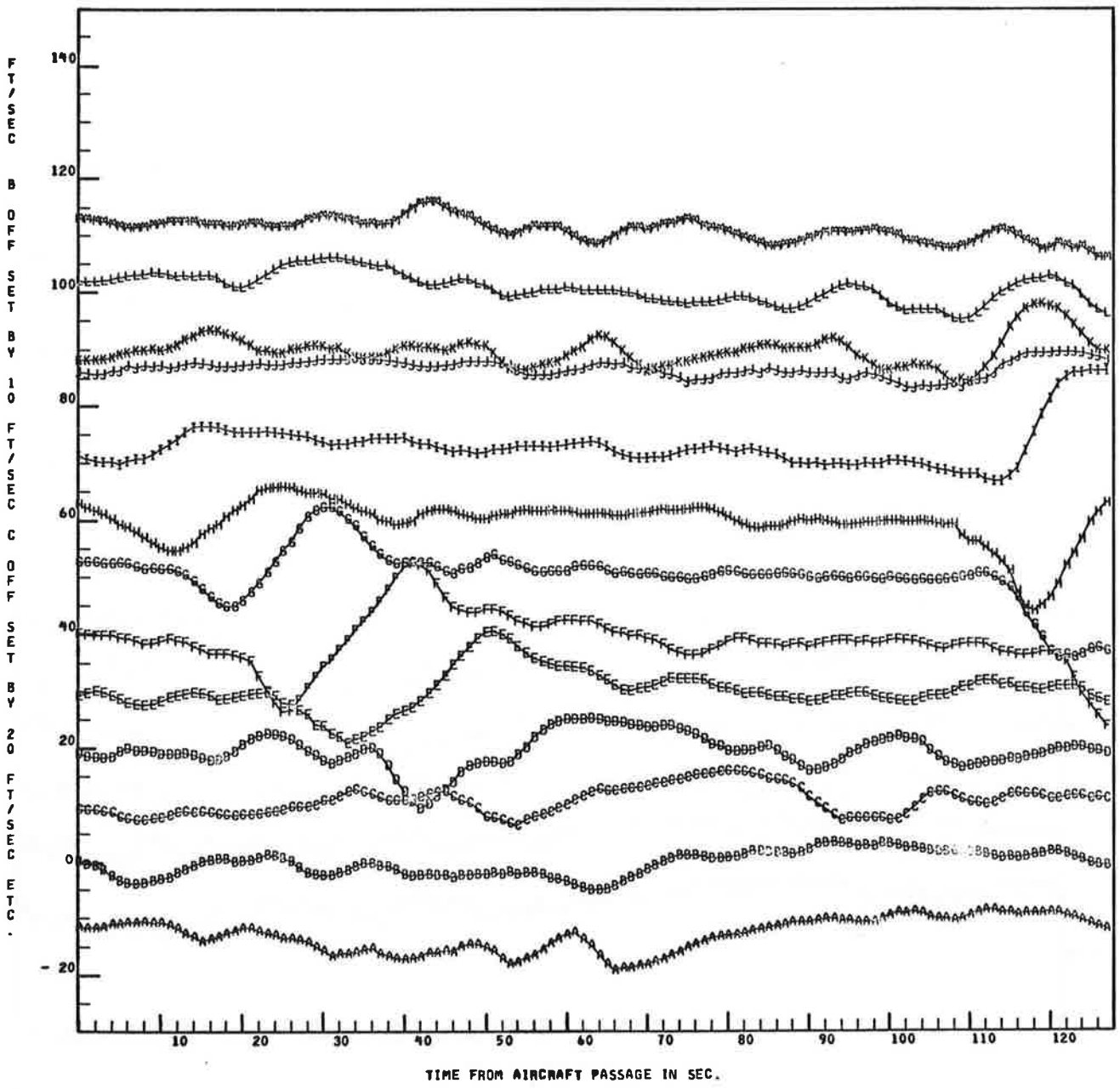


Fig. 4-22 - Groundwind Sensor Data Averaged over 5-sec Intervals (Sensors 101-113)

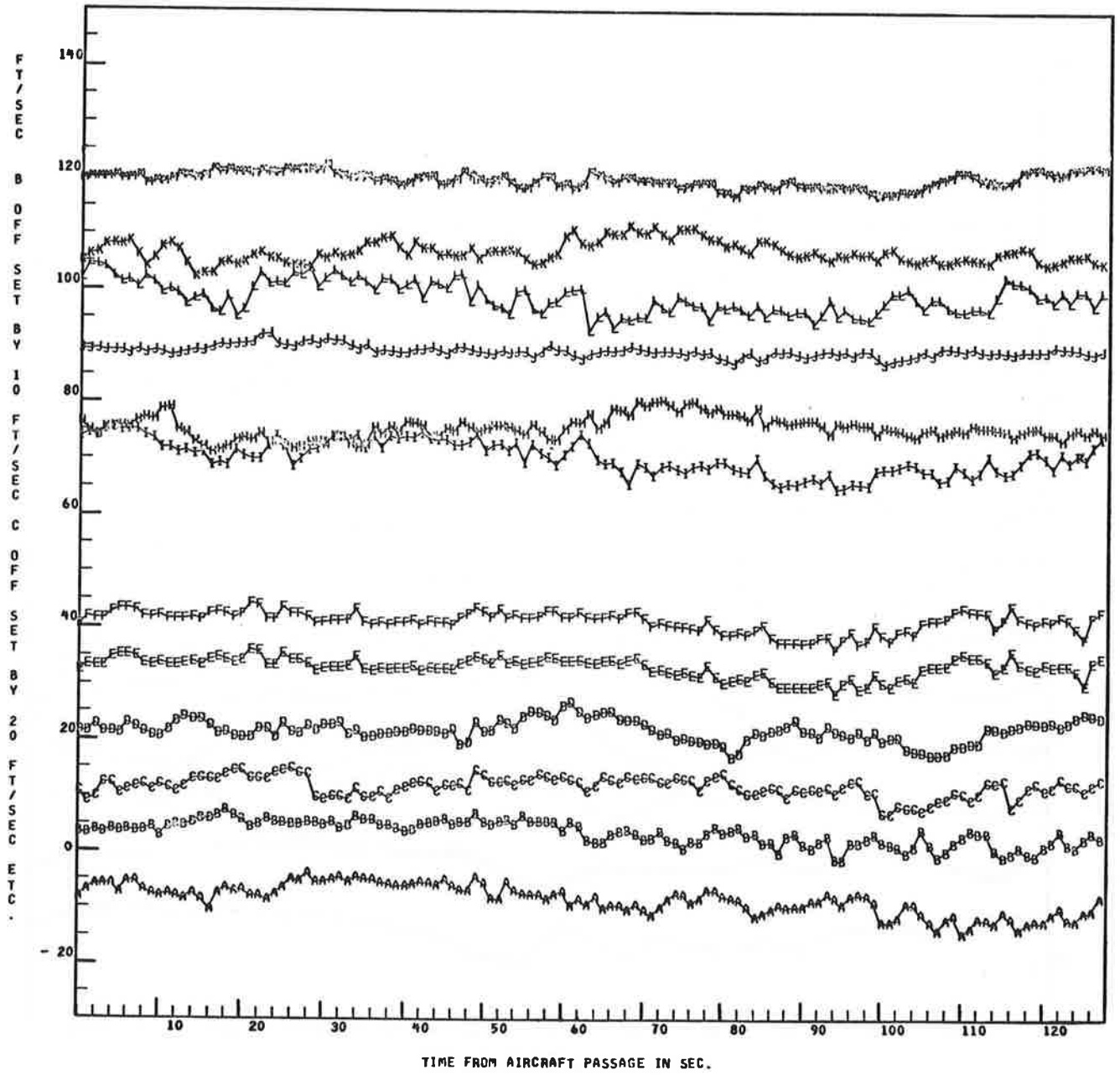


Fig.4-23 - Groundwind Sensor Data Averaged over 1-sec Intervals (Sensors 114-126)

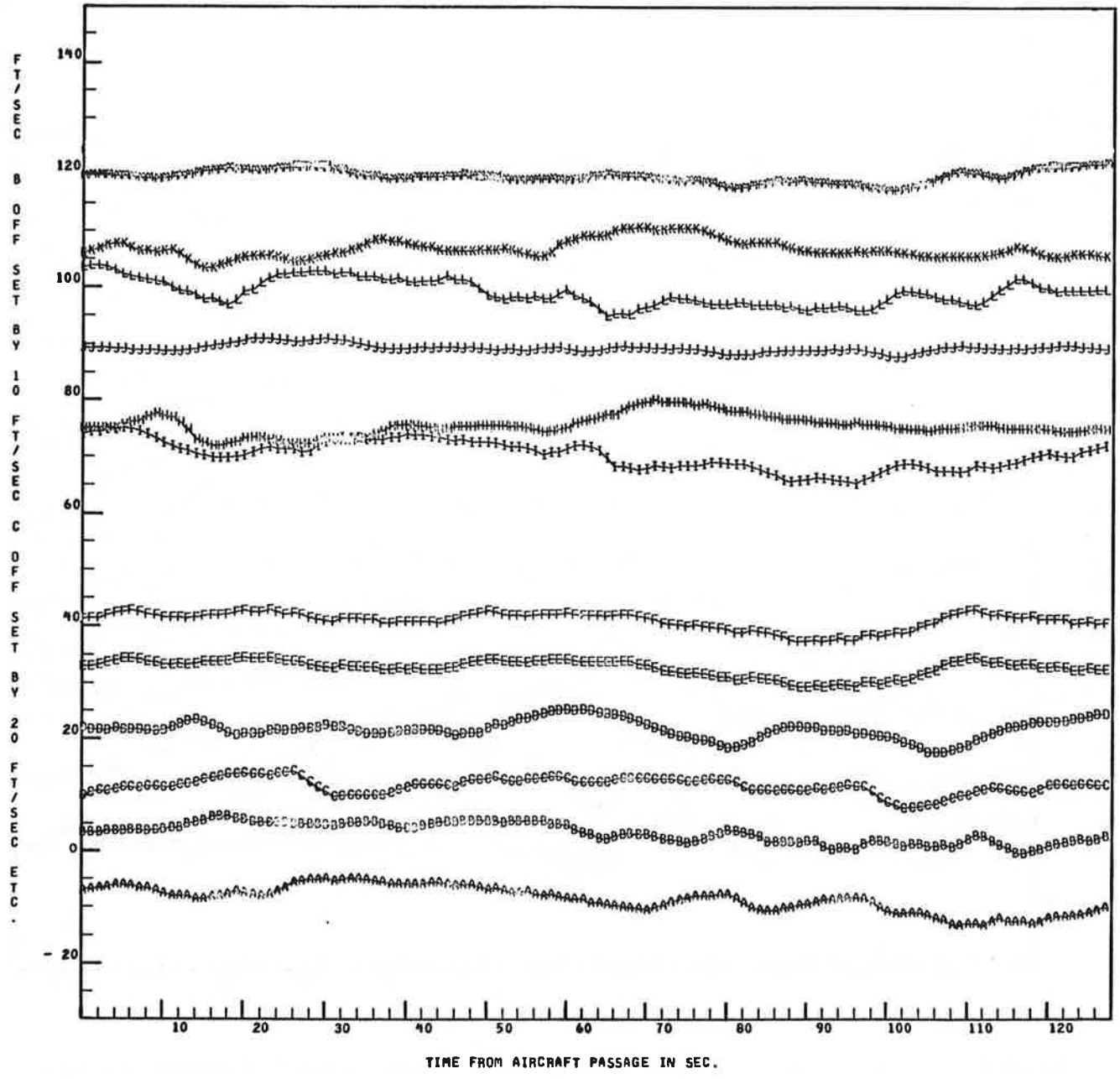


Fig.4-24 - Groundwind Sensor Data Averaged over 5-sec Intervals (Sensors 114-126)

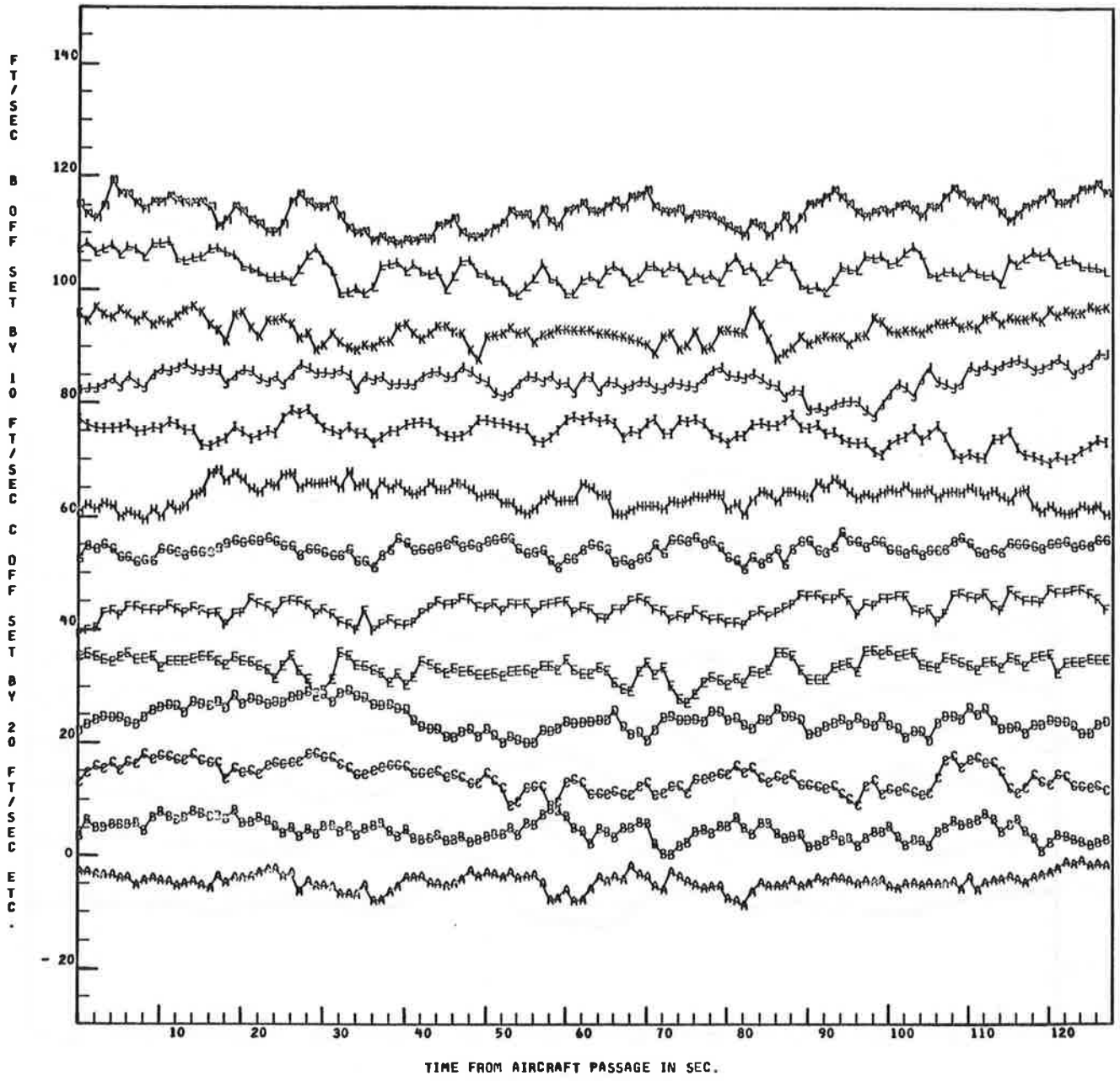


Fig. 4-27 - Groundwind Sensor Data Averaged over 1-sec Intervals (Sensors 214-226)

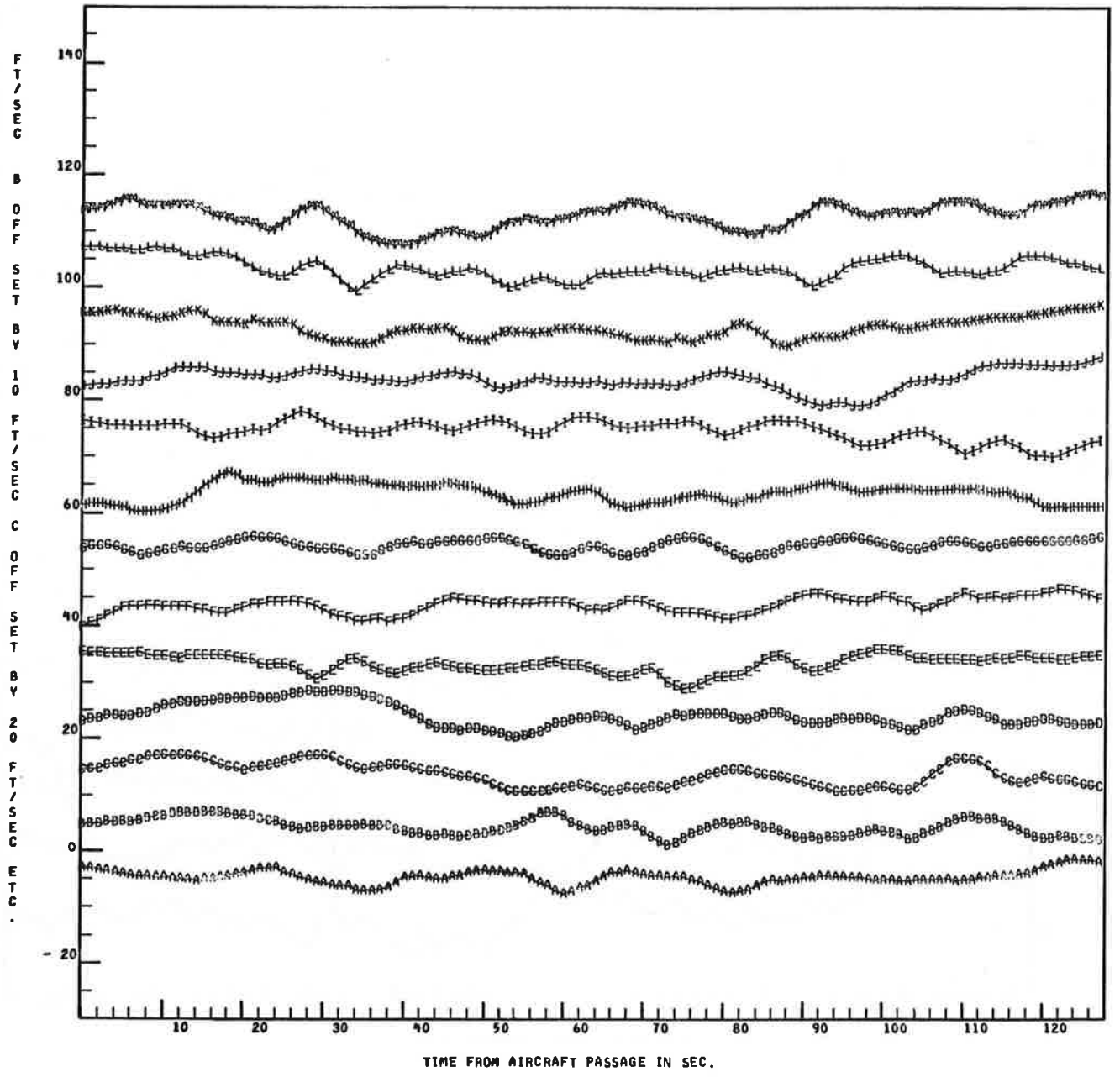


Fig.4-28 - Groundwind Sensor Data Averaged over 5-sec Intervals (Sensors 214-226)

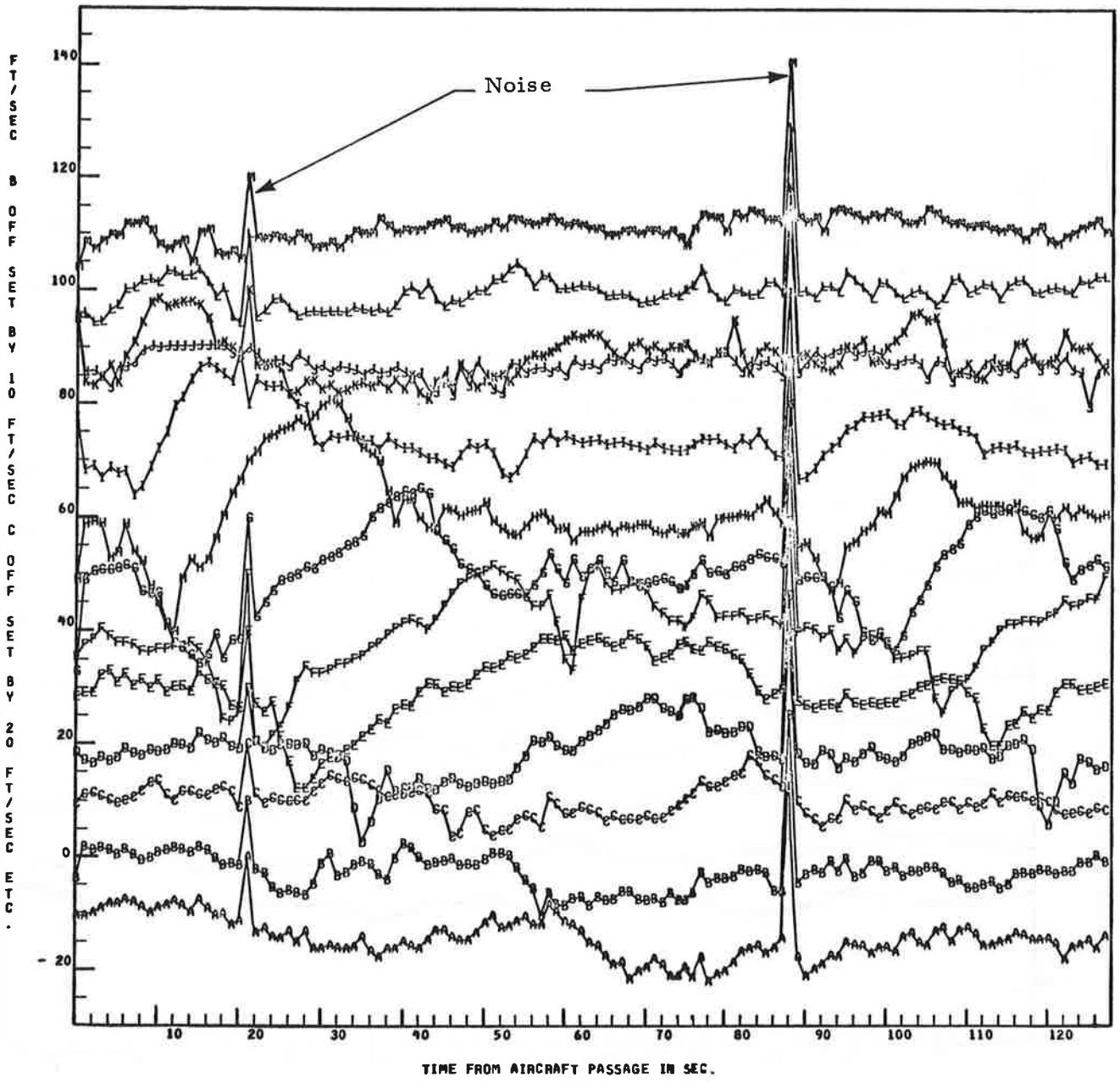


Fig. 4-29 - Groundwind Sensor Data Averaged over 1-sec Intervals (Sensors 101-113)

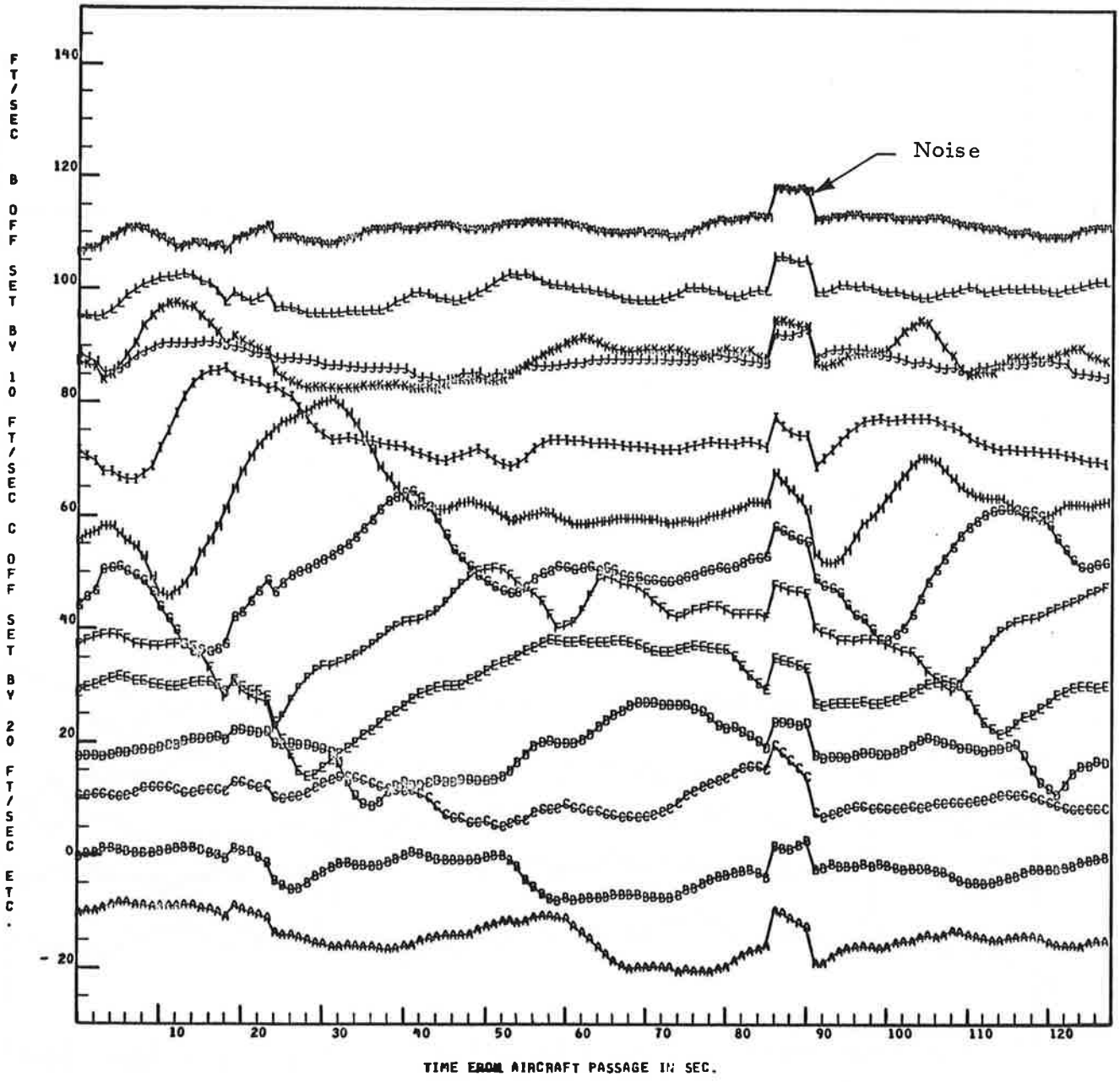


Fig.4-30 - Groundwind Sensor Data Averaged over 5-sec Intervals (Sensors101-113)

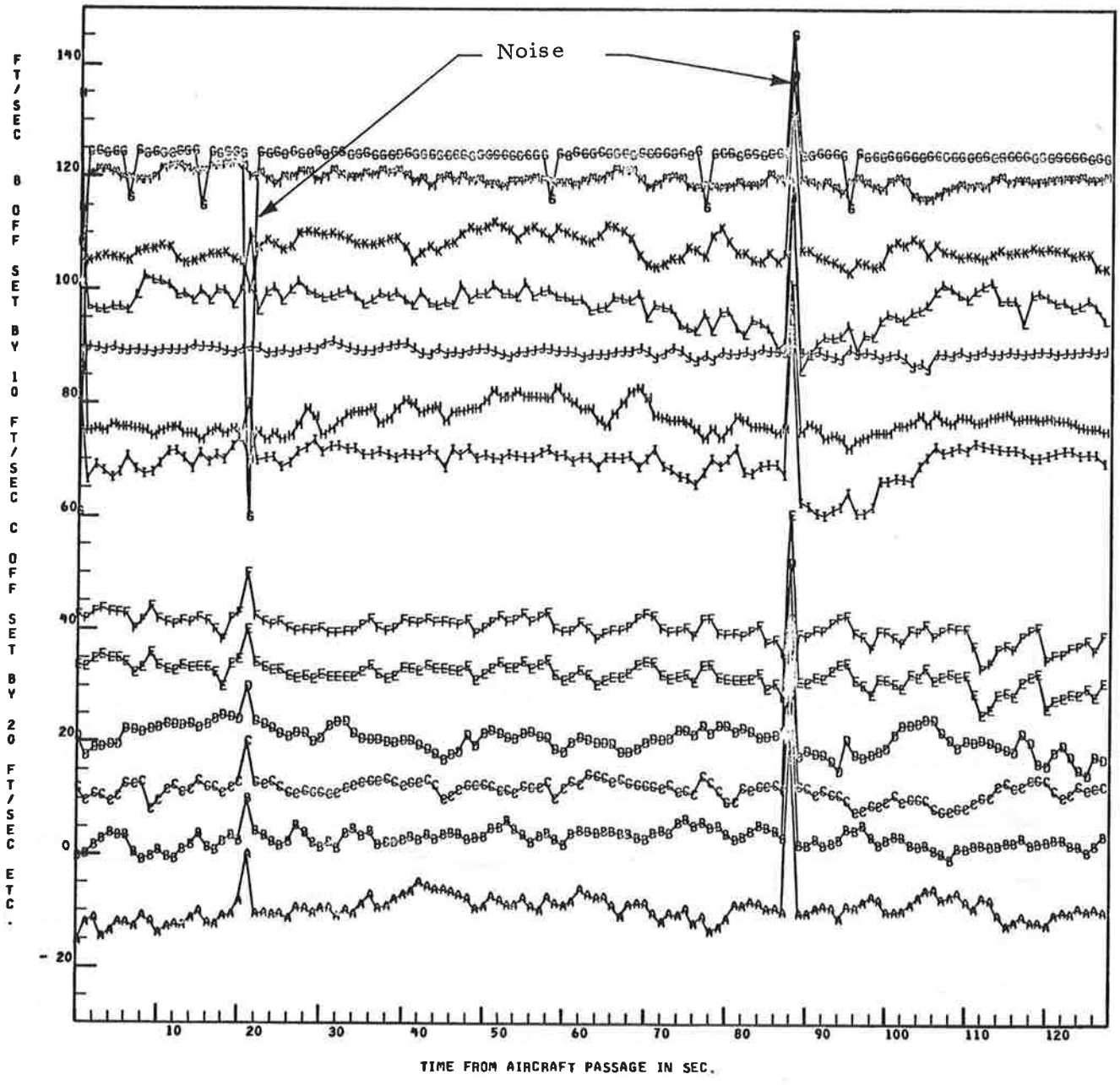


Fig.4-31 - Groundwind Sensor Data Averaged over 1-sec Intervals (Sensors114-126)

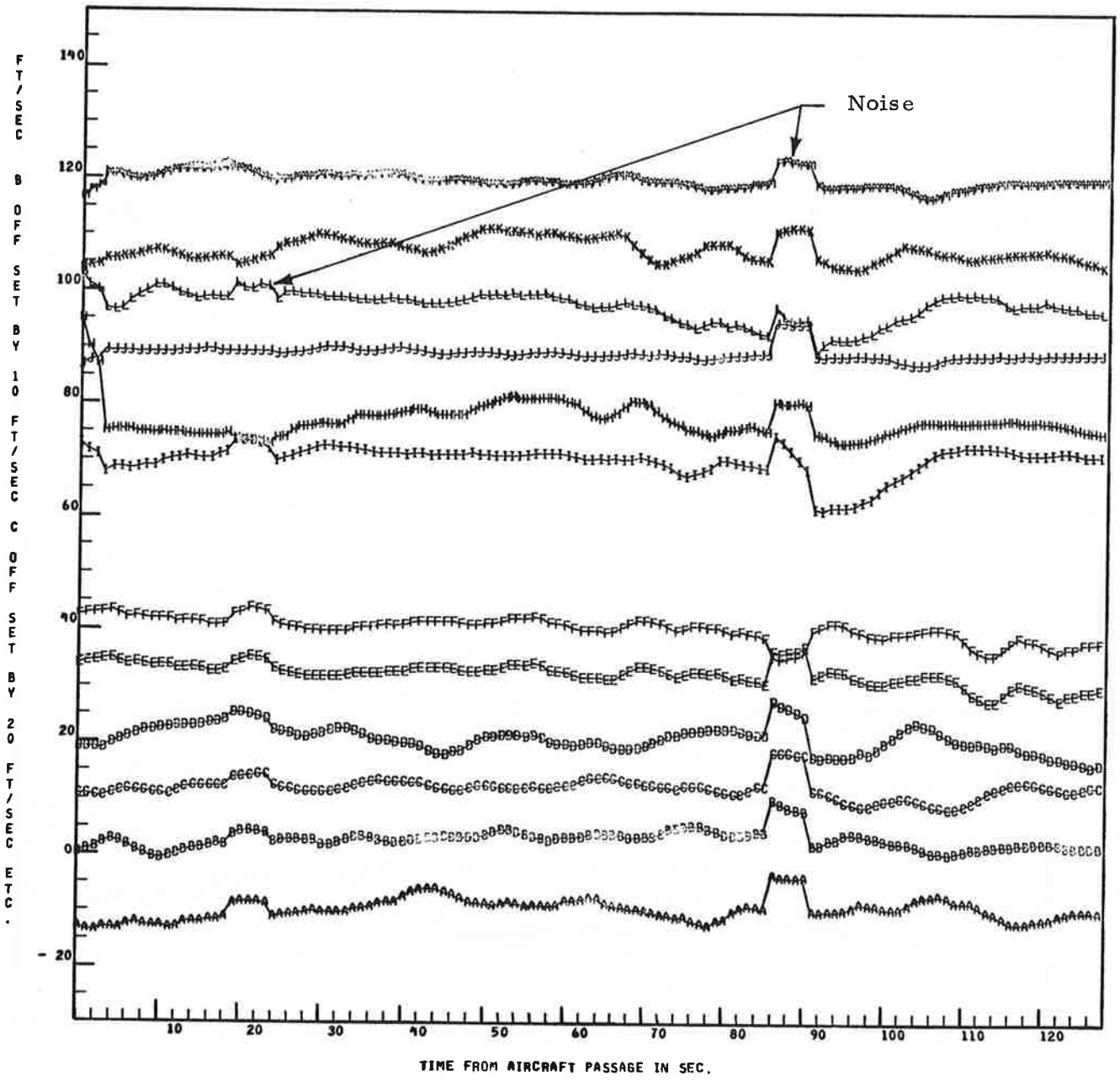


Fig.4-32 - Groundwind Sensor Data Averaged over 5-sec Intervals (Sensors 114-126)

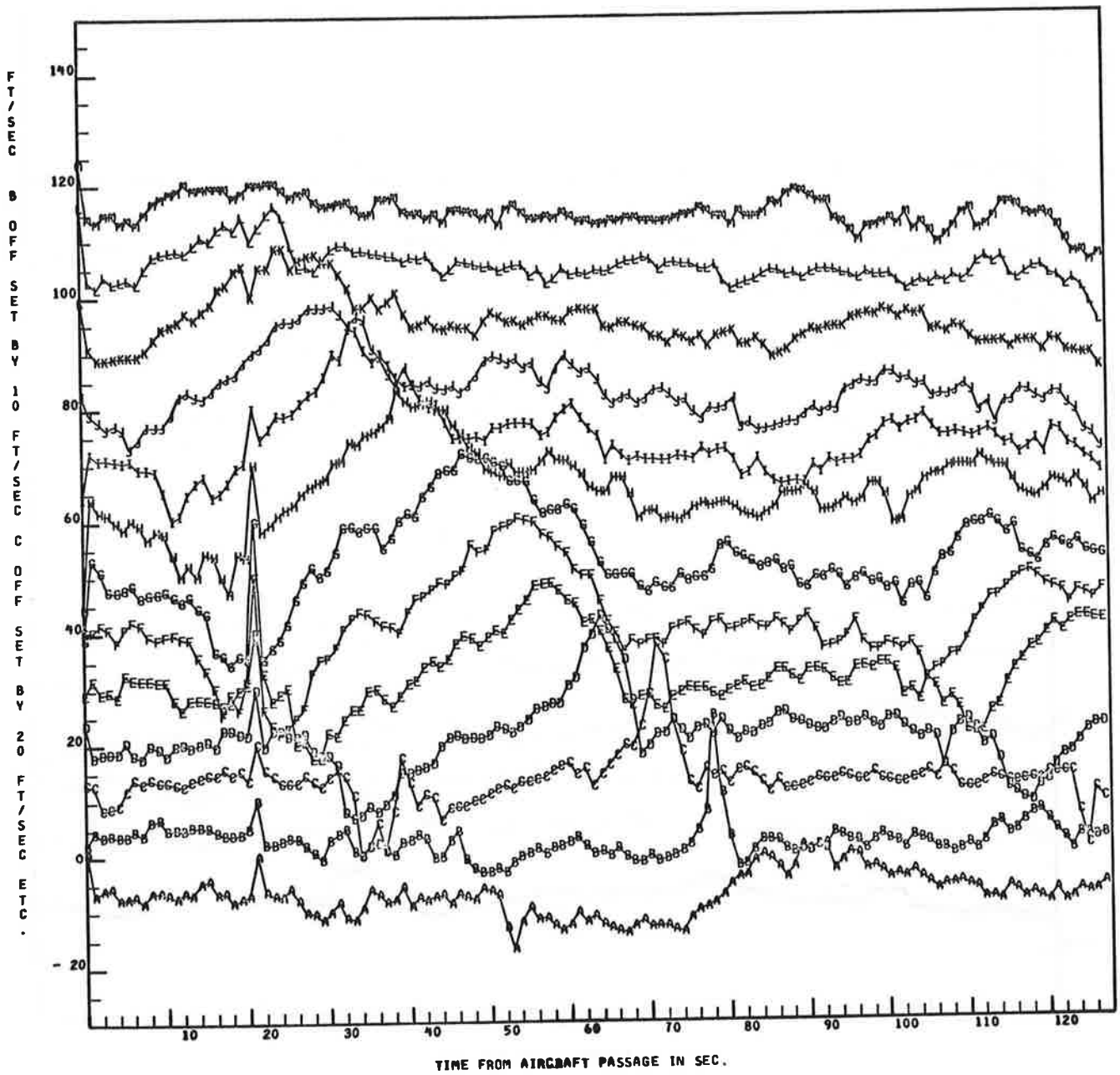


Fig. 4-33 - Groundwind Sensor Data Averaged over 1-sec Intervals (Sensors 201-213)

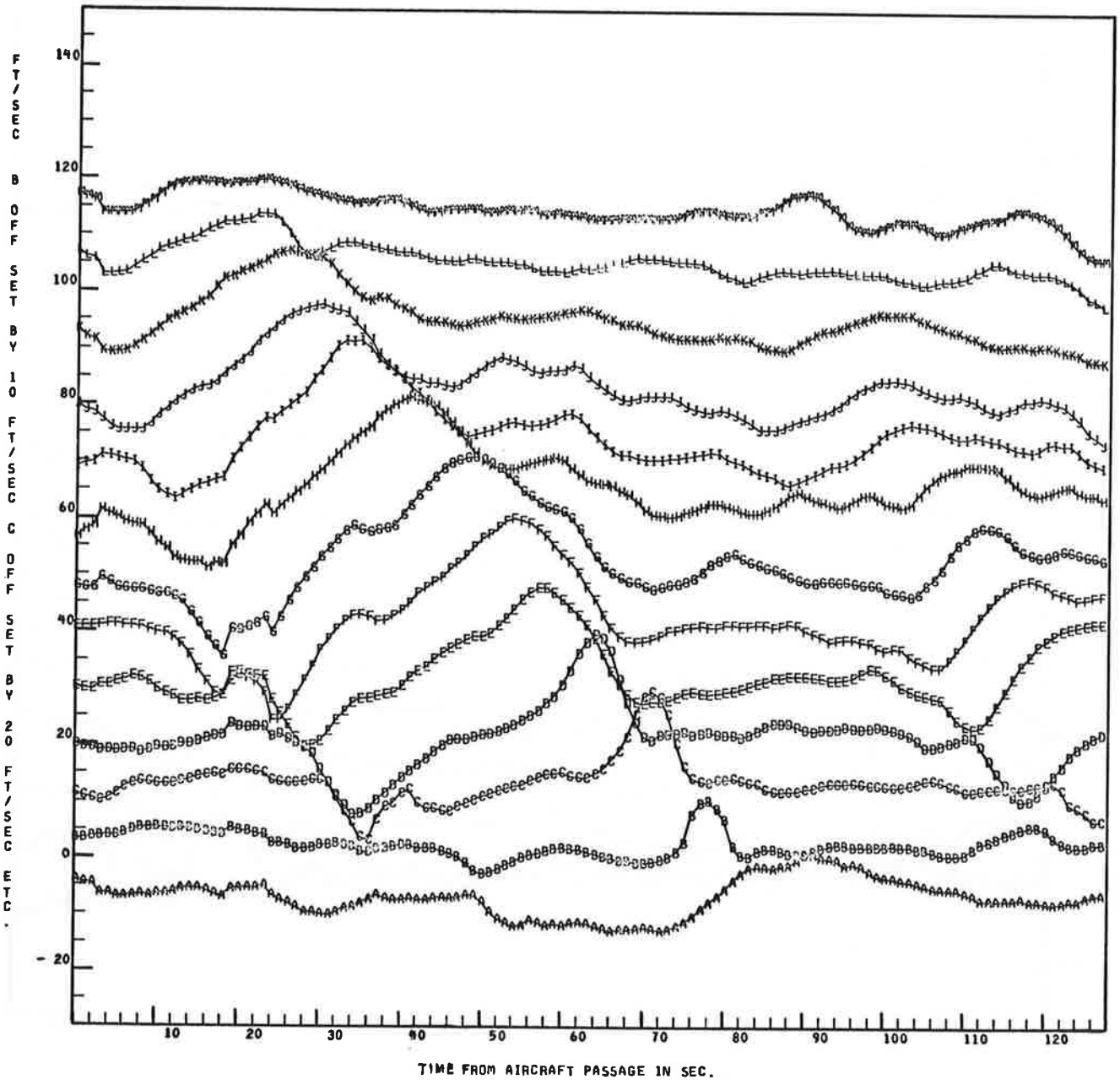


Fig.4-34 - Groundwind Sensor Data Averaged over 5-sec Intervals (Sensors 201-213)

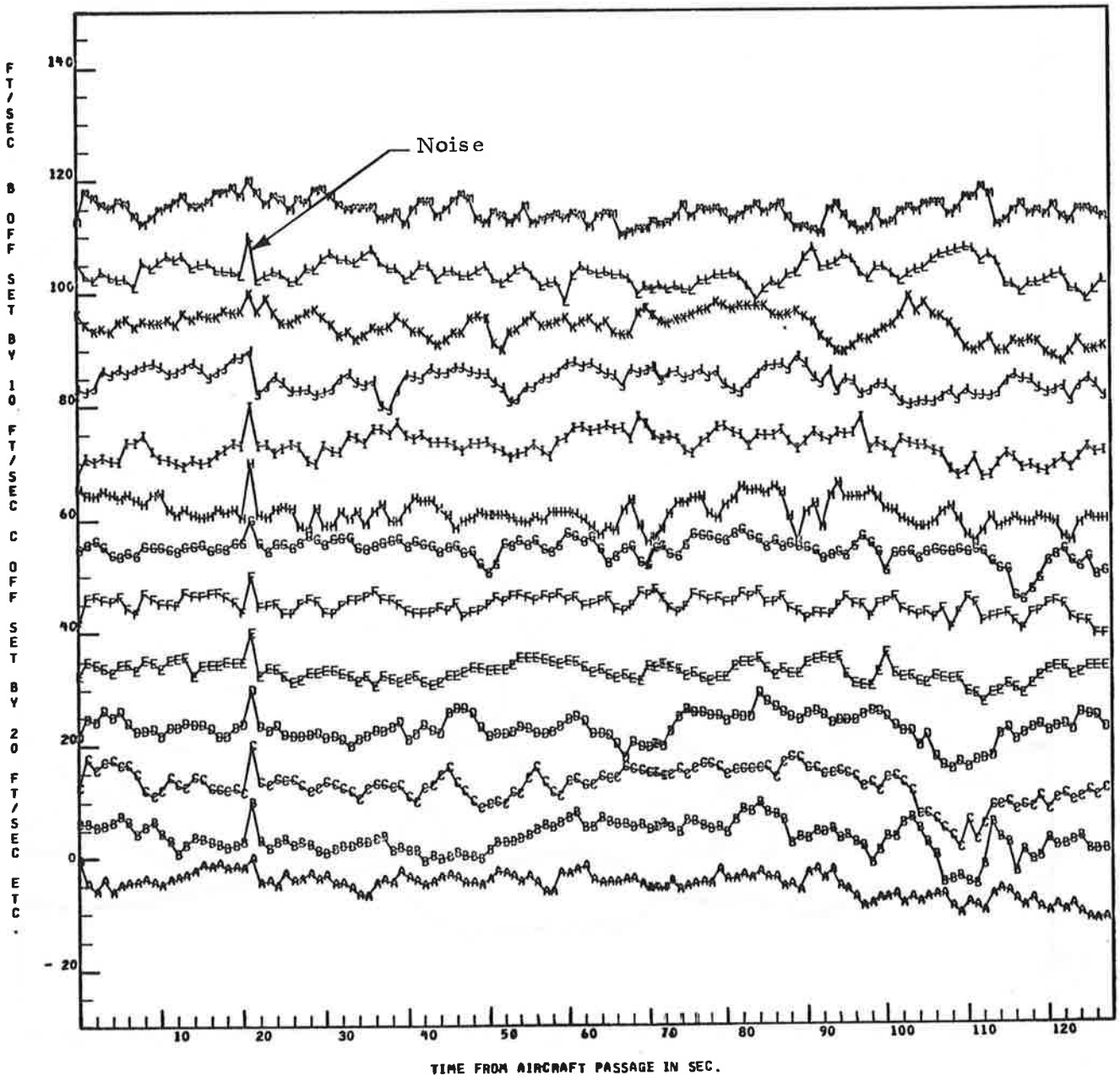


Fig. 4-35 - Groundwind Sensor Data Averaged over 1-sec Intervals (Sensors 214-226)

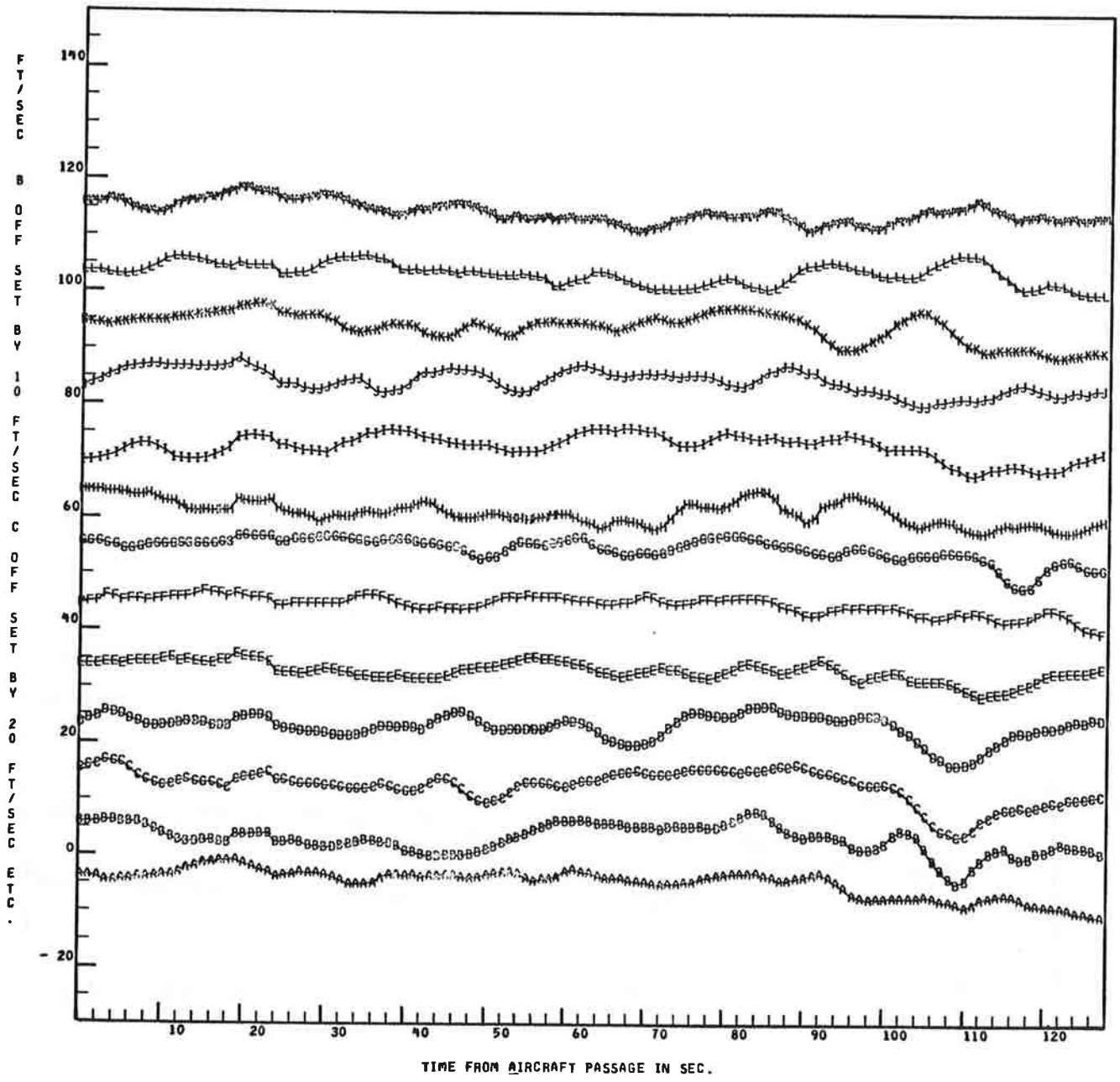


Fig. 4-36 - Groundwind Sensor Data Averaged over 5-sec Intervals (Sensors 214-226)

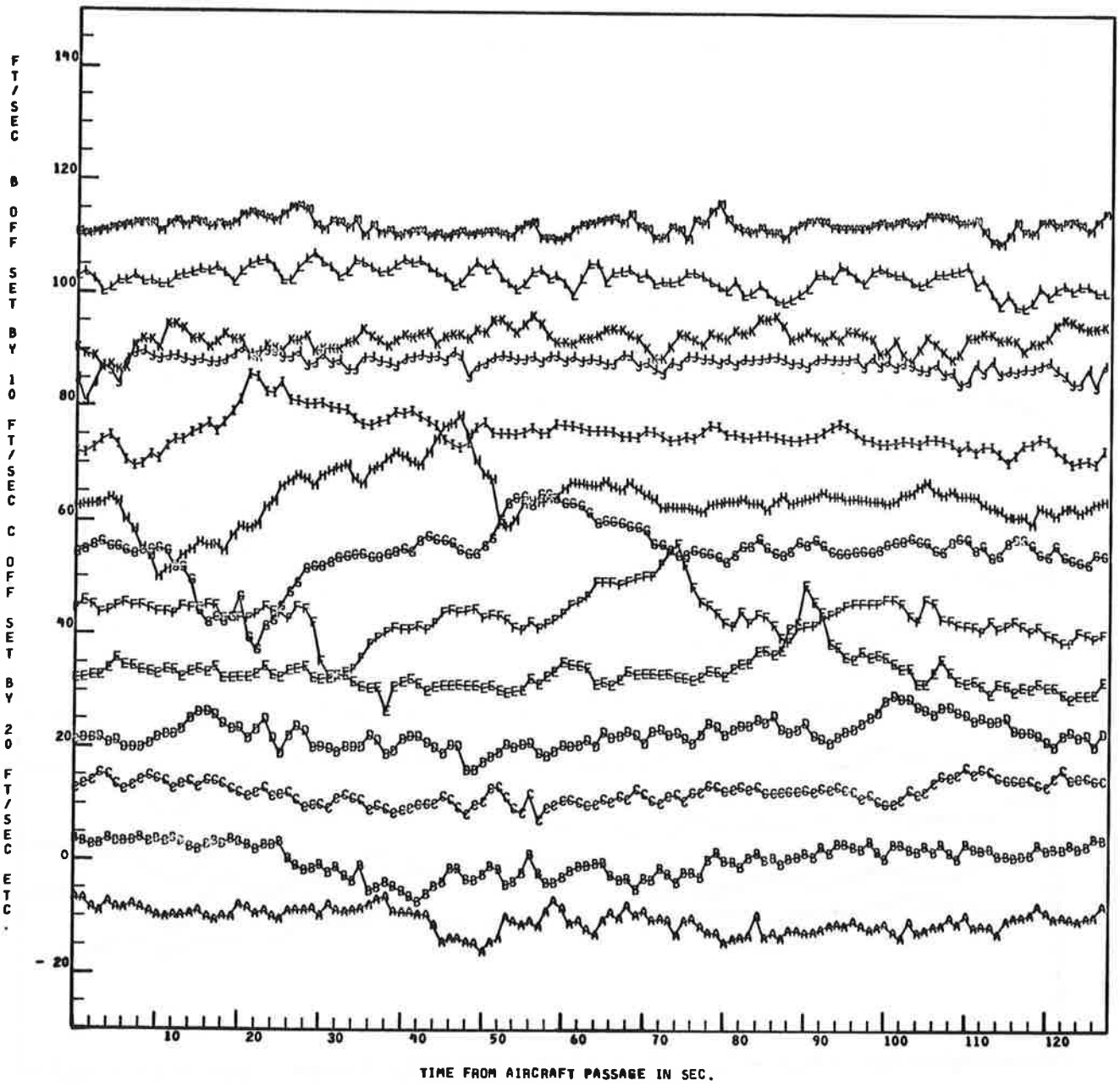


Fig.4-37 - Groundwind Sensor Data Averaged over 1-sec Intervals (Sensors 101-113)

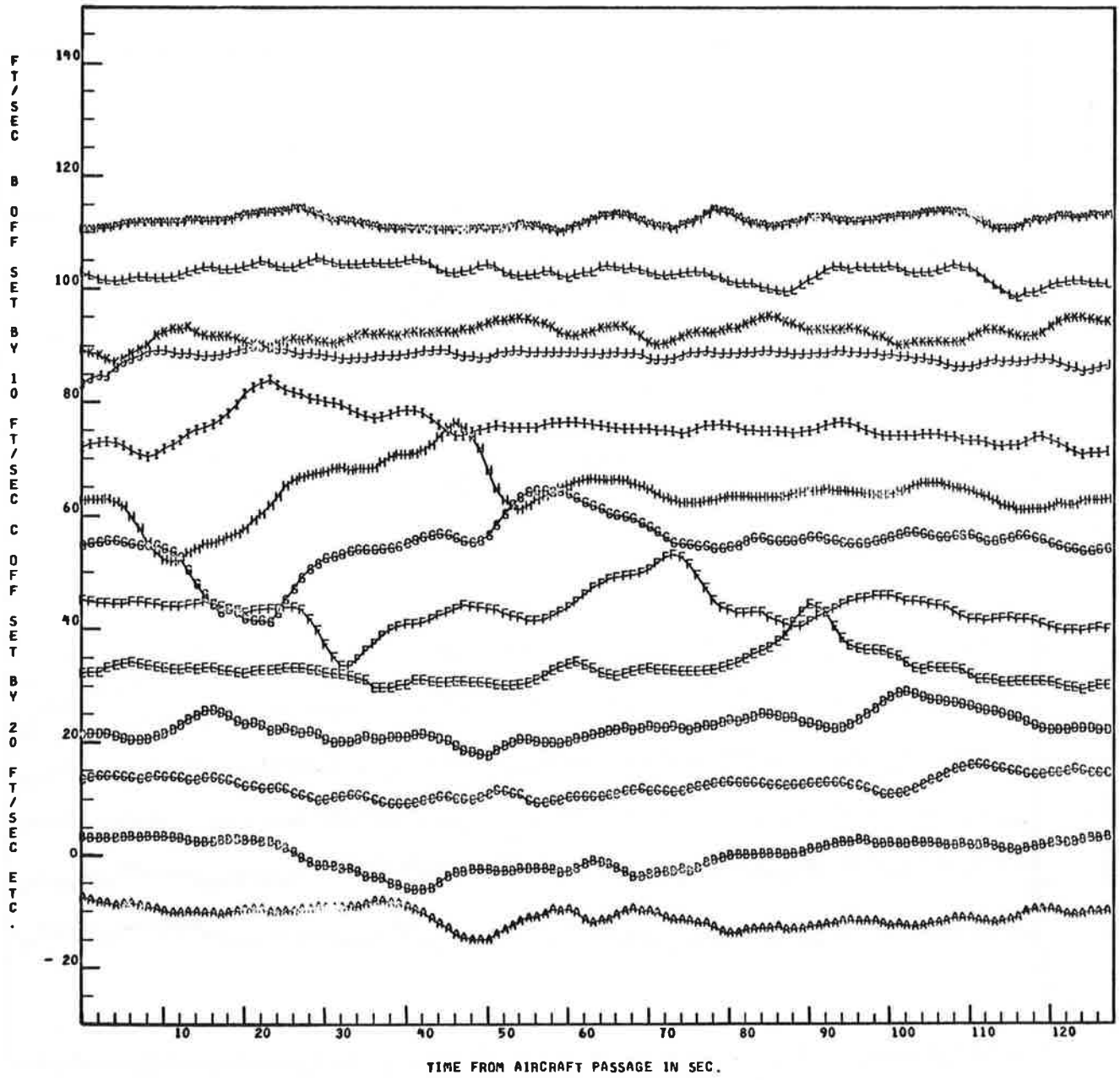


Fig. 4-38 - Groundwind Sensor Data Averaged over 5-sec Intervals (Sensors 101-113)

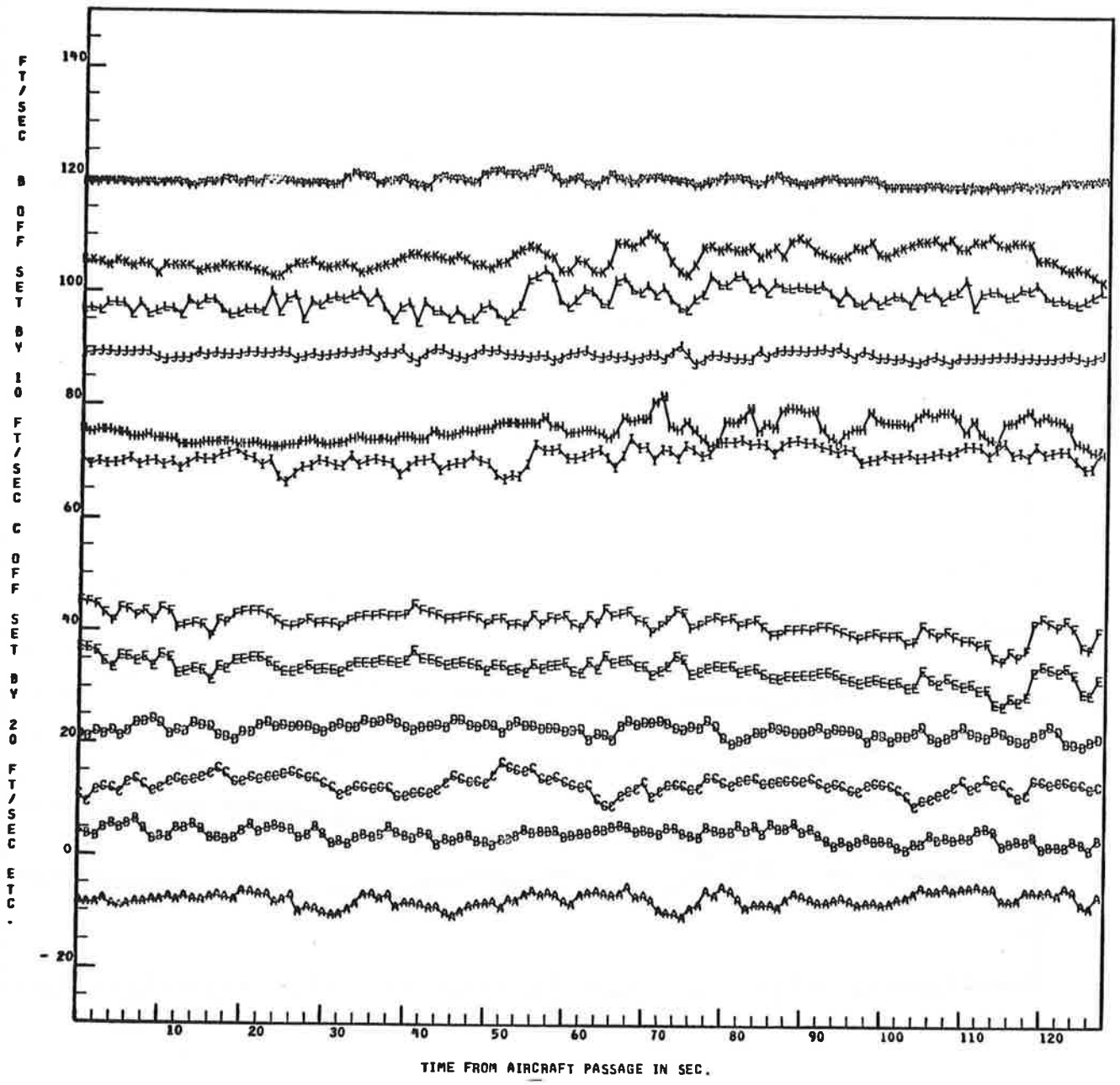


Fig.4-39 - Groundwind Sensor Data Averaged over 1-sec Intervals (Sensors 114-126)

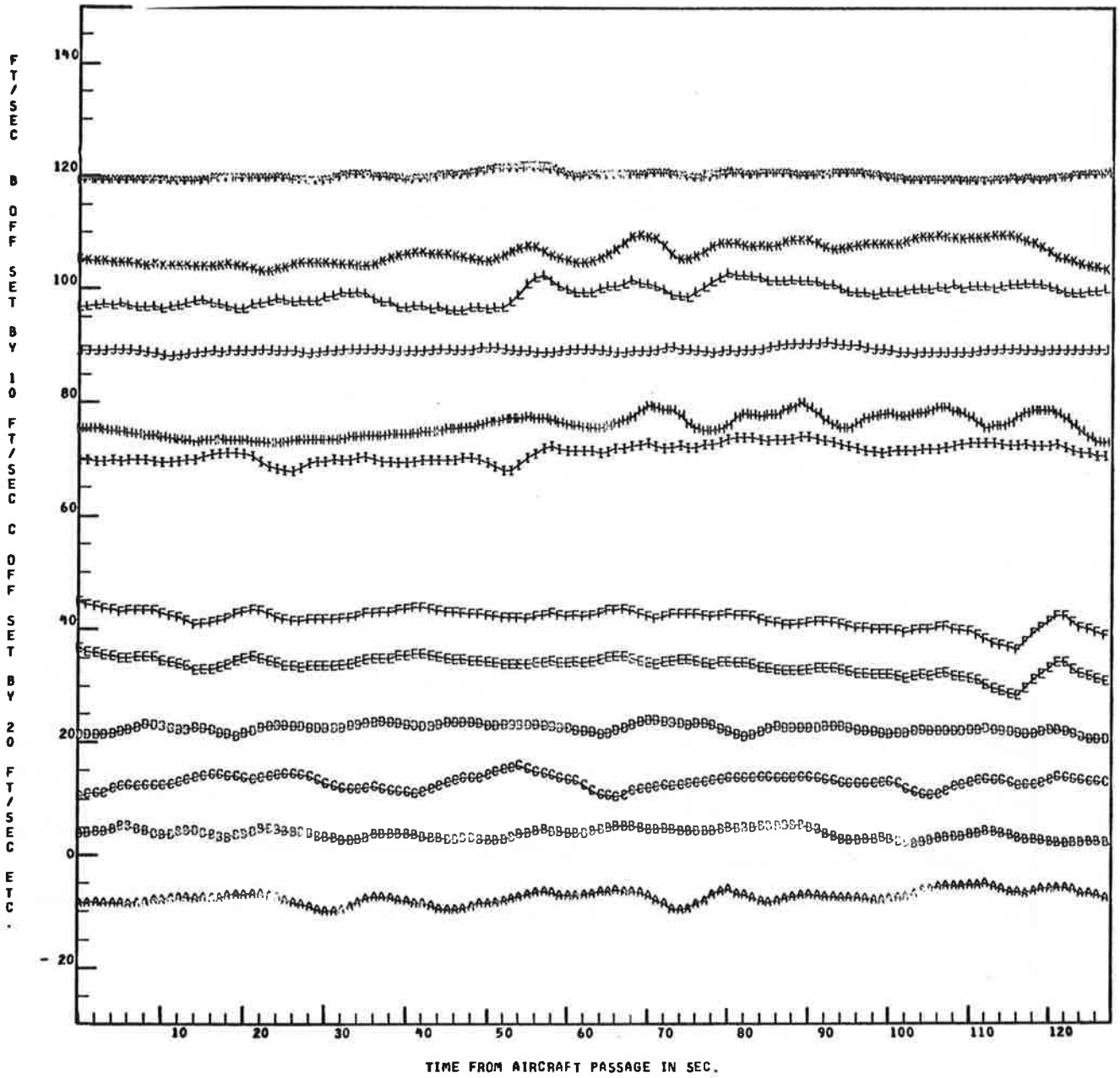


Fig.4-40 - Groundwind Sensor Data Averaged over 5-sec Intervals (Sensors 114-126)

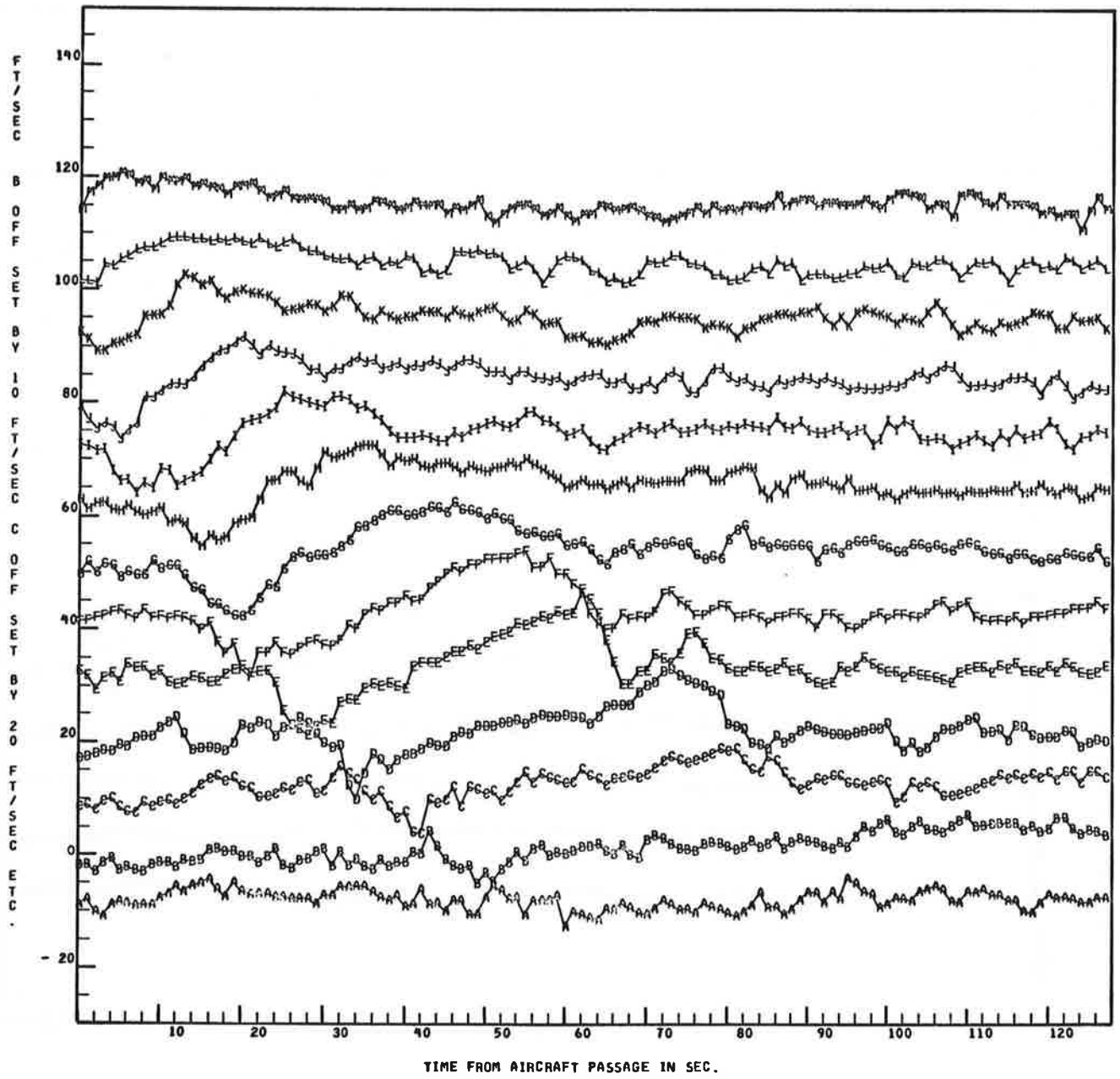


Fig. 4-41 - Groundwind Sensor Data Averaged over 1-sec Intervals (Sensors 201-213)

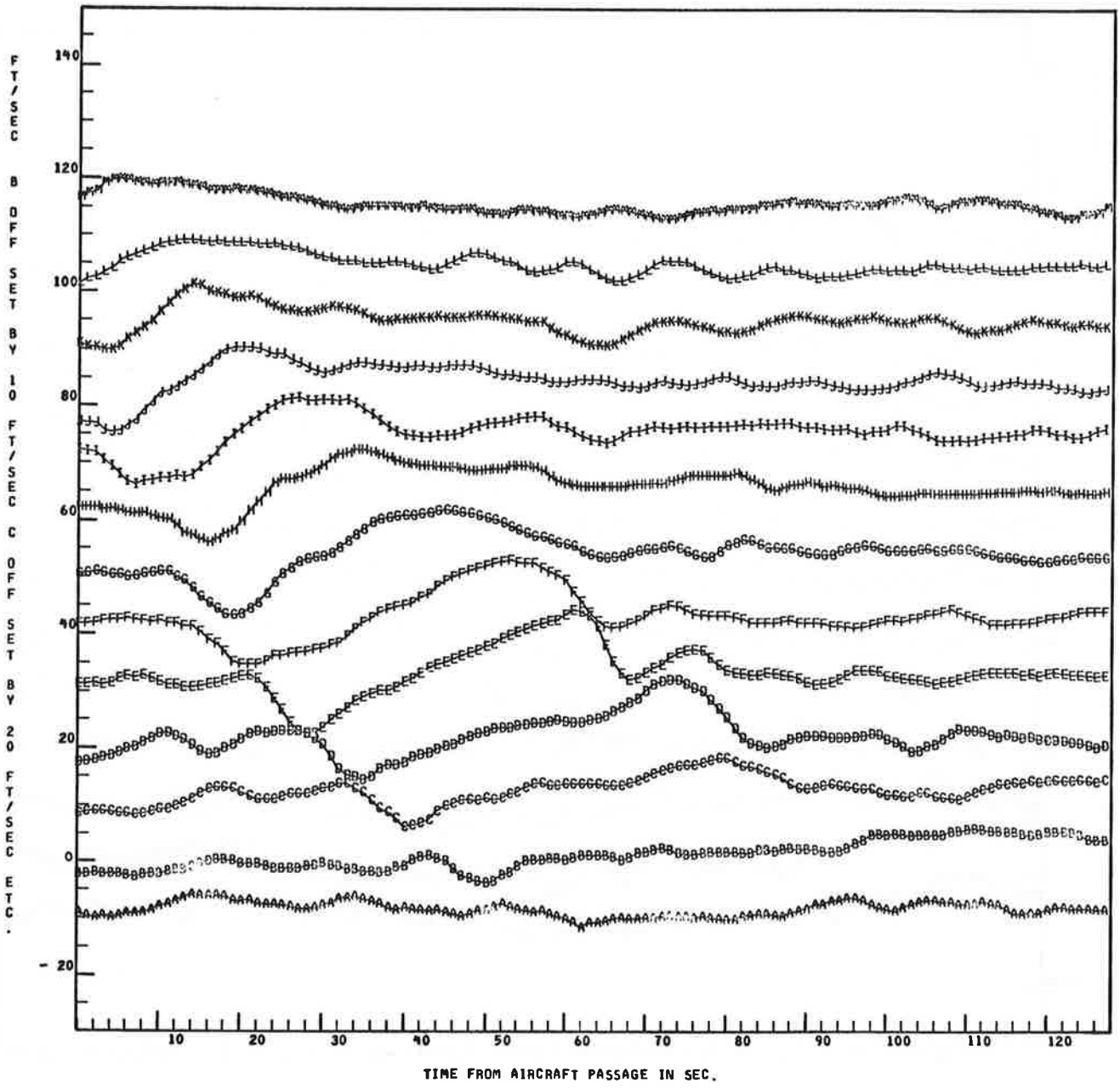


Fig.4-42 - Groundwind Sensor Data Averaged over 5-sec Intervals (Sensors 201-213)

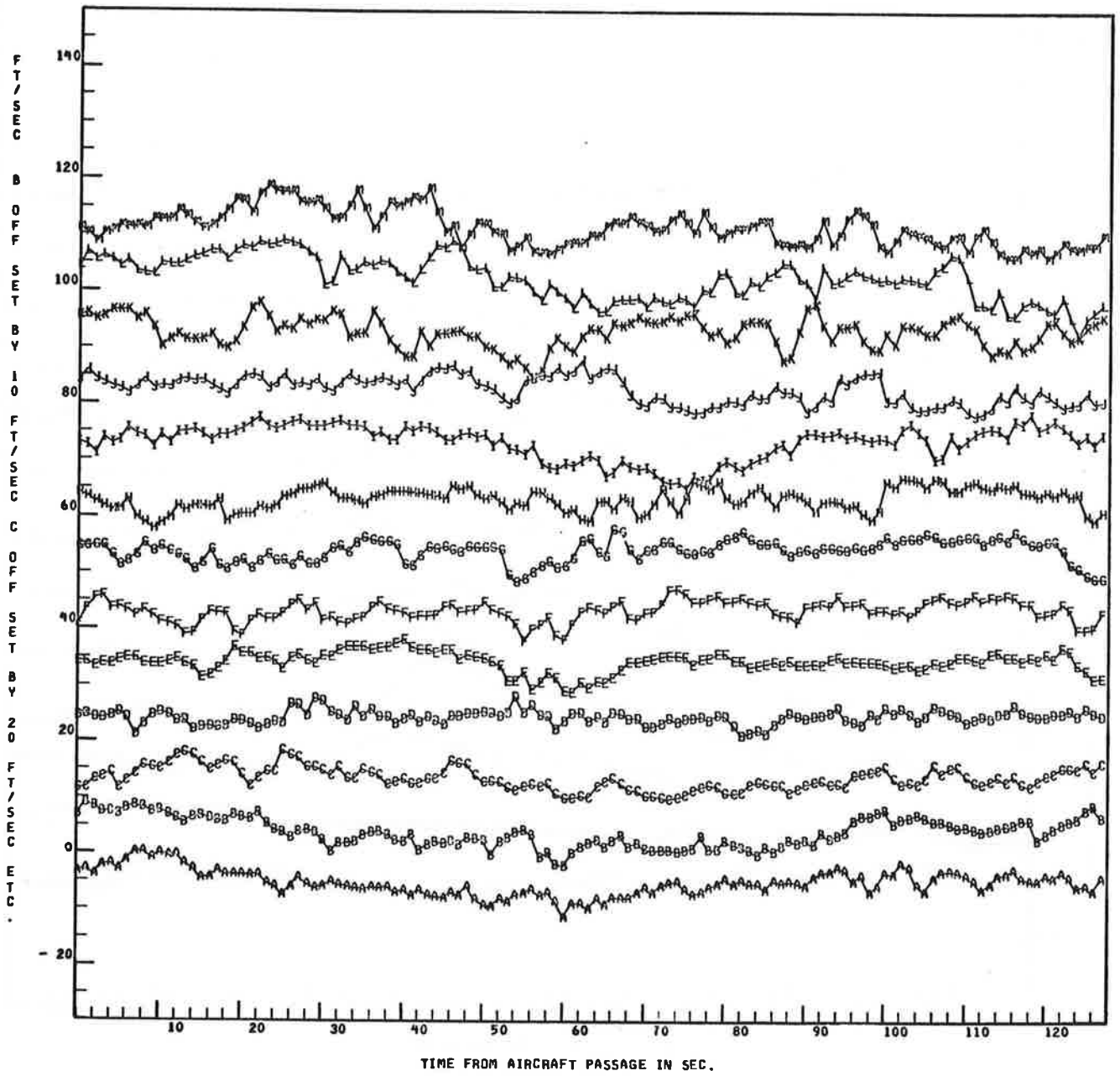


Fig.4-43 - Groundwind Sensor Data Averaged over 1-sec Intervals (Sensors 214-226)

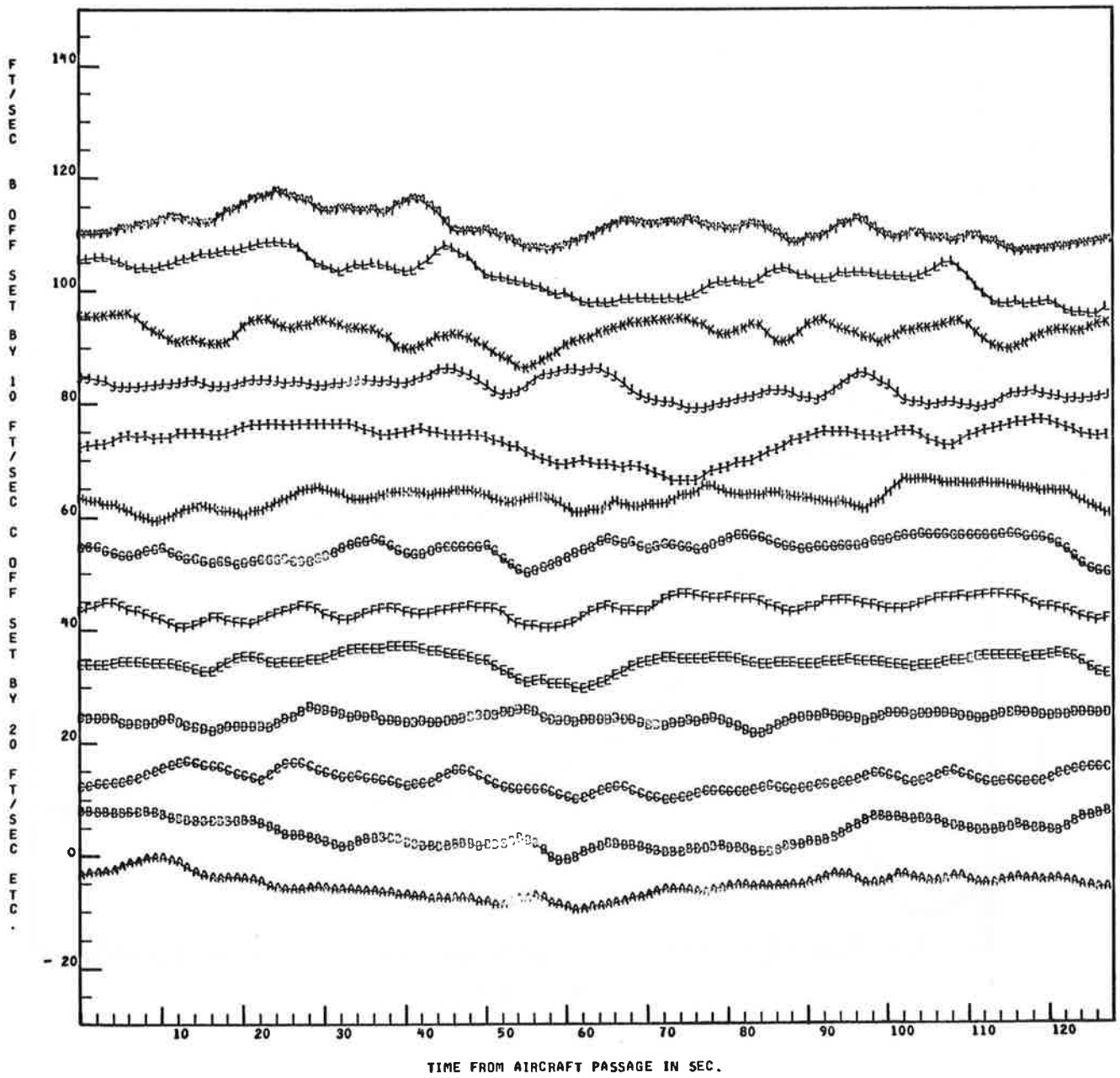


Fig. 4-44 - Groundwind Sensor Data Averaged over 5-sec Intervals (Sensors 214-226)

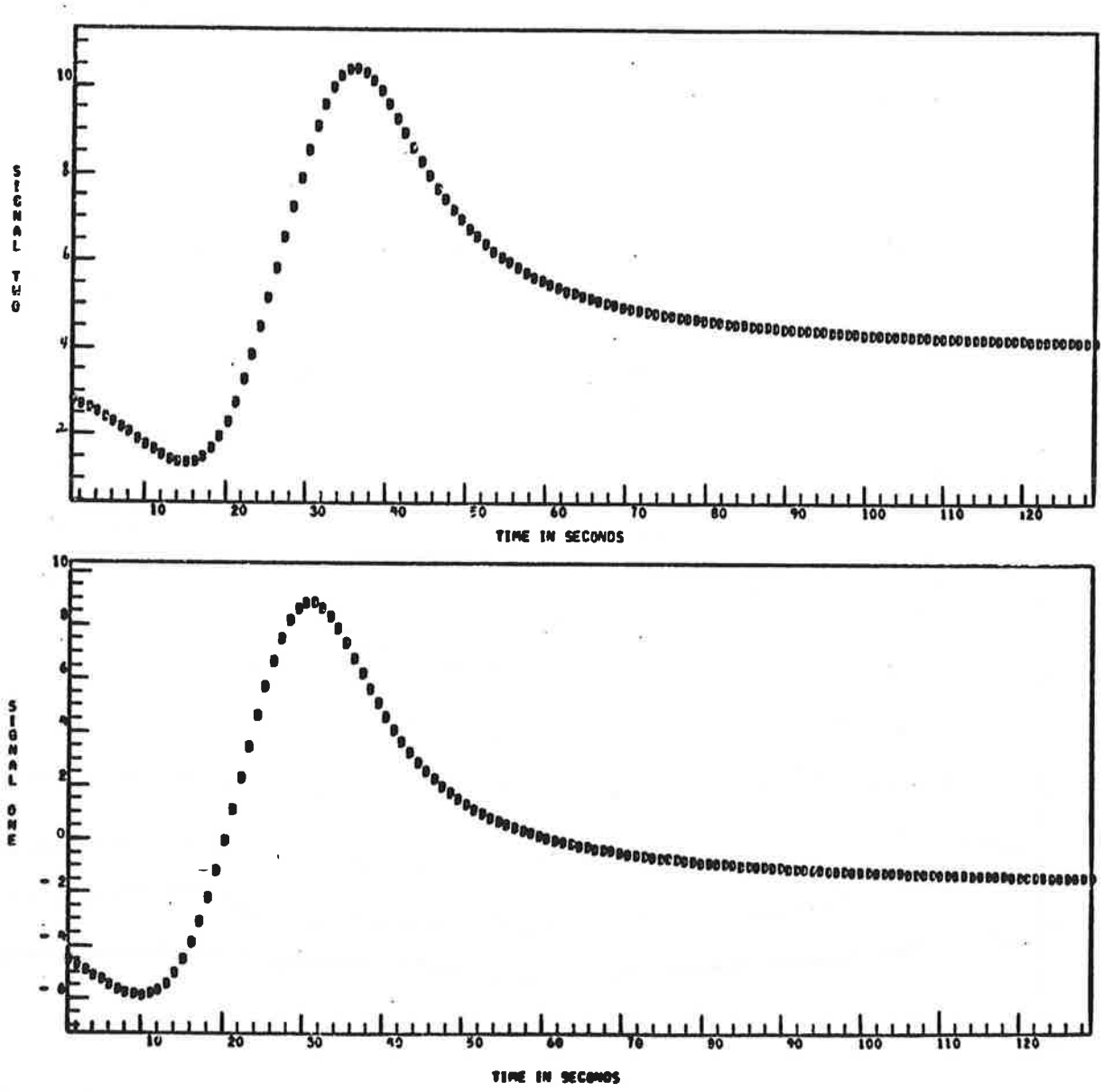


Fig. 4-45 - Theoretical Groundwind Signatures for Sensors at 200 and 250 ft, Respectively, on Port Side of Sensor Line 1 (Sensors 109, 108)

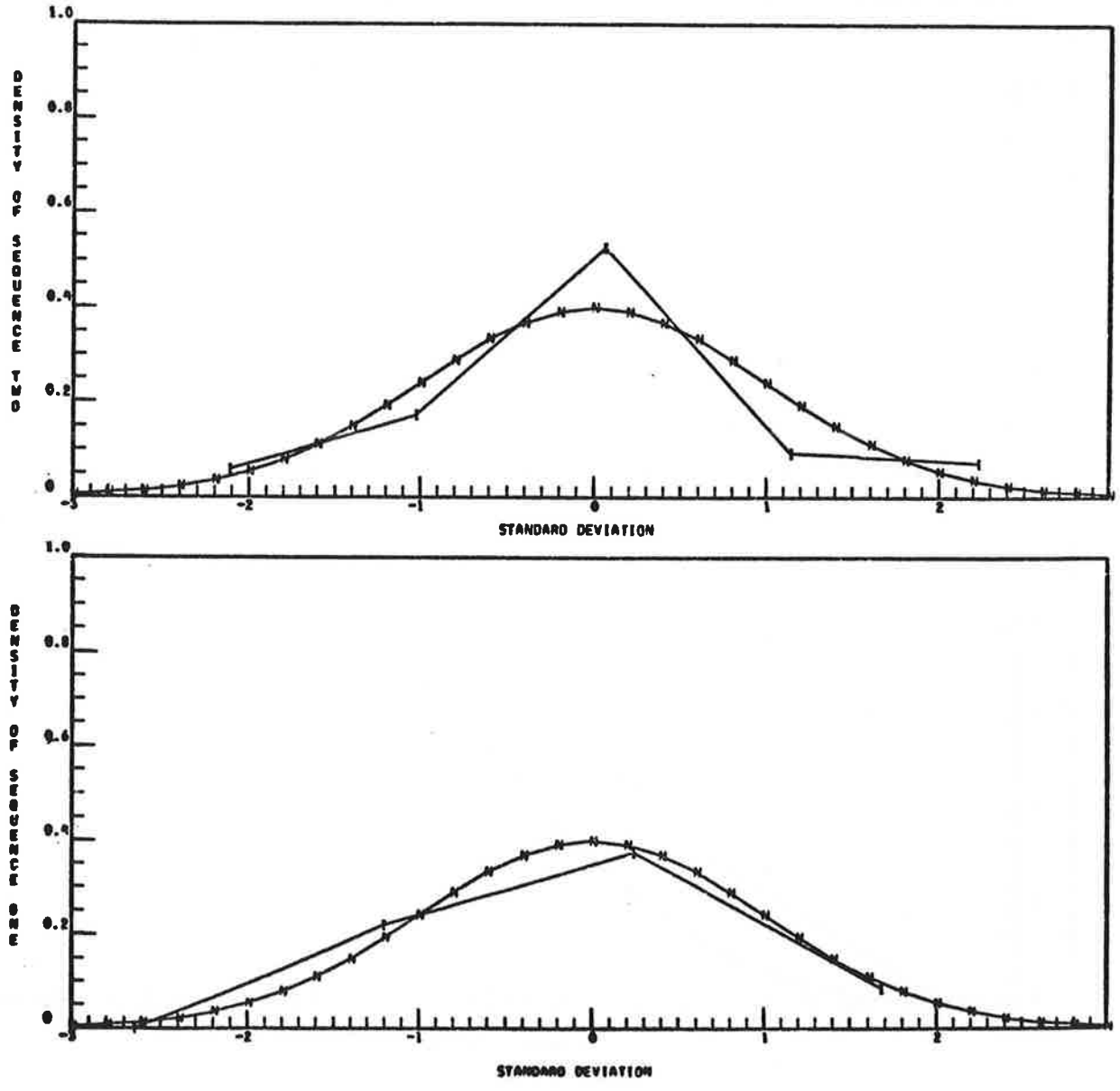


Fig. 4-46 - Probability Distribution of Theoretical Sensor Data Compared to Normal Distributions

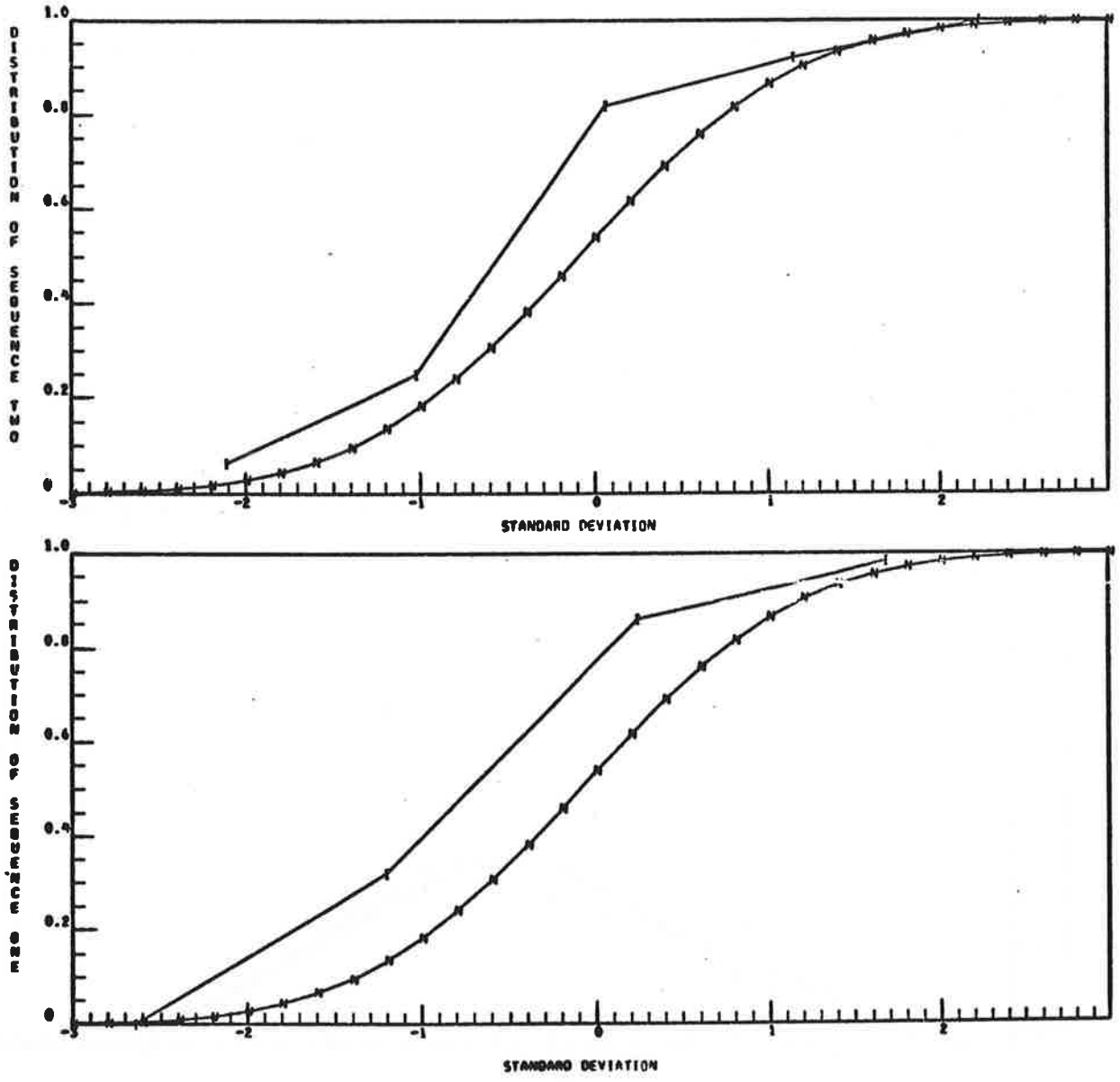


Fig. 4-47 - Cumulative Distribution of Theoretical Sensor Data Compared to Normal Cumulative Distribution

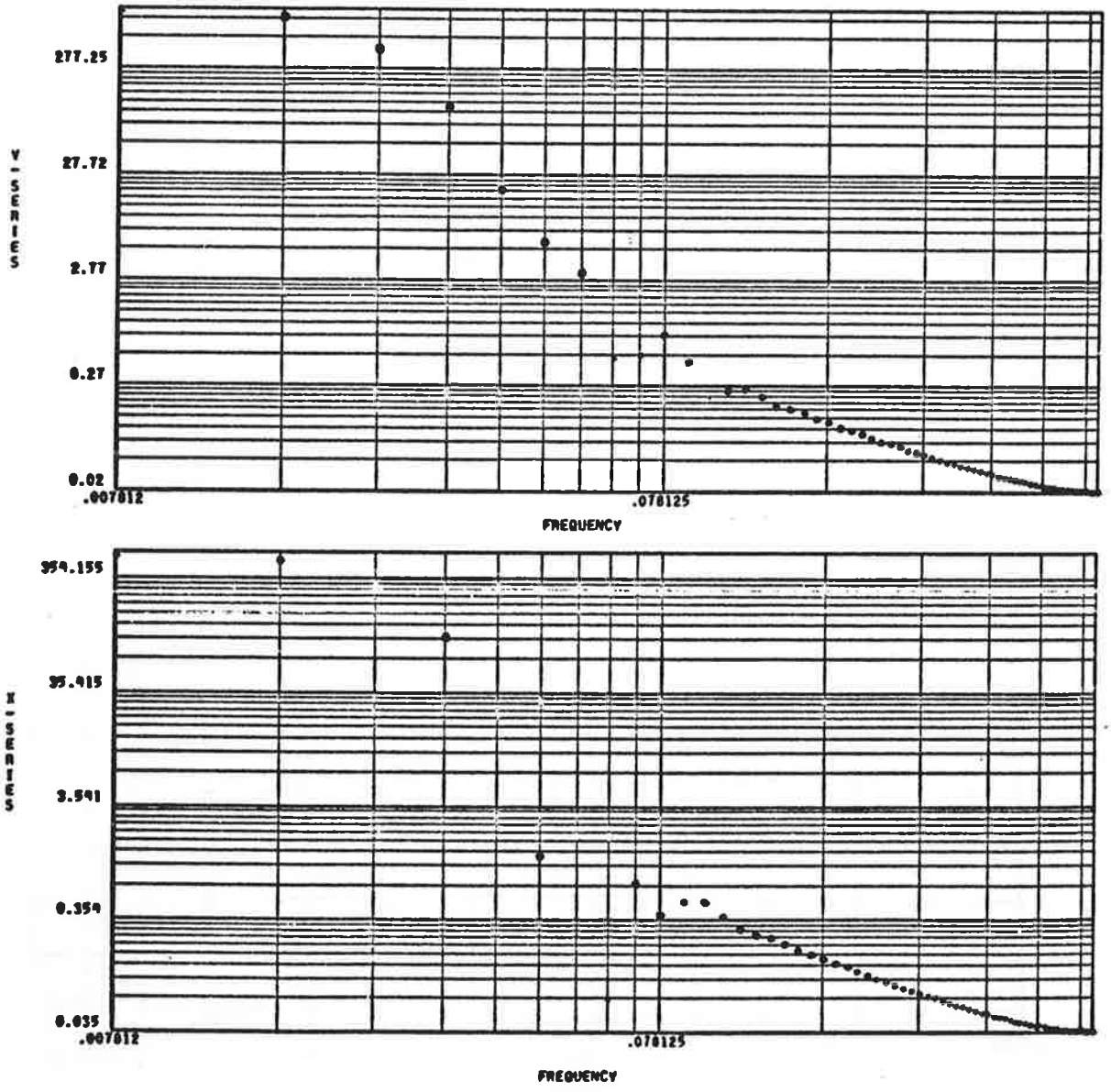


Fig. 4-48 - Power Spectral Density of Theoretical Sensor Data

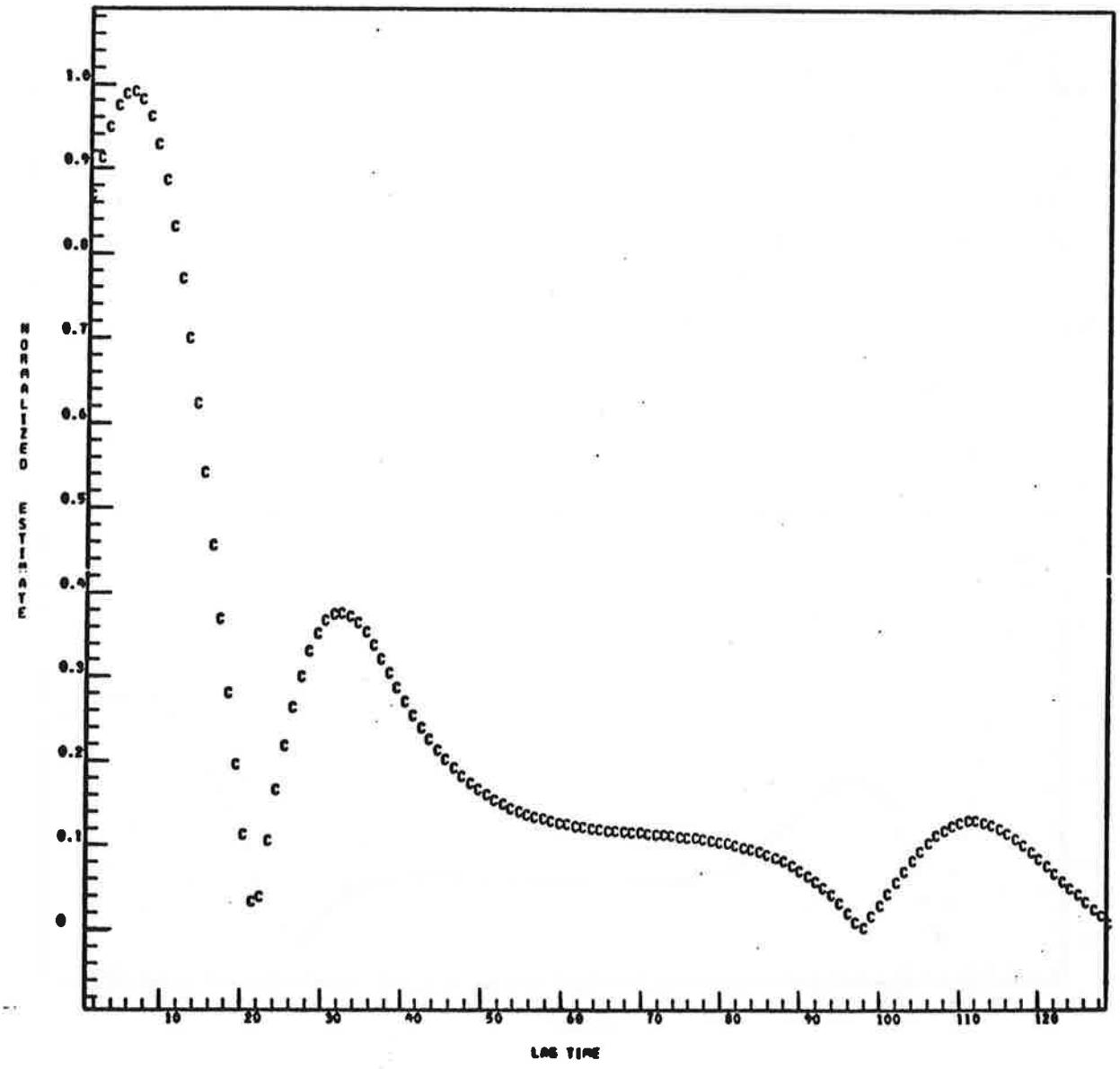


Fig. 4-51 - Cross-Correlation Functions of Theoretical Sensor Data

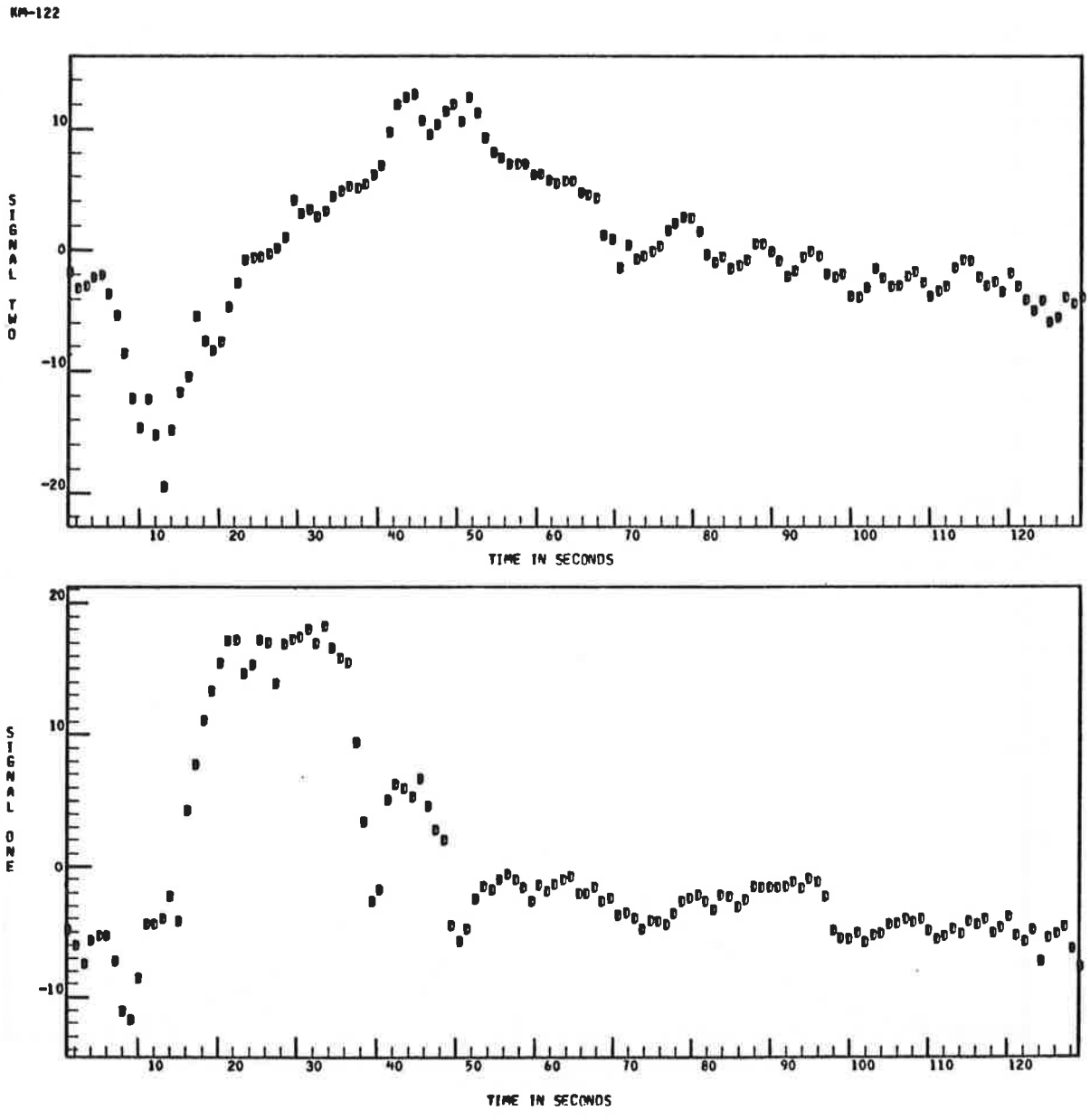


Fig. 4-52 - Actual Groundwind Signatures for Sensors at 200 and 250 ft, Respectively, on Port Side of Sensor Line 1

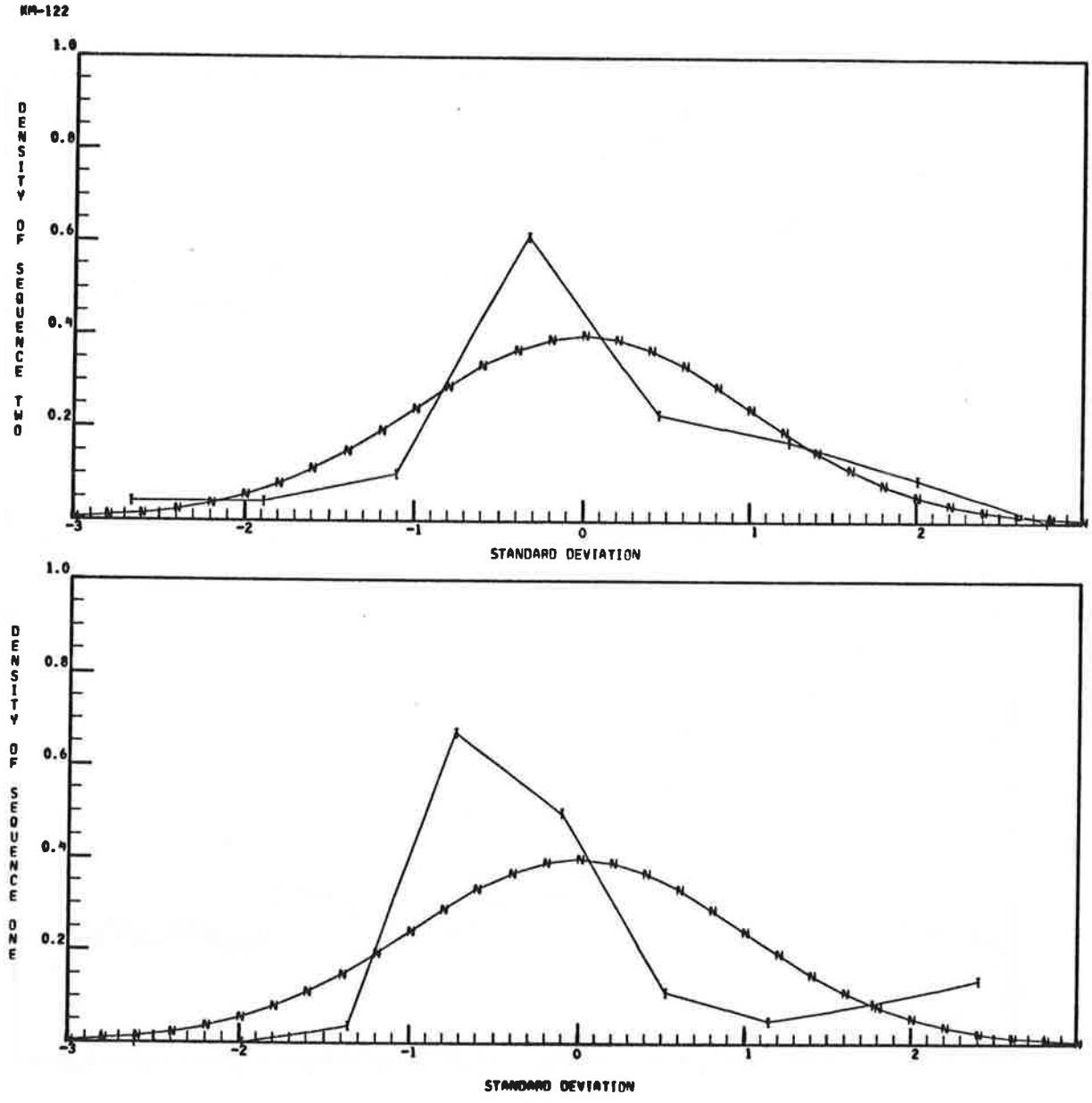


Fig. 4-53 - Probability Distributions of Actual Sensor Data Compared to Normal Distributions

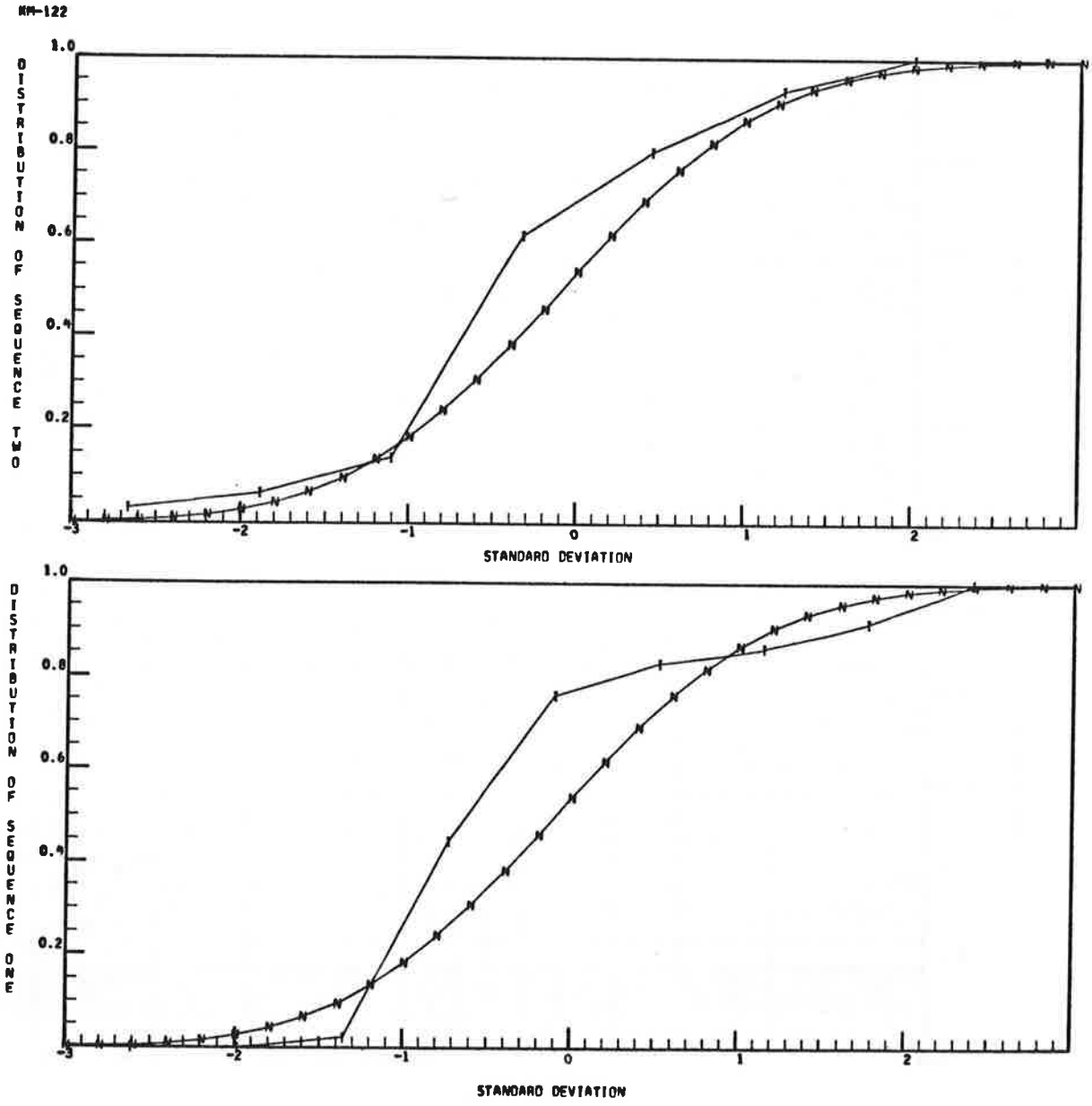


Fig. 4-54 - Cumulative Distributions of Actual Sensor Data Compared to Normal Cumulative Distributions

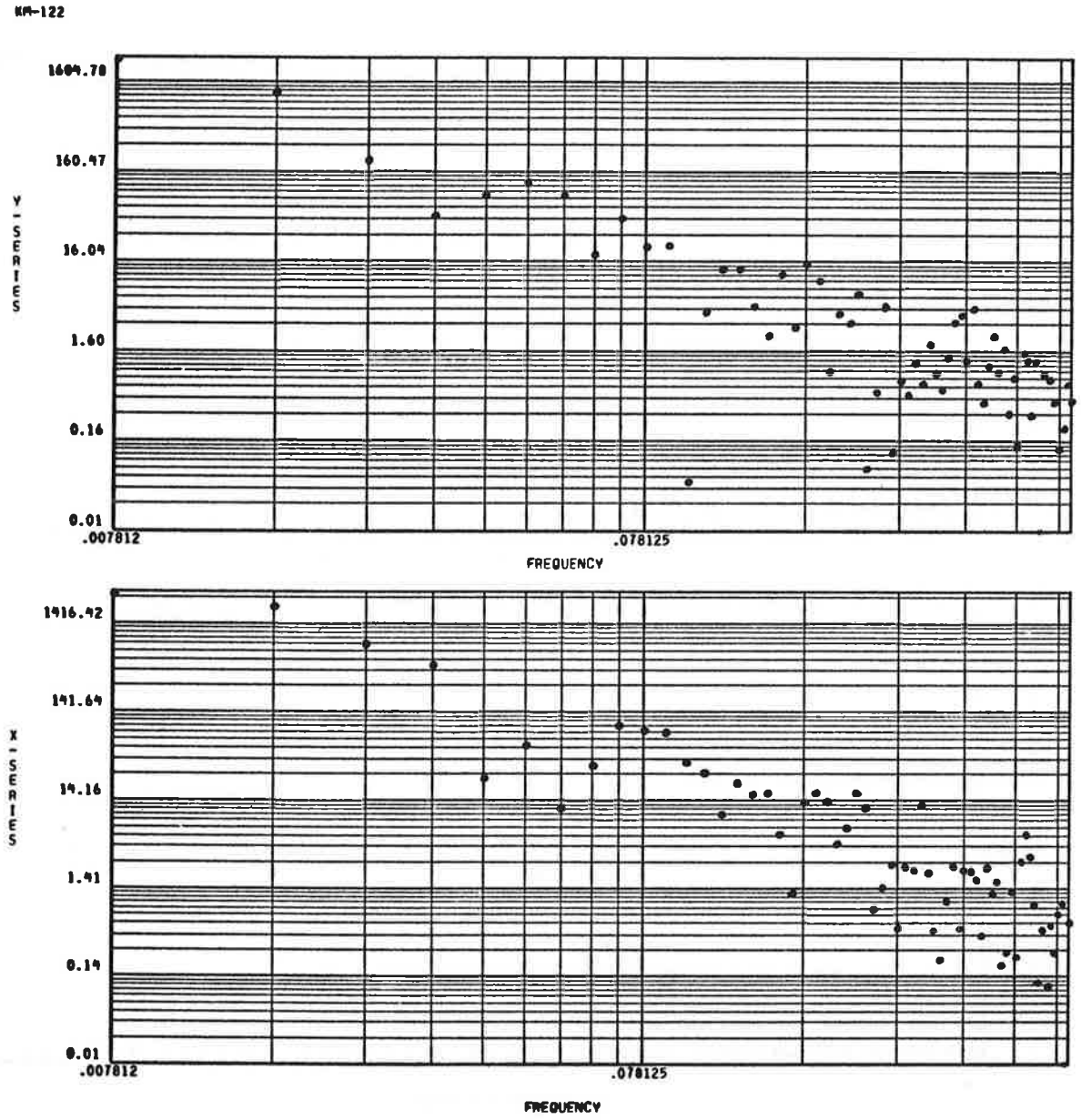


Fig. 4-55 - Power Spectral Density of Actual Sensor Data

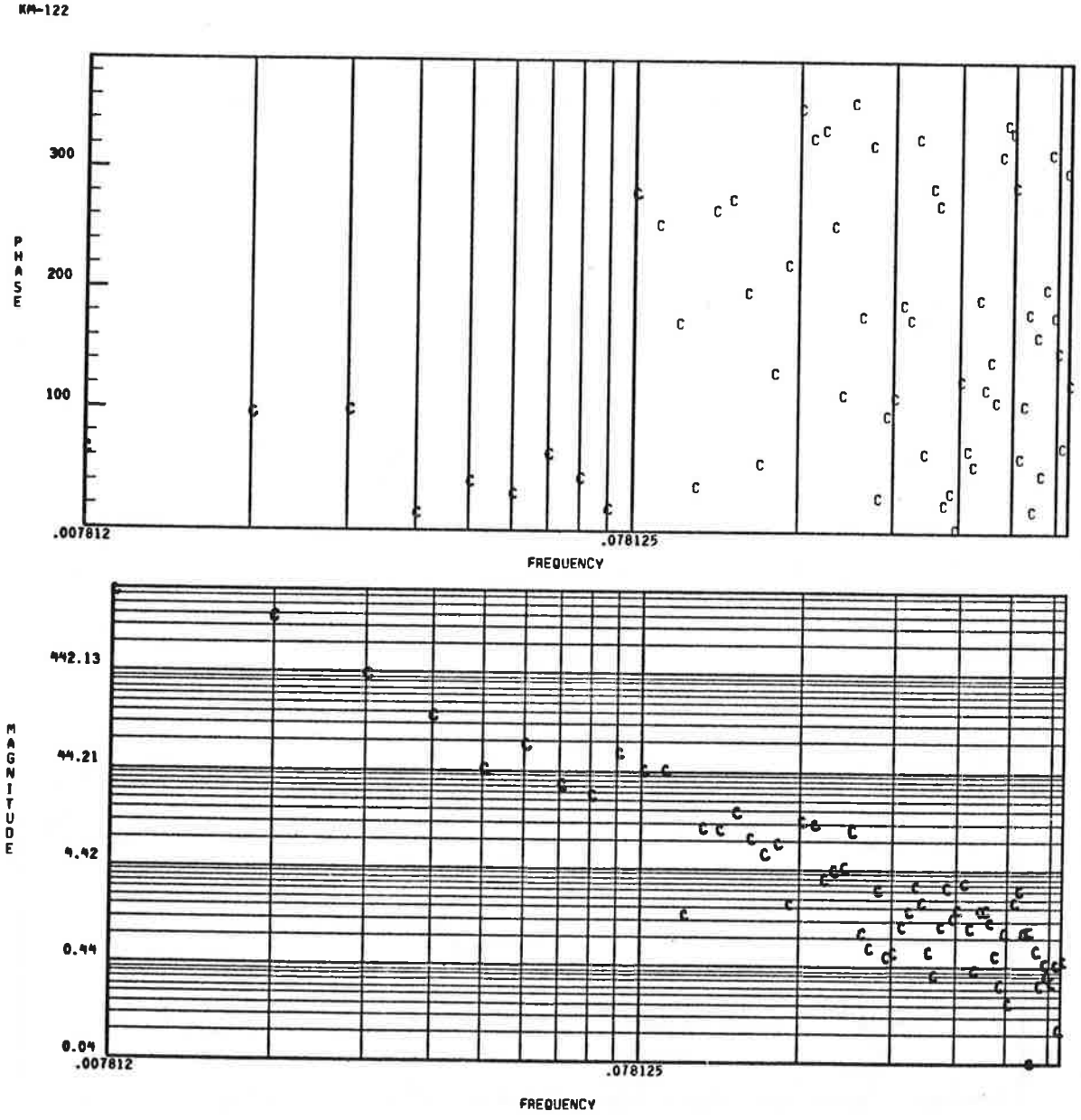


Fig. 4-56 - Cross Spectral Density (Phase and Magnitude) of Actual Sensor Data

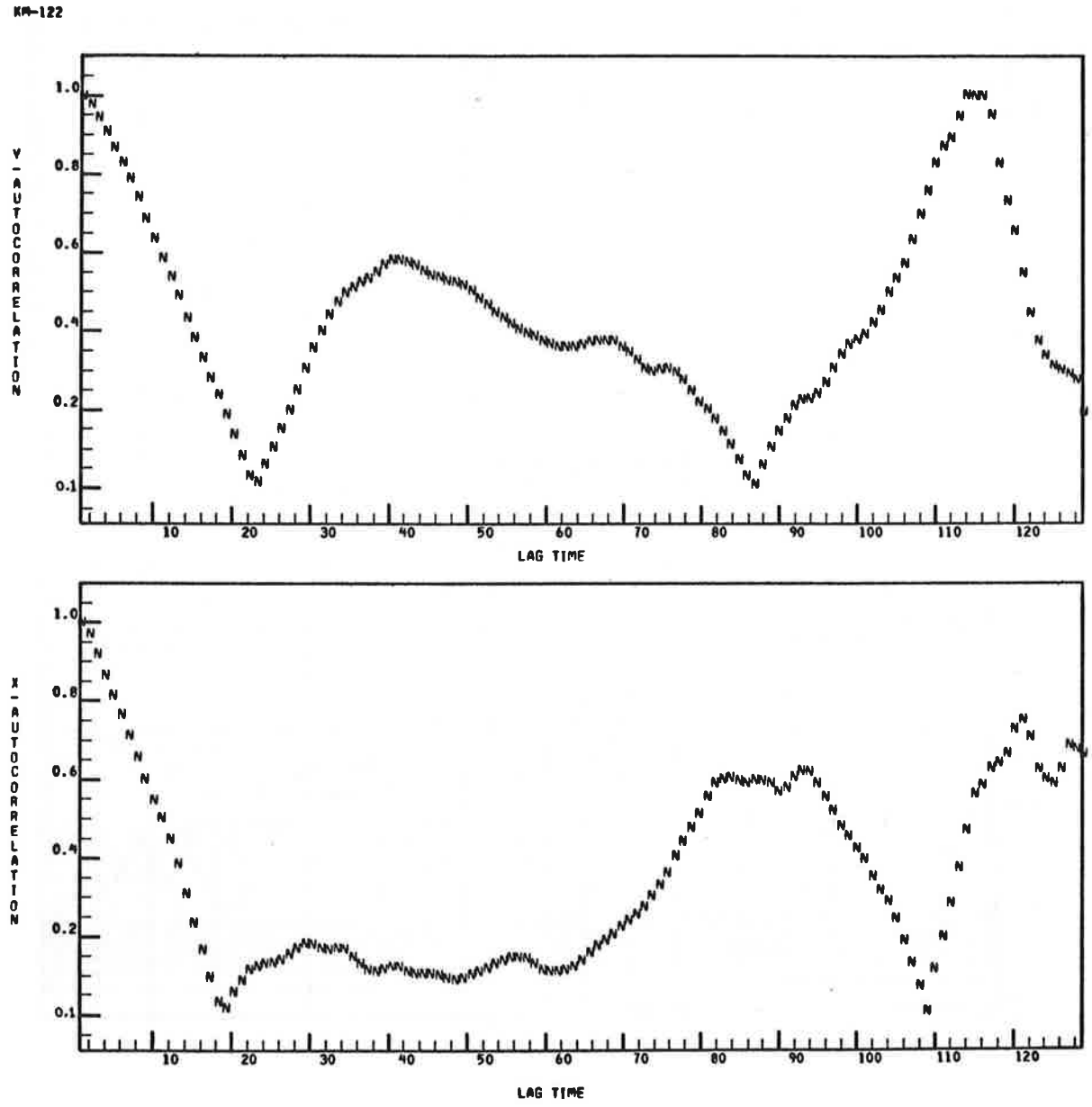


Fig. 4-57 - Autocorrelation Functions of Actual Sensor Data

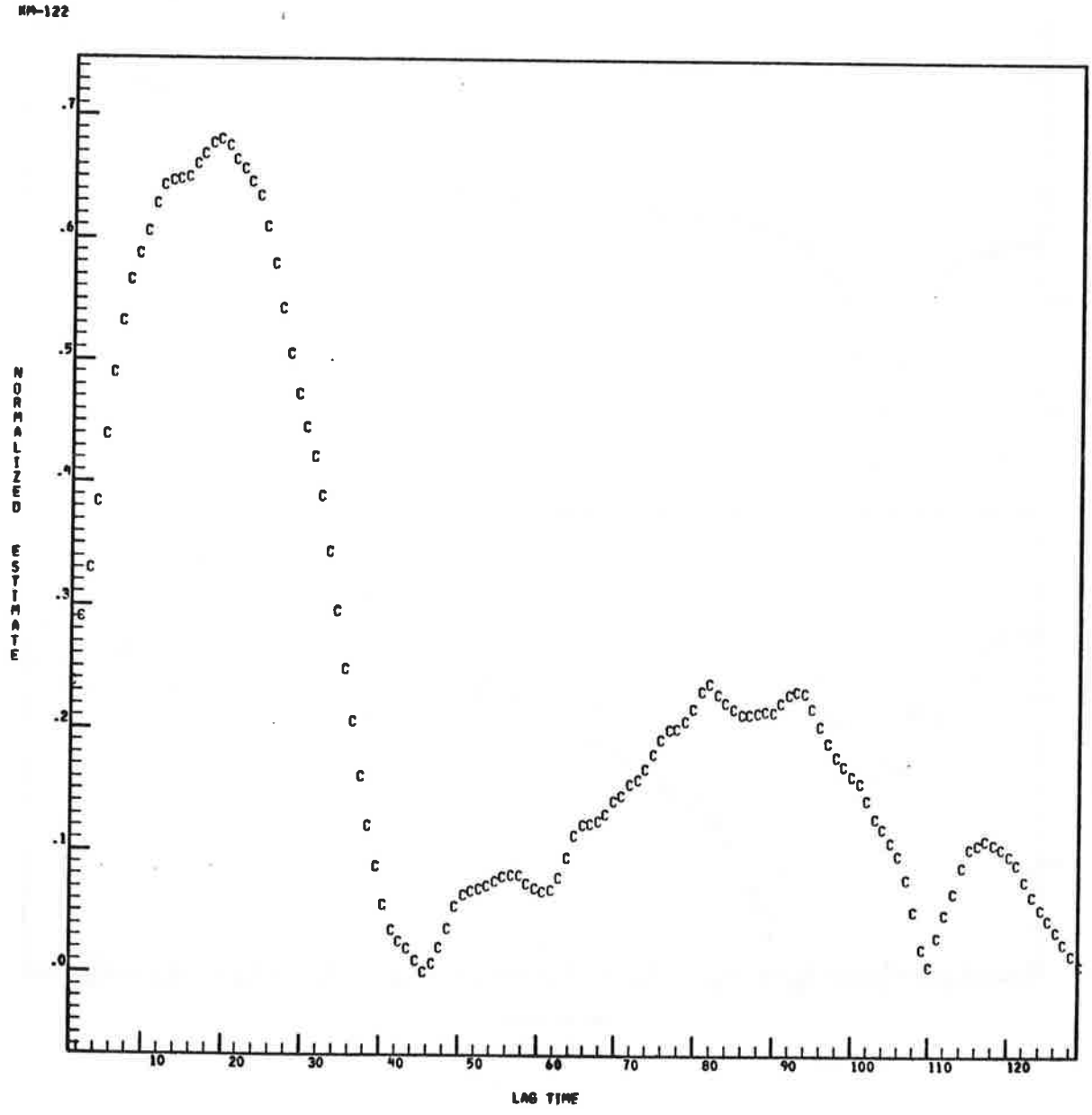


Fig.4-58 - Cross-Correlation Function of Actual Sensor Data

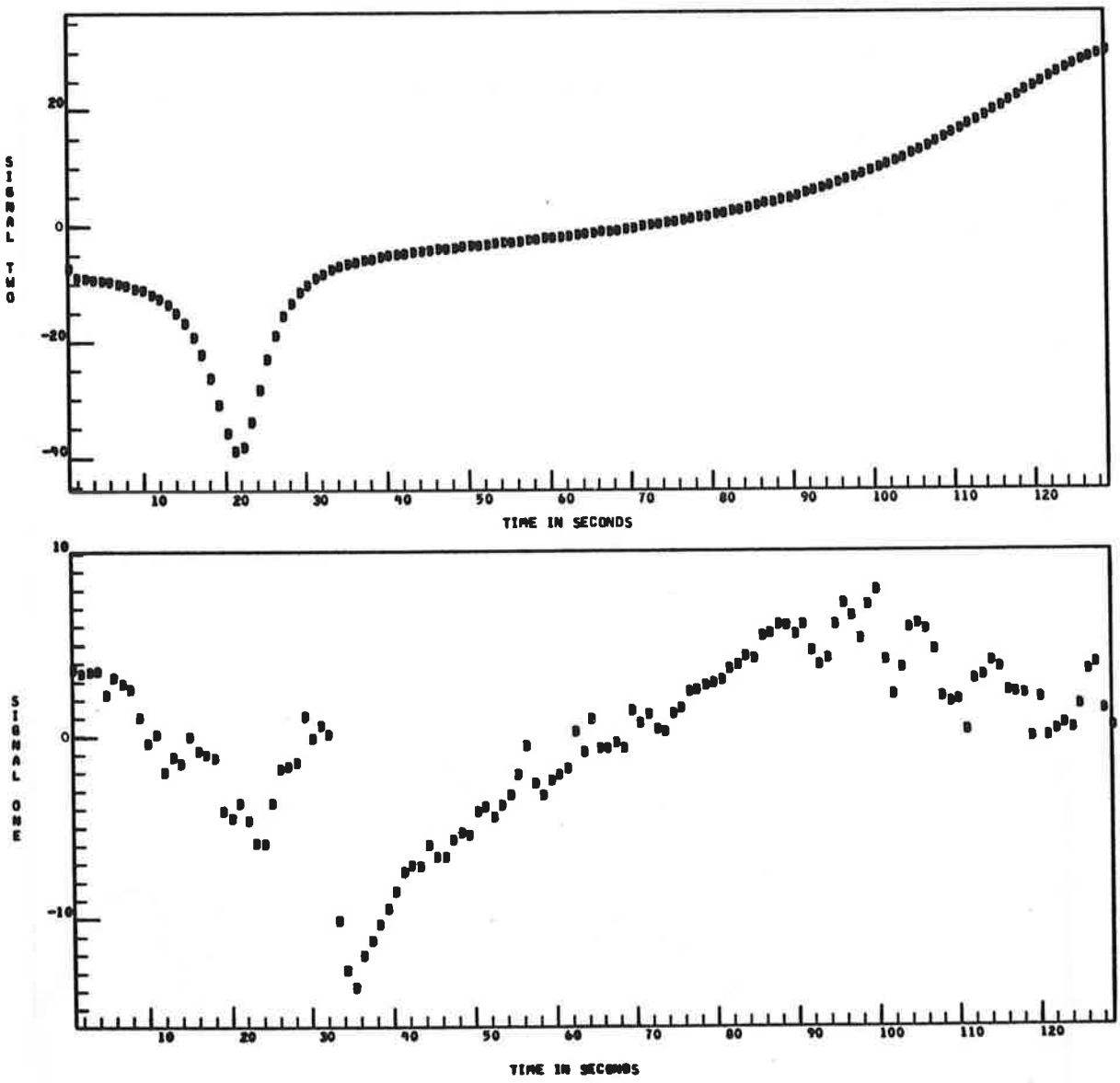


Fig. 4-59 - Comparison of Experimental (Signal 1) and Theoretical (Signal 2) Groundwind Signatures

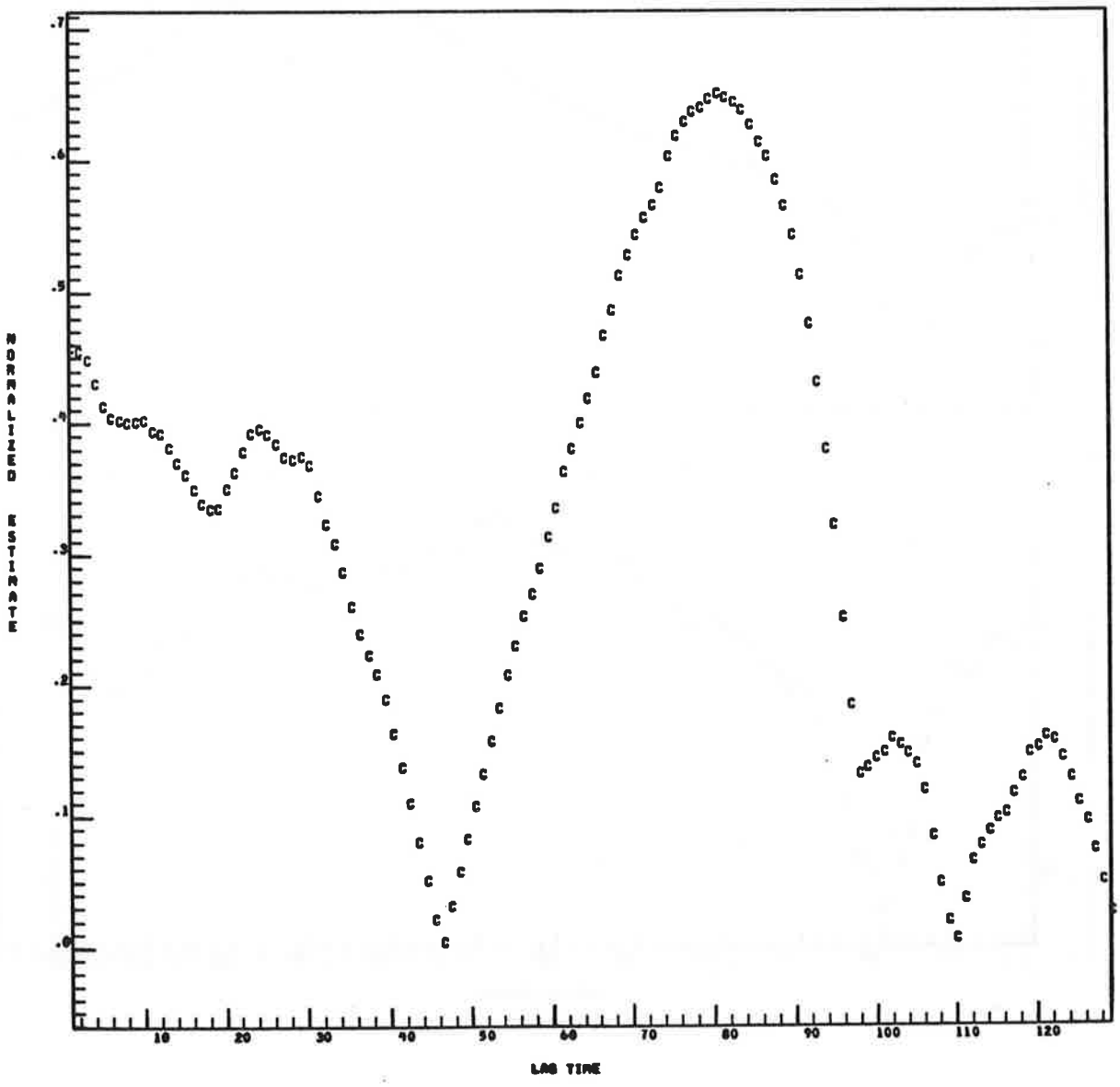


Fig. 4-60 - Cross-Correlation Between Experimental and Theoretical Groundwind Signatures

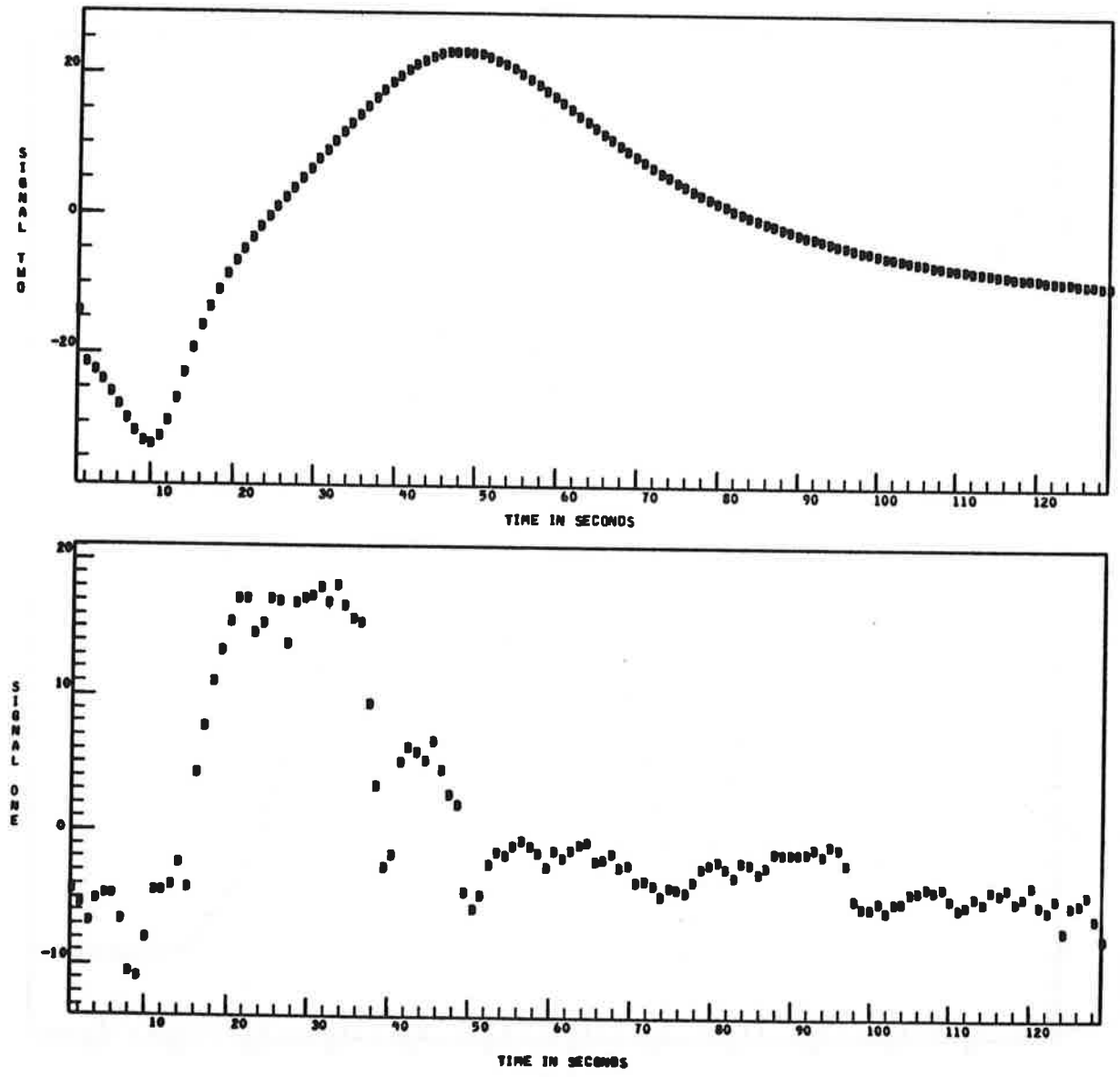


Fig. 4-63 - Comparison of Experimental (Signal 1) and Theoretical (Signal 2) Groundwind Signatures

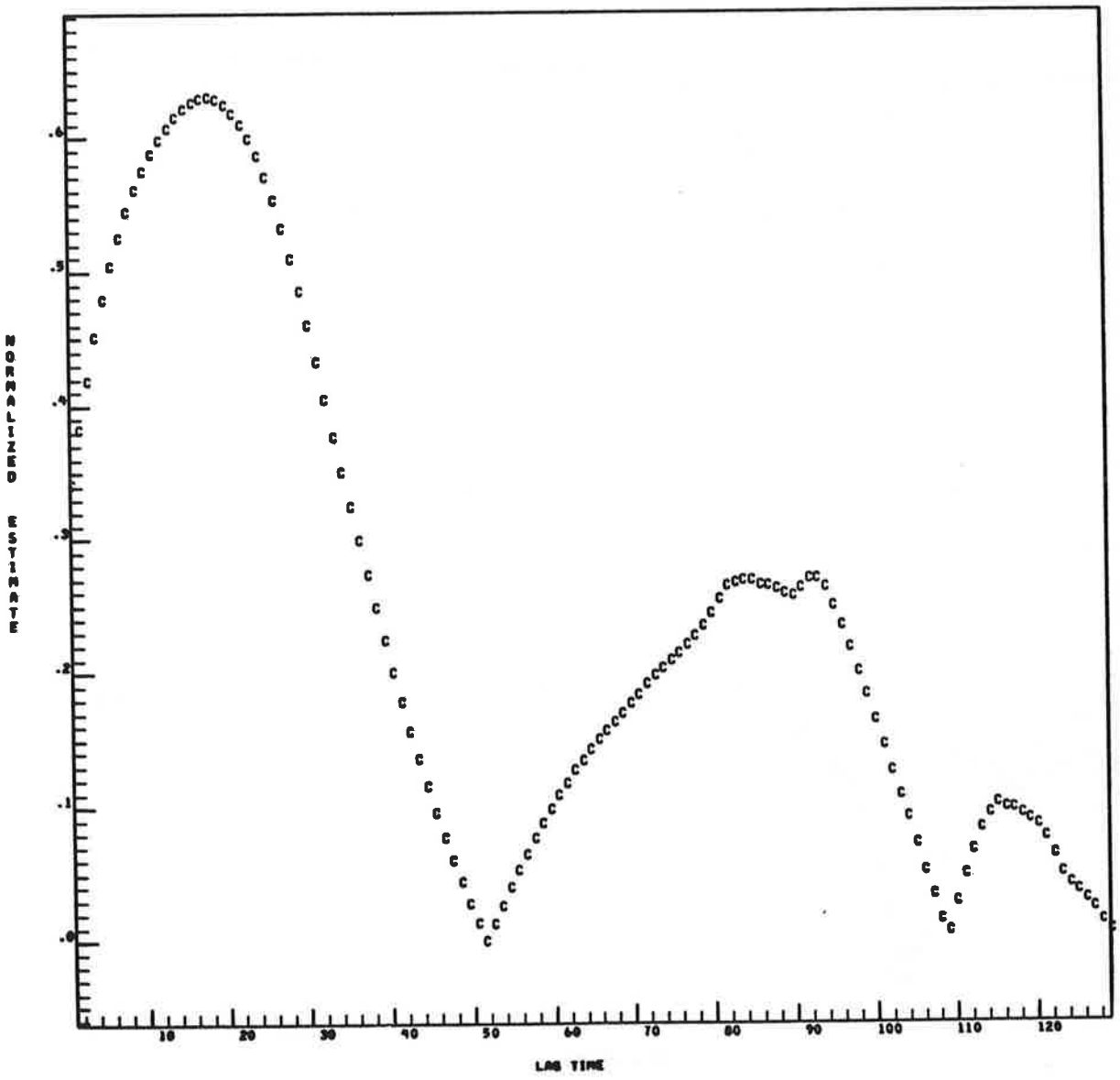


Fig. 4-64 - Cross-Correlation Between Experimental and Theoretical Groundwind Signatures

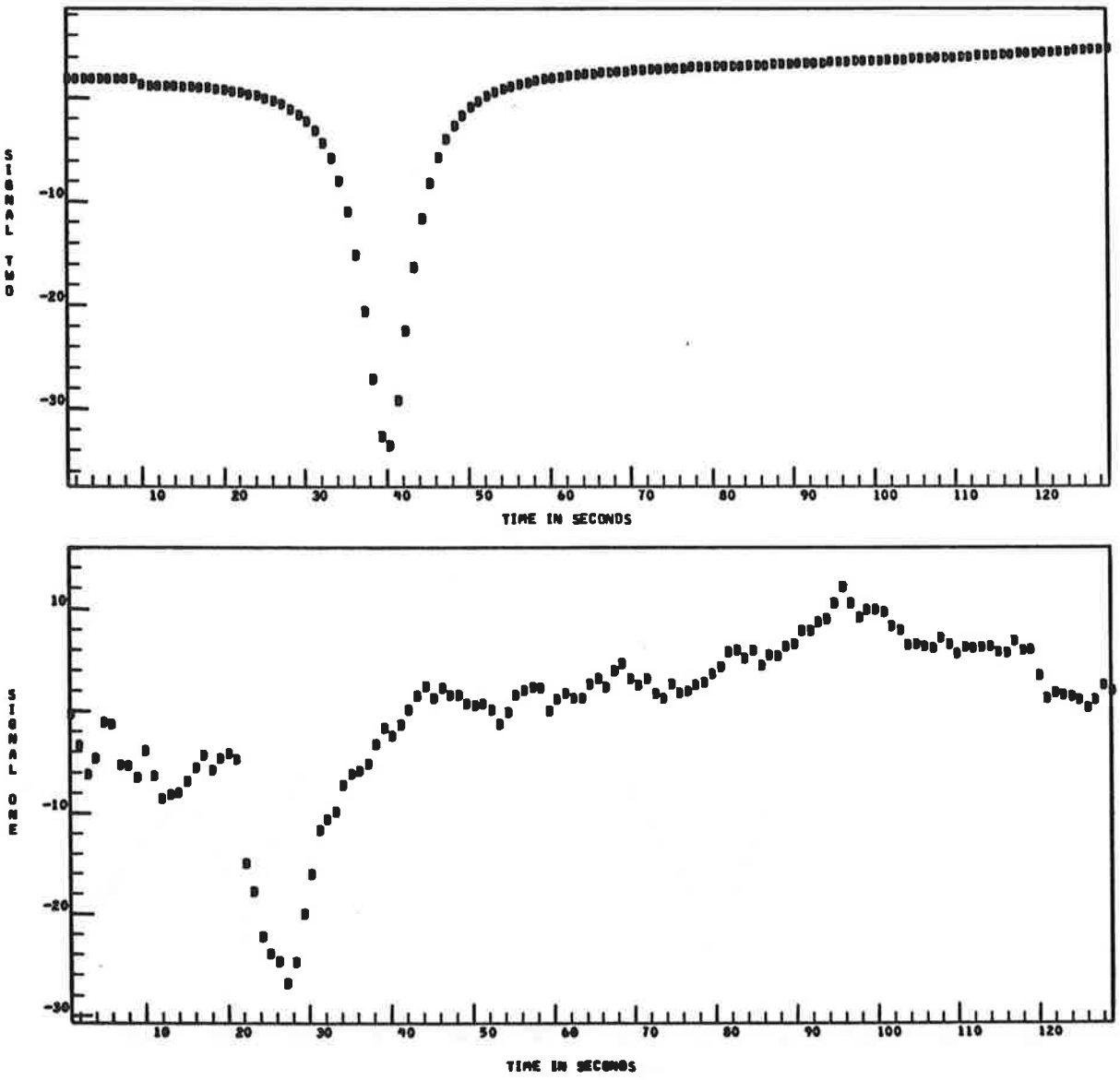


Fig. 4-65 - Comparison of Experimental (Signal 1) and Theoretical (Signal 2) Groundwind Signatures

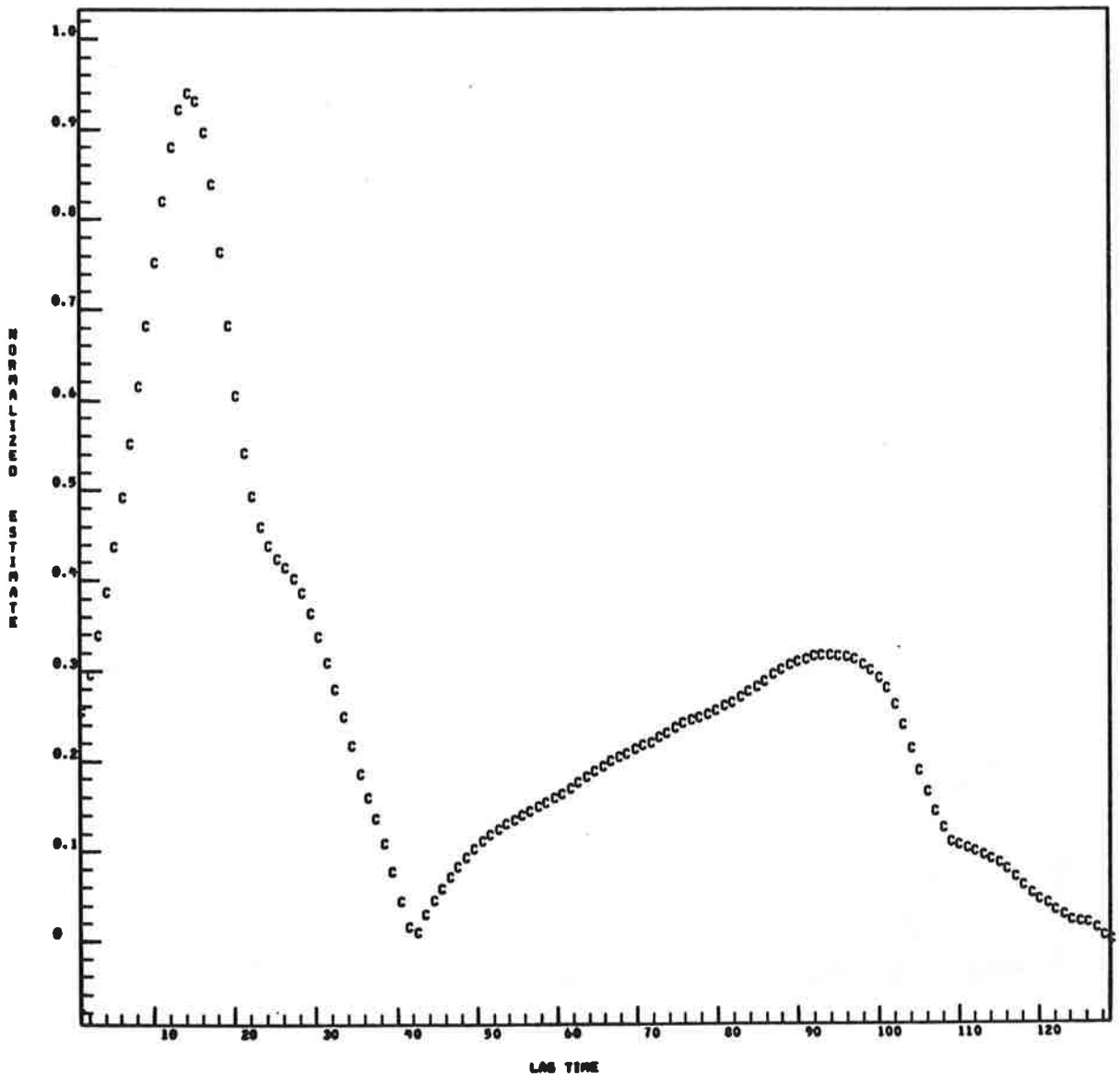


Fig. 4-66 - Cross-Correlation Between Experimental and Theoretical Groundwind Signatures

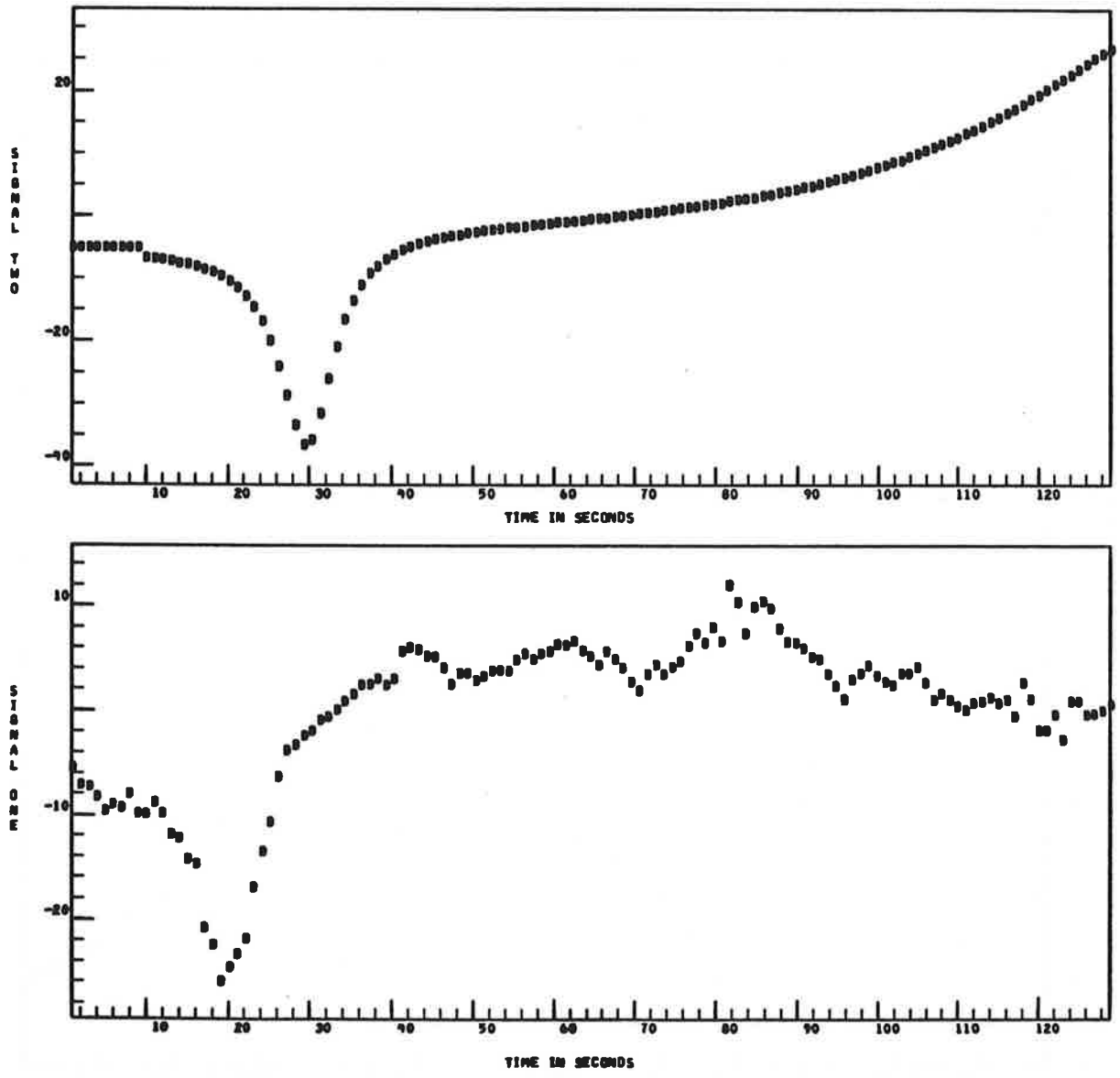


Fig. 4-67 - Comparison of Experimental (Signal 1) and Theoretical (Signal 2) Groundwind Signatures

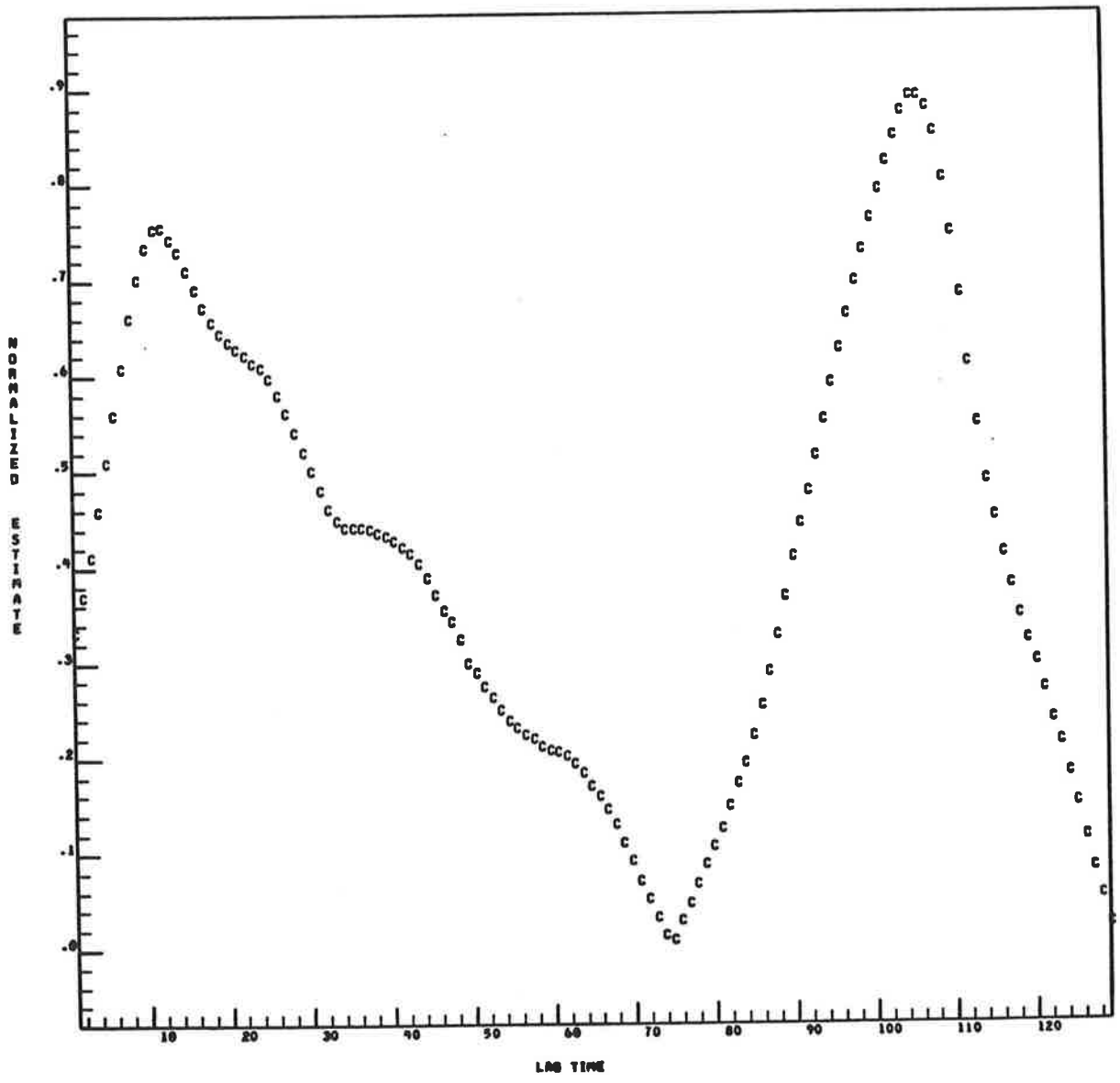


Fig. 4-68 - Cross-Correlation Between Experimental and Theoretical Groundwind Signatures

## 5. ANALYSIS OF METEOROLOGICAL MEASUREMENTS

When the K122 tape was recorded, only the tower 1 meteorological instrumentation was operational. This limited the scope of the analysis of the meteorological data since no temperature lapse rate data were available. Hence, parameters depending on lapse rate, such as Richardson number, could not be computed. The three-component wind data at the 20 and 40-foot elevations were processed by the STAT program to yield mean wind speeds, variances and directions. This information was then processed by the MET program to yield wind profiles, friction velocities, roughness lengths, wind shear and energy dissipation rates. A detailed description of the meteorological measurements and their processing in the MET program are given in Ref. 1. Theoretical wind profiles were computed based on the computed friction velocities, computed roughness lengths and estimated Pasquill class. Results are shown in Figs. 5.1 through 5.6 for the analysis of the meteorological data taken during landing of the Boeing 747 at 0/2/16. The processed data were taken over the 128-second period following passage of the aircraft over sensor line 1. The computer line-printer output data are shown in Fig. 5-1, and plots of the computed wind speed and direction profiles are shown in Figs. 5-2 through 5-6. As shown in Fig. 5-1, a horizontal wind speed profile was computed based on fitting the wind data at the two tower elevations to a power law profile of the form:

$$\frac{\bar{u}}{V_{ref}} = \left(\frac{z}{z_{ref}}\right)^{p} \tag{5.1}$$

where $\bar{u}$ is the horizontal wind speed, z is height above ground level, $Z_{ref}$ is the selected reference height and $V_{ref}$ and p are parameters to be determined in the curve fit. The computed profile is listed in Fig. 5-1 along with the three curve fit parameters. A plot of this profile is shown in Fig. 5-2 compared to the

measured data at the two elevations. A wind direction profile, relative to the runway centerline, was computed based on a linear fit of the data at the two elevations. The computed direction profile is listed in Fig. 5-1 along with the two curve fit constants, and a plot of the direction profile is shown in Fig. 5-3. The vertical wind speed profile was computed based on a quadratic fit which forced a zero vertical velocity at ground level. The computed profile is given in Fig. 5-1 along with the curve fit constants, and a plot of the profile is shown in Fig. 5-4 along with the measured data at the two elevations.

The friction velocity $u^*$ is computed from two different equations. The first is based on an assumed logarithmic wind profile and requires velocity measurements at two elevations:

$$u^* = k \frac{\bar{u}_1 - \bar{u}_2}{\ell n (z_1/z_2)} \tag{5.2}$$

where k is the von Karman constant, 0.4, and $\bar{u}_1$ and $\bar{u}_2$ are the measured velocities at $z_1$ and $z_2$. The second makes use of the measured variance $\sigma_u$ in the wind speed at a single elevation:

$$u^* = \sigma_u/2.5 \tag{5.3}$$

The friction velocity determined from Eq. (5.2) was calculated using the wind speed measurements at the two tower elevations. This value is listed as USTAR(1,2) in Fig. 5-1. Friction velocities based on Eq. (5.3) were calculated for both tower elevations. These values are listed as USTARP(1) for the 20-foot elevation and USTARP(2) for the 40-foot elevation in Fig. 5-1. An average of these three values is listed as the tower 1 value. The friction velocities calculated from Eq. (5.3) are seen to vary by a factor of 2 from the 20-foot elevation to the 40-foot elevation, with the lower elevation value being twice as high as the value calculated from Eq. (5.2).

Roughness lengths $z_o$ were calculated from measured wind speeds at two elevations by assuming a logarithmic profile:

$$\ln z_o = \frac{\frac{\bar{u}_1}{\bar{u}_2} \ln z_2 - \ln z_1}{\bar{u}_1/\bar{u}_2 - 1} \tag{5.4}$$

and from the measured horizontal wind speed $\bar{u}$ and variance in the vertical wind speed $\sigma_w$ at a single elevation:

$$\ln z_o = \ln z - 0.5 \frac{\bar{u}}{\sigma_w} \tag{5.5}$$

The value computed from Eq. (5.4) is listed in Fig. 5-1 as ZO(1, 2), and the values computed from Eq. (5.5) are listed as ZO P(1) for the 20-foot elevation and ZO P(2) for the 40-foot elevation. A large variation is noted in the three computed values. As with the friction velocties, an average of the three values is listed in Fig. 5-1 as the tower 1 value.

A gradient of the horizontal wind velocity was computed from

$$\frac{d\bar{u}}{dz} = \frac{\bar{u}_2 - \bar{u}_1}{z_2 - z_1} \tag{5.6}$$

and is listed in Fig. 5-1 as VGRAD (1, 2).

Theoretical wind profiles were calculated based on a Pasquill class power law profile and a logarithmic profile. The Pasquill class power law constant was selected from the "average cloudiness" Pasquill class criteria (Ref. 4):

Table 5-1
AVERAGE CLOUDINESS PASQUILL CLASS CRITERIA

| Wind Speed (m/sec) | < 2 | 2-4 | 4-6 | >6 |
|---|---|---|---|---|
| Pasquill Class | A | B | C | D |
| Power Law Constant | .15 | .17 | .20 | .26 |

where the wind speed for use in Table 5-1 was obtained by extrapolating the previously obtained power law profile to the 10-foot elevation. This extrapolated wind velocity was also taken as the reference velocity $V_{ref}$ at the 10-foot reference altitude $z_{ref}$. The computed Pasquill class profile is listed in Fig. 5-1 along with the three parameters $V_{ref}$, $z_{ref}$ and the Pasquill class power-law constant which is listed as PPASQ. Note that the Pasquill class power-law constant value 0.17 compares rather closely with the fitted power law value 0.20. A plot of the Pasquill class profile is shown in Fig. 5-5 compared with the two measured values. The Pasquill class profile is seen to fit the two measured values very closely and to compare very well with the fitted power-law profile (Fig. 5-2).

A theoretical logarithmic wind profile was calculated from

$$\frac{\bar{u}}{u^*} = \frac{1}{k} \ell n \frac{z}{z_o} \tag{5.7}$$

where the friction velocity and roughness length were taken as the previously obtained averaged tower 1 data. The computed profile is listed in Fig. 5-1, and a plot of the profile is shown in Fig. 5-6. The logarithmic profile based on the previously obtained average roughness length and friction velocity is seen to not compare well with the measured data and fitted power curve in Fig. 5-2 or the Pasquill class profile in Fig. 5-5.

Wind shear gradients of the three-component wind data were obtained by taking differences for all three components as in Eq. (5.6). The U, V and W components are in the directions along the extended runway centerline aft of the landing aircraft, normal to the runway to the starboard side, and in the vertical direction upward, respectively. The computed values are listed in Fig. 5-1 as DUDZ(1, 2), DVDZ(1, 2) and DWDZ(1, 2).

The turbulent energy dissipation rates, $\epsilon$, were calculated by using three different equations for both tower elevations (20 and 40-foot) where wind velocity data were taken. The three equations are

$$\epsilon^{1/3} = \frac{u^*}{k^{1/3} z^{1/3}} \tag{5.8}$$

where $u^*$ has been previously determined,

$$\epsilon^{1/3} = \frac{1}{2^{1/3}} \frac{\bar{u} k^{2/3}}{\ell n (z/z_o)} \tag{5.9}$$

which is the equivalent of Eq. (5.8), assuming a logarithmic profile, and

$$\epsilon^{1/3} = \frac{\sigma_u}{2.5 k^{1/3} z^{1/3}} \tag{5.10}$$

which is also equivalent to Eq. (5.8), assuming the relation

$$u^* = \sigma_u / 2.5 \tag{5.11}$$

The computed $\epsilon^{1/3}$ values are listed in Fig. 5-1, with EPS13A, EPS13C and EPS13D corresponding to Eqs. (5.8), (5.9) and (5.10), respectively; and I = 1 and 2 corresponding to the 20 and 40-foot tower elevations, respectively. The EPS13B label is extended for an $\epsilon^{1/3}$ calculation taking into account Richardson number. Since the required temperature lapse rate measurements were not taken during this test series, this calculation was not made, and the computer printed zero for these values.

The friction velocity $u^*$ at a given location is defined as the square root of the cross-correlation between the horizontal and vertical components of wind velocity at that location. These cross-correlations were made for the measured horizontal and vertical wind data at the two tower elevations. Shown in Fig. 5-7 are the measured horizontal and vertical components at the 20-foot elevation for the 128-second time interval following passage of the Boeing 747 over sensor line 1 at 0/2/16. The cross correlation is given in Fig. 5-8. The data are normalized to $\sqrt{RX0*RY0}$, where RX0 and RY0 are the autocorrelations of the two separate curves at zero lag time. From the cross correlation at zero lag time, a friction velocity of 0.230 feet/second is determined for the 20-foot elevation. Performing a similar analysis of the 40-foot elevation data (Figs. 5-9 and 5-10) yields a friction velocity of 0.659 feet/second. Although these values are not as nearly equal as one might hope for, since the friction velocity is generally assumed to be constant at all elevations, they are certainly within the same order of magnitude, and they compare favorably with the friction velocity of 0.7946 feet/second determined from Eq. (5.2) (See Fig. 5-1, USTAR(1, 2)).

As pointed out in the preceding paragraphs, some of the meteorological parameters have widely different values depending on the method of calculation. It may be determined during the course of the wake vortex test program or in the analysis of data that many of these parameters are of no real value in correlating wake vortex transport behavior to meteorological conditions, and these parameters may be disposed of in the data analysis program. Of those parameters determined to be of value, the most appropriate method of calculations must be determined by an analysis of test data.

```
HORIZONTAL WIND SPEED PROFILE

  ALTITUDE,FT   VELOCITY,FT/SEC

    .0000           .0000
   .1000+02        .8121+01
   .2000+02        .9297+01
   .3000+02        .1006+02
   .4000+02        .1064+02
   .5000+02        .1112+02
   .6000+02        .1152+02
   .7000+02        .1187+02
   .8000+02        .1219+02
   .9000+02        .1247+02
   .1000+03        .1273+02
   .1100+03        .1297+02
   .1200+03        .1319+02
   .1300+03        .1340+02
   .1400+03        .1359+02

  VREF=  .8121+01 FT/SEC,  ZREF=  .1000+02 FT,  P=  .20

WIND DIRECTION PROFILE

  ALTITUDE,FT   DIRECTION, DEGREES

    .0000          -.7512+02
   .1000+02        -.7556+02
   .2000+02        -.7600+02
   .3000+02        -.7644+02
   .4000+02        -.7688+02
   .5000+02        -.7732+02
   .6000+02        -.7776+02
   .7000+02        -.7820+02
   .8000+02        -.7864+02
   .9000+02        -.7908+02
   .1000+03        -.7953+02
   .1100+03        -.7997+02
   .1200+03        -.8041+02
   .1300+03        -.8085+02
   .1400+03        -.8129+02

  COEF(1)= -.7512+02

  COEF(2)= -.4407-01

VERTICAL WIND SPEED PROFILE

  ALTITUDE,FT   VELOCITY,FT/SEC

    .0000           .0000
   .1000+02        -.2087+00
```

**Fig. 5-1 - MET Program Line Printer Output**

```
   .8000+02          .1177+02
   .9000+02          .1201+02
   .1000+03          .1222+02
   .1100+03          .1242+02
   .1200+03          .1261+02
   .1300+03          .1278+02
   .1400+03          .1294+02

  VREF=  .8121+01 FT/SEC,  ZREF=  .1000+02 FT,  PPASQ=  .17

THEORETICAL WIND PROFILES

  * LOG PROFILE (NEUTRAL STABILITY)

  ALTITUDE,FT  VELOCITY,FT/SEC

   .0000            .0000
   .1000+02         .2067+02
   .2000+02         .2352+02
   .3000+02         .2519+02
   .4000+02         .2637+02
   .5000+02         .2729+02
   .6000+02         .2804+02
   .7000+02         .2867+02
   .8000+02         .2922+02
   .9000+02         .2971+02
   .1000+03         .3014+02
   .1100+03         .3053+02
   .1200+03         .3089+02
   .1300+03         .3122+02
   .1400+03         .3152+02

U,V,W WIND SHEAR

  DUDZ(1,2)=  .6376-02  FT/SEC/FT

  DVDZ(1,2)=  .3007+00  FT/SEC/FT

  DWDZ(1,2)=  .3376-01  FT/SEC/FT

  * TOWER1  DUDZ=  .6374-02  DVDZ=  .3007+00  DWDZ=  .3376-01  FT/SEC/FT

DISSIPATION RATE

  I      EPS13A      EPS13B      EPS13C      EPS13D

  1    .3227+00    .0000       .3252+00    .7175+00  FT**(2/3)/SEC
  2    .6062+00    .0000       .2470+00    .9971+00  FT**(2/3)/SEC
```

Fig. 5-1 (Continued)

```
   .2000+02        -.2951+00
   .3000+02        -.3614+00
   .4000+02        -.4173+00
   .5000+02        -.4666+00
   .6000+02        -.5111+00
   .7000+02        -.5521+00
   .8000+02        -.5902+00
   .9000+02        -.6260+00
   .1000+03        -.6599+00
   .1100+03        -.6921+00
   .1200+03        -.7228+00
   .1300+03        -.7524+00
   .1400+03        -.7808+00

  COEF(1)=  .0000

  COEF(2)=  .0000

  COEF(3)= -.6599-01

FRICTION VELOCITY

  USTAR(1,2)=  .7946+00  FT/SEC

  USTARP(1)=  .1435+01  USTARP(2)=  .2706+01  FT/SEC

  TOWER 1      .165+01  FT/SEC

ROUGHNESS LENGTH

  Z0(1,2)=  .1856+00  FT

  ZOP(1)=  .9253-02  ZOP(2)=  .2307-02  FT

  TOWER 1      .657-01  FT

GRADIENT OF HORIZONTAL WIND COMPONENT

  VGRAD(1,2)=  .6068-01  VGRAD

  TOWER 1      .607-01  FT/SEC/FT

PASQUIL CLASS WIND PROFILE

  ALTITUDE,FT  VELOCITY,FT/SEC

   .0000          .0000
   .1000+02       .3263+01
   .2000+02       .9297+01
   .3001+02       .9960+01
   .4000+02       .1046+02
   .5000+02       .1086+02
   .6000+02       .1121+02
   .7000+02       .1150+02
```

Fig. 5-1 - (Concluded)

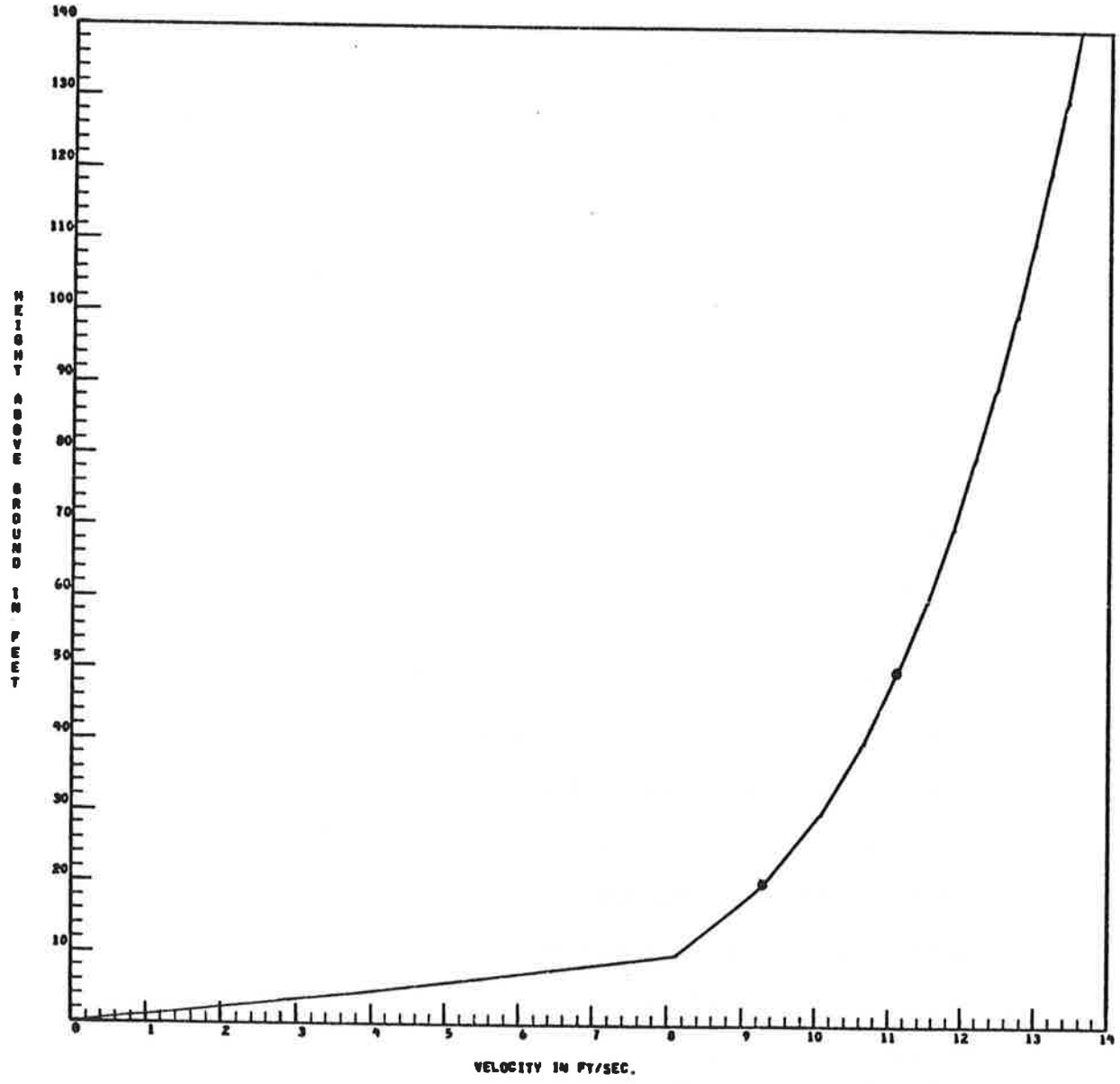


Fig. 5-2 - Horizontal Wind Speed Profile

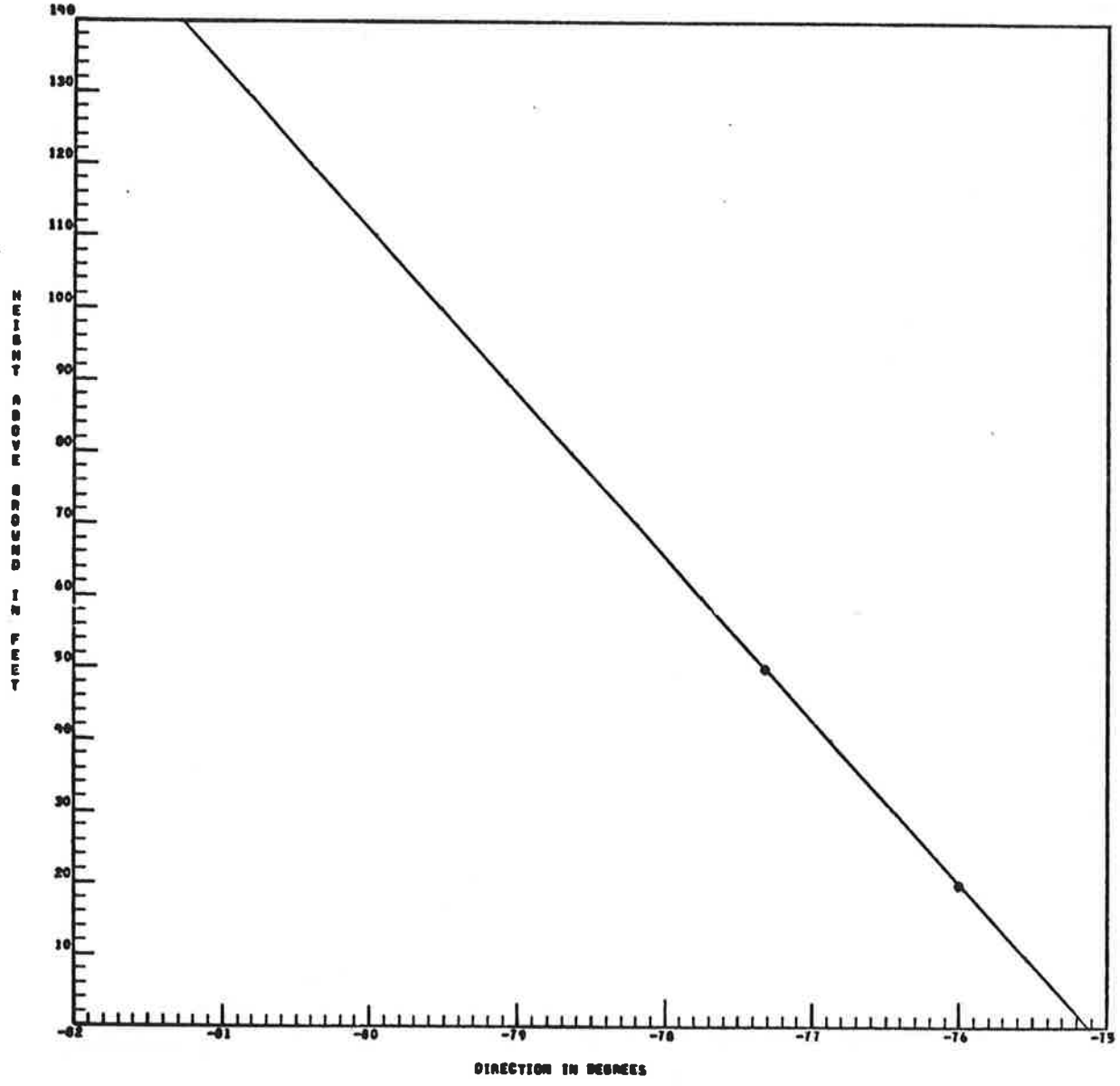


Fig. 5-3 - Wind Direction Profile

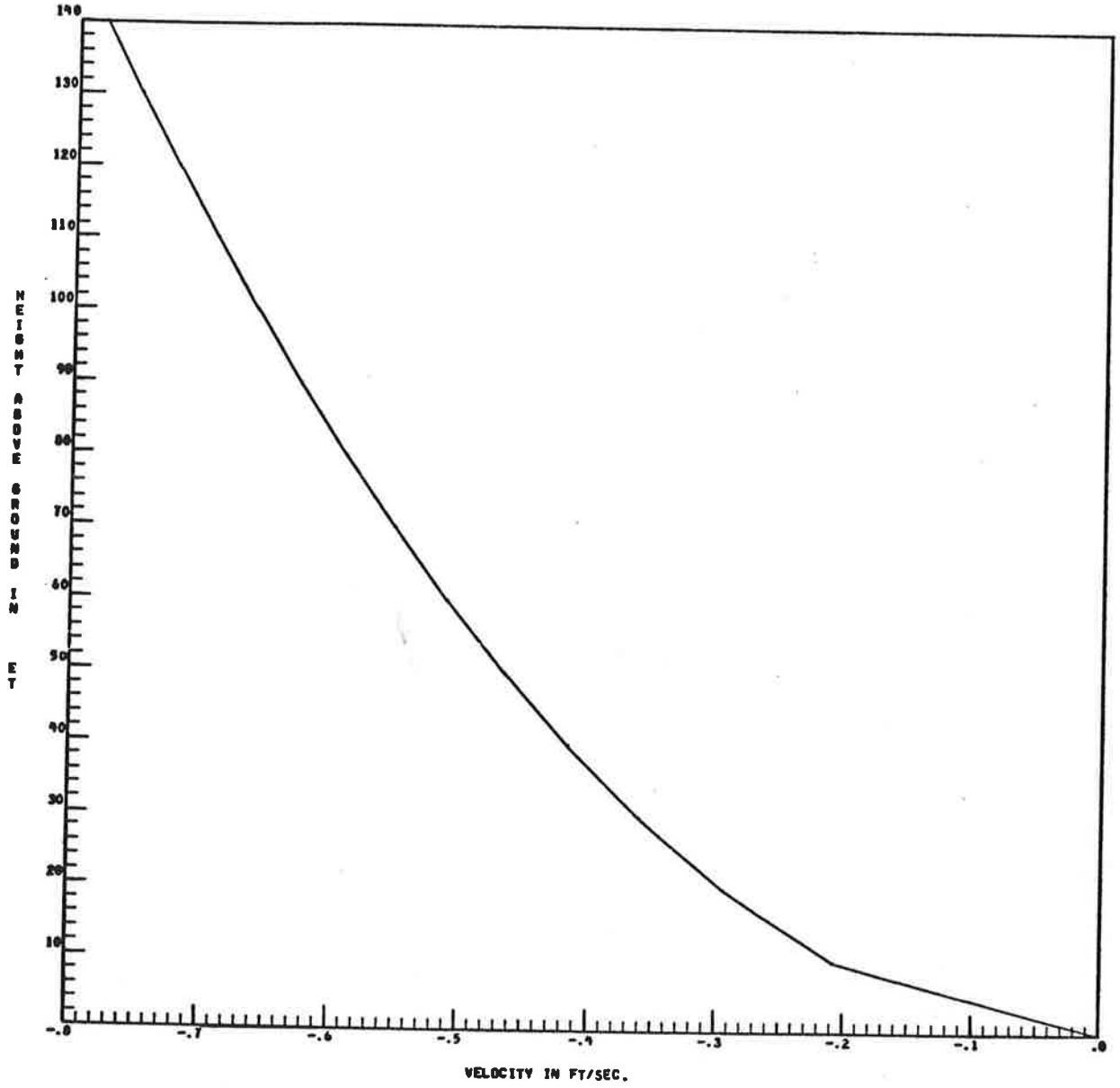


Fig. 5-4 - Vertical Wind Profile

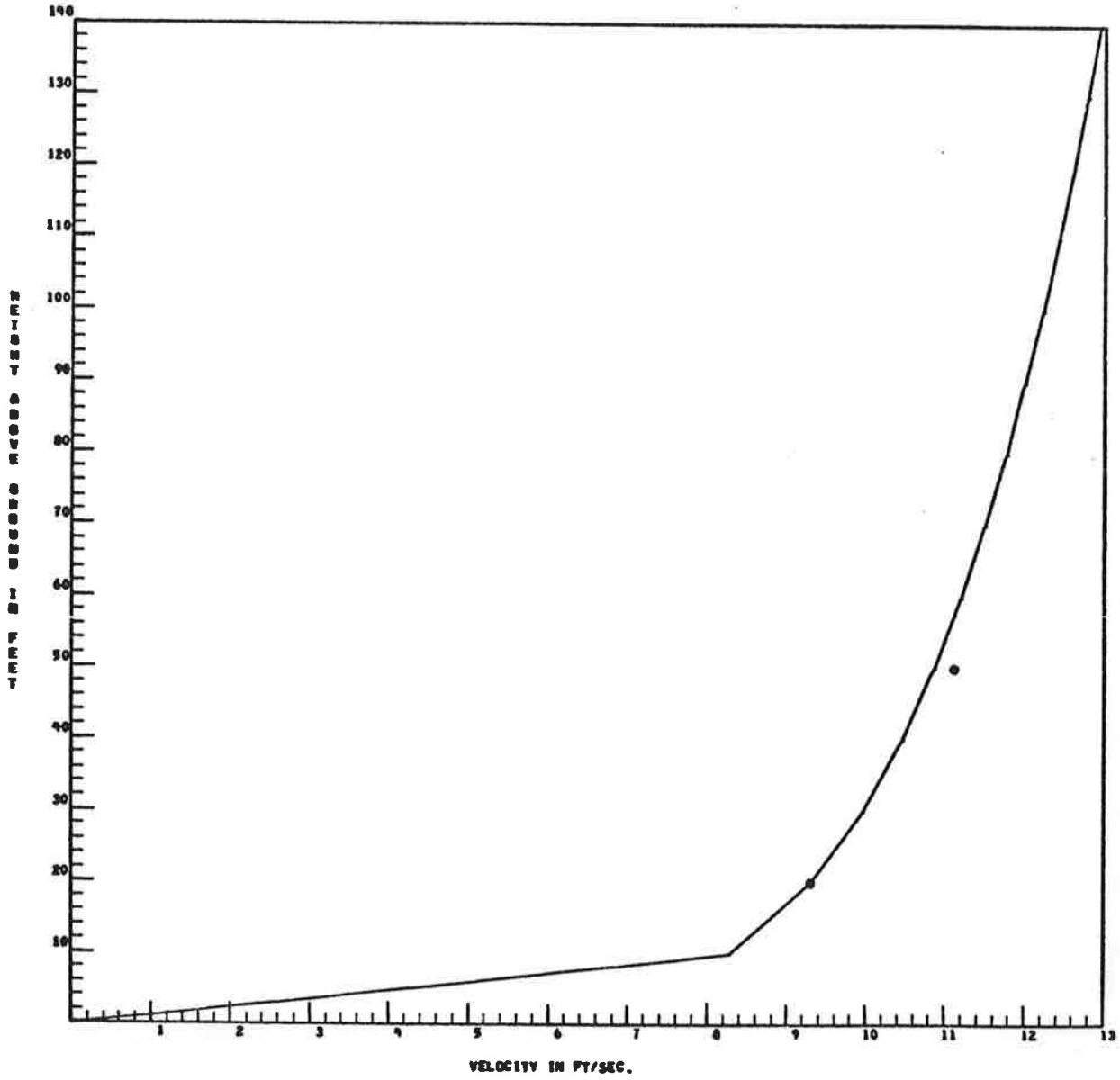


Fig. 5-5 - Pasquill Class Profile

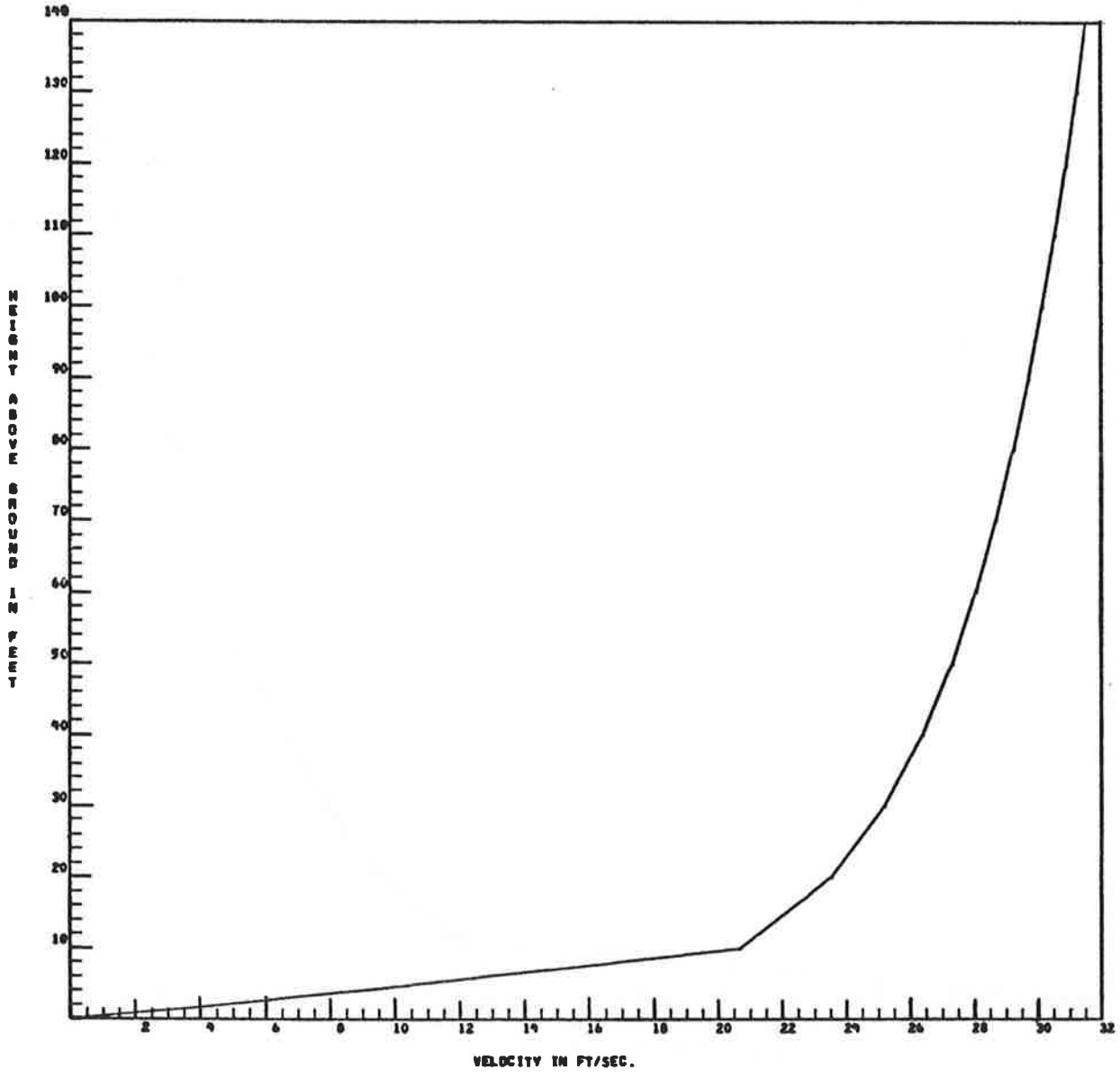


Fig. 5-6 - Logarithmic Wind Profile

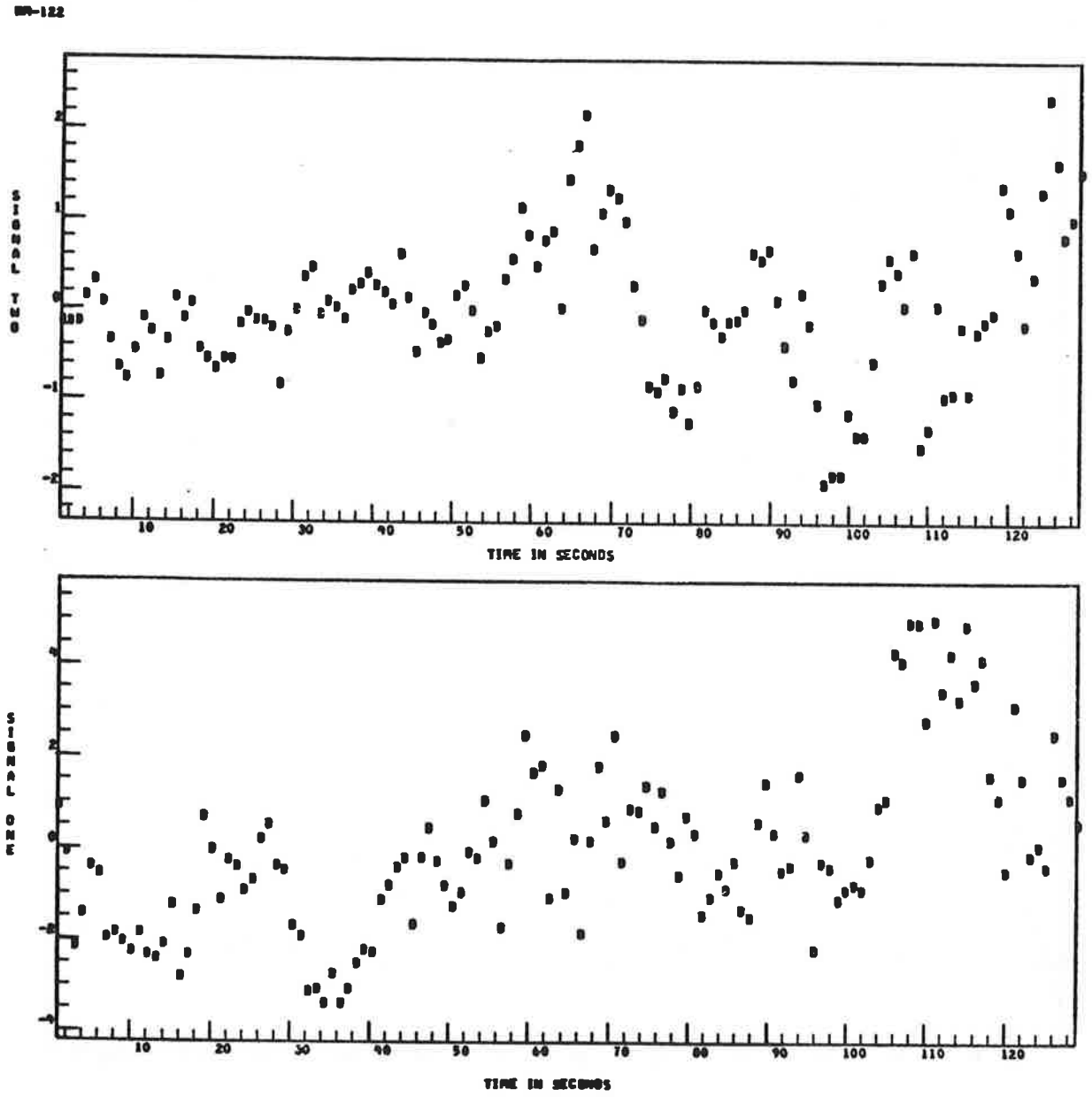


Fig. 5-7 - Horizontal and Vertical Components of Wind Velocity at 20-Foot Elevation

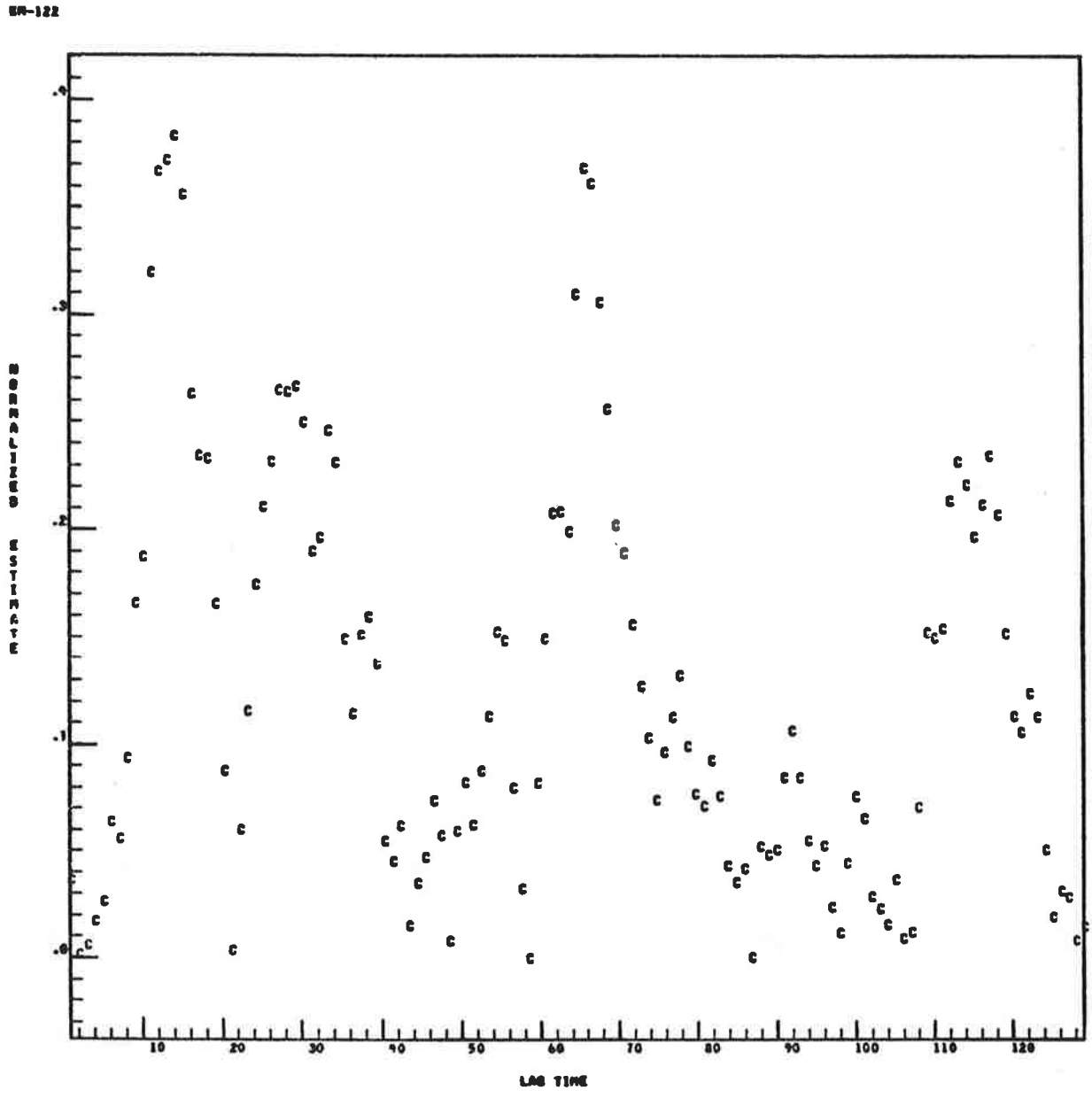


Fig. 5-8 - Cross Correlation Function of Horizontal and Vertical Wind Components at 20-Foot Elevation

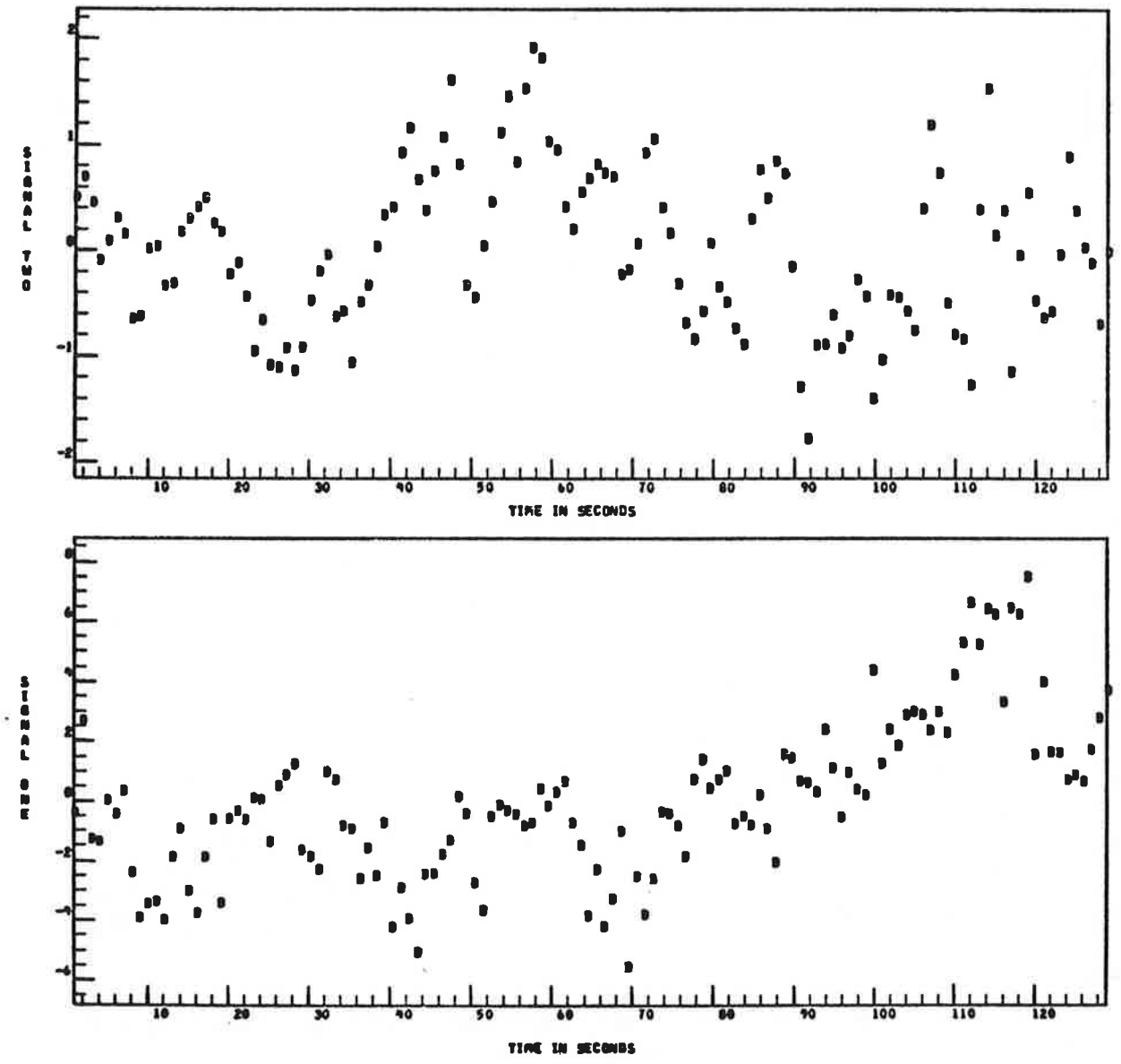


Fig. 5-9 - Horizontal and Vertical Components of Wind Velocity at 40-Foot Elevation

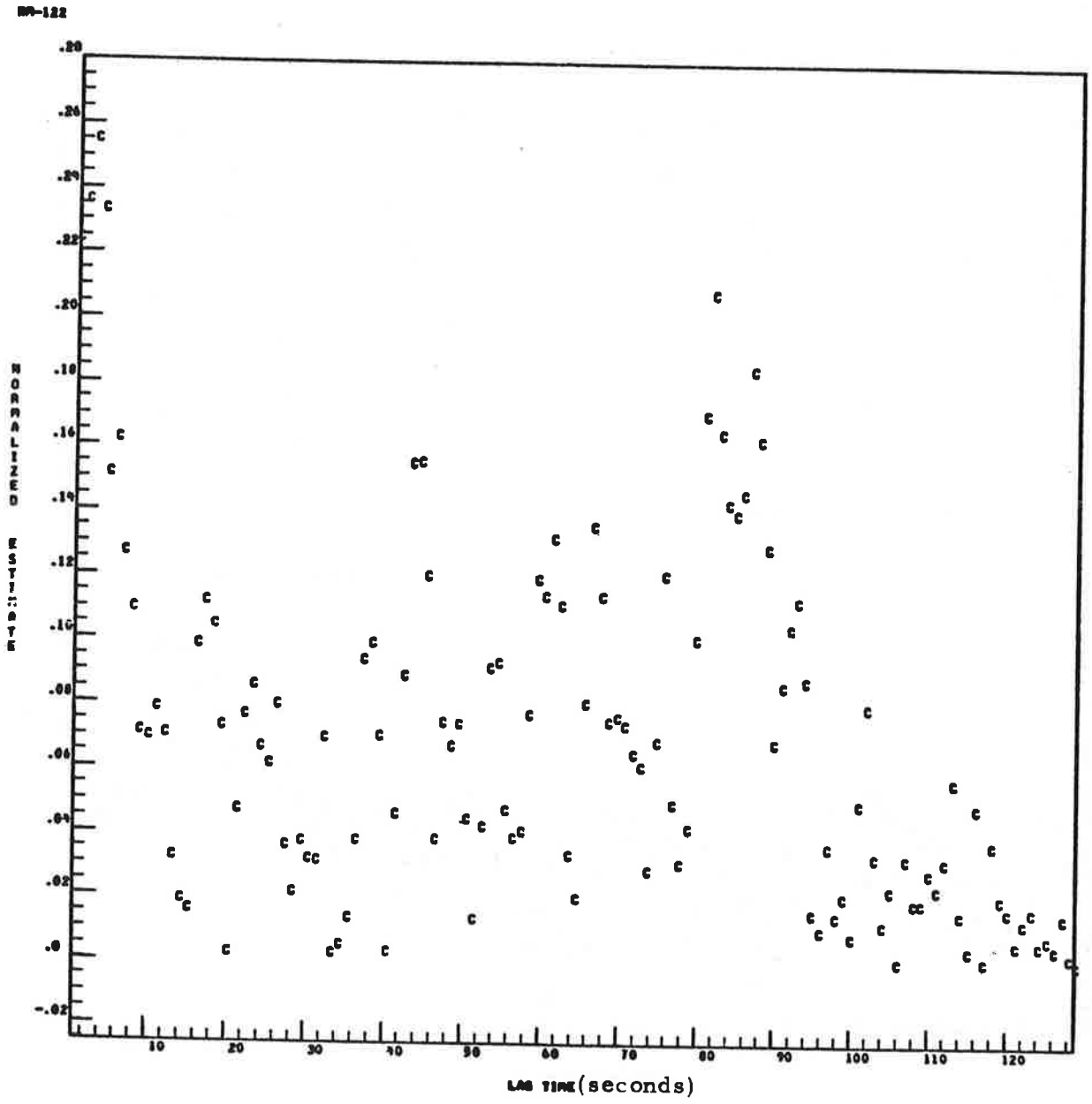


Fig. 5-10 - Cross-Correlation Function of Horizontal and Vertical Wind Components at 40-Foot Elevation

# 6. CONCLUSIONS AND RECOMMENDATIONS

The output of groundwind vortex sensors and tower-mounted wind, pressure and temperature measuring devices at the Department of Transportation wake vortex test site at Kennedy International Airport can be processed, analyzed and displayed by means of a computerized data processing system developed under this research program. Vortex tracks have been predicted on the basis of an expanded transport code incorporated into the above system and utilizing the observed meteorological parameters as inputs. The capability to compare observed and predicted vortex transport characteristics has been demonstrated. The results of the program indicate that the ground-wind propellor anemometer vortex sensor array provides a good indication of the near-ground vortex behavior; wind shear and turbulence profiles can be extracted from the tower-mounted meteorological sensors; and the computed vortex tracks can be correlated with the experimental measurements.

The investigation of statistical processing techniques did not yield an algorithm for analyzing ground-wind sensor data which was a positive improvement over the existing TSC algorithms. It was noted, however, that smoothing the data with a 5-second moving average effectively removed random wind fluctuations to reveal the characteristic vortex wind signature.

On basis of the results of the present research effort, the following specific recommendations are proposed:

1. A broad data base should be established of vortex wake and meteorological measurements for continued analysis.

2. Analysis should be conducted of wake vortex and meteorological measurements and predicted vortex tracks in the above data base to verify and refine the Predictive Model and to examine input requirements for implementing the Predictive Model at any airport.

# APPENDIX A – VORCOM DETAILED FLOW CHARTS

MAIN ROUTINE DRIVER

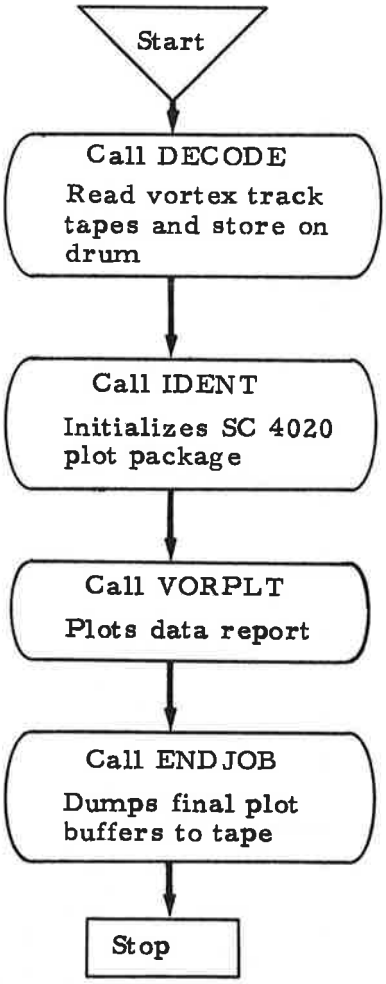

## Subroutine DECODE

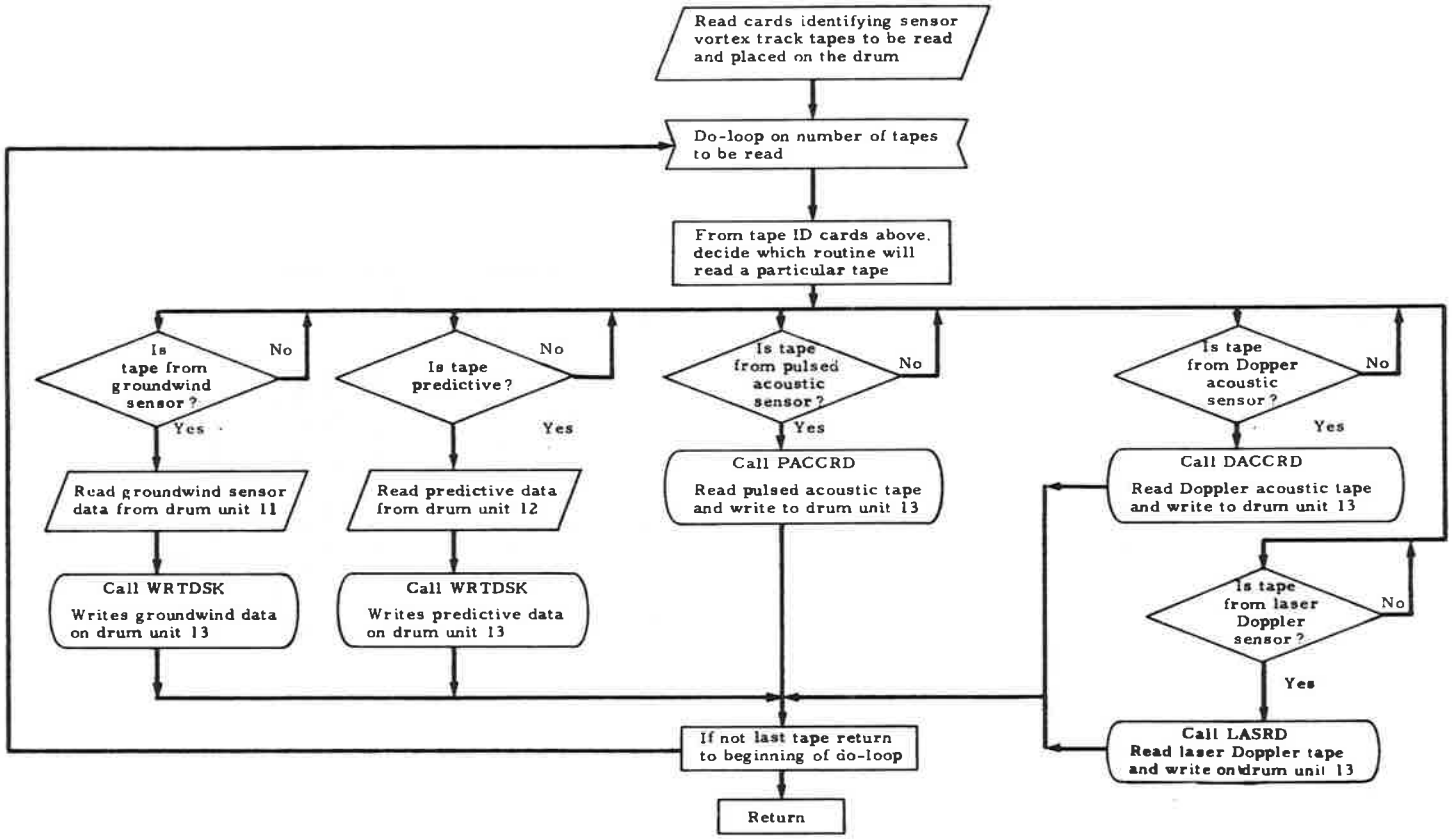

## Function FL

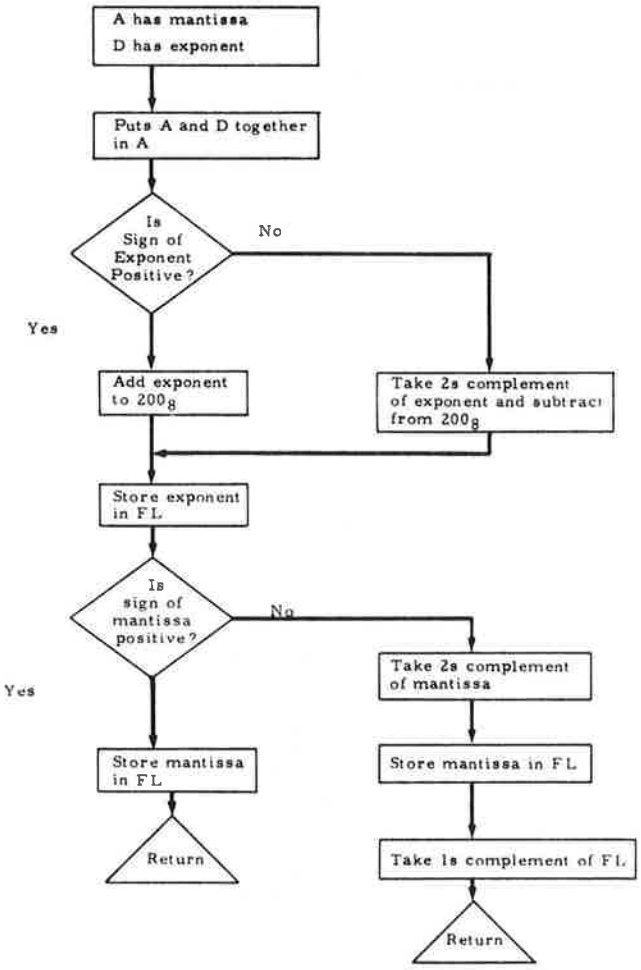
A has mantissa
D has exponent
Puts A and D together in A
Is Sign of Exponent Positive?
No
Yes
Add exponent to 200g
Take 2s complement of exponent and subtract from 200g
Store exponent in FL
Is sign of mantissa positive?
No
Yes
Take 2s complement of mantissa
Store mantissa in FL
Store mantissa in FL
Return
Take 1s complement of FL
Return

## Subroutine WRTDSK

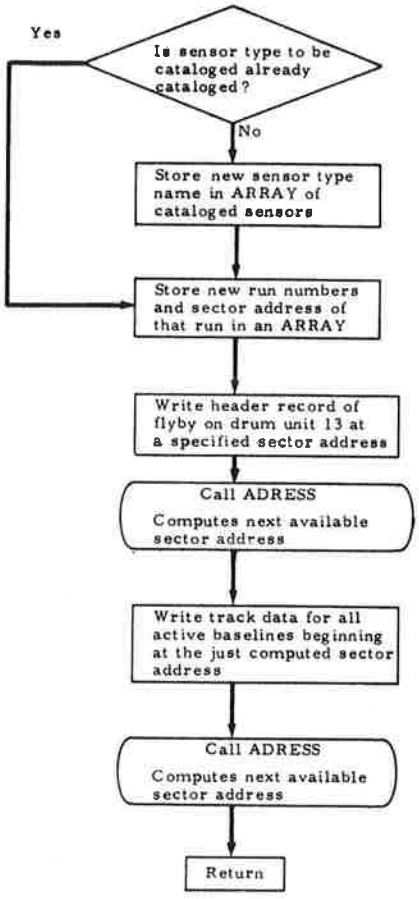

Subroutine RETREV

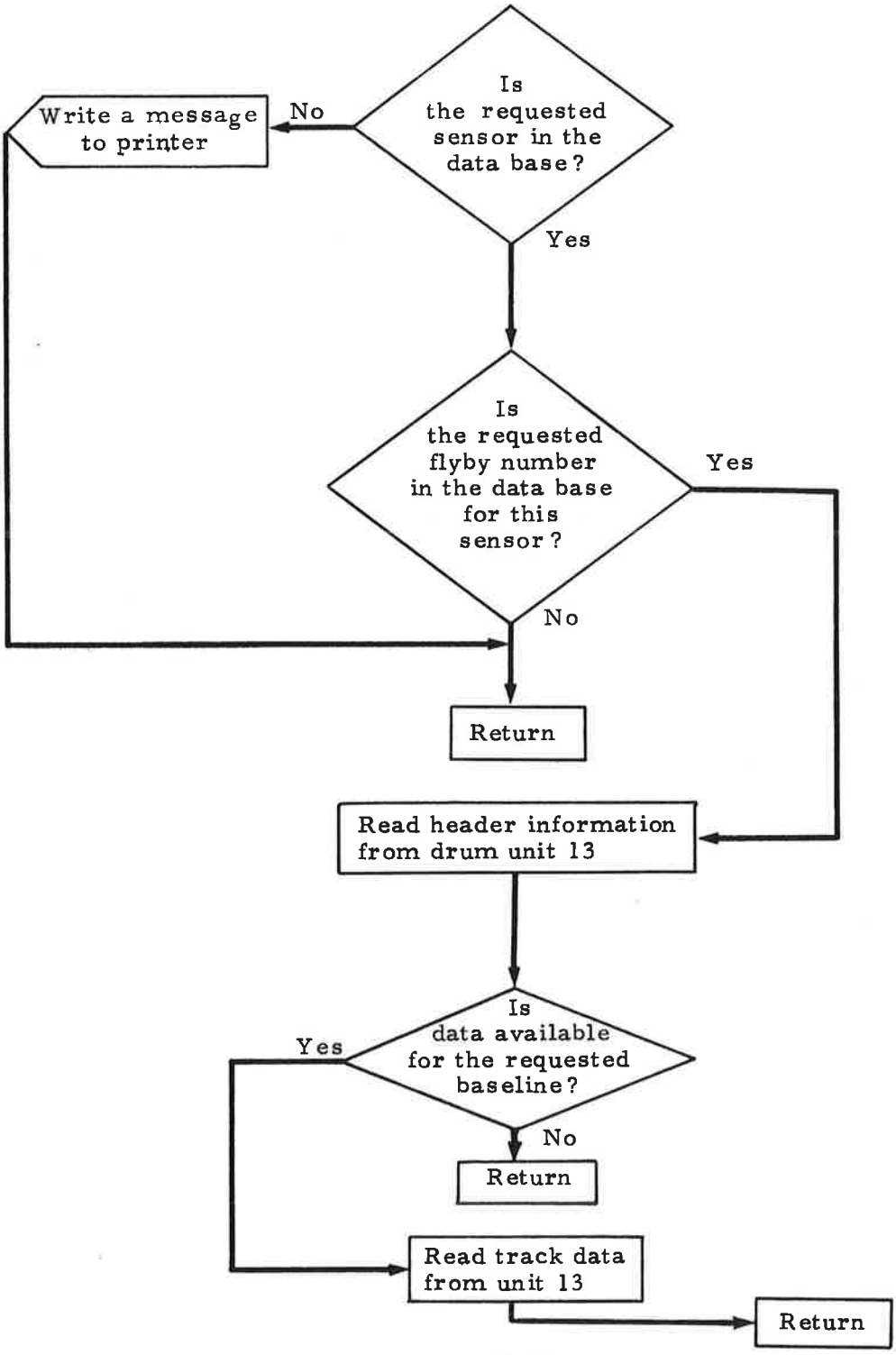

Subroutine RDTAP

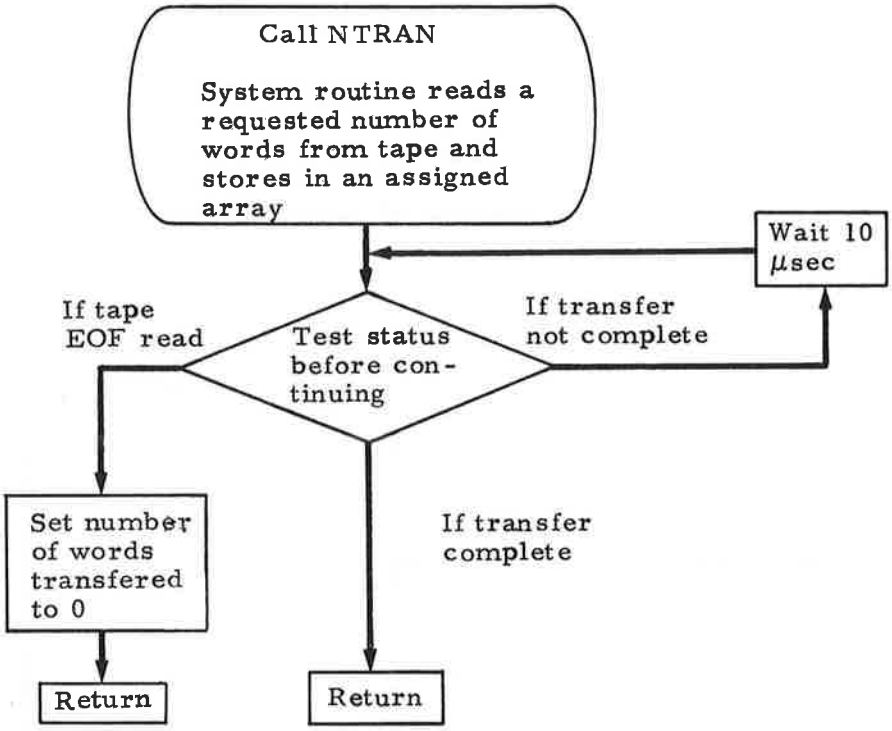

## Subroutine DECODE

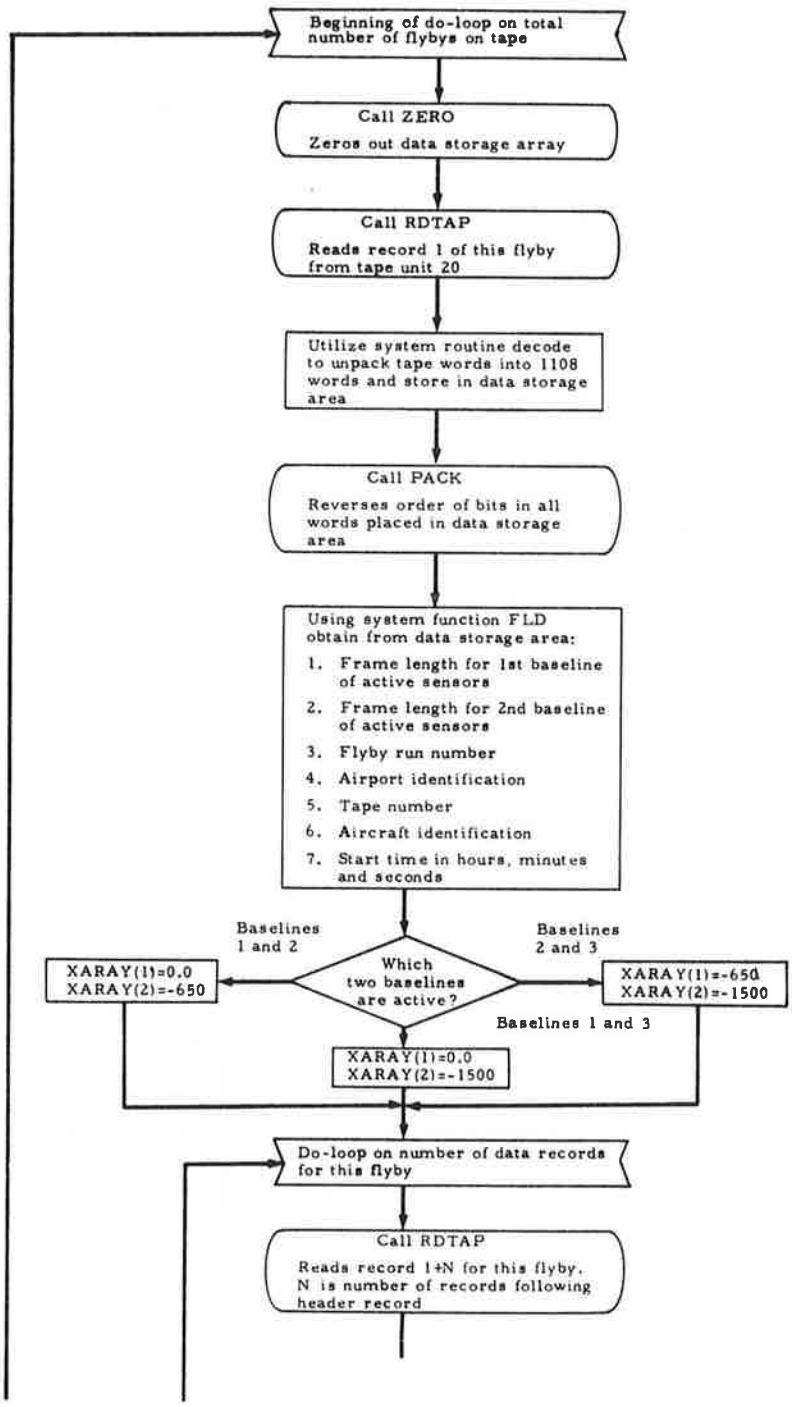

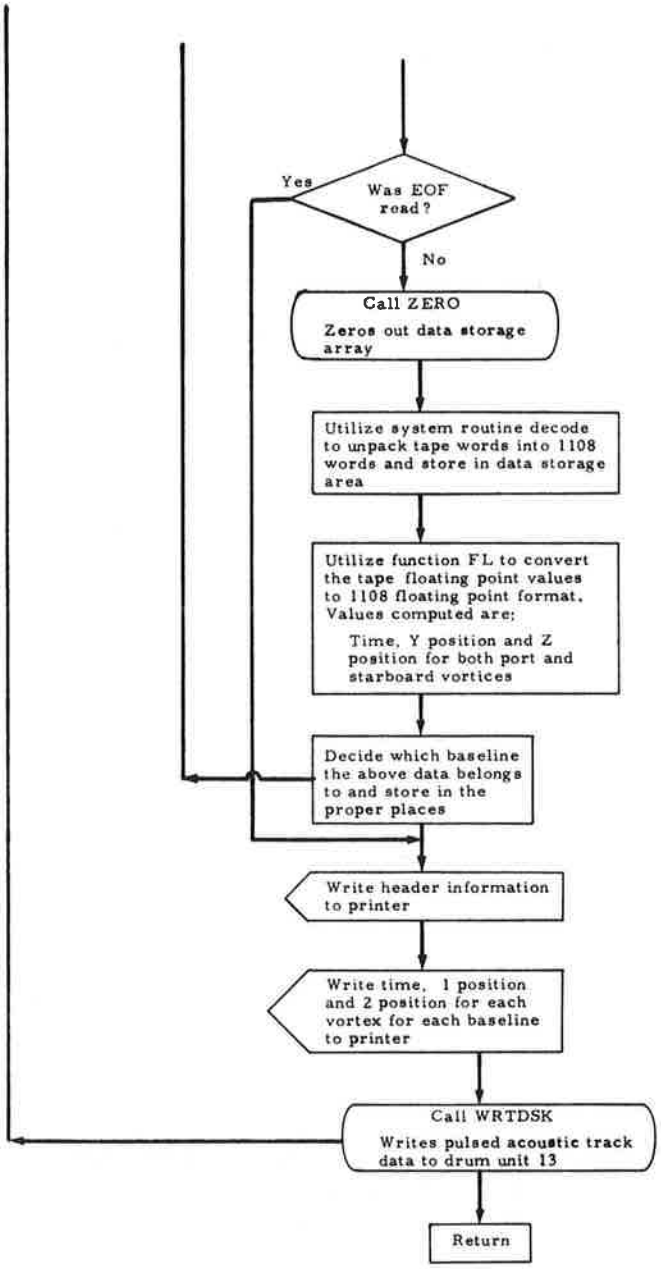
Was EOF read?
Yes
No
Call ZERO
Zeros out data storage array
Utilize system routine decode to unpack tape words into 1108 words and store in data storage area
Utilize function FL to convert the tape floating point values to 1108 floating point format. Values computed are:
Time, Y position and Z position for both port and starboard vortices
Decide which baseline the above data belongs to and store in the proper places
Write header information to printer
Write time, 1 position and 2 position for each vortex for each baseline to printer
Call WRTDSK
Writes pulsed acoustic track data to drum unit 13
Return

## Subroutine LASRD

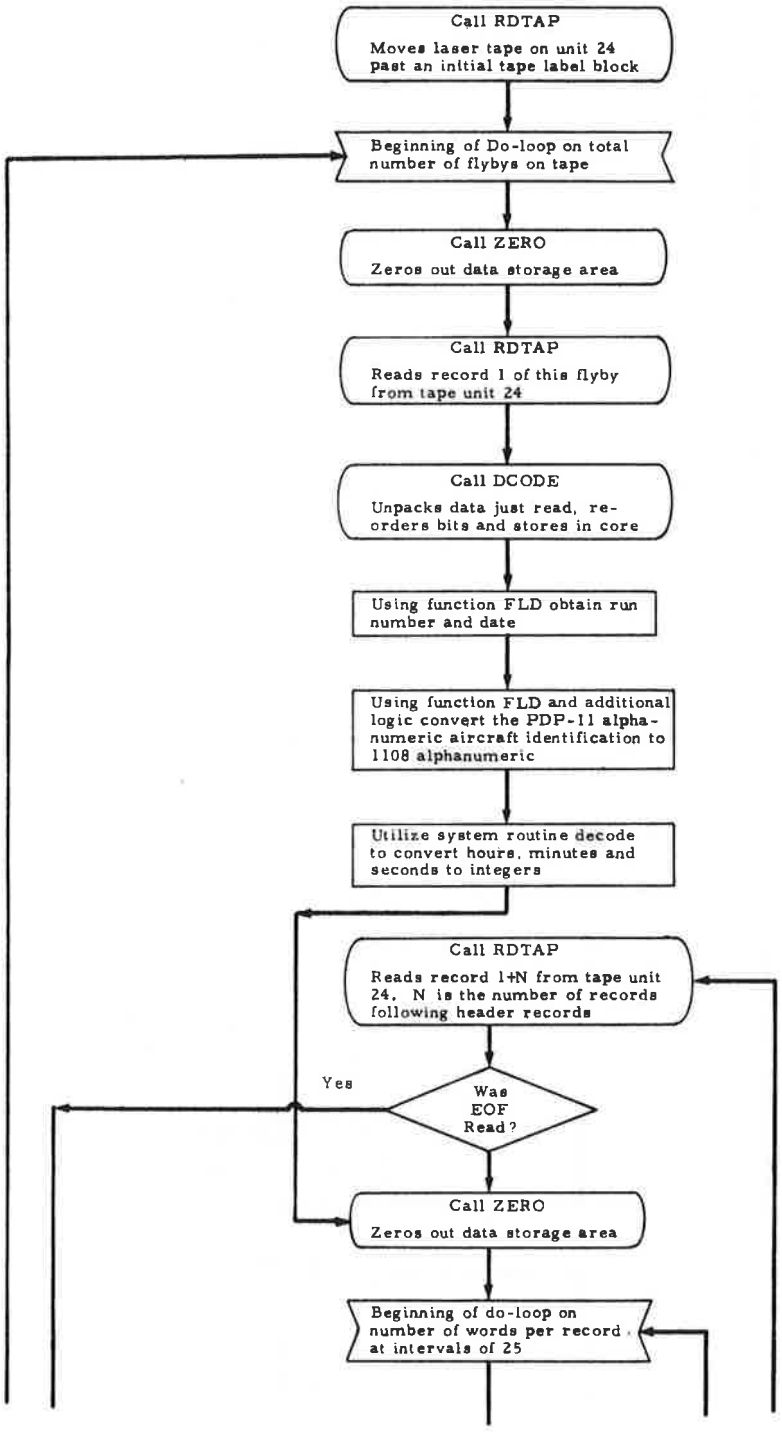

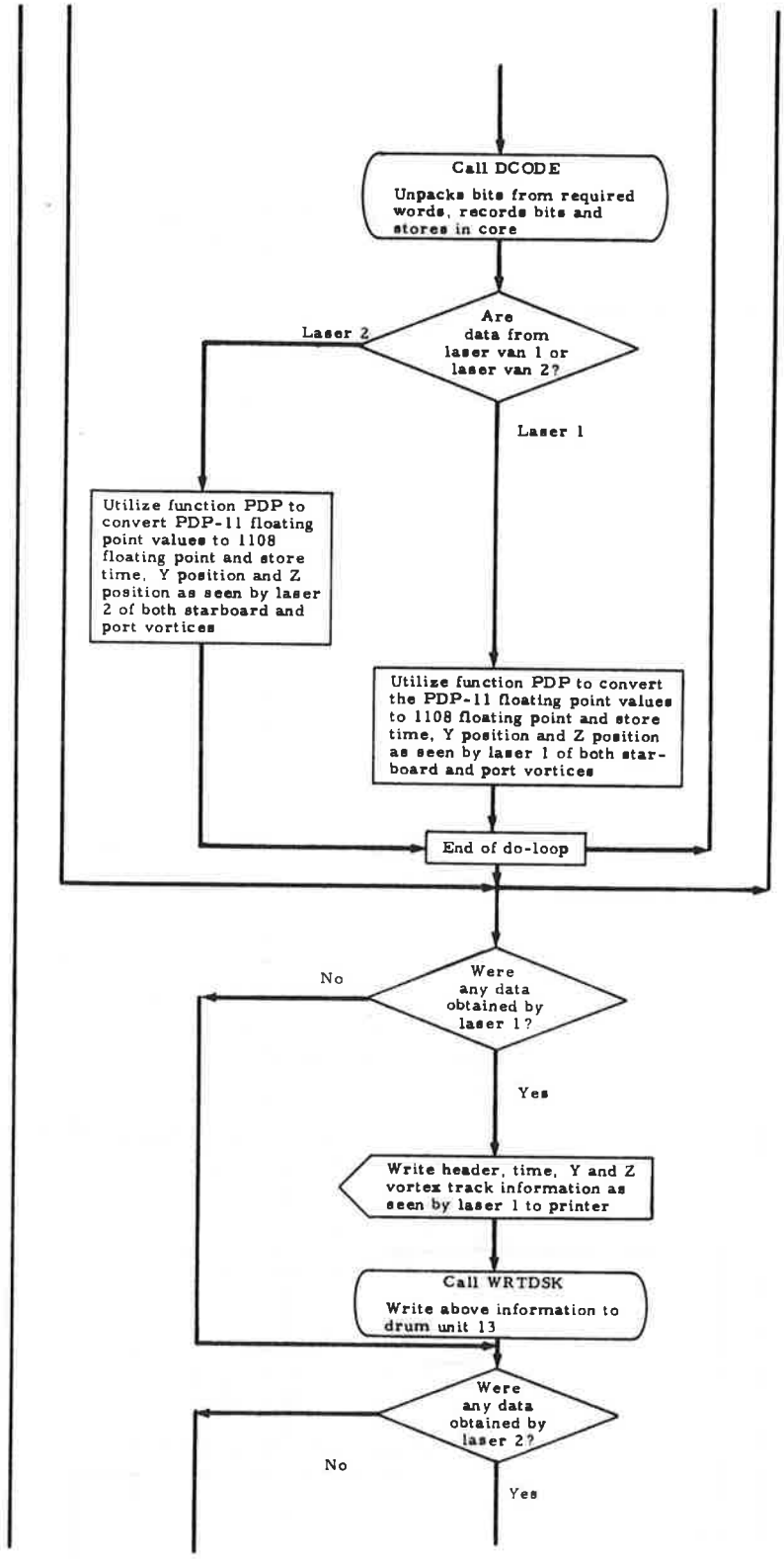
Call DCODE
Unpacks bits from required words, records bits and stores in core
Are data from laser van 1 or laser van 2?
Laser 2
Laser 1
Utilize function PDP to convert PDP-11 floating point values to 1108 floating point and store time, Y position and Z position as seen by laser 2 of both starboard and port vortices
Utilize function PDP to convert the PDP-11 floating point values to 1108 floating point and store time, Y position and Z position as seen by laser 1 of both starboard and port vortices
End of do-loop
Were any data obtained by laser 1?
No
Yes
Write header, time, Y and Z vortex track information as seen by laser 1 to printer
Call WRTDSK
Write above information to drum unit 13
Were any data obtained by laser 2?
No
Yes

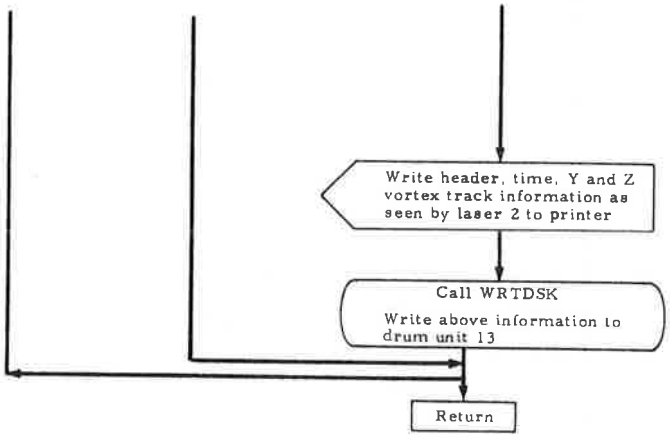
Write header, time, Y and Z vortex track information as seen by laser 2 to printer
Call WRTDSK
Write above information to drum unit 13
Return

## Subroutine DACCRD

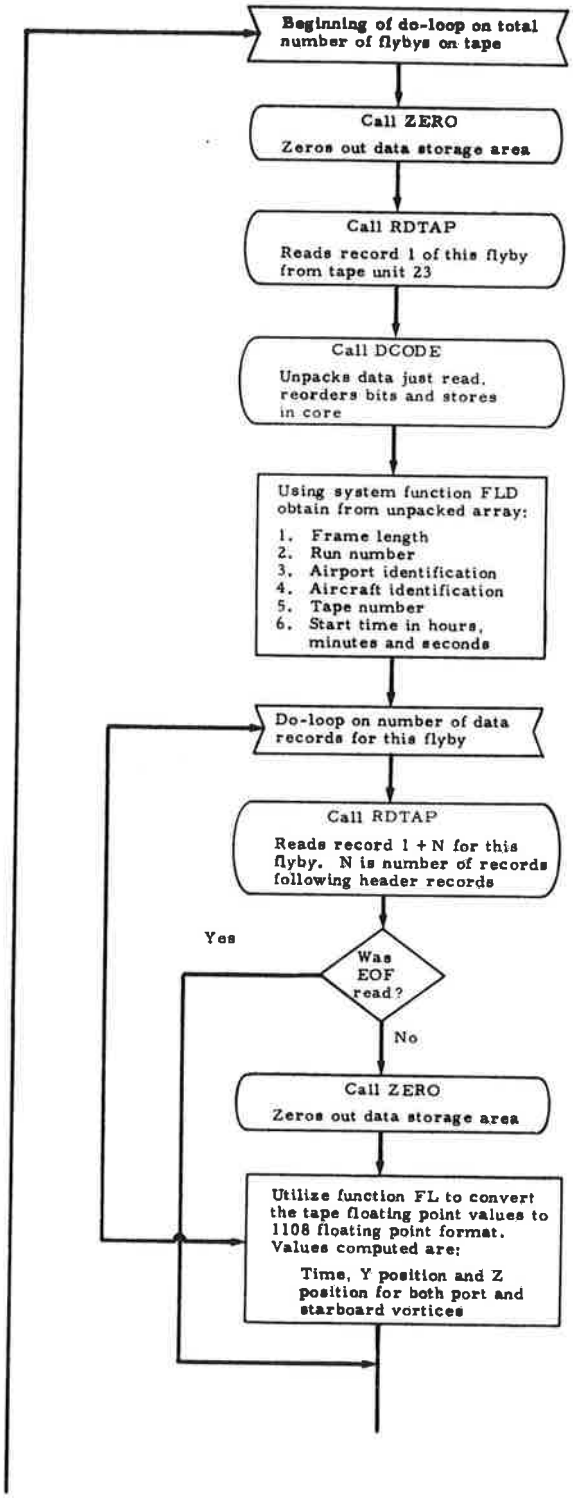

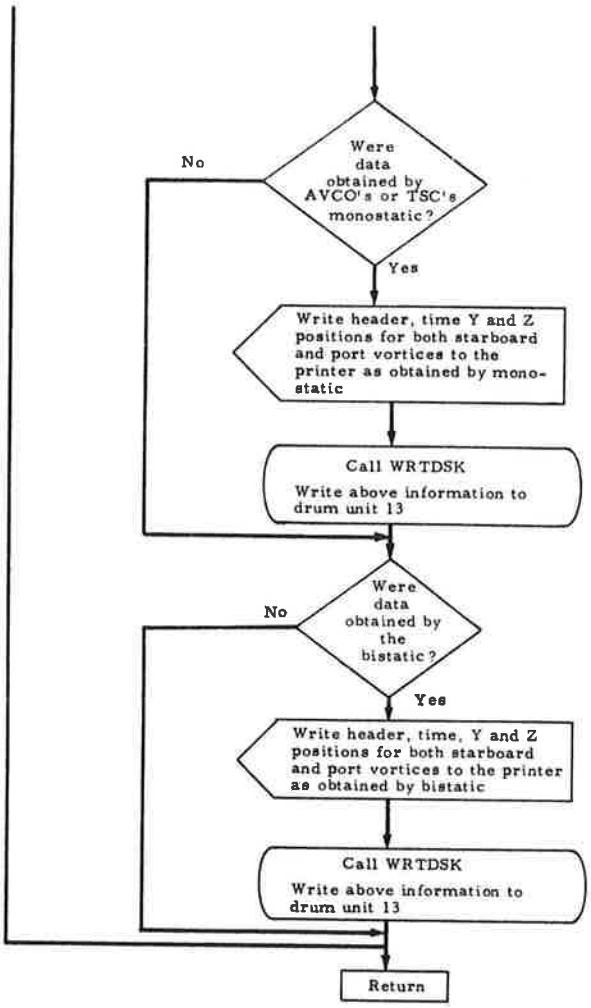
Were data obtained by AVCO's or TSC's monostatic?
No
Yes
Write header, time Y and Z positions for both starboard and port vortices to the printer as obtained by mono-static
Call WRTDSK
Write above information to drum unit 13
Were data obtained by the bistatic?
No
Yes
Write header, time, Y and Z positions for both starboard and port vortices to the printer as obtained by bistatic
Call WRTDSK
Write above information to drum unit 13
Return

## Subroutine VORPLT

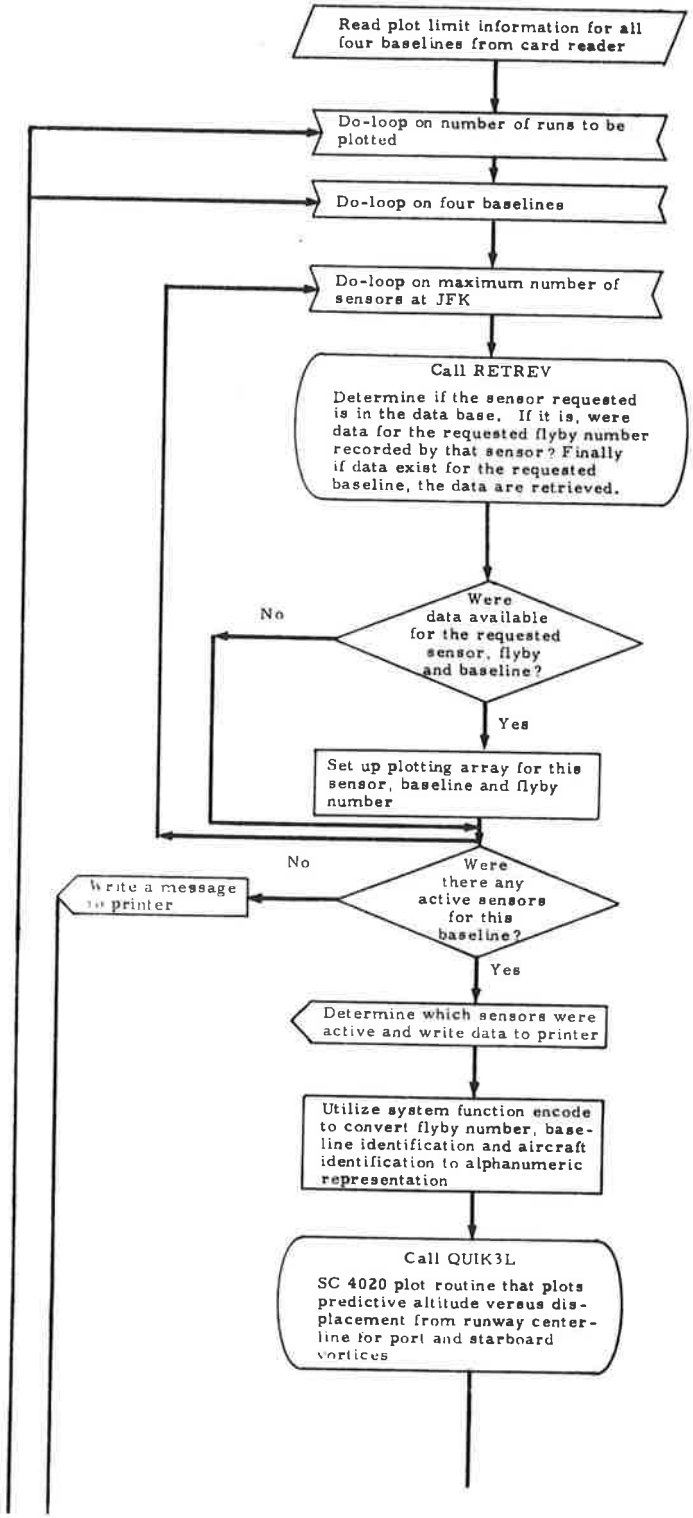

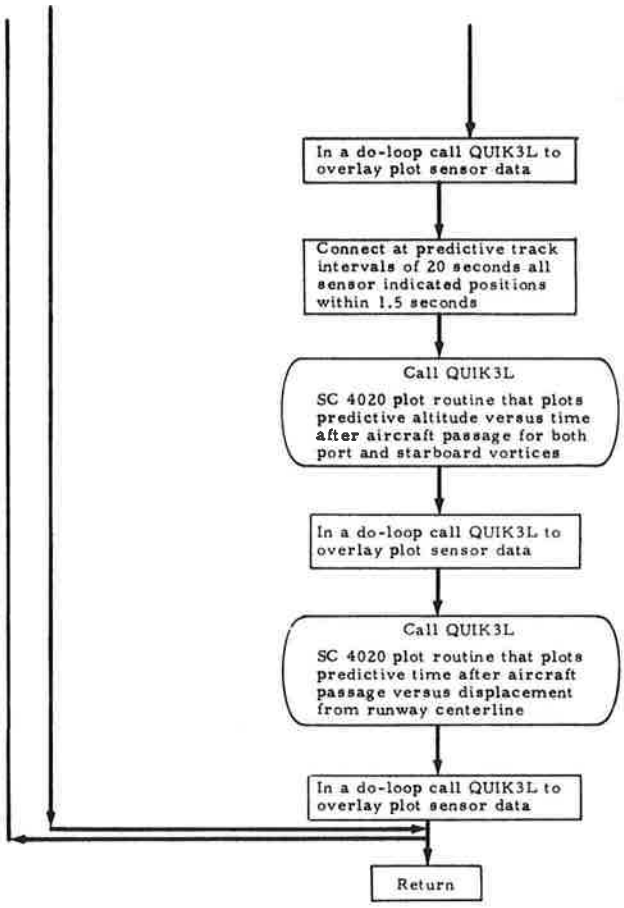
In a do-loop call QUIK3L to overlay plot sensor data
Connect at predictive track intervals of 20 seconds all sensor indicated positions within 1.5 seconds
Call QUIK3L
SC 4020 plot routine that plots predictive altitude versus time after aircraft passage for both port and starboard vortices
In a do-loop call QUIK3L to overlay plot sensor data
Call QUIK3L
SC 4020 plot routine that plots predictive time after aircraft passage versus displacement from runway centerline
In a do-loop call QUIK3L to overlay plot sensor data
Return

# APPENDIX B – MET AND PREDIC DETAILED PROGRAM

MAINC (Driver)

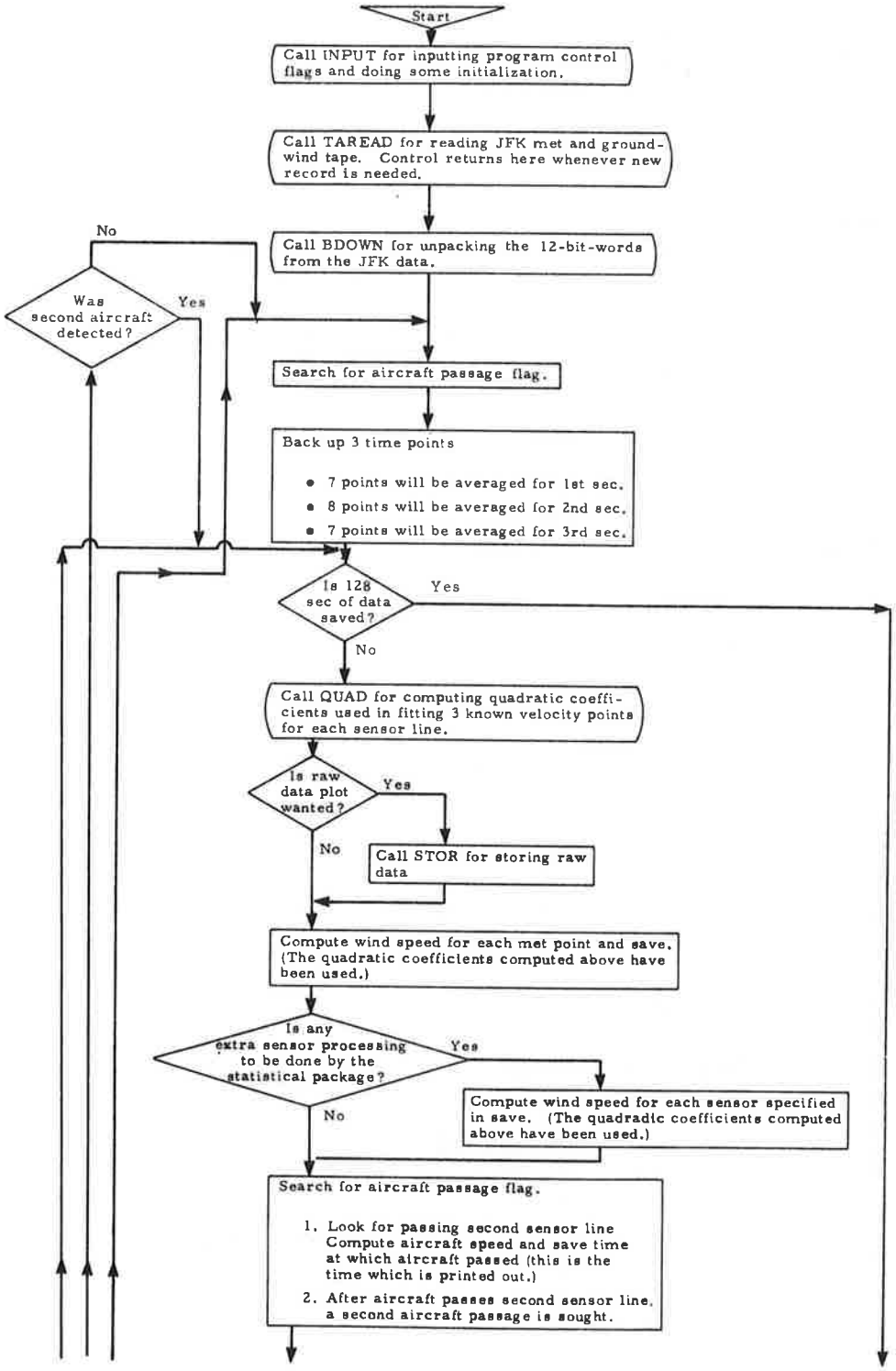

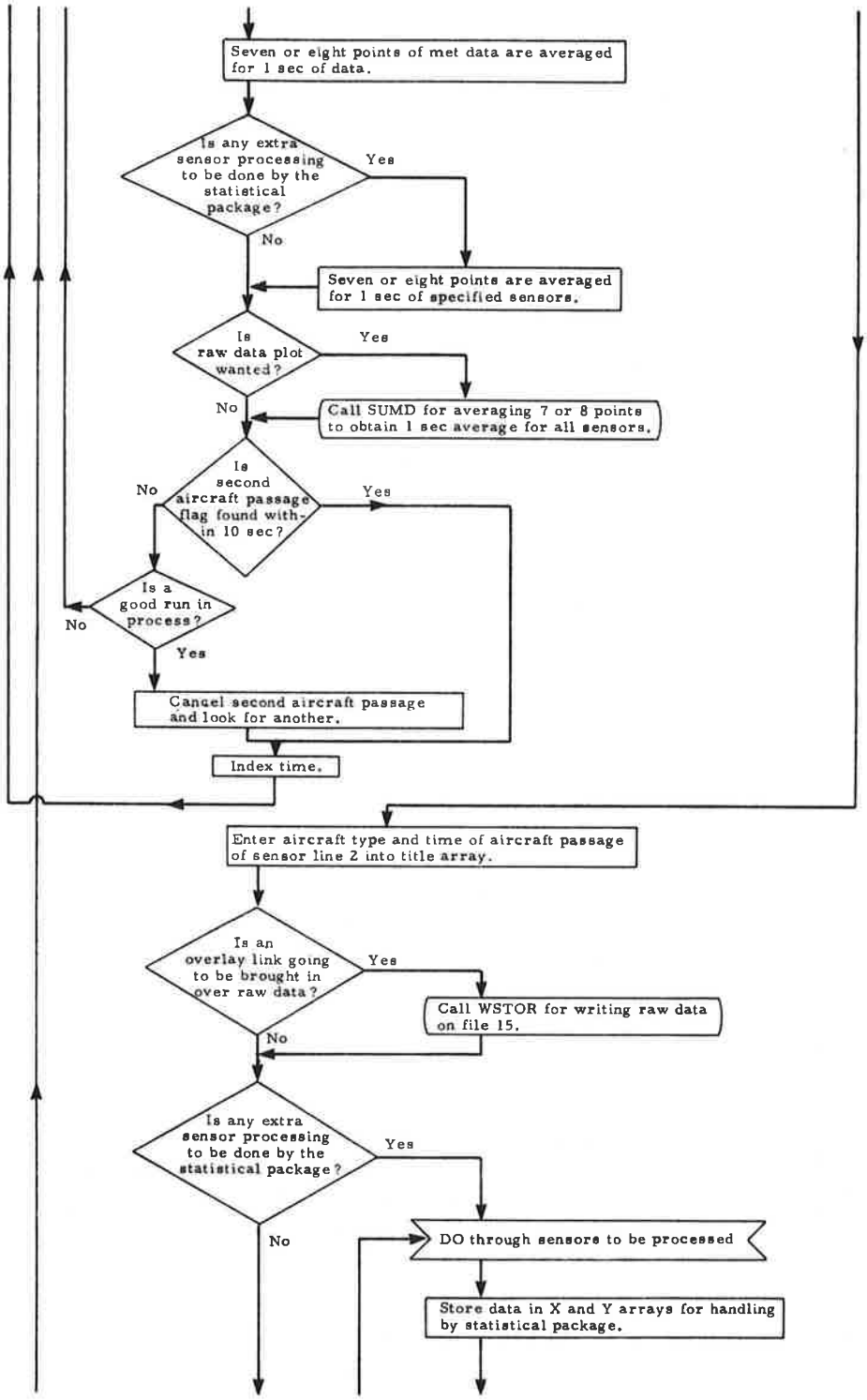
Seven or eight points of met data are averaged for 1 sec of data.
Is any extra sensor processing to be done by the statistical package?
Yes
No
Seven or eight points are averaged for 1 sec of specified sensors.
Is raw data plot wanted?
Yes
No
Call SUMD for averaging 7 or 8 points to obtain 1 sec average for all sensors.
Is second aircraft passage flag found within 10 sec?
No
Yes
Is a good run in process?
No
Yes
Cancel second aircraft passage and look for another.
Index time.
Enter aircraft type and time of aircraft passage of sensor line 2 into title array.
Is an overlay link going to be brought in over raw data?
Yes
Call WSTOR for writing raw data on file 15.
No
Is any extra sensor processing to be done by the statistical package?
Yes
No
DO through sensors to be processed
Store data in X and Y arrays for handling by statistical package.

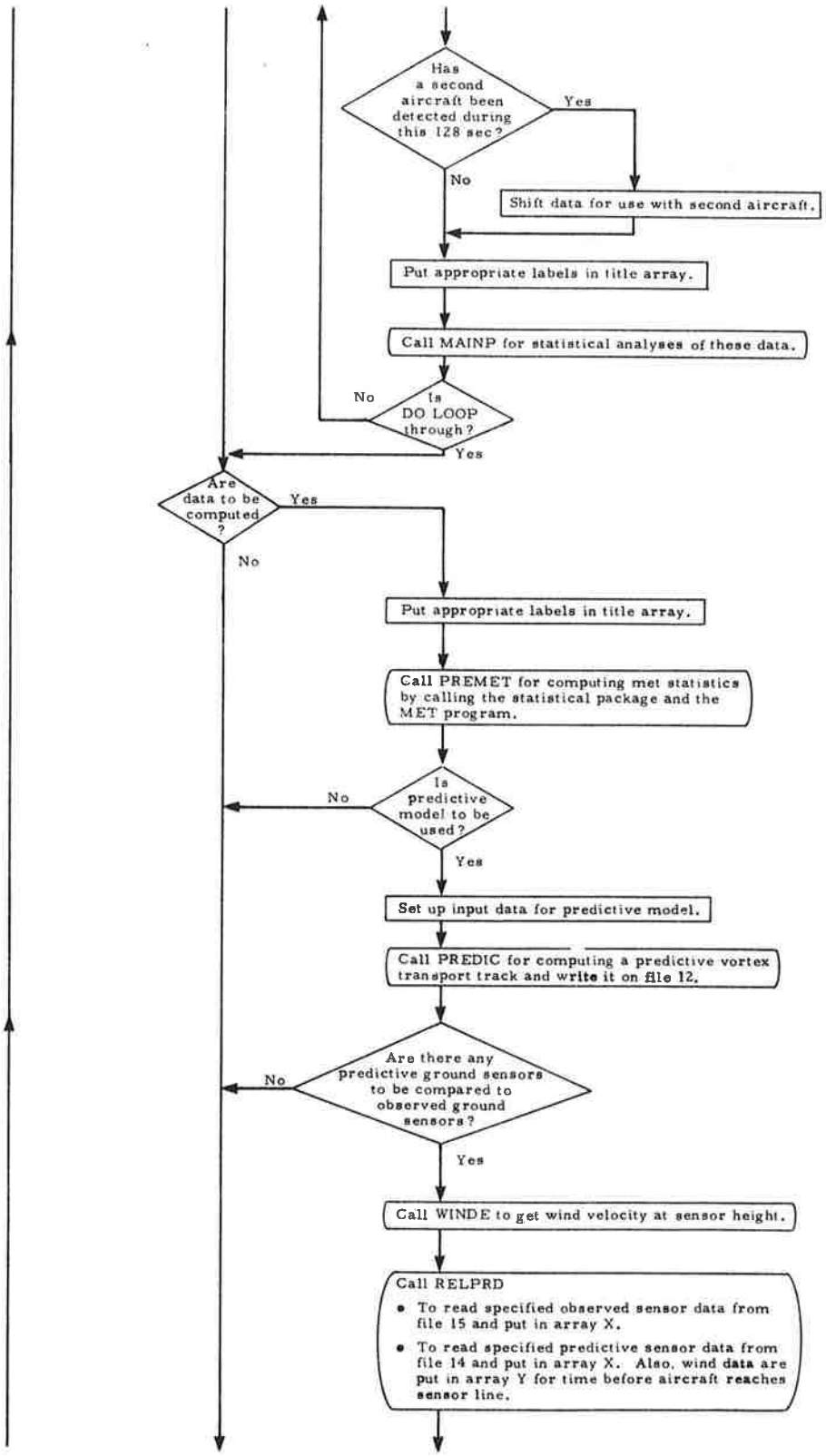
Has a second aircraft been detected during this 128 sec?
Yes
No
Shift data for use with second aircraft.
Put appropriate labels in title array.
Call MAINP for statistical analyses of these data.
No
Is DO LOOP through?
Yes
Are data to be computed ?
Yes
No
Put appropriate labels in title array.
Call PREMET for computing met statistics by calling the statistical package and the MET program.
No
Is predictive model to be used?
Yes
Set up input data for predictive model.
Call PREDIC for computing a predictive vortex transport track and write it on file 12.
No
Are there any predictive ground sensors to be compared to observed ground sensors?
Yes
Call WINDE to get wind velocity at sensor height.
Call RELPRD
• To read specified observed sensor data from file 15 and put in array X.
• To read specified predictive sensor data from file 14 and put in array X. Also, wind data are put in array Y for time before aircraft reaches sensor line.

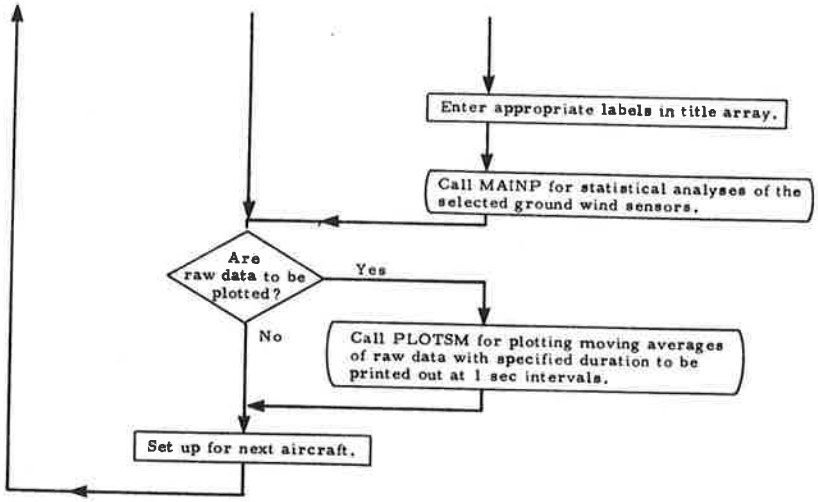
Enter appropriate labels in title array.
Call MAINP for statistical analyses of the selected ground wind sensors.
Are raw data to be plotted?
Yes
No
Call PLOTSM for plotting moving averages of raw data with specified duration to be printed out at 1 sec intervals.
Set up for next aircraft.

PREMET

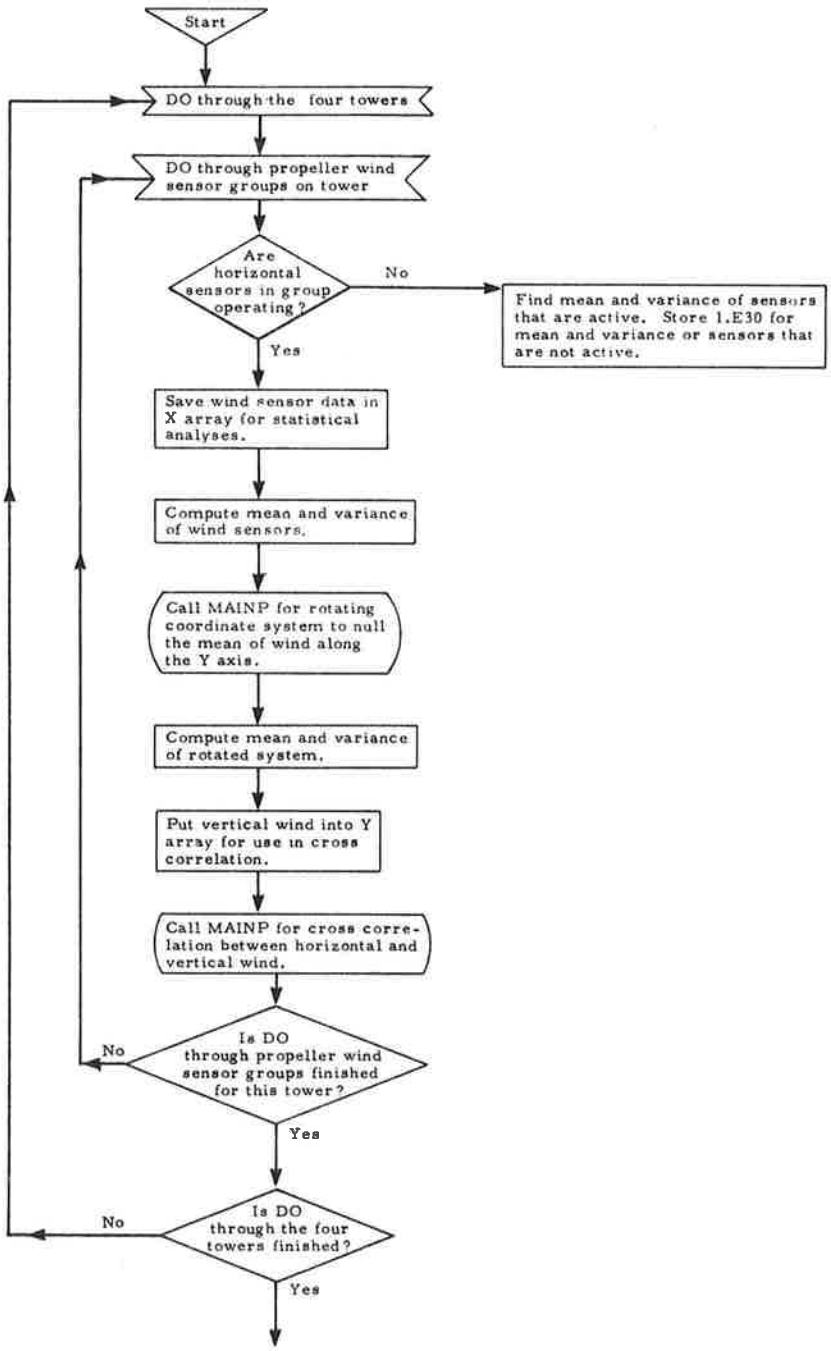
Start
DO through the four towers
DO through propeller wind sensor groups on tower
Are horizontal sensors in group operating?
No
Find mean and variance of sensors that are active. Store 1.E30 for mean and variance or sensors that are not active.
Yes
Save wind sensor data in X array for statistical analyses.
Compute mean and variance of wind sensors.
Call MAINP for rotating coordinate system to null the mean of wind along the Y axis.
Compute mean and variance of rotated system.
Put vertical wind into Y array for use in cross correlation.
Call MAINP for cross correlation between horizontal and vertical wind.
Is DO through propeller wind sensor groups finished for this tower?
No
Yes
Is DO through the four towers finished?
No
Yes

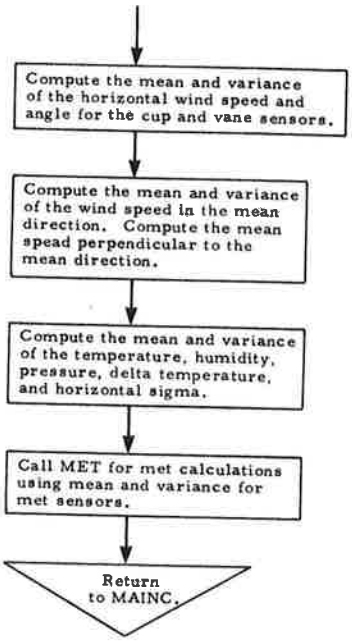
Compute the mean and variance of the horizontal wind speed and angle for the cup and vane sensors.
Compute the mean and variance of the wind speed in the mean direction. Compute the mean spead perpendicular to the mean direction.
Compute the mean and variance of the temperature, humidity, pressure, delta temperature, and horizontal sigma.
Call MET for met calculations using mean and variance for met sensors.
Return to MAINC.

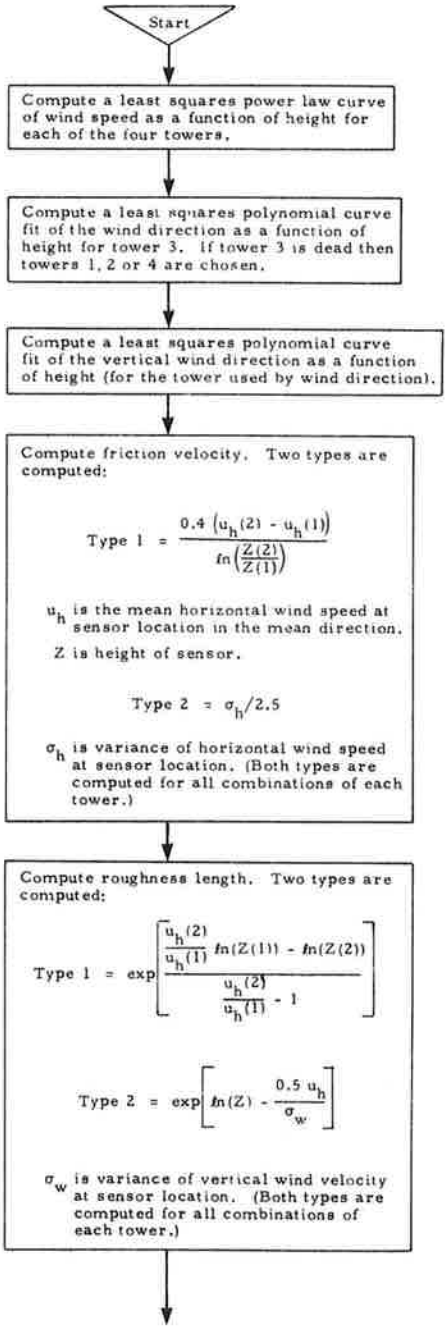
Start
Compute a least squares power law curve of wind speed as a function of height for each of the four towers.
Compute a least squares polynomial curve fit of the wind direction as a function of height for tower 3. If tower 3 is dead then towers 1, 2 or 4 are chosen.
Compute a least squares polynomial curve fit of the vertical wind direction as a function of height (for the tower used by wind direction).
Compute friction velocity. Two types are computed:
Type 1 = 0.4 (u_h(2) - u_h(1)) / ln(Z(2)/Z(1))
u_h is the mean horizontal wind speed at sensor location in the mean direction.
Z is height of sensor.
Type 2 = σ_h/2.5
σ_h is variance of horizontal wind speed at sensor location. (Both types are computed for all combinations of each tower.)
Compute roughness length. Two types are computed:
Type 1 = exp[ (u_h(2)/u_h(1)) ln(Z(1)) - ln(Z(2)) / (u_h(2)/u_h(1)) - 1 ]
Type 2 = exp[ ln(Z) - 0.5 u_h / σ_w ]
σ_w is variance of vertical wind velocity at sensor location. (Both types are computed for all combinations of each tower.)

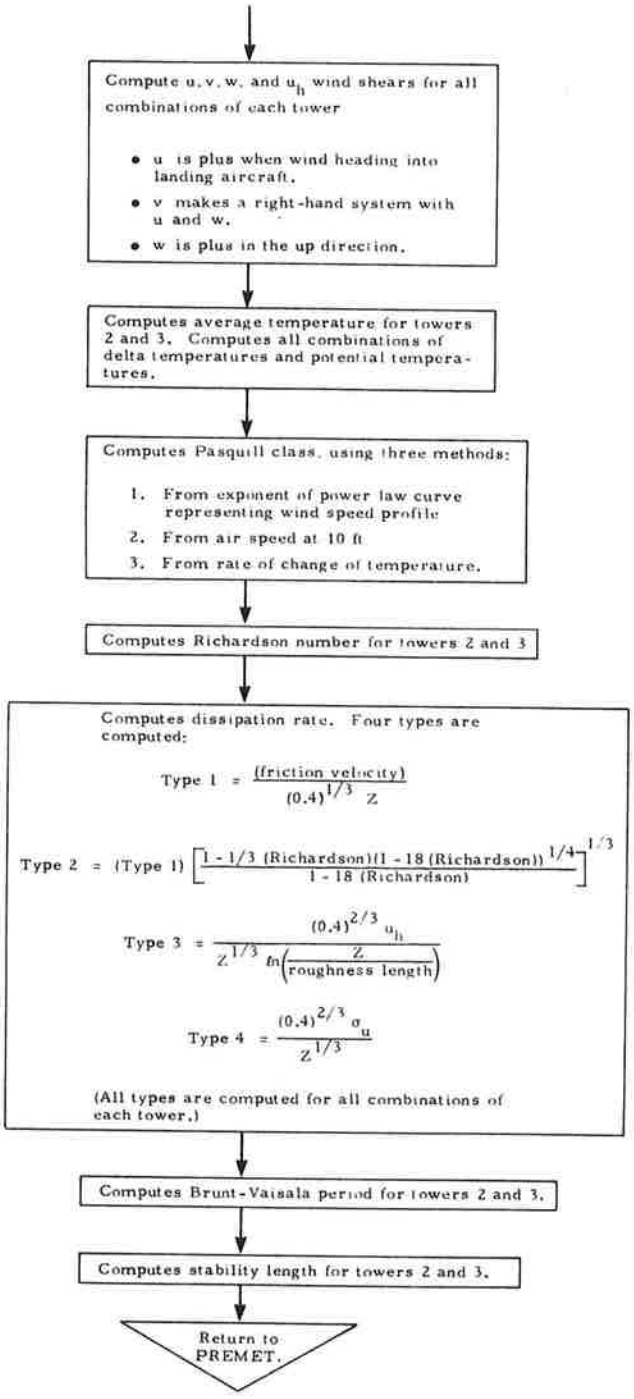
Compute u, v, w, and $u_h$ wind shears for all combinations of each tower
• u is plus when wind heading into landing aircraft.
• v makes a right-hand system with u and w.
• w is plus in the up direction.
Computes average temperature for towers 2 and 3. Computes all combinations of delta temperatures and potential temperatures.
Computes Pasquill class, using three methods:
1. From exponent of power law curve representing wind speed profile
2. From air speed at 10 ft
3. From rate of change of temperature.
Computes Richardson number for towers 2 and 3
Computes dissipation rate. Four types are computed:
Type 1 = (friction velocity) / $(0.4)^{1/3}$ Z
Type 2 = (Type 1) $\left[\frac{1 - 1/3\ (\text{Richardson})(1 - 18\ (\text{Richardson}))^{1/4}}{1 - 18\ (\text{Richardson})}\right]^{1/3}$
Type 3 = $\frac{(0.4)^{2/3}\ u_h}{Z^{1/3}\ \ln\left(\frac{Z}{\text{roughness length}}\right)}$
Type 4 = $\frac{(0.4)^{2/3}\ \sigma_u}{Z^{1/3}}$
(All types are computed for all combinations of each tower.)
Computes Brunt-Vaisala period for towers 2 and 3.
Computes stability length for towers 2 and 3.
Return to PREMET.

## STATISTICS PROGRAM (STAT)

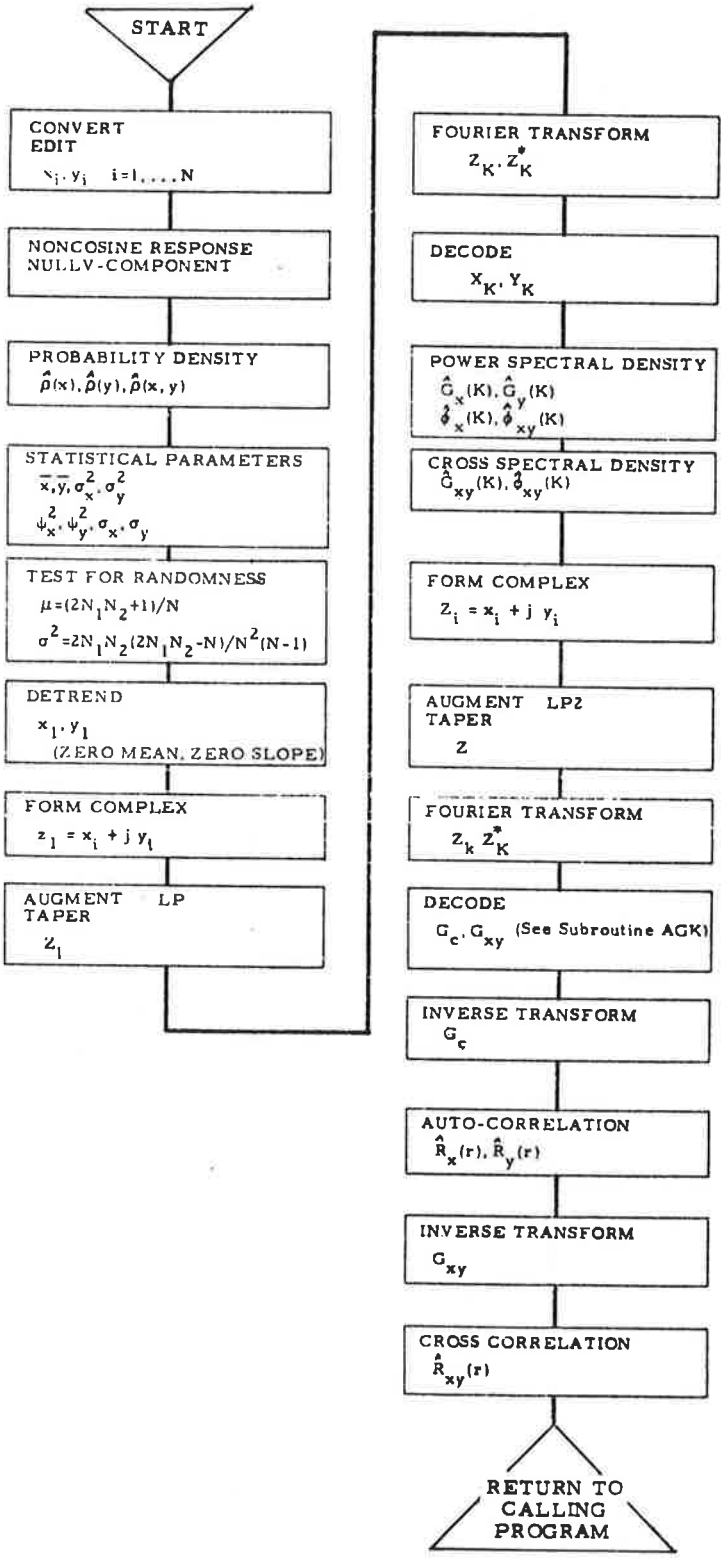

NOTE: Statements within dashed lines not used.

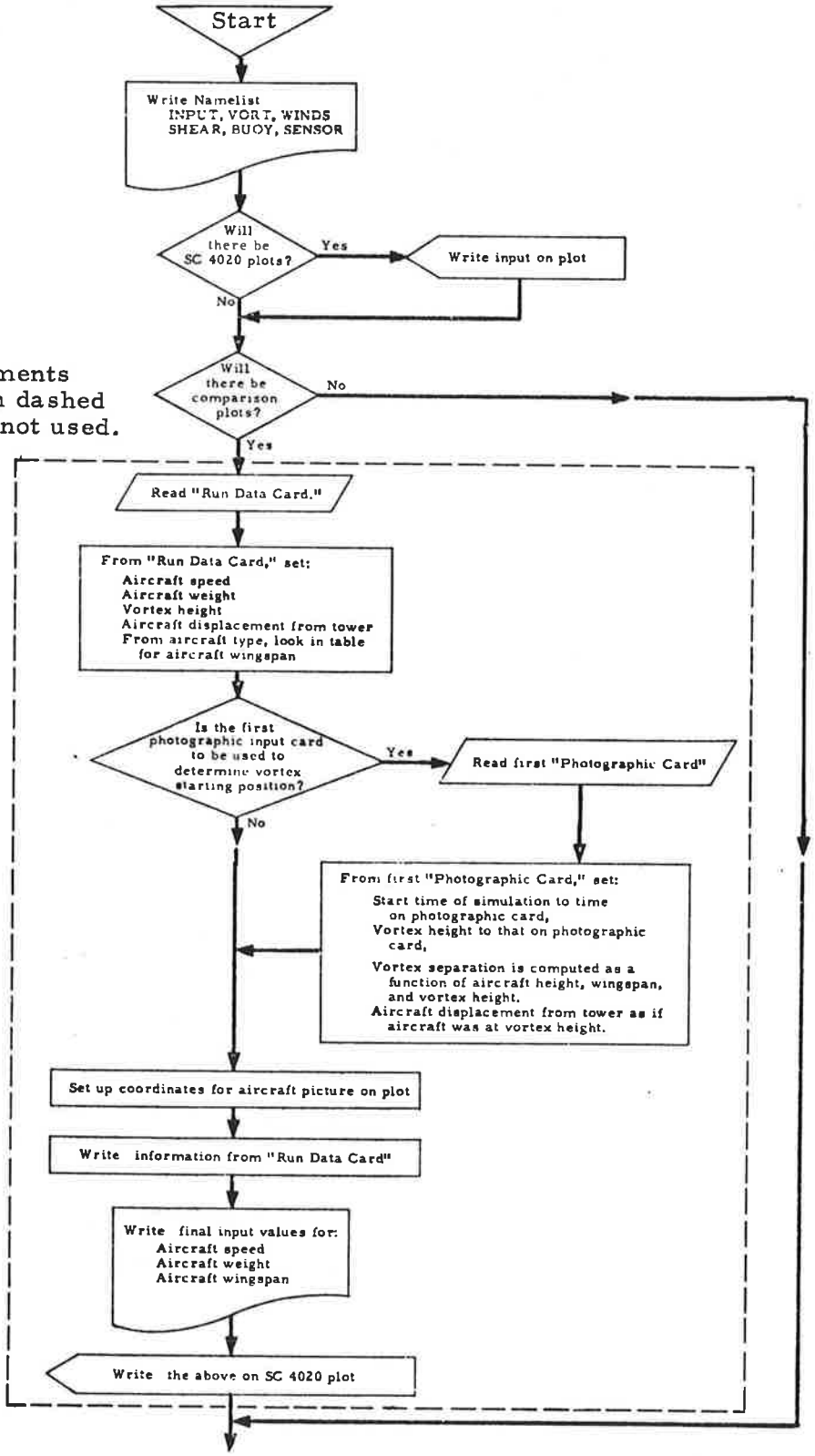

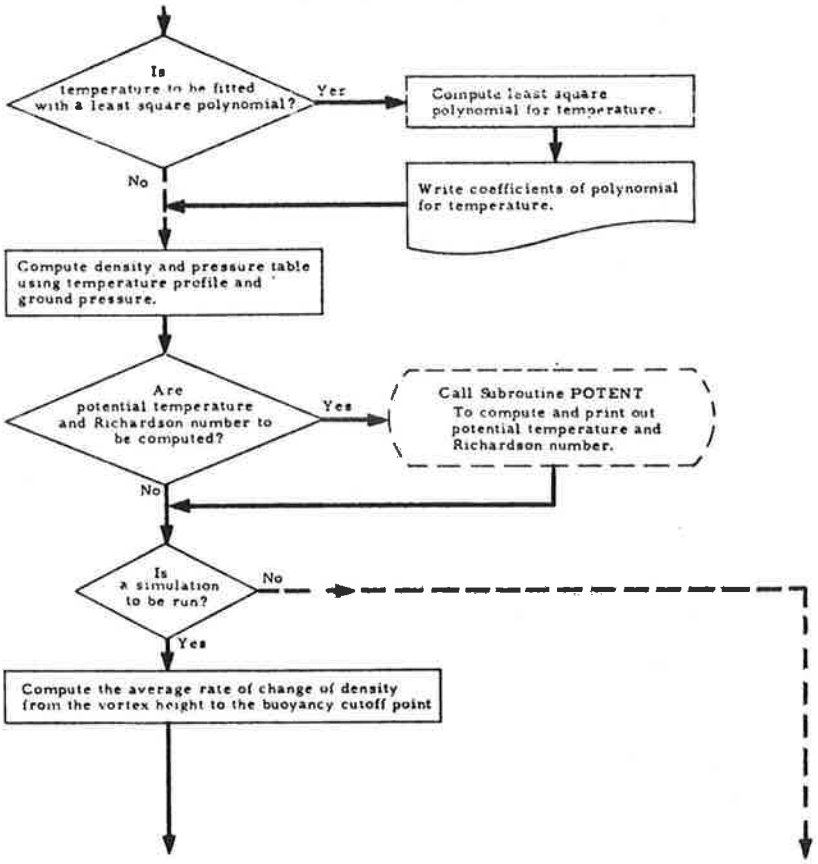
Is temperature to be fitted with a least square polynomial?
Yes
Compute least square polynomial for temperature.
No
Write coefficients of polynomial for temperature.
Compute density and pressure table using temperature profile and ground pressure.
Are potential temperature and Richardson number to be computed?
Yes
Call Subroutine POTENT
To compute and print out potential temperature and Richardson number.
No
Is a simulation to be run?
No
Yes
Compute the average rate of change of density from the vortex height to the buoyancy cutoff point

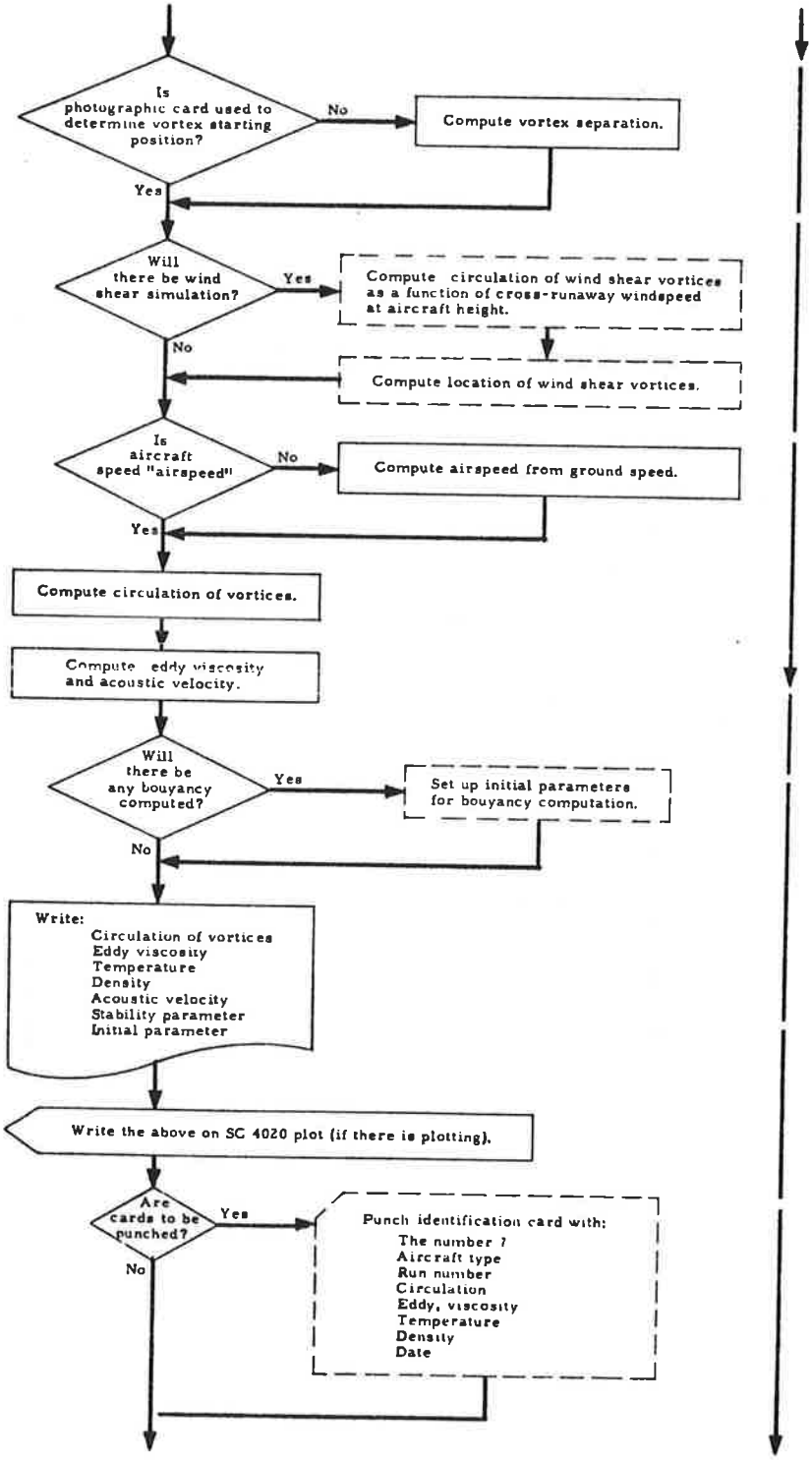
Is photographic card used to determine vortex starting position?
No
Compute vortex separation.
Yes
Will there be wind shear simulation?
Yes
Compute circulation of wind shear vortices as a function of cross-runaway windspeed at aircraft height.
No
Compute location of wind shear vortices.
Is aircraft speed "airspeed"
No
Compute airspeed from ground speed.
Yes
Compute circulation of vortices.
Compute eddy viscosity and acoustic velocity.
Will there be any bouyancy computed?
Yes
Set up initial parameters for bouyancy computation.
No
Write:
Circulation of vortices
Eddy viscosity
Temperature
Density
Acoustic velocity
Stability parameter
Initial parameter
Write the above on SC 4020 plot (if there is plotting).
Are cards to be punched?
Yes
Punch identification card with:
The number 7
Aircraft type
Run number
Circulation
Eddy, viscosity
Temperature
Density
Date
No

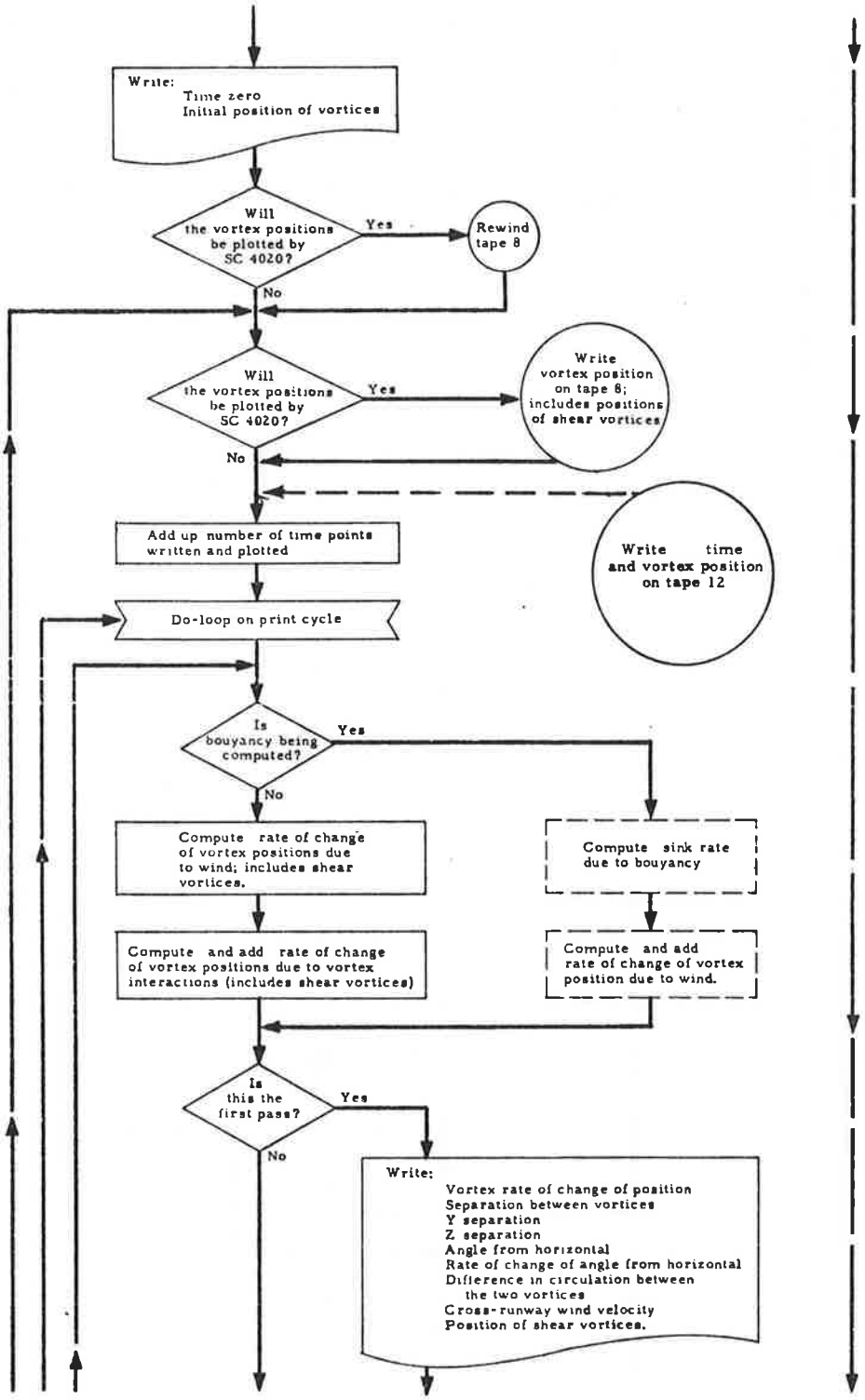
Write:
Time zero
Initial position of vortices
Will the vortex positions be plotted by SC 4020?
Yes
Rewind tape 8
No
Will the vortex positions be plotted by SC 4020?
Yes
Write vortex position on tape 8; includes positions of shear vortices
No
Write time and vortex position on tape 12
Add up number of time points written and plotted
Do-loop on print cycle
Is bouyancy being computed?
Yes
No
Compute rate of change of vortex positions due to wind; includes shear vortices.
Compute sink rate due to bouyancy
Compute and add rate of change of vortex positions due to vortex interactions (includes shear vortices)
Compute and add rate of change of vortex position due to wind.
Is this the first pass?
Yes
No
Write:
Vortex rate of change of position
Separation between vortices
Y separation
Z separation
Angle from horizontal
Rate of change of angle from horizontal
Difference in circulation between the two vortices
Cross-runway wind velocity
Position of shear vortices.

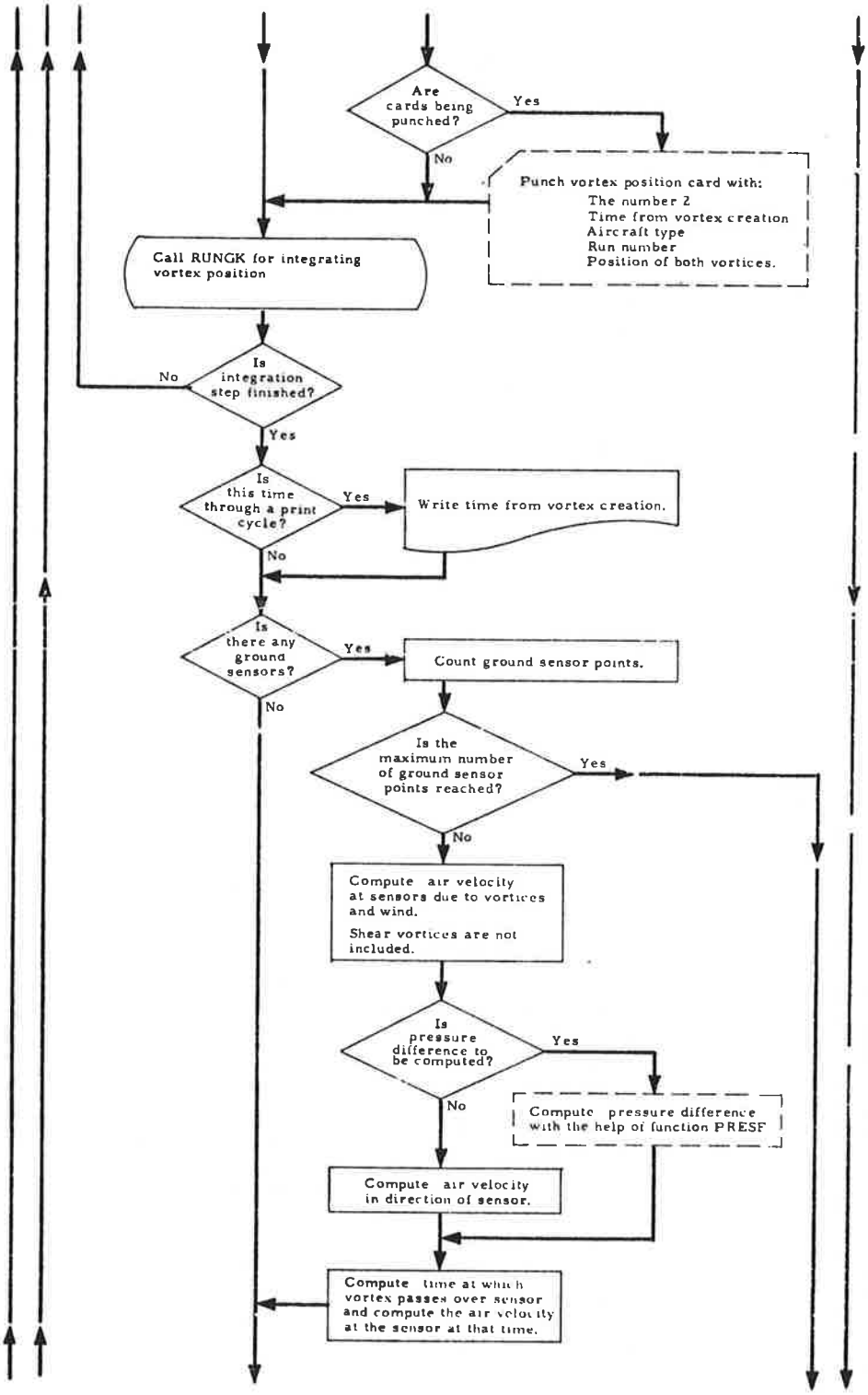
Are cards being punched?
Yes
No
Punch vortex position card with:
The number 2
Time from vortex creation
Aircraft type
Run number
Position of both vortices.
Call RUNGK for integrating vortex position
Is integration step finished?
No
Yes
Is this time through a print cycle?
Yes
Write time from vortex creation.
No
Is there any ground sensors?
Yes
Count ground sensor points.
No
Is the maximum number of ground sensor points reached?
Yes
No
Compute air velocity at sensors due to vortices and wind.
Shear vortices are not included.
Is pressure difference to be computed?
Yes
No
Compute pressure difference with the help of function PRESF
Compute air velocity in direction of sensor.
Compute time at which vortex passes over sensor and compute the air velocity at the sensor at that time.

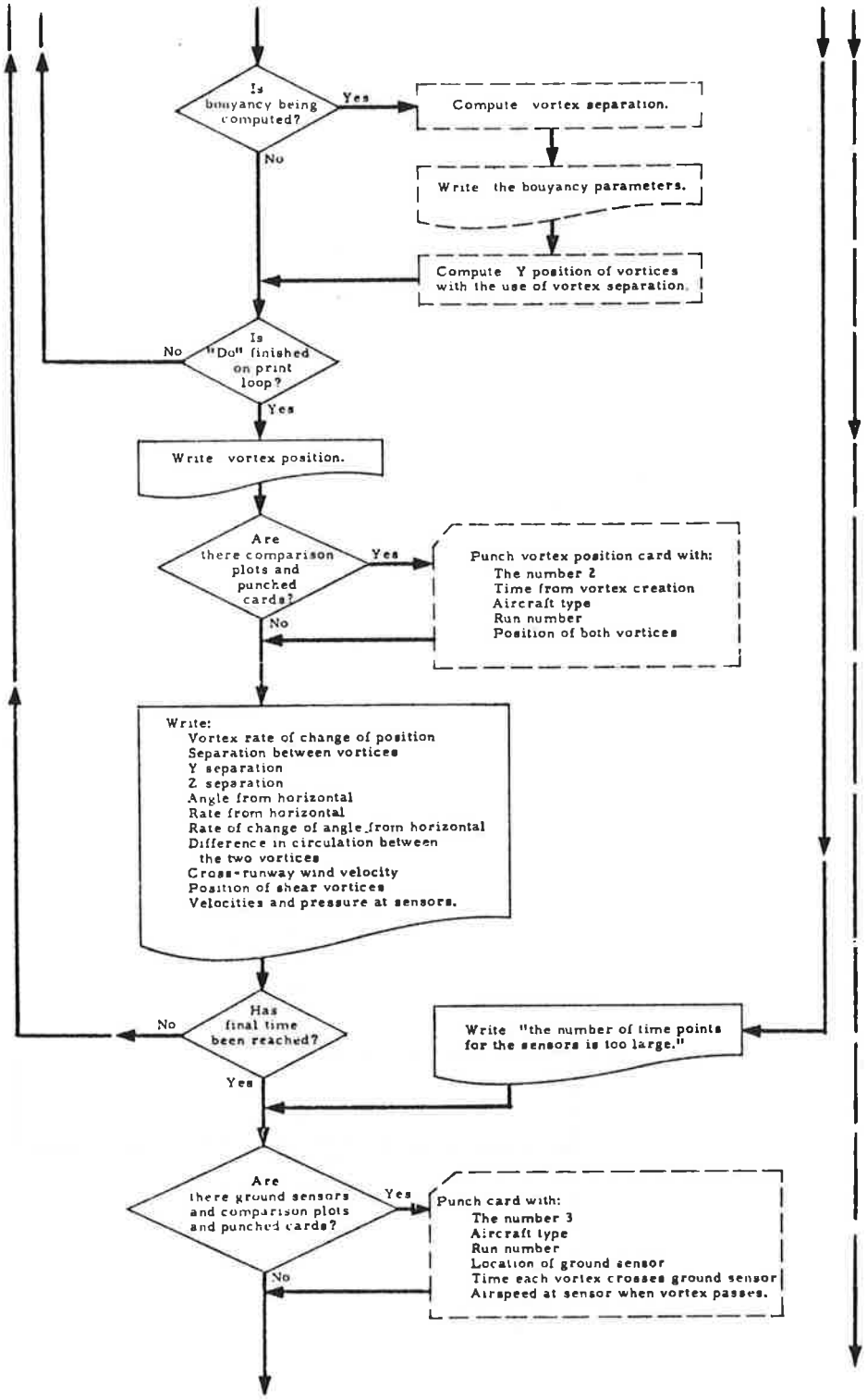
Is buoyancy being computed?
Yes
No
Compute vortex separation.
Write the bouyancy parameters.
Compute Y position of vortices with the use of vortex separation.
Is "Do" finished on print loop?
No
Yes
Write vortex position.
Are there comparison plots and punched cards?
Yes
No
Punch vortex position card with:
The number 2
Time from vortex creation
Aircraft type
Run number
Position of both vortices
Write:
Vortex rate of change of position
Separation between vortices
Y separation
Z separation
Angle from horizontal
Rate from horizontal
Rate of change of angle from horizontal
Difference in circulation between the two vortices
Cross-runway wind velocity
Position of shear vortices
Velocities and pressure at sensors.
Has final time been reached?
No
Yes
Write "the number of time points for the sensors is too large."
Are there ground sensors and comparison plots and punched cards?
Yes
No
Punch card with:
The number 3
Aircraft type
Run number
Location of ground sensor
Time each vortex crosses ground sensor
Airspeed at sensor when vortex passes.

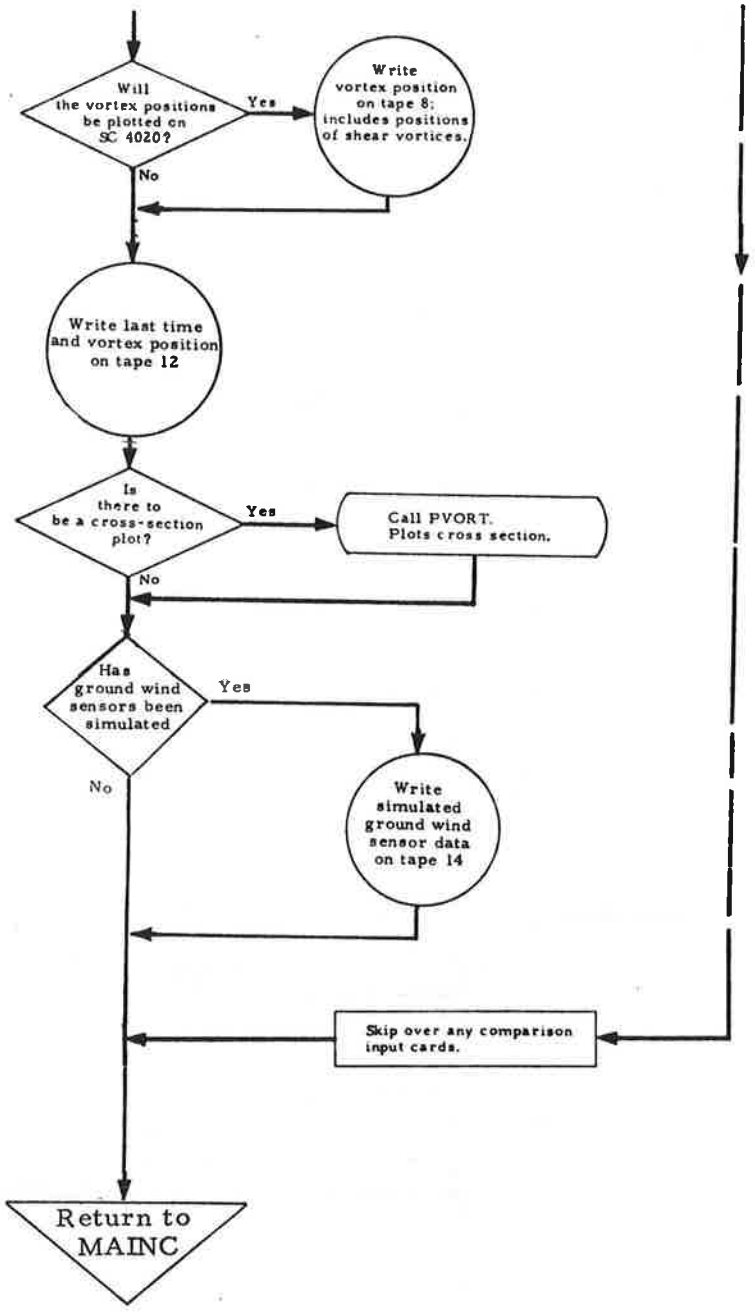
Will the vortex positions be plotted on SC 4020?
Yes
Write vortex position on tape 8; includes positions of shear vortices.
No
Write last time and vortex position on tape 12
Is there to be a cross-section plot?
Yes
Call PVORT. Plots cross section.
No
Has ground wind sensors been simulated
Yes
Write simulated ground wind sensor data on tape 14
No
Skip over any comparison input cards.
Return to MAINC

PROGRAM COORDINATE SYSTEM

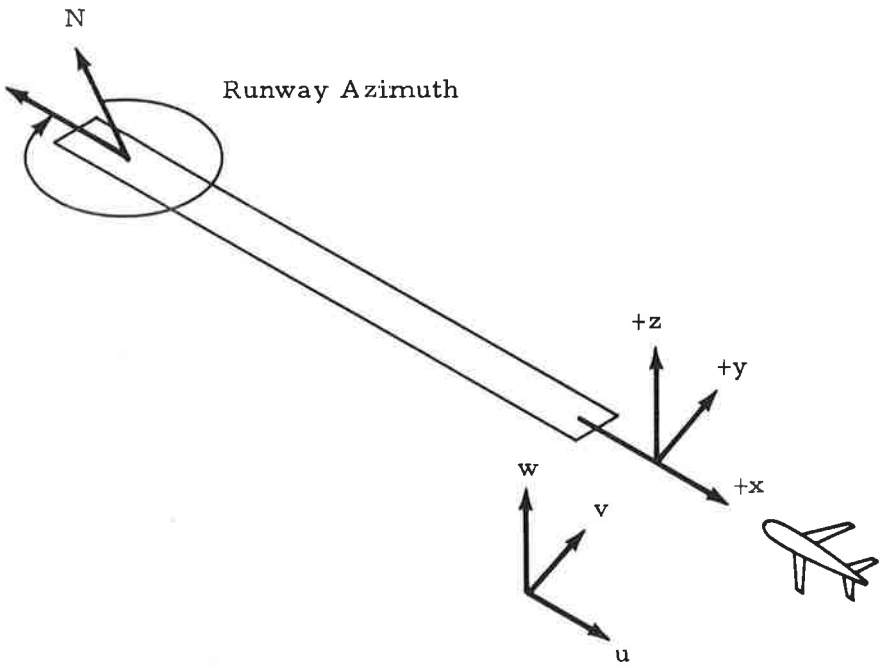

## APPENDIX C – INPUT FOR MET AND PREDIC PROGRAM

There are two types of input for the MET and PREDIC program:

1. Input cards to control the program's operation
2. Magnetic tape which contains meteorological and groundwind data along with aircraft flags.

### Input Cards

The first card is a title card where the first 30 caricatures appear on all the printed titles. The next group of input cards is for namelist INTAPE (described in Chart C-1). The last two groups of input cards is for namelists STATF and STATD. The variables in these namelists are for controlling the statistical program. They are preset and need not be changed.

### Magnetic Tape

The magnetic tape that this program currently reads is TSC's two base line groundwind sensor line JFK tapes.

NAMELIST (INTAPE)

| | |
|---|---|
| ISREC | NUMBER OF RECORDS TO SKIP |
| ISFRAM | NUMBER OF FRAMES TO SKIP |
| IRWIND | FLAG<br>IRWIND = 0 DO NOT REWIND INPUT TAPE<br>IRWIND = 1 REWIND INPUT TAPE BEFOR STARTING |
| NRUN | NUMBER OF RUNS (IF NRUN = 0 THEN PROGRAM TERMINATES) |
| IRAW | FLAG<br>IRAW = 0 NO PLOTTING OF RAW DATA<br>IRAW .GE. 1 PLOT RAW DATA ('IRAW' SECOND AVERAGES AT 1 SECOND INTERVALS)<br>IRAW MUST BE ODD |
| METDAT | FLAG<br>METDAT = 0 NO MET DATA<br>METDAT = 1 MET DATA |
| NPRED | FLAG<br>NPRED = 0 NO PREDICTION<br>NPRED = 1 PREDICTION COMPUTED (METDAT MUST EQUAL 1) |
| NSENG | NUMBER OF SENSOR GROUPS TO PROCESS |
| MSENG(2,5) | SENSOR GROUPS TO BE PROCESSED<br>ONE OR TWO SENSORS CAN BE IN A GROUP.<br>THE SECOND SUBSCRIPT INDICATES THE GROUP.<br>WHERE THE FIRST SUBSCRIPT INDICATES THE MEMBER OF THE GROUP.<br>100 OR 200 IS ADDED TO THE SENSOR NUMBER TO INDICATE SENSOR LINE 1 OR SENSOR LINE 2. |
| LINES(4) | FLAG FOR SENSOR LINES WANTED<br>LINES(L) = 1 INDICATES SENSOR LINE L IS WANTED<br>LINES(L) = 0 INDICATES SENSOR LINE L IS NOT WANTED |
| LSENGC(26,4) | SENSORS TO BE CROSS CORRELATED WITH THE PREDICTED.<br>THE FIRST SUBSCRIPT IS SENSOR NUMBER<br>THE SECOND SUBSCRIPT IS SENSOR LINE NUMBER<br>LSENGC = 1 SENSOR TO BE CROSS CORRELATED<br>LSENGC = 0 SENSOR NOT TO BE CROSS CORRELATED<br>'IRAW','METDAT', AND 'NPRED' MUST NOT BE ZERO |
| ISEN(3,18) | FLAG TO INDICATE MET SENSORS ACTIVE<br>ISEN(N,M)=0 THIS SENSOR NOT ACTIVE<br>ISEN(N,M)=1 THIS SENSOR IS ACTIVE |

Chart C-1 - Description of Input Cards for Namelist INTAPE

## APPENDIX D – OUTPUT FOR MET AND PREDIC PROGRAM

The two main outputs are MET data on the printer and predictive tracks on tape unit 12.

Printer output from MET is by way of name list with the following definitions:

| | | | | |
|---|---|---|---|---|
| PLAW | (1, 1) | Tower 1 | Reference Height | Power Law for Horizontal Wind Speed Profile |
| | (2, 1) | | Reference Velocity | |
| | (3, 1) | | Exponent | |
| | (1, 2) | Tower 2 | | |
| | (2, 2) | | | |
| | (3, 2) | | | |
| | (1, 3) | Tower 3 | | |
| | (2, 3) | | | |
| | (3, 3) | | | |
| | (1, 4) | Tower 4 | | |
| | (2, 4) | | | |
| | (3, 4) | | | |
| NPOLY | | | Order of Polynominal | Horizontal Wind Direction Profile |
| COEF | (1) | | Coefficients for Polynominal | |
| COEF | (2) | | | |
| COEF | (3) | | | |
| COEFV | (3) | | Coefficient for Vertical Wind Profile* | |
| USTAR1 | (1) | 20 and 40 ft Tower 1 | | Friction Velocity Type 1 $\frac{0.4*(u_h(2) - u_h(2)}{\ell n\left(\frac{Z(2)}{Z(1)}\right)}$ |
| | (2) | 20 and 40 ft Tower 2 | | |
| | (3) | 25 and 50 ft Tower 3 | | |
| | (4) | 25 and 100 ft Tower 3 | | |
| | (5) | 25 and 135 ft Tower 3 | | |
| | (6) | 25 and 140 ft Tower 3 | | |
| | (7) | 50 and 100 ft Tower 3 | | |
| | (8) | 50 and 135 ft Tower 3 | | |
| | (9) | 50 and 140 ft Tower 3 | | |
| | (10) | 100 and 135 ft Tower 3 | | |
| | (11) | 100 and 140 ft Tower 3 | | |
| | (12) | 135 and 140 ft Tower 3 | | |
| | (13) | 20 and 30 ft Tower 4 | | |
| | (14) | Avg. of 1 → 13 for Type 1 Friction Velocity | | |

*$V = COEFV(3) * \sqrt{Z}$

| | | | |
|---|---|---|---|
| USTAR2 | (1) | 20 ft Tower 1 | Friction Velocity Type 2 $\frac{\sigma_h}{2.5}$ |
| | (2) | 40 ft Tower 1 | |
| | (3) | 20 ft Tower 2 | |
| | (4) | 40 ft Tower 2 | |
| | (5) | 25 ft Tower 3 | |
| | (6) | 50 ft Tower 3 | |
| | (7) | 100 ft Tower 3 | |
| | (8) | 135 ft Tower 3 | |
| | (9) | 140 ft Tower 3 | |
| | (10) | 20 ft Tower 4 | |
| | (11) | 30 ft Tower 4 | |
| | (12) | Avg. of 1 – 11 for Type 2 Fric. Vel. | |
| USTAR4 | (1) | Tower 1 | Average Friction Velocity for Tower (Type 1 and 2) |
| | (2) | Tower 2 | |
| | (3) | Tower 3 | |
| | (4) | Tower 4 | |
| ROUGH1 | (1) | 20 and 40 ft Tower 1 | Roughness Length Type 1 $\exp\left[\frac{\frac{u_h(2)}{u_h(1)}\ell n(z(1) - \ell n(z(2))}{\frac{u_h(2)}{u_h(1)} - 1}\right]$ |
| | (2) | 20 and 40 ft Tower 2 | |
| | (3) | 25 and 50 ft Tower 3 | |
| | (4) | 25 and 100 ft Tower 3 | |
| | (5) | 25 and 135 ft Tower 3 | |
| | (6) | 25 and 140 ft Tower 3 | |
| | (7) | 50 and 100 ft Tower 3 | |
| | (8) | 50 and 135 ft Tower 3 | |
| | (9) | 50 and 140 ft Tower 3 | |
| | (10) | 100 and 135 ft Tower 3 | |
| | (11) | 100 and 140 ft Tower 3 | |
| | (12) | 135 and 140 ft Tower 3 | |
| | (13) | 20 and 30 ft Tower 4 | |
| | (14) | Avg. of 1 – 13 for Type 1 Roughness Length | |
| ROUGH2 | (1) | 20 ft Tower 1 | Roughness Length Type 2 $\exp\left(\ell n(Z) - .5\frac{u_h}{\sigma_w}\right)$ |
| | (2) | 40 ft Tower 1 | |
| | (3) | 20 ft Tower 2 | |
| | (4) | 40 ft Tower 2 | |
| | (5) | 25 ft Tower 3 | |
| | (6) | 50 ft Tower 3 | |
| | (7) | 100 ft Tower 3 | |
| | (8) | 135 ft Tower 3 | |
| | (9) | 140 ft Tower 3 | |
| | (10) | 20 ft Tower 4 | |
| | (11) | 30 ft Tower 4 | |
| | (12) | Avg. of 1 – 11 for Type 2 Roughness Length | |
| ROUGH4 | (1) | Tower 1 | Average Roughness Length For Tower (Type 1 and 2) |
| | (2) | Tower 2 | |
| | (3) | Tower 3 | |
| | (4) | Tower 4 | |

| | | |
|---|---|---|
| VGRAD(1, 1) | 20 and 40 ft Tower 1 | u Wind Shear |
| (1, 2) | 20 and 40 ft Tower 2 | |
| (1, 3) | 25 and 50 ft Tower 3 | |
| (1, 4) | 25 and 100 ft Tower 3 | |
| (1, 5) | 25 and 135 ft Tower 3 | |
| (1, 6) | 25 and 140 ft Tower 3 | |
| (1,7) | 50 and 100 ft Tower 3 | |
| (1, 8) | 50 and 135 ft Tower 3 | |
| (1, 9) | 50 and 140 ft Tower 3 | |
| (1, 10) | 100 and 135 ft Tower 3 | |
| (1, 11) | 100 and 140 ft Tower 3 | |
| (1, 12) | 135 and 140 ft Tower 3 | |
| (1, 13) | 20 and 30 ft Tower 4 | |
| (1, 14) | Avg. of 1 – 13 for u Wind Shear | |
| VGRAD(2, 1) | 20 and 40 ft Tower 1 | v Wind Shear |
| (2, 2) | 20 and 40 ft Tower 2 | |
| (2, 3) | 25 and 50 ft Tower 3 | |
| (2, 4) | 25 and 100 ft Tower 3 | |
| (2, 5) | 25 and 135 ft Tower 3 | |
| (2, 6) | 25 and 140 ft Tower 3 | |
| (2, 7) | 50 and 100 ft Tower 3 | |
| (2, 8) | 50 and 135 ft Tower 3 | |
| (2, 9) | 50 and 140 ft Tower 3 | |
| (2, 10) | 100 and 135 ft Tower 3 | |
| (2, 11) | 100 and 140 ft Tower 3 | |
| (2, 12) | 135 and 140 ft Tower 3 | |
| (2, 13) | 20 and 30 ft Tower 4 | |
| (2, 14) | Avg. of 1 – 13 for v Wind Shear | |
| VGRAD(3, 1) | 20 and 40 ft Tower 1 | w Wind Shear |
| (3, 2) | 20 and 40 ft Tower 2 | |
| (3, 3) | 25 and 50 ft Tower 3 | |
| (3, 4) | 25 and 100 ft Tower 3 | |
| (3, 5) | 25 and 135 ft Tower 3 | |
| (3, 6) | 25 and 140 ft Tower 3 | |
| (3, 7) | 50 and 100 ft Tower 3 | |
| (3, 8) | 50 and 135 ft Tower 3 | |
| (3, 9) | 50 and 140 ft Tower 3 | |
| (3, 10) | 100 and 135 ft Tower 3 | |
| (3, 11) | 100 and 140 ft Tower 3 | |
| (3, 12) | 135 and 140 ft Tower 3 | |
| (3, 13) | 20 and 30 ft Tower 4 | |
| (3, 14) | Avg. of 1 – 13 for w Wind Shear | |
| VGRAD(4, 1) | 20 and 40 ft Tower 1 | $u_h$ Wind Shear |
| (4, 2) | 20 and 40 ft Tower 2 | |
| (4, 3) | 25 and 50 ft Tower 3 | |
| (4, 4) | 25 and 100 ft Tower 3 | |
| (4, 5) | 25 and 135 ft Tower 3 | |
| (4, 6) | 25 and 140 ft Tower 3 | |
| (4, 7) | 50 and 100 ft Tower 3 | |

| | | | |
|---|---|---|---|
| VGRAD | (4, 8) | 50 and 135 ft Tower 3 | $u_h$ Wind Shear |
| | (4, 9) | 50 and 140 ft Tower 3 | |
| | (4, 10) | 100 and 135 ft Tower 3 | |
| | (4, 11) | 100 and 140 ft Tower 3 | |
| | (4, 12) | 135 and 140 ft Tower 3 | |
| | (4, 13) | 20 and 30 ft Tower 4 | |
| | (4, 14) | Avg. of 1 – 13 for $u_h$ Wind Shear | |
| HORGR4 | (1) | Tower 1 | Average u Wind Shear for Each Tower |
| | (2) | Tower 2 | |
| | (3) | Tower 3 | |
| | (4) | Tower 4 | |
| TEMP | (1) | 10 ft Tower 2 | Temperature |
| | (2) | 40 ft Tower 2 | |
| | (3) | 10 ft Tower 3 | |
| | (4) | 50 ft Tower 3 | |
| | (5) | 140 ft Tower 3 | |
| TEMPA2 | | Average Temp. for Tower 2 | |
| TEMPA3 | | Average Temp. for Tower 3 | |
| TEMP | (6) | ΔT from (10 to 40 ft) Tower 2 | $C^o$/100 ft |
| | (7) | ΔT from (10 to 50 ft) Tower 3 | |
| | (8) | ΔT from (10 to 140 ft) Tower 3 | |
| ATEMP | | Average ΔT from Tower 3 | |
| TEMP | (9) | Potential Temp. from (10 to 40 ft) Tower 2 | |
| | (10) | Potential Temp. from (10 to 50 ft) Tower 3 | |
| | (11) | Potential Temp. from (10 to 140 ft) Tower 3 | |
| APTEMP | | Average Potential Temp. from Tower 3 | |
| PRESH | | Pressure | |
| HUMED | | Humidity | |
| IPASQ | (1, 1) | Tower 1 | Pasquill Class According to Power of Power Law Curve |
| | (1, 2) | Tower 2 | |
| | (1, 3) | Tower 3 | |
| | (1, 4) | Tower 4 | |
| | (2, 1) | Tower 1 | Pasquill Class According to Air Speed at 10 ft level |
| | (2, 2) | Tower 2 | |
| | (2, 3) | Tower 3 | |
| | (2, 4) | Tower 4 | |
| | (3, 2) | Tower 2 | Pasquill Class According to dT/dZ |
| | (3, 3) | Tower 3 | |
| RICH | (1) | Richardson Number, Tower 2 | |
| | (2) | Richardson Number, Tower 3 | |
| | (3) | Average Richardson Number | |
| DISIP | (1, 1) | 20 ft Tower 1 | Dissipation Rate Type 1 = $\frac{\text{(Friction Velocity)}}{(.4)^{1/3} z}$ |
| | (2, 1) | 40 ft Tower 1 | |
| | (3, 1) | 20 ft Tower 2 | |
| | (4, 1) | 40 ft Tower 2 | |
| | (5, 1) | 25 ft Tower 3 | |
| | (6, 1) | 50 ft Tower 3 | |
| | (7, 1) | 100 ft Tower 3 | |
| | (8, 1) | 135 ft Tower 3 | |

| | | |
|---|---|---|
| DISIP | (9, 1) | 140 ft Tower 3 |
| | (10, 1) | 20 ft Tower 4 |
| | (11, 1) | 30 ft Tower 4 |
| | (12, 1) | Avg. of 1 – 11 for Dissipation Rate of Type 1 |
| DISIP | (1, 2) | 20 ft Tower 1 |
| | (2, 2) | 40 ft Tower 1 |
| | (3, 2) | 20 ft Tower 2 |
| | (4, 2) | 40 ft Tower 2 |
| | (5, 2) | 25 ft Tower 3 |
| | (6, 2) | 50 ft Tower 3 |
| | (7, 2) | 100 ft Tower 3 |
| | (8, 2) | 135 ft Tower 3 |
| | (9, 2) | 140 ft Tower 3 |
| | (10, 2) | 20 ft Tower 4 |
| | (11, 2) | 30 ft Tower 4 |
| | (12, 2) | Avg. of 1 – 11 for Dissipation Rate of Type 2 |
| DISIP | (1, 3) | 20 ft Tower 1 |
| | (2, 3) | 40 ft Tower 1 |
| | (3, 3) | 20 ft Tower 2 |
| | (4, 3) | 40 ft Tower 2 |
| | (5, 3) | 25 ft Tower 3 |
| | (6, 3) | 50 ft Tower 3 |
| | (7, 3) | 100 ft Tower 3 |
| | (8, 3) | 135 ft Tower 3 |
| | (9, 3) | 140 ft Tower 3 |
| | (10, 3) | 20 ft Tower 4 |
| | (11, 3) | 30 ft Tower 4 |
| | (12, 3) | Avg. of 1 – 11 for Dissipation Rate of Type 3 |
| DISIP | (1, 4) | 20 ft Tower 1 |
| | (2, 4) | 40 ft Tower 1 |
| | (3, 4) | 20 ft Tower 2 |
| | (4, 4) | 40 ft Tower 2 |
| | (5, 4) | 25 ft Tower 3 |
| | (6, 4) | 50 ft Tower 3 |
| | (7, 4) | 100 ft Tower 3 |
| | (8, 4) | 135 ft Tower 3 |
| | (9, 4) | 140 ft Tower 3 |
| | (10, 4) | 20 ft Tower 4 |
| | (11, 4) | 30 ft Tower 4 |
| | (12, 4) | Avg. of 1 – 11 for Dissipation Rate of Type 4 |
| | (13, 1) | Tower 1 |
| | (13, 2) | Tower 2 |
| | (13, 3) | Tower 3 |
| | (13, 4) | Tower 4 |
| BRUNT2 | | Brunt-Vaisala Period for Tower 2 |
| BRUNT3 | | Brunt-Vaisala Period for Tower 3 |
| STAB2 | | Stability Length for Tower 2 |
| STAB3 | | Stability Length for Tower 3 |

Dissipation Rate Type 2

$$= (\text{Type 1}) \frac{\left((1 - \frac{1}{3}(\text{RICH}) * (1 - 18(\text{RICH}))^{1/4}\right)^{1/3}}{(1 - 18\,(\text{RICH}))^{1/3}}$$

Dissipation Rate Type 3

$$\frac{0.4^{2/3}\, u_h}{z^{1/3}\, \ell n \left(\frac{z}{(\text{Roughness Length})}\right)}$$

Dissipation Rate Type 4

$$= \frac{0.4^{2/3}\, \sigma_n}{z^{1/3}}$$

Average Dissipation Rate for Each Tower (Types 1, 2, 3, 4)

The predictive tracks on tape unit 12 is read by VORCOM for plotting.

## APPENDIX F – REPORT OF INVENTIONS

The objective of the contract was fulfilled including: (1) the development of a comprehensive computer program for the analysis of JFK MET/GW tapes; (2) the processing and data reduction of the MET/GW tapes supplied by DOT-TSC; and (3) statistical analysis of groundwind sensor tracks. In satisflying the above program objectives no innovation, discovery, improvement or invention was made.

## REFERENCES


1. Wilson, D. J., M. R. Brashears, E. A. Carter and K. R. Shrider, "Wake Vortex Predictive System," Report FAA-RD-72-108 (also LMSC-HREC TR D306226), Lockheed Missiles & Space Company, Huntsville, Ala., 1972.

2. Brashears, M. R., and J. N. Hallock, "Aircraft Wake Vortex Transport Model," AIAA J. of Aircraft, Vol. 11, May 1974, pp. 265-272.

3. Brashears, M. R. et al., "Analysis of Predicted Aircraft Wake Vortex Transport and Comparison with Experiment," Report FAA-RD-74-74.I and II April 1974.

4. Brashears, M. R., S. J. Robertson, B. C. Johnson, C. Fan and K. R. Shrider, "Wake Vortex Transport Considerations and Meterological Data Analysis — Wake Vortex Predictions Systems Study," LMSC-HREC TR D390424, Lockheed Missiles & Space Company, Huntsville, Ala., November 1974.

5. Winston, B. P., DOT-TSC report to be published.